

12. SITE 758¹

Shipboard Scientific Party²

HOLE 758A

Date occupied: 12 June 1988
Date departed: 24 June 1988
Time on hole: 11 days, 5 hr
Position: 5°23.049'N, 90°21.673'E
Bottom felt (rig floor; m; drill-pipe measurement): 2934.5
Distance between rig floor and sea level (m): 10.87
Water depth (drill-pipe measurement; corrected m): 2923.6
Total depth (rig floor; corrected m): 3611.3
Penetration (m): 676.8
Number of cores: 73
Total length of cored section (m): 676.8
Total core recovered (m): 453.83
Core recovery (%): 67
Oldest sediment cored:
Depth sub-bottom (m): 527.1
Nature: clayey tuff
Earliest age: Santonian
Latest age: early Campanian
Measured velocity (km/s): 1.7–4.5
Hard rock:
Depth sub-bottom (m): 498.9
Nature: plagioclase phyric basalt
Measured velocity (km/s): 4.5–5.1
Basement:
Depth sub-bottom (m): 517.45
Nature: slightly plagioclase phyric to aphyric basalt
Measured velocity (km/s): 3.8–4.4

HOLE 758B

Date occupied: 15 June 1988
Date departed: 15 June 1988
Time on hole: 11 hr, 15 min
Position: 5°23.037'N, 90°21.670'E
Bottom felt (rig floor; m; drill-pipe measurement): 2936.5
Distance between rig floor and sea level (m): 10.87
Water depth (drill-pipe measurement; corrected m): 2925.6
Total depth (rig floor; corrected m): 3032.5
Penetration (m): 96.0
Number of cores: 10
Total length of cored section (m): 96.0
Total core recovered (m): 98.68

Core recovery (%): 102

Oldest sediment cored:

Depth sub-bottom (m): 96.0
Nature: nannofossil ooze with clay and foraminifers
Earliest age: late Miocene
Measured velocity (km/s): 1.55

HOLE 758C

Date occupied: 15 June 1988
Date departed: 15 June 1988
Time on hole: 7 hr, 45 min
Position: 5°23.043'N, 90°21.668'E
Bottom felt (rig floor; m; drill-pipe measurement): 2933.1
Distance between rig floor and sea level (m): 10.87
Water depth (drill-pipe measurement; corrected m): 2922.2
Total depth (rig floor; corrected m): 2942.5
Penetration (m): 9.4
Number of cores: 1
Total length of cored section (m): 9.4
Total core recovered (m): 9.40
Core recovery (%): 100
Oldest sediment cored:
Depth sub-bottom (m): 9.4
Nature: clayey nannofossil ooze with foraminifers
Earliest age: Pleistocene
Measured velocity (km/s): 1.48

Principal results: Ocean Drilling Program (ODP) Site 758 (proposed Site NER-1C) is on the southeast side of one of the large en echelon blocks that characterize the Ninetyeast Ridge between the Equator and 10°N. Together, the three drilling locations of Leg 121 on the Ninetyeast Ridge are designed to sample the basement through time and the sedimentary section through both time and latitude. Site 758 is the northern point of that transect, and it is located roughly halfway between Deep Sea Drilling Project (DSDP) Sites 216 and 217.

Specific objectives at Site 758 were to sample basement for basalt geochemistry at a location as far north as possible to study evolution of the Kerguelen/Ninetyeast hot spot as well as vertical changes within the basement. Borehole televiwer (BHTV) logging sought breakouts as an indicator of *in-situ* stresses that are possibly related to compression of the Indo-Australian plate. Sampling was also planned to provide material for constructing a detailed northward-motion curve for the Indian plate from paleomagnetic studies, with particular emphasis on the Eocene and younger section to study the slowing of the Indian plate during collision with Asia. This location also forms the northern site in the south-north paleoceanographic/climatic transect. Here, particular emphasis could be placed in studying the evolution of the monsoonal climate regime as driven by the uplift of the Himalayas and Tibet and modified by variations caused by the Milankovitch mechanism.

The proposed site location was picked at time 1730 hr on the seismic-reflection survey carried out during *Robert D. Conrad* Cruise 2705 (RC2705). The original drilling plan was to drill two sites—one for Neogene objectives and one for Paleogene and basement objectives. Because of severe time constraints and increased faith in the

¹ Peirce, J., Weissel, J., et al., 1989. *Proc. ODP, Init. Repts.*, 121: College Station, TX (Ocean Drilling Program).

² Shipboard Scientific Party is as given in the list of Participants preceding the contents.

minicone system for reentry, a single combined location was chosen in order to save several days of drilling time at the expense of condensing the Neogene section by 20%.

The site survey tracks are widely spaced. The orientation of the approach survey to the perceived structural grain (N45°E) was picked from a combination of seismic, Sea Beam, and Seasat data. The survey was conducted outside the Global Positioning System (GPS) satellite window and therefore is less accurately positioned than the previous surveys during Leg 121. The area around the site is much more heavily faulted (usually to the surface) than was apparent from the original RC2705 site survey.

Hole 758A was cored with the advanced hydraulic piston corer (APC) and extended core barrel (XCB) systems to refusal at 422 m below seafloor (mbsf). A minicone was set onto a relatively hard bottom, the ship was offset, and Hole 758B was APC cored to 96 mbsf to overlap the coring interval in Hole 758A. Hole 758C consists of a mud-line core that was taken because of correlation uncertainties evident when Core 121-758B-1H was split.

Hole 758A was reentered and cored with the rotary core barrel (RCB) to a total depth of 677 mbsf. The logging program was not completed because of poor hole conditions. The seismic stratigraphic and geochemical logs were run from 40 to 405 mbsf, and the BHTV was run from 525 to 610 mbsf. The quality of the BHTV log processed aboard ship is inadequate for interpretation; post-cruise processing may improve it.

Five lithologic units are recognized at Site 758:

Unit I (0–122 mbsf): Holocene to middle Miocene nannofossil ooze. This unit is divided into two subunits:

Subunit IA (0–25 mbsf): Holocene to lowermost Pleistocene alternating layers of light gray nannofossil ooze with clay and foraminifers and layers of dark gray nannofossil ooze with foraminifers. The layers are 10–110 cm thick and have gradational contacts. Subunit IA contains six major ash layers, 5–34 cm thick, and several thin, green ash layers, which are 1–2 cm thick. The thicker ash layers are graded, fine upward, commonly have sharp basal contacts, and locally contain pumice fragments.

Subunit IB (25–122 mbsf): lowermost Pleistocene to middle Miocene light gray to white nannofossil ooze with clay, foraminifers, and micrite. The calcium carbonate content of Subunit IB is higher than that of Subunit IA, and it increases downcore as the clay content decreases. Gray ash beds, 2–15 cm thick, and thin, green ash beds, 1–2 cm thick, are less common in this subunit than in Subunit IA.

Unit II (122–367 mbsf): middle Miocene to lower Maestrichtian chalk. Unit II is divided into two subunits:

Subunit IIA (121–296 mbsf): middle Miocene to lower Paleocene nannofossil and calcareous nannofossil chalk, very pale brown to white in color and mottled and bioturbated. The calcium carbonate content is more than 80%. Rare chert pebbles occur.

Subunit IIB (296–367 mbsf): upper Maestrichtian to upper Campanian, greenish gray calcareous chalk with nannofossils, foraminifers, and clay. The subunit has some occurrences of pyrite, chert pebbles, dark ash layers, and porcellanite intervals up to 11 cm long. *Inoceramus* and other shell fragments are common. The calcium carbonate content decreases with depth from about 90% to less than 60% within Subunit IIB.

Unit III (367–431 mbsf): Campanian greenish gray calcareous clay with varicolored patches (similar to a camouflage pattern). This unit contains several chert pebbles, porcellanite stringers up to 20 cm long, *Inoceramus* and other shell fragments, some ash beds, and rare microfaults.

Unit IV (431–499 mbsf): Campanian greenish gray tuff with minor interbeds of ashy calcareous chalk. Unit IV also contains silt- to lapilli-sized lithic and pumice fragments in graded beds, pyrite, rounded basalt pebbles (<1 cm diameter), and minor amounts of shell fragments.

Unit V (499–677 mbsf): Campanian(?) basalts, which are medium grained, petrographically uniform, and aphyric to sparsely plagioclase and clinopyroxene phyrlic. The 29 flow units recovered include five pillowed flows. Vesicles and amygdules are rare in the upper flow units and common in the lower flow units. Eight intervals of interbedded tuff similar to Unit IV were recovered, including one layer at 602 mbsf which is dated as younger than Turonian. The thickness of any one of these volcanoclastic intervals is no more than a few meters, and they are more sporadic with depth. Pillows are in-

terbedded with 1-m-thick flows below 640 mbsf. The lower flow units are less than 3 m thick and are characterized by sharp, cryptocrystalline selvages. The flow units become thicker and more massive upsection, where the average thickness exceeds 10 m. One unit is more than 20 m thick. Shipboard analyses do not indicate any significant geochemical trends with depth.

Basalt recovery was spectacular (>70%) until the pillow units were reached, and museum-scale (up to 3.37 m long) pieces of unbroken rock were repeatedly recovered from the thickest flow units. The upper flow units are interpreted as ponded sheet flows; the lower flow units are thin sheet flows interbedded with pillowed flows. The ashes are geochemically distinct from the flows. Some ashes were deposited by falling through the water column and others as turbidity flows. No accretionary lapilli were recovered, indicating that the sources of the ashes were more than 10 km distant. We interpret these observations to mean that the ashes were produced at volcanic islands not immediately adjacent to the site, whereas the lavas were erupted locally in deep water. There is no indication that any of the basaltic units were erupted subaerially.

The Cretaceous/Tertiary boundary sequence is incomplete, and the best estimated position of boundary is between cores at 296 mbsf. The uppermost Maestrichtian and the lowermost Paleocene appear to be absent. Fossil assemblages change from tropical to higher latitude forms at about 305 mbsf.

Site 758 was originally chosen to penetrate an expanded Paleogene section at the northern end of Ninetyeast Ridge. This objective was especially important because neither Site 216 nor 217 recovered a complete Paleogene section. Unfortunately, the Paleogene section at Site 758 is also incomplete, with several unconformities. Preliminary indications, based only on calcareous nannofossil dates, are that all or parts of the zones below CP1b, CP3(?), and CP9 to CP14 are missing in the Paleogene.

In contrast to the poor quality of the Paleogene section, the Neogene section appears to be excellent. The double APC-cored sections of the upper 100 m (Holocene to upper Miocene) are correlatable on a centimeter scale using the magnetic susceptibility profiles. The magnetostratigraphic record is superb down to the top of Chron 6. All known geomagnetic reversals are clearly recorded in the shipboard data, except for the two Reunion events. Below this depth, the quality of the paleomagnetic record deteriorates as the calcium carbonate content increases and the clay content decreases. The visible alternations in Subunit IA may correlate with climatic variations and/or tectonic events in the Himalayas. This section also contains a very complete Holocene to Miocene tephrochronology of silicic ashes from the Indonesian Arc. The Toba ash (~75,000 yr) is tentatively identified at 1.5 to 1.8 mbsf. This replicated section is an excellent example of the value of double APC coring. Cores from Hole 758B showed that commonly 1–2 m of section either was not cored or was highly disturbed between every pair of piston cores. The double APC section is three times as valuable as a single APC section.

BACKGROUND AND OBJECTIVES

This section includes a brief synopsis of overall drilling objectives on Ninetyeast Ridge and discusses in detail the goals for Site 758, the northern site drilled on the ridge during Leg 121. A more complete discussion of the overall objectives and their implications is in the "Leg 121 Background and Objectives" chapter (this volume).

Northern Site 758

Site 758 lies along the crest of Ninetyeast Ridge, midway between DSDP Sites 216 and 217 (Fig. 1). As the northernmost site of the three-site transect along the ridge, the chosen site position is where basement can be easily reached by drilling. Basement age at this location is predicted to be 80 Ma, according to hot-spot models of Duncan (1978) and Duncan et al. (in press). Figure 2 shows the paleogeography of the site at its predicted basement age.

The site is at 5°23.05'N, 90°21.67'E, in a water depth of 2924 m. This area of Ninetyeast Ridge is broken into several

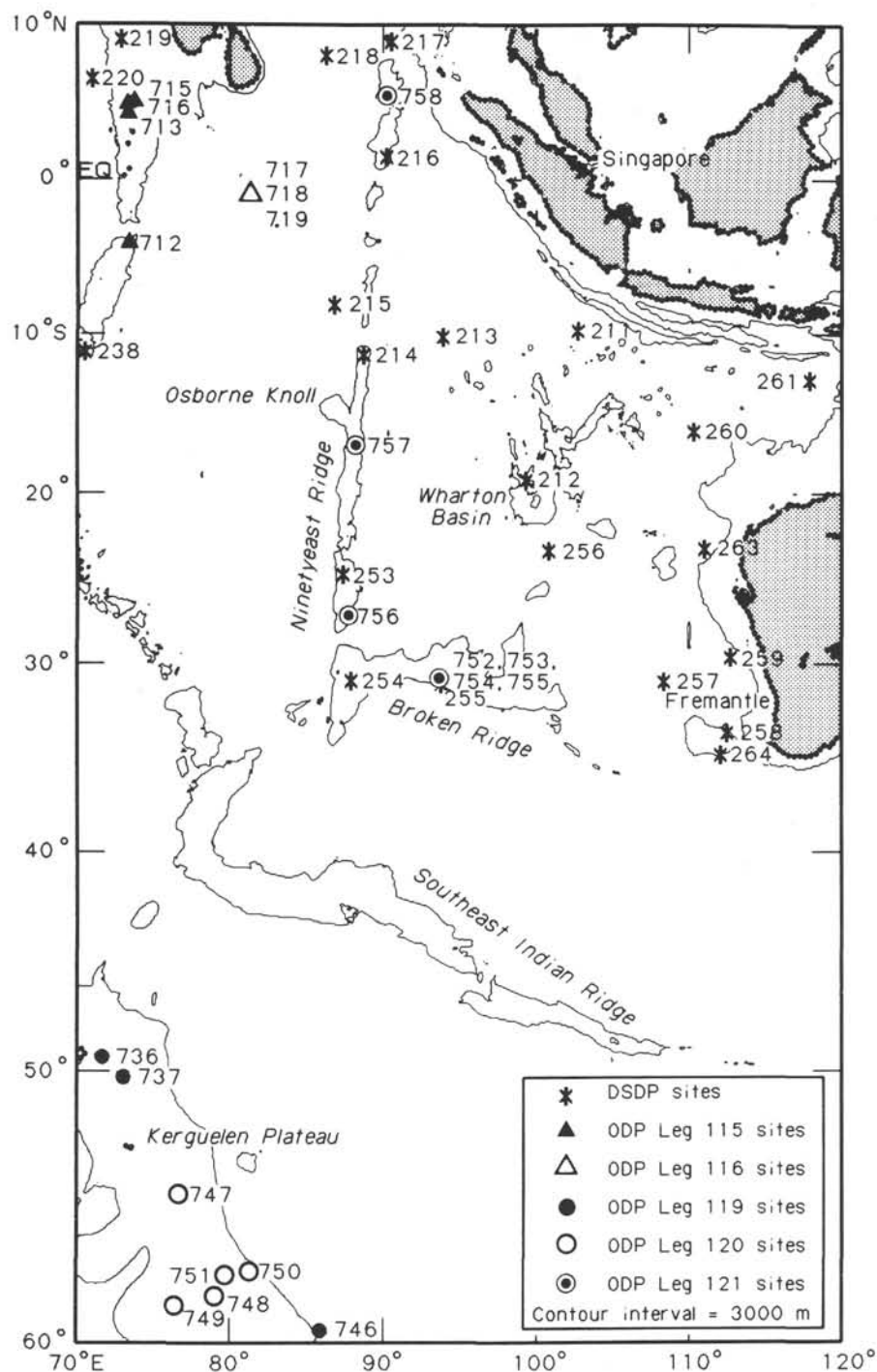


Figure 1. Location of Site 758 at the northern end of Ninetyeast Ridge and other ODP and DSDP sites in the Indian Ocean.

large, en echelon blocks, and Site 758 is on the southeast side of one of those blocks (see Figs. 55 and 56, "Seismic Stratigraphy" section, this chapter). Three holes were cored at Site 758 (see "Operations" section, this chapter). The deepest hole reached a total depth of 677 mbsf, after penetrating 431 m of hemipelagic and pelagic sediments, 68 m of tuff, and 178 m of basaltic flows with some interbeds of tuff.

Objectives

The objectives for drilling Ninetyeast Ridge fall into three broad categories: petrology, northward motion of the Indian plate, and paleoceanography/paleoclimatology.

A basic premise of the petrologic objectives on Leg 121 was to sample the volcanism of the Kerguelen/Ninetyeast hot spot

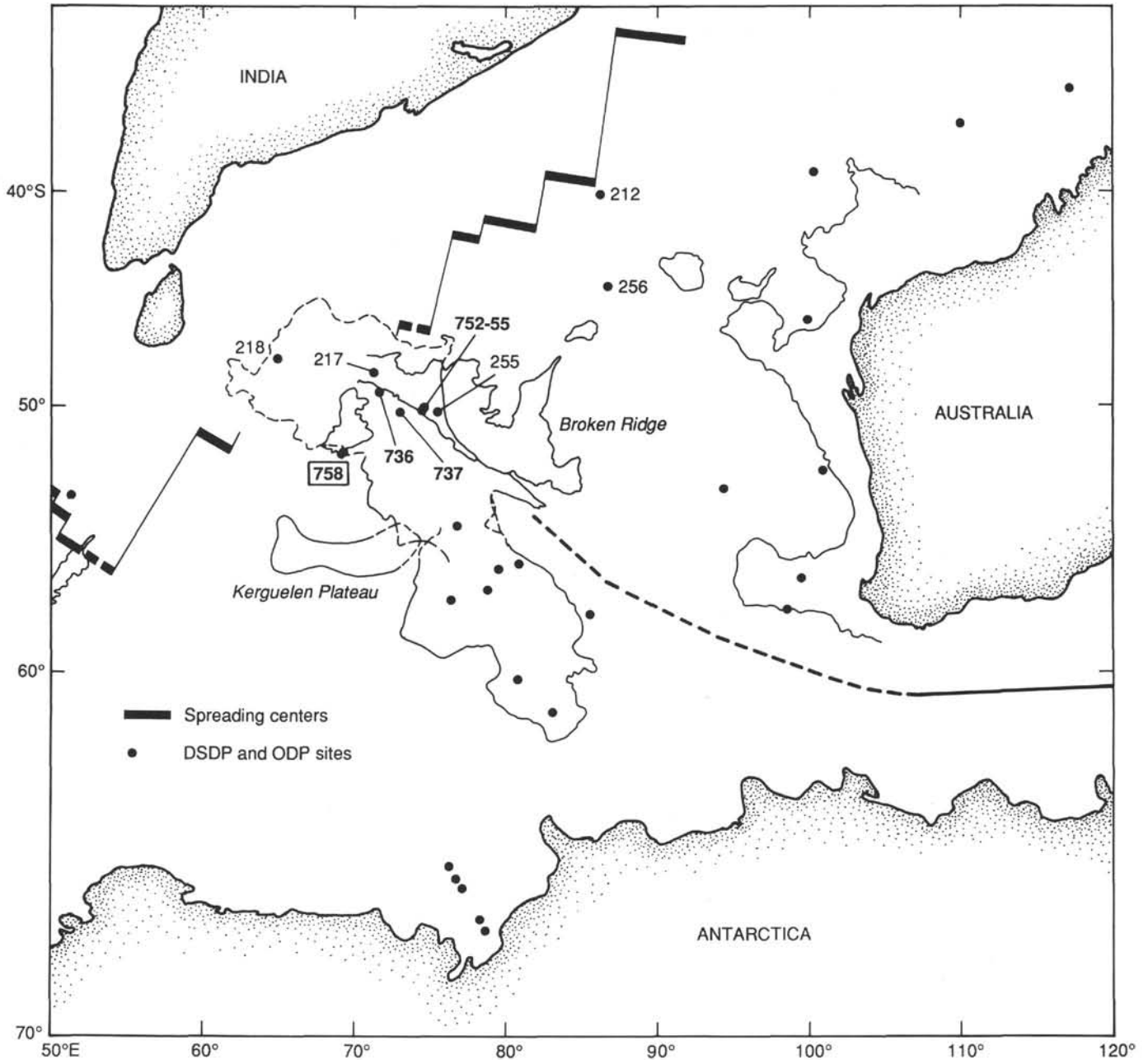


Figure 2. Reconstruction for 80 Ma, showing the position of Site 758 and adjacent features at the same time as its basement age, as predicted by Duncan et al. (in press). Overlap between the Kerguelen Plateau and Ninetyeast Ridge is due to younger volcanic construction and, presumably, to the manner of reconstruction which shows the northern Kerguelen Plateau fixed in its present-day coordinates (after model by Royer et al., in press).

through time, by sampling along the length of the Ninetyeast Ridge to study variations on a long time scale and also by sampling vertically to study variations within individual volcanic sections on a short time scale. With the unexpected discovery at Broken Ridge of an extensive ash sequence, which was produced presumably by the Kerguelen/Ninetyeast hot spot, sampling proximal ashes and basement rocks produced by the same volcanic source through the same time period (Late Cretaceous to middle Eocene) became more important.

In particular, Site 758 provided an opportunity to sample volcanic ash and basement of Campanian age, which was the unsampled interval between Sites 754 and 755 in the section at Broken Ridge. Furthermore, the seismic interpretation at the

proposed location suggested the presence of a clear basement reflector below the reverberant reflectors. This interpretation indicated that there was an excellent chance to drill unequivocal basement for the first time on Ninetyeast Ridge.

The primary objective of the paleomagnetic studies of the Ninetyeast Ridge sites is to precisely define the slowing of the northward motion of the Indian plate during and after its collision with Asia. We know that it slowed by a factor of three from the rate before collision (~ 15 cm/yr, 70 to ~ 50 Ma) to the rate after collision (~ 5 cm/yr, after 40 Ma; Molnar and Tapponnier, 1975; Peirce, 1978; Patriat and Achache, 1984), but the details of its deceleration are unknown. The manner in which the Indian plate slowed during the middle and late Eocene may pro-

vide clues about the tectonic style of the deformation that developed between India and Asia during the early stages of collision.

At Site 758, the ash section and the flows should provide excellent paleolatitude data for the Indian plate in the Late Cretaceous, but this is not the age of prime interest. The seismic interpretation predicted a thick Paleogene section at this location. A stable paleomagnetic signal extracted from the expected carbonate lithology would have further constrained the deceleration of the Indian plate. Unfortunately, this hope was frustrated by the unexpectedly incomplete and abbreviated Paleogene section that was actually drilled.

An additional, related objective at this site was to study the terrigenous component of sedimentation after collision. As discussed briefly in the "Leg 121 Background and Objectives" chapter, abundant evidence suggests that major uplift of the Himalayas and Tibet did not occur until well after collision, but the sequence and timing of tectonic events is not well understood. Because of its proximity to the Ganges-Brahmaputra drainage system, Site 758 may contain a sedimentary record of these events. The location of the site above the sedimentary distribution channels of the Bengal Fan means that the section there is thin enough to penetrate and is not interrupted by turbidites; hence, recovery was unimpeded by extensive sandy intervals.

One goal for a north-south paleoceanographic transect in the eastern Indian Ocean was to recover fossil records that contain a mixture of species from two different climatic assemblages, such as temperate and subtropical. Because many of the biostratigraphic time scales are based on the fossil record from one climatic zone (usually subtropical), it is often difficult to relate the fossils from one climatic assemblage to those of another with an accurate determination of relative stratigraphic ages. This confusion is further complicated by the time-transgressive nature of many critical biostratigraphic datums toward the ecological limits of any particular form. Sites with mixed zonal assemblages allow biostratigraphers to construct interzonal relationships and thus build more robust time scales with wider applicability.

At Site 758, one particular objective was to recover a continuous section of mixed tropical to subtropical Paleogene assemblages to compare with the higher latitude assemblages of the same age recovered farther south on the transect. In the Maestrichtian and Campanian part of the section, the same objectives apply, except that Site 758 was in temperate latitudes and closer to the two southern sites on the transect. Given the incomplete Paleogene section at Site 758, properly meeting these objectives is difficult for that age range. Fortunately, this situation does not apply for the Upper Cretaceous, and the objectives for the northern end of the paleoceanographic transect for that time frame should be attainable.

A unifying theme of the objectives of most of the ODP sites in the northern Indian Ocean is to study the impact of the uplift of the Himalayas and the Tibetan Plateau on sedimentation rates (increased terrigenous input) and the development of the monsoonal climate regime (which is ultimately driven by the seasonal differences in air temperature over the Indian Ocean and the Tibetan Plateau). ODP Leg 116 (Cochran, Stow, et al., 1989) focused on the Bengal Fan deposits derived from Himalayan uplift, and ODP Leg 117 (Prell, Niitsuma, et al., 1989) studied the history of monsoon development in the Arabian Sea.

Site 758 provides an opportunity to complement those studies at a location where the Himalayan component of sedimentation is hemipelagic, instead of turbiditic (as at the Bengal Fan sites of ODP Leg 116). Its low-latitude location in proximity to a sedimentary source area, which was probably affected in vary-

ing degrees by Pleistocene glaciation, offers a unique opportunity to study climatic variations. In this setting, the difference in the sedimentary signal between glacial and interglacial periods should be particularly dramatic. These climatic variations have been related to variations in the input of solar energy related to variations in Earth's orbital geometry (Milankovitch cycles) at other ODP sites (e.g., Srivastava, Arthur, et al., 1987). Seasonal monsoonal variations are superimposed on this glacial-interglacial pattern. Site 758 is the only ODP site that lies within the influence of the monsoons to the east of the Indian subcontinent. As such, it provides an important complement to the sites west of India in the Arabian Sea. Furthermore, it offers us the opportunity for high-resolution study of climatic fluctuations superimposed on longer time scale tectonic variations.

Because the preceding objectives required detailed sampling and complete recovery of the section, double APC coring (with offset core depths) was planned as a high-priority secondary procedure if time allowed. Fortunately, there was time for a second APC hole (Hole 758B), and the quality of the shipboard correlations between holes and with both the paleontological and magnetostratigraphic time scales (Berggren et al., 1985; Bolli et al., 1985; Harland et al., 1982) exceeded our expectations.

Pelagic records of eolian dust accumulation provide quantitative estimates of both the intensity of zonal winds and the aridity of the eolian source areas (Rea et al., 1985). One important paleoclimatological goal of Leg 121 was to recover continuous stratigraphic sections of Cenozoic age in order to analyze the eolian record. Ninetyeast Ridge is ideally located for this study because it lies between the great deserts of Africa and Australia and therefore should receive an adequate supply of dust. Furthermore, locations on top of the ridge are protected from abyssal reworking and should have fewer unrecognized contributions from hemipelagic input. The backtrack history of the three sites on Ninetyeast Ridge (see Fig. 16 of the "Leg 121 Background and Objectives" chapter) will provide a paleoclimatic record that spans nearly 50° of latitude.

The position of Site 758 during the Paleogene was in the trade-winds belt, just as Site 757 was during the Neogene. Thus, these two sites should have similar paleoclimatic records for those different time intervals. However, the poor quality of the Paleogene section present at Site 758 may mean that this objective cannot be fully met.

The objective of completing a full suite of logging runs, including the BHTV, became a top priority at Site 758 after the early termination of operations at Site 757. The BHTV data are particularly useful in measuring (1) the orientation of break-outs, which are an indicator of *in-situ* stress, and (2) the true thickness of the volcanoclastic material intercalated with the basaltic units. The measurement of *in-situ* stress at this location is particularly important because the site position is where deformation of the Indo-Australian plate is indicated by focal plane solutions of earthquakes (Stein and Okal, 1978). Similar stresses, presumably related, created folds in the Bengal Fan sediments that were drilled on Leg 116 (Sites 717-719, Fig. 1; Cochran, Stow, et al., 1989). The pervasive occurrence of young faults observed on the seismic data acquired during the approach survey ("Seismic Stratigraphy" section and the "Ninetyeast Ridge Underway Geophysics" chapter, this volume) is a further indication of high stresses at this location.

Two further objectives for Site 758 were defined aboard ship by the scientific party. The first is to study the tephrochronology of the Indonesian volcanic arc. Site 758 will provide the first opportunity to do this work beyond the depth of a conventional piston core. The second is to study in detail the behavior of the Earth's magnetic field during one or more polarity transitions. The terrigenous component in the upper Neogene sedi-

ment should preserve an excellent paleomagnetic record in this section. Initial shipboard results indicate that both of these studies will have an excellent section with which to work.

OPERATIONS

Cocos Island to Site 758 Transit

JOIDES Resolution departed from Cocos Island atoll immediately after disembarking one of the galley personnel and sailed for the northern site of the Ninetyeast Ridge drilling campaign. While under way, the new sand line was spooled onto the forward sand line winch. On 11 June, one day before reaching Site 758, the ship crossed the equator and another batch of polliwogs was initiated into the honorable order of shellbacks and introduced to the mysteries of Neptunus Rex.

The seismic gear was streamed to begin the site location survey at 0245 hr, 12 June. A different location, designated prospective Site NER-1C, was chosen instead of the two previous prospective Sites NER-1A and NER-1B. Because we had less time available than originally called for, prospective Site NER-1C was positioned (as approved by the Pollution Prevention and Safety Panel) to achieve the scientific objectives at a single site instead of at both prospective Sites NER-1A and NER-1B. The site survey was conducted, for the first time during this leg, without the aid of GPS navigation. The seismic gear was retrieved at 1145 hr after the second pass over the site, but the beacon was not dropped so that a third pass over the site using the precision depth recorders (PDR) could be used to refine the actual drop point. A beacon was dropped at 1325 hr to officially begin Site 758.

While on site, significant currents that ran contrary to published charts developed. These currents intermittently exceeded 3 kt, prompting our deployment of the current meter. Shore-based work will be conducted to plot current directions and strength.

Site 758

Hole 758A

The ship was offset 114 m southeast of the beacon (05°23.049'N, 90°21.673'E; Fig. 3) and an APC/XCB bottom-hole assembly (BHA) including the nonmagnetic drill collar was made up. The BHA was run to the seafloor, and we successfully took a 6-m-long mud-line core to establish the working water depth at 2923.6 m. An oxidized layer in the mud-line core is identified as the actual seafloor surface material. Eleven piston cores were then taken, with total recovery exceeding 100% (Table 1). Cores 121-758A-3H through 121-758A-11H were magnetically oriented using the Eastman Whipstock Multishot camera system. Piston corer refusal was defined by 70,000-lb overpull in sticky clay-rich sediment, forcing us to change to XCB operations.

XCB coring advanced the hole from 102.4 to 421.5 mbsf. The first 220 m of this interval experienced unusually easy coring, and recovery ranged from 5.0 to 9.8 m per core. The abundance of chert and porcellanite increases below 220 mbsf, and from their first occurrence at 350 mbsf, layers of this material took their toll on both recovery and the life of the XCB cutting shoes. Diamond shoes were used for six of the next nine core runs, but coring resulted in both slow penetration and disturbed recovery. At Core 121-758A-46X the core barrel became stuck in the BHA and required continuous jarring for 30 min to dislodge. On deck, we found that the box connection of the cutting shoe adaptor sub was slightly swollen, which must have interfered with reentry of the pin end of the seal bore drill collar. The hole was then displaced with 12 ppg mud in preparation for terminating XCB coring and pulling the drill pipe from the hole.

Before we abandoned Hole 758A, a minicone was assembled and dropped to mark the hole for reentry and deepening with the RCB system. The minicone was modified with a small mud skirt to keep it from disappearing into the crater at the top of the hole, which is apparently what had happened to the cone dropped at Site 752 (see "Operations" section, "Site 752" chapter, this volume).

The pipe was pulled clear of the seafloor at 0440 hr, and *JOIDES Resolution* was offset about 26 m south in order to complete a double APC-cored sequence (Fig. 3).

Hole 758B

After determining that the PDR depth was 2 m deeper at the location for Hole 758B, a mud-line core was attempted to achieve both mud-line capture and an adequate overlap with the coring breaks of Hole 758A. The overlap and sub-bottom depth correlations are very good (see "Paleomagnetism" section, this chapter), but the mud-line core apparently missed about 0.5 m of the surface sediments. Nevertheless, 10 APC cores were taken to a depth of 96 mbsf, with a total recovery in excess of 100% (Table 1). Cores 121-758B-3H through 121-758B-10H were magnetically oriented like the cores from Hole 758A. The pipe was then pulled clear of the seafloor at 1558 hr, and the vessel was offset 10 m north (Fig. 3).

Laboratory analyses of the oriented piston cores indicated that applied pump pressure prior to firing the piston corer serves to stabilize the camera. The results obtained using this approach are more coherent than those obtained by simply lowering the Multishot. Nevertheless, paleomagnetic analyses of the cores still show a clear drift in the downhole declination data in reversed polarity zones (Fig. 4). This drift was first attributed to torque in the drill pipe resulting from pressure-up to fire the APC. Opposite trends in the declination between the two drill holes, however, do not substantiate that hypothesis. The causes of the drift in the paleomagnetic data are still open to discussion.

Hole 758C

A final mud-line APC core was attempted to capture the elusive oxidized seafloor sediments that were missed in Hole 758B and to dispel any ambiguity between the positions of the tops of the holes (Table 1). We were successful again in taking a mud-line core, and the pipe was immediately pulled to the deck to change over to the RCB system. The bit was on deck at 2350 hr, 15 June.

Hole 758A (First Reentry)

A new RBI C-4 bit was made up to a conventional RCB BHA, and the pipe was tripped once more to the seafloor. The vibration-isolation TV frame with the TV and Mesotech sonar was made up around the pipe and lowered until the seafloor came into view and the minicone and flotation balls could be seen as targets on the sonar. The ship was maneuvered over the minicone in 12 min, and the drill pipe was stabbed successfully into the cone on the first attempt. Reentry occurred at 0615 hr on June 16. The combination of a firm clay-rich mud at the seafloor and the mudskirt enhancement held the minicone so that every aspect of the cone was clearly visible on the TV image, including the bull's-eye paint job. The cone had not settled into the crater at the top of the hole nor had it been obscured by the cuttings piled around the edge, as seemed to have happened in previous deployments of the minicone. The TV image showed that two of the three flotation balls were still attached to the edge of the cone.

The TV frame was recovered, and the drill pipe was run to the bottom of the hole without encountering any fill or bridges. RCB coring commenced at 421.5 mbsf and continued to 583.2

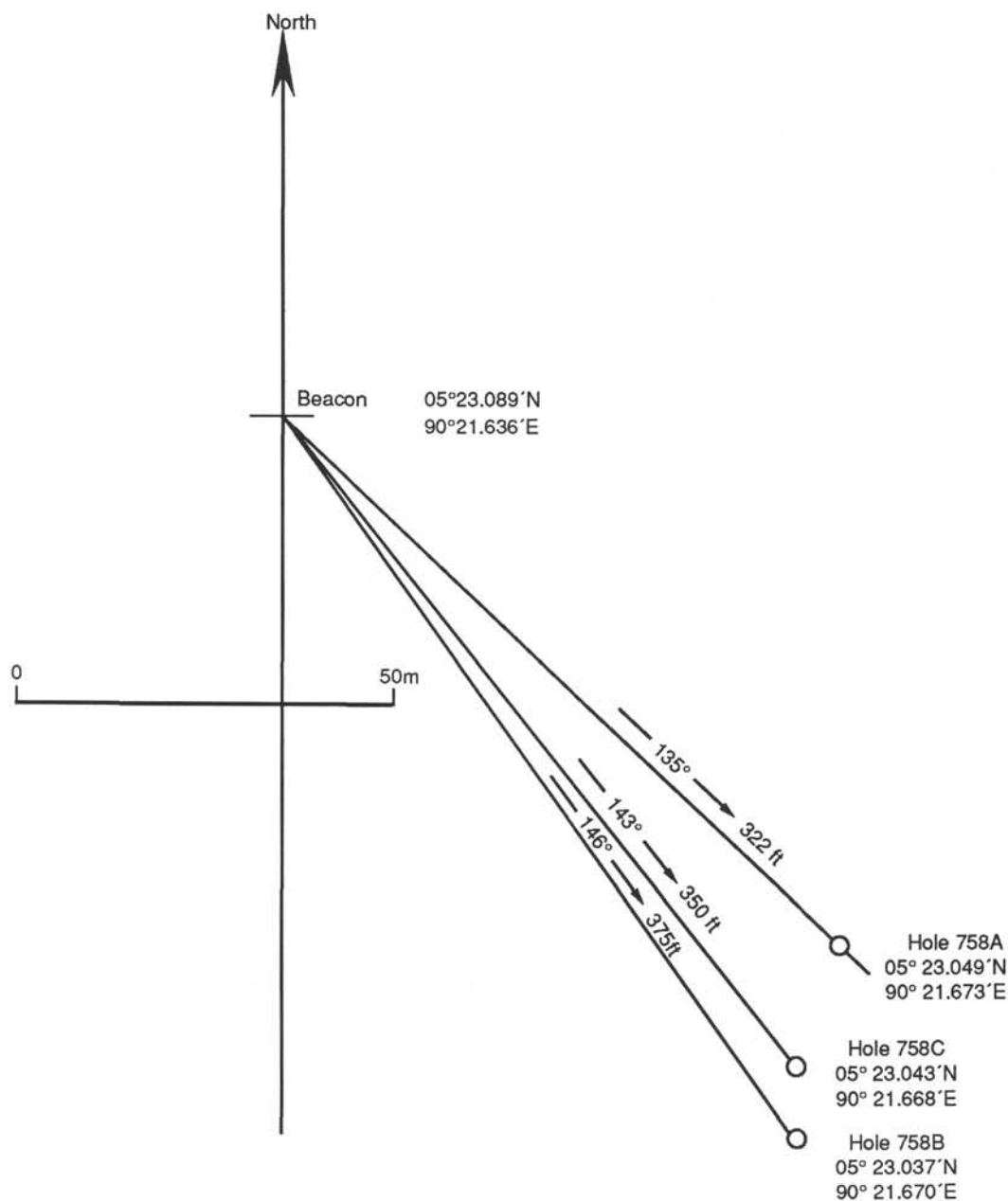


Figure 3. Offset locations of the Site 758 holes relative to the final beacon position.

mbsf (Table 1). Cores 121-758A-47R to 121-758A-53R were easily drilled in limestone, with penetration at about 30 m/hr. Basalt was first found in Core 121-758A-54R at 495 mbsf, along with interbedded sediments, although acoustic basement in the seismic records was interpreted at 650 mbsf. Below Core 121-758A-57R the formation is almost exclusively basalt, and penetration rates ranged from 2 to 4 m/hr. The rock proved extremely conducive to coring, however. Several cores achieved near full recovery and contained unbroken pieces of basalt up to 3.3 m long. After Core 121-758A-63R, the pipe was pulled to change bits. The first RCB bit had accumulated 35.2 rotating hr and was pulled to avoid cutting an undergauge hole or experiencing sudden failure, even though it had shown no overt signs of incipient failure. The hole was displaced with high viscosity mud and the pipe was pulled out of the hole. The bit reached the rig floor at 0115 hr, 19 June, and was found to be in amaz-

ingly good condition (only $1/16$ -in. undergauge)—it could have been mistaken for a bit with 30 hr or more in sediments instead of in basalt.

Hole 758A (Second Reentry)

An identical RBI C-4 RCB bit was made up to the BHA with a mechanical bit release (MBR), and the pipe was run back in to reenter the hole. After the telemetry pod, which had developed an internal power supply problem, was replaced, the TV-sonar system was deployed and run to the bottom of the pipe with minimal difficulties despite a strong surface current (up to 3 kt) that developed while the ship was on site. The minicone was spotted immediately, and maneuvering and stabbing took only 3 min. The cone was still highly visible a little above the seafloor, and the missing flotation ball had mysteriously reappeared. Reentry occurred at 0913 hr on 19 June.

Table 1. Coring summary, Site 758.

Core no.	Date (June 1988)	Time (local)	Depth		Length		Recovery (%)
			top (mbsf)	bottom (mbsf)	cored (m)	recovered (m)	
121-758A-							
1H	12	2225	0.0	6.0	6.0	6.11	102.0
2H	13	0005	6.0	15.6	9.6	10.02	104.4
3H	13	0110	15.6	25.2	9.6	10.00	104.1
4H	13	0205	25.2	34.8	9.6	10.05	104.7
5H	13	0255	34.8	44.4	9.6	9.98	104.0
6H	13	0350	44.4	54.0	9.6	9.97	104.0
7H	13	0440	54.0	63.7	9.7	10.02	103.3
8H	13	0530	63.7	73.4	9.7	9.94	102.0
9H	13	0655	73.4	83.1	9.7	9.95	102.0
10H	13	0745	83.1	92.8	9.7	9.97	103.0
11H	13	0910	92.8	102.4	9.6	9.99	104.0
12X	13	1015	102.4	112.1	9.7	9.55	98.4
13X	13	1105	112.1	121.7	9.6	9.63	100.0
14X	13	1155	121.7	131.4	9.7	6.63	68.3
15X	13	1240	131.4	141.0	9.6	5.46	56.9
16X	13	1320	141.0	150.7	9.7	5.99	61.7
17X	13	1400	150.7	160.4	9.7	5.65	58.2
18X	13	1435	160.4	170.0	9.6	6.17	64.3
19X	13	1510	170.0	179.7	9.7	6.83	70.4
20X	13	1550	179.7	189.3	9.6	4.66	48.5
21X	13	1625	189.3	199.0	9.7	7.76	80.0
22X	13	1715	199.0	208.7	9.7	5.13	52.9
23X	13	1800	208.7	218.3	9.6	8.49	88.4
24X	13	1840	218.3	228.0	9.7	6.22	64.1
25X	13	1930	228.0	237.7	9.7	8.13	83.8
26X	13	2005	237.7	247.3	9.6	7.44	77.5
27X	13	2100	247.3	256.9	9.6	1.70	17.7
28X	13	2150	256.9	266.6	9.7	9.58	98.7
29X	13	2235	266.6	276.3	9.7	5.87	60.5
30X	13	2315	276.3	285.9	9.6	6.16	64.1
31X	14	0000	285.9	295.6	9.7	9.75	100.0
32X	14	0050	295.6	305.3	9.7	9.42	97.1
33X	14	0145	305.3	314.9	9.6	9.63	100.0
34X	14	0235	314.9	324.6	9.7	9.81	101.0
35X	14	0335	324.6	334.3	9.7	3.27	33.7
36X	14	0435	334.3	343.9	9.6	4.05	42.2
37X	14	0550	343.9	352.6	8.7	0.72	8.3
38X	14	0755	352.6	357.6	5.0	3.20	64.0
39X	14	0940	357.6	367.3	9.7	2.13	21.9
40X	14	1115	367.3	377.0	9.7	2.80	28.8
41X	14	1225	377.0	386.6	9.6	7.39	77.0
42X	14	1355	386.6	396.3	9.7	5.33	54.9
43X	14	1530	396.3	399.6	3.3	0.70	21.2
44X	14	1725	399.6	405.6	6.0	0.60	10.0
45X	14	2005	405.6	415.2	9.6	0.30	3.1
46X	15	0000	415.2	421.5	6.3	0.40	6.4
47R	16	1200	421.5	431.2	9.7	3.45	35.5
48R	16	1335	431.2	440.9	9.7	6.04	62.2
49R	16	1450	440.9	450.6	9.7	0.75	7.7
50R	16	1610	450.6	460.2	9.6	4.35	45.3
51R	16	1735	460.2	469.9	9.7	5.90	60.8
52R	16	1855	469.9	479.6	9.7	3.52	36.3
53R	16	2010	479.6	489.2	9.6	0.93	9.7
54R	16	2330	489.2	498.9	9.7	2.50	25.8
55R	17	0310	498.9	508.4	9.5	7.04	74.1
56R	17	0445	508.4	517.9	9.5	4.02	42.3
57R	17	0905	517.9	527.1	9.2	3.23	35.1
58R	17	1410	527.1	536.5	9.4	9.42	100.0
59R	17	1830	536.5	545.9	9.4	8.87	94.3
60R	18	0005	545.9	555.1	9.2	8.03	87.3
61R	18	0430	555.1	564.3	9.2	8.17	88.8
62R	18	1200	564.3	573.8	9.5	4.30	45.2
63R	18	1805	573.8	583.2	9.4	9.91	105.0
64R	19	2055	583.2	592.7	9.5	4.37	46.0
65R	20	0310	592.7	602.1	9.4	7.26	77.2
66R	20	0825	602.1	611.5	9.4	8.05	85.6
67R	20	1600	611.5	620.8	9.3	8.36	89.9
68R	20	2235	620.8	630.2	9.4	5.63	59.9
69R	21	0300	630.2	639.4	9.2	6.86	74.5
70R	21	0700	639.4	648.6	9.2	2.95	32.0
71R	21	1325	648.6	658.0	9.4	4.90	52.1
72R	21	2215	658.0	667.6	9.6	7.47	77.8
73R	22	0300	667.6	676.8	9.2	5.00	54.3
					676.8	453.83	67.1

The pipe was run to total depth at 583.2 mbsf, and only 10 m of easily washable fill was encountered en route. RCB coring resumed in solid basalt, with penetration rates as slow as 1.6 m/hr. Two more days of uninterrupted basalt coring ended at 676.8 mbsf in order to allow sufficient time to log the hole before departure for Singapore. No lithologic boundary that could ex-

Table 1 (continued).

Core no.	Date (June 1988)	Time (local)	Depth		Length		Recovery (%)
			top (mbsf)	bottom (mbsf)	cored (m)	recovered (m)	
121-758B-							
1H	15	0700	0.0	9.5	9.5	9.88	104.0
2H	15	0800	9.5	18.9	9.4	9.59	102.0
3H	15	0900	18.9	28.4	9.5	9.95	105.0
4H	15	0950	28.4	38.0	9.6	9.71	101.0
5H	15	1045	38.0	47.7	9.7	9.94	102.0
6H	15	1140	47.7	57.3	9.6	9.83	102.0
7H	15	1230	57.3	67.0	9.7	9.99	103.0
8H	15	1320	67.0	76.7	9.7	10.04	103.5
9H	15	1410	76.7	86.3	9.6	9.91	103.0
10H	15	1505	86.3	96.0	9.7	9.84	101.0
					96.0	98.68	102.8
121-758C-							
1H	15	1645	0.0	9.4	9.4	9.40	100.0
					9.4	9.40	100.0

plain the seismic basement reflector was reached. Total basalt penetration after first contact was 178 m, with an admirable recovery rate of over 69%. Because of the slow penetration rates, heavy-wall drilling joints were used at the top of the string for Cores 121-758A-55R through 121-758A-73R. A multistation drift survey covering the entire hole was conducted with the Multishot while recovering Core 121-758A-67R. The four measurements, from 3555, 3512, 3458, and 3385 m below rig floor (mbrf), were found to be 1° to 1.5° from vertical.

The hole was conditioned for logging by sweeping with 40 bbl of polymer mud and then running the bit up to 100 mbsf and back to bottom. The wiper trip encountered no bridges, but 23 m of accumulated fill was readily pumped away. Seven hole volumes of seawater were flushed at a high pump rate. The rotary shifting tool was run, and the MBR was actuated to release the bit with no problems. The aft sand line was corrosion treated while the shifting tool was recovered. The hole was then treated with KCl-added gel mud and appeared to be in fine condition for the extensive logging program planned.

The end of the pipe was positioned at 2977.2 mbrf (42.7 mbsf) for the first logging attempt. The seismic stratigraphic string (DIL-BHC-GR) was run but could not be calibrated. After some investigation the problem was determined to be an unexpectedly deep air/water interface, and calibration had been first attempted in air. The tools were finally run into the pipe and stopped on an obstruction in the pipe at 2531 mbrf, more than 400 m above the end of the pipe. Circulation at 300–500 psi was enough to get the logging tools past the unknown obstruction and into the open hole, only to have the tools stopped again by a firm bridge at 3340 mbrf (405 mbsf) in the hole. The available sediment interval was logged, and the seismic stratigraphic string was recovered.

The geochemical suite (GST-ACT-NGT-CNL) was made up and run to log the same sediment interval before we made another wiper trip to open more of the hole. This tool string also encountered the pipe obstruction, which apparently was caused by bent drill pipe, at 2531 mbrf, but we were able to force it through with 250 gal/min circulation. The other bridge at 3340 mbrf also stopped this tool, and the open-hole interval up to the end of the pipe was logged. The second suite of logging tools was back on deck at 0520 hr on 23 June.

A second wiper trip was made, without a bit this time, to ensure no obstacles in running the logs. No bridges were felt, although there seemed to be some drag in the 70-m zone immediately over basement. In retrospect, this would have been the

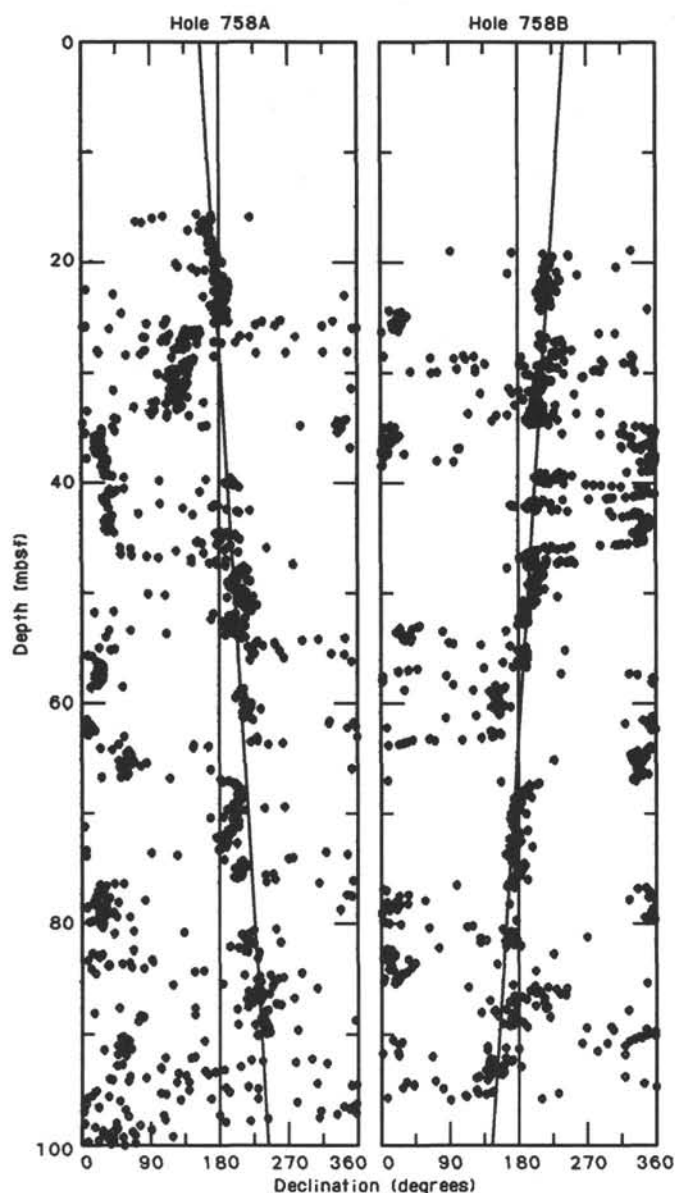


Figure 4. Oriented paleomagnetic declination records after alternating field demagnetization at 9 mT show opposing directions of downhole drift in Holes 758A and 758B.

point where the bent pipe joints (which were later confirmed) entered the top of the hole. It is not clear, however, why the bent pipe did not present noticeable drag lower in the hole. Basement appeared to be wide open and no fill was encountered as the MBR top connecting sub easily reached total depth. KCl-added mud was again pumped to replace the volume lost during the wiper trip.

The end of the pipe was set at 525 mbsf, about 30 m lower than the first basalt contact, for the next set of logging runs. The seismic stratigraphic logging suite (DIL-BHC-GR) was run in and again encountered the bent pipe restriction before being lowered into open hole. One bridge or ledge was worked past just beyond the end of the pipe, but another firm bridge at 545.4 mbsf stopped the tool. The open interval of basement to the end of the pipe was logged, and the tools were retrieved.

With about 12 hr left before we needed to trip the drill pipe and depart the site, we made our final attempt to log basement with the BHTV. A third short wiper trip to bottom that suc-

ceeded in knocking out bridges required 30,000–40,000 lb at three locations in the basement section of the hole. The hole was displaced with KCl-added mud across the sediment section and 10.3 ppg weighted mud in basement. The end of the pipe was set at 553.5 mbsf, thereby theoretically exposing 123 m of “ideal” basement. The BHTV was made up and run, but was quickly back on deck with a flooded cablehead. A new pigtail was installed, and the tool was again lowered and worked to the bottom of the pipe. The tool hung up momentarily at the end of the MBR, but successfully entered into open hole, only to be stopped at 610 mbsf. The hole was logged up from 610 mbsf to the pipe-up position at 553.5 mbsf. The pipe was picked up, exposing another 30 m of basalt that was also logged. A second run was made from 555.5 up to 525.5 mbsf. The BHTV appeared to be operating at less than optimum performance during the entire exercise. No breakouts in the rock were immediately recognized. Total operating time had expired, and BHTV deployment was ended and the tool was returned to the rig floor.

The drill pipe was pulled for the final time on Leg 121 and coated with Coat-415 internal corrosion inhibitor while tripping out. Three obviously bent joints of 5-in. drill pipe were found at the expected location in the drill string, accounting for the recurring obstruction detected on each logging run. The BHA was broken down piece by piece for storage in the main deck racks, and the MBR top connector was on deck at 1330 hr on 24 June, ending Leg 121 operations after a total of 12 days on site.

Depth and magnetometer surveys were conducted on the transit from Site 758 to Singapore port call. Arrival in Singapore, and the end of Leg 121, was at 0830 (local time), 28 June 1988.

LITHOSTRATIGRAPHY AND SEDIMENTOLOGY

Sediments of Holocene to early Campanian age were recovered from three continuously cored holes at Site 758 before drilling was terminated at 677 mbsf in basalt in Hole 758A. Five lithologic units are identified: Unit I, 121.7 m of middle Miocene to Holocene nannofossil ooze; Unit II, 245.6 m of upper Campanian to middle Miocene chalk; Unit III, 63.9 m of Campanian volcanic clay; Unit IV, 67.4 m of Campanian tuff; and Unit V, 178.2 m of basalt (Table 2 and Fig. 5).

Lithologic Unit I

Subunit IA

The nannofossil ooze of Unit I is divided into two subunits based on terrigenous clay content. Subunit IA includes the intervals from Cores 121-758A-1H through 121-758A-4H (0.0–25.2 mbsf), Cores 121-758B-1H through 121-758B-3H-4 (0.0–22.4 mbsf), and Core 121-758C-1H (0.0–9.4 mbsf) (Table 2). At the top of the subunit is a 46-cm-thick layer of brown (10YR 5/3) clayey nannofossil ooze of Holocene age, based on the presence of *Emiliana huxleyi* (see “Biostratigraphy” section, this chapter). This brown layer represents the oxidized interval at the top of the sedimentary section. The dominant lithology of Subunit IA consists of alternating layers of light nannofossil ooze with clay and foraminifers and layers of dark clayey nannofossil ooze with foraminifers. Differentiation between the two oozes is based on color and terrigenous clay content. Subunit IA also contains several thick volcanic ash layers, numerous thin ashes, pumice blebs, and one large pumice fragment.

The alternating light and dark ooze layers, 10 to 110 cm thick, are sparsely to moderately mottled and bioturbated. The bedding contacts between the light and dark beds generally are gradual, over a 5- to 15-cm interval. The contacts between dark and underlying light beds appear more mottled and diffuse in comparison with the more abrupt contacts between the light

Table 2. Lithologic units at Site 758.

Unit	Core interval	Depth (mbsf)	Lithology	Age
IA	758A-1H to -4H	0.0–25.2	Nannofossil ooze with foraminifers and clay and clayey nannofossil ooze with foraminifers	Holocene to early Pleistocene
	758B-1H to -3H-4	0.0–22.4		
	758C-1H	0.0–9.4		
IB	758A-4H to -14X	25.2–121.7	Nannofossil ooze with clay, foraminifers, and micrite	early Pleistocene middle Miocene
	758B-3H-4 to -10H	22.4–96.0		
IIA	758A-14X to -32X	121.7–295.6	Nannofossil chalk and calcareous nannofossil chalk	middle Miocene to early Paleocene
IIB	758A-32X to -40X	295.6–367.3	Calcareous chalk with nannofossils, foraminifers, and clay	late Maestrichtian to Campanian
III	758A-40X to -48R	367.3–431.2	Volcanic clay with foraminifers	Campanian
IV	758A-49R to -54R-CC	431.2–498.6	Tuff with basalt pebbles, shells, and ashy calcareous chalk interbeds	Campanian
V	758A-54R-CC to -73R	498.6–676.8	Basalt with minor tuff interbeds	Campanian or older(?)

layers overlying the dark beds. The light intervals are gray (5Y 6/1) to light gray (5Y 7/1), and the darker intervals are gray (5Y 5/1), dark gray (5Y 4/1), and olive gray (5Y 5/2). The dark beds contain 10% to 20% more clay and, correspondingly, less calcium carbonate than the light beds (see Table 16 in the “Organic Chemistry” section, this chapter, and Fig. 6A).

Subunit IA contains several major ash beds and numerous thin ash layers. The colors of the massive ash beds vary among olive gray (5Y 4/2), light gray (10YR 7/1), dark gray (5Y 4/1), and black (N2/). Thickness ranges from 5 to 34 cm, and these beds exhibit sharp basal contacts. Several of the ash beds are clearly graded, fining upward. The uppermost massive ash, in Section 121-758A-1H-2, 0–34 cm (1.50–1.84 mbsf), is probably the Toba ash (Fig. 7), which was deposited approximately 75,000 yr BP (Ninkovitch, 1978). The thin, distinct ash layers are 1–2 cm thick and vary in color from green (10YR 6/3) to dark gray (5Y 4/1). Commonly, two to four discrete layers occur in close proximity, within a 5–10-cm sedimentary section. Black (10YR 2/1) pumice blebs are scattered throughout Subunit IA, and a pumice fragment, 1 cm long, was found at 86–87 cm in Section 121-758B-1H-3. A peculiar rock, 2 cm long, with a spindle, oblong shape and consisting of pyrite and clear glassy crystals was found at 117–119 cm in Section 121-758B-1H-5, within a massive ash layer.

Grain-size analyses of the bulk unconsolidated sediments of Unit I were conducted on three samples from every core, which is a low sampling density relative to the observed lithologic variations. Subunit IA has a fairly constant grain size between 6.44 and 5.55 ϕ (11.5 to 21.3 μm) (Table 3 and Fig. 8).

Smear slide analyses indicate that nannofossils are the dominant sediment component throughout Subunit IA. Foraminiferal content ranges from 5% to 25%, while diatoms and radiolarians compose 5% or less of this subunit.

Subunit IB

Subunit IB includes Cores 121-758A-4H to 121-758A-14X (25.2–121.7 mbsf) and 121-758B-3H-4 to 121-758B-10H (22.4–96.0 mbsf) (Table 2) and consists of nannofossil ooze with clay, foraminifers, and micrite. The major differences between Sub-

units IA and IB are increases in both calcium carbonate content (Table 16 and Fig. 6) and the amount of micrite. The ooze is mottled and bioturbated, and the color grades downsection from gray (5Y 6/1) and light gray (5Y 7/1) to white (10YR 8/1). Variations in sediment color become less discernible downsection as the relatively clay-rich darker colored beds become less distinct. The upper half of the subunit contains a few massive, dark gray (5Y 5/1) to dark grayish brown (2.5YR 3/2) 2–15-cm-thick ash beds and numerous, thin green (10YR 6/3) and dark gray (5Y 4/1) ash layers. The ash beds are usually characterized by sharp basal contacts and, in places, exhibit graded bedding, fining upward. Black (10YR 2/1) pumice blebs occur sporadically throughout Subunit IB.

Nannofossils are the dominant sediment component in Subunit IB, forming 60% to 72% of the sediment. Foraminiferal content ranges from 1% to 10%, generally decreasing downsection. Diatoms and radiolarians comprise up to 2% of the upper half of this subunit, but are essentially absent from the lower half. Clay concentration decreases from 20% at the top to only a trace amount at the bottom of the subunit.

At the transition from Subunit IA to Subunit IB, the grain size increases abruptly and then decreases, perhaps in relation to the decreasing concentration of foraminifers. The rather spiky appearance of the grain-size data below 60 mbsf (Fig. 8) is considered suspect, because in some cases the sediment could not be fully disaggregated prior to analysis.

Lithologic Unit II

Subunit IIA

The chalk of Unit II is divided into two subunits on the basis of several lesser lithologic variations. Subunit IIA, in Cores 121-758A-14X to 121-758A-32X (121.7–295.6 mbsf) (Table 2), consists of nannofossil, calcareous, and, in places, foraminiferal chinks with a mean calcium carbonate content of 88% (Table 16 and Fig. 6B). The chalk occurs as 2–12-cm long drilling biscuits that are separated by up to 10 cm of drilling slurry. Mottling varies from moderate to extremely faint, and bioturbation is moderate to strong. The chinks are very pale brown (10YR 7/3) in Cores 121-758A-14X to 121-758A-17X, white (10YR 8/2) from Cores 121-758A-17X to 121-758A-27X, and a mixture of these two colors in Cores 121-758A-27X to 121-758A-32X. Several intervals of faint laminae bedding occur in Cores 121-758A-27X to 121-758A-31X.

The degree of lithification appears to decrease abruptly between Cores 121-758A-27X and 121-758A-28X, where the sediment changes from pure chalk to a mixed lithology of chalk and ooze. This mixture reverts back to 100% chalk at the base of Core 121-758A-29X. The mean calcium carbonate content increases from 86% in the chinks prior to the lithology change to 95% in the partly ooze cores (Table 16 and Fig. 6B). This transition occurs across the unconformity that spans nearly the entire Eocene, 37 to 58 Ma.

Light gray (10YR 6/1) to pale brown (10YR 6/3) isolated chert pebbles on a millimeter scale occur within Cores 121-758A-19X to 121-758A-22X and 121-758A-27X. Chert nodules, approximately 5 cm in diameter, were found in Cores 121-758A-29X to 121-758A-31X. An isolated pyrite clast, 0.5 \times 2.3 cm, was found at 38–39 cm in Section 121-758A-14X-1. Faint black ash blebs are sporadically distributed through Cores 121-758A-21X to 121-758A-32X.

Nannofossils are the dominant component of Subunit IIA, making up 40% to 70% of the sediment. Foraminiferal content ranges from 5% to 30% in Cores 121-758A-14X to 121-758A-22X, but decreases to generally less than 5% in the lower cores of this subunit. Radiolarians compose up to 5% of this subunit whereas diatoms occur in only trace amounts.

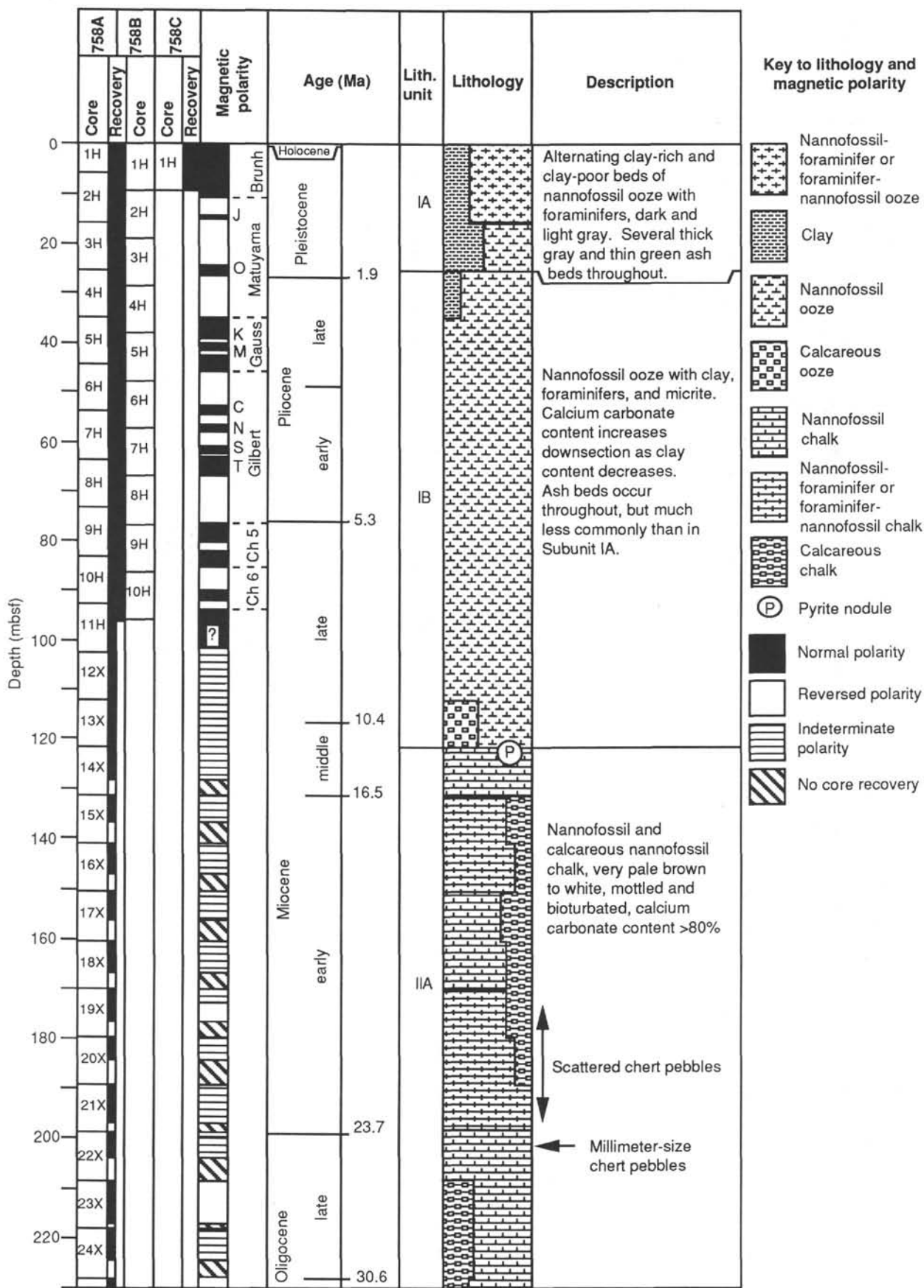


Figure 5. Site 758 summary diagram.

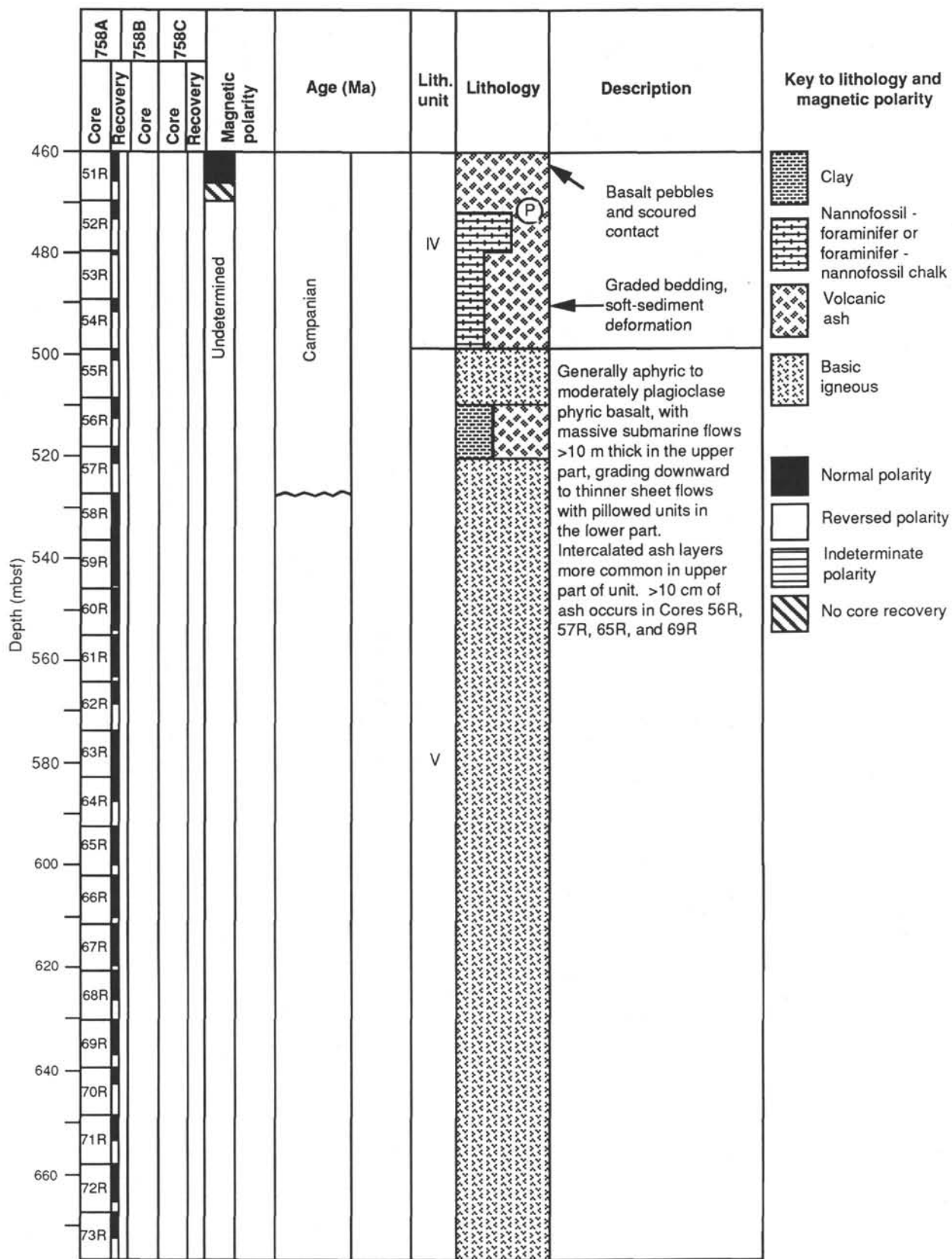


Figure 5 (continued).

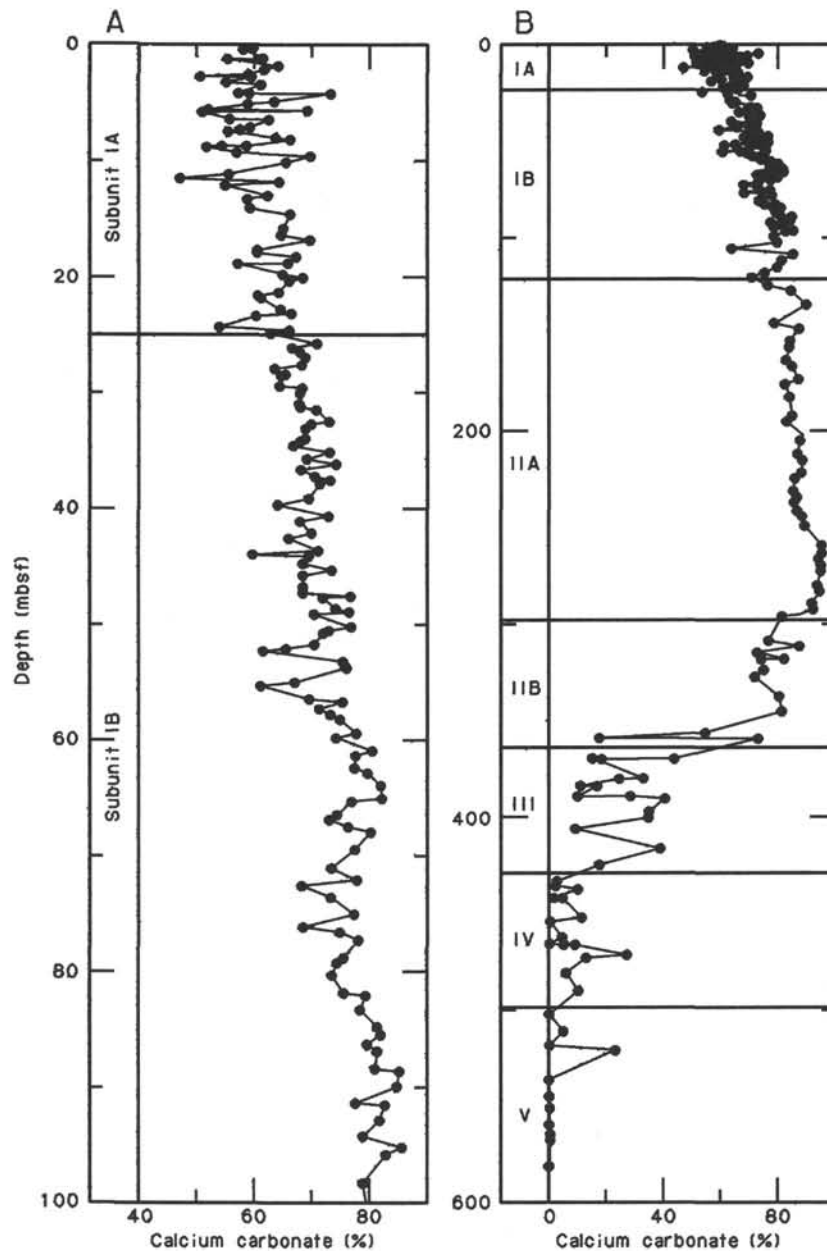


Figure 6. Calcium carbonate content profiles for Site 758. **A.** Samples from 0 to 100 mbsf in Hole 758A, 1 to 96 mbsf in Hole 758B, and 0 to 9 mbsf in Hole 758C. Although the absolute sub-bottom depths are not identical in all three holes, analysis of the volume magnetic susceptibility stratigraphies (see "Paleomagnetism" section) suggests that the holes are offset by no more than 2 to 3 m. Therefore, moderate resolution comparison of the combined calcium carbonate profiles is acceptable. **B.** All samples from Holes 758A, 758B, and 758C.

The Cretaceous/Tertiary boundary sequence occurs between Cores 121-758A-31X and 121-758A-32X, the same interval that, coincidentally, separates Subunits IIA and IIB. The sedimentary sequence at the boundary is not well defined in the recovered cores because the lowermost Paleocene and uppermost Maestrichtian are absent (see "Biostratigraphy" section). Core 121-758A-31X, which appears similar to overlying chalks, is a white (10YR 8/2) to very pale brown (10YR 7/2) chalk with white mottles exhibiting gray halos and a chert pebble, 6 × 3 cm, in the interval from 7.5 to 11.5 cm in Section 1. Section 7 and the core catcher of Core 121-758A-31X appear more indurated than the overlying sections.

Subunit IIB

Subunit IIB, in Cores 121-758A-32X to 121-758A-40X (295.6–367.3 mbsf) (Table 2), consists of calcareous, nannofossil, and foraminiferal chalks, commonly in the form of drilling biscuits, which are mottled and bioturbated. These chalks are fundamentally different from the overlying chalks. First, calcium carbonate content decreases from 90% in Subunit IIA to less than 60% downsection (Table 16 and Fig. 6B). Second, in conjunction with the decrease in calcium carbonate content, the chalks grade in color from white (10YR 8/2) and very pale brown (10YR 8/3) to light and dark greenish gray (5GY 5/1 and 5G 4/1). Subunit

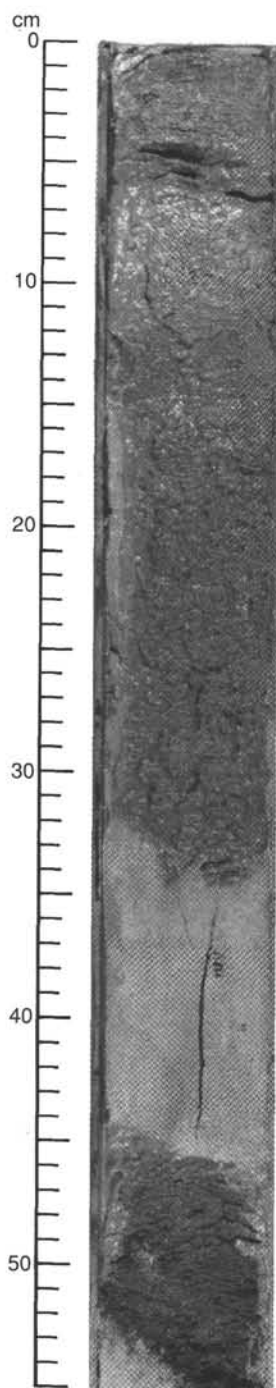


Figure 7. The uppermost massive, gray ash (Toba ash) in lithologic Unit I (0–34 cm) overlying a black ash from 45–55 cm in Section 121-758A-1H-2.

IIB contains thick *Inoceramus* fragments and thin-shelled molluscan fragments. These shell fragments are locally abundant, and the individual valves are up to 2.5 cm long. The diffuse ash layers and ash blebs that occur throughout this subunit highlight the mottles and burrow structures. Subunit IIB also has scattered stringers, up to 11 cm thick, of chert and porcellanite; pyrite at 84 cm in Section 121-758A-34X-3; and horizontal green laminae in bundles 1–2-cm thick common in Cores 121-758A-36X and 121-758A-38X.

Table 3. Grain-size analyses of the bulk sediment from Unit I, Hole 758A.

Core, section, interval (cm)	Depth (mbsf)	Mean diameter	
		(μm)	(ϕ)
1H-2, 65	2.15	21.30	5.55
1H-4, 65	5.15	19.90	5.65
1H-CC, 5	5.80	11.50	6.44
2H-2, 65	8.15	16.40	5.93
2H-4, 65	11.15	17.80	5.81
2H-CC, 5	15.82	14.50	6.11
3H-2, 66	17.76	20.20	5.63
3H-4, 136	21.46	19.10	5.71
3H-CC, 5	25.35	16.30	5.94
4H-2, 125	27.95	29.00	5.11
4H-4, 125	30.95	33.10	4.92
4H-CC, 5	35.01	19.20	5.70
5H-2, 125	37.55	25.80	5.28
5H-4, 125	40.55	18.30	5.77
5H-CC, 5	44.55	22.80	5.45
6H-2, 125	47.15	19.10	5.71
6H-4, 125	50.15	13.40	6.22
6H-6, 125	53.15	17.50	5.84
7H-2, 125	56.75	15.90	5.97
7H-4, 125	59.75	15.00	6.06
7H-6, 125	62.75	9.50	6.72
8H-2, 125	66.45	31.20	5.00
8H-4, 125	69.45	14.00	6.16
8H-6, 125	72.45	11.60	6.43
9H-2, 125	76.15	27.50	5.18
9H-4, 125	79.15	15.60	6.00
9H-6, 125	82.15	28.20	5.15
10H-2, 90	85.50	19.70	5.67
10H-4, 95	88.55	8.90	6.81
10H-6, 95	91.55	18.30	5.77
11H-2, 95	95.25	10.90	6.52
11H-4, 95	98.25	23.70	5.40
11H-6, 95	101.25	14.00	6.16
12X-2, 95	104.85	15.70	5.99
12X-4, 95	107.85	16.20	5.95
12X-6, 95	110.85	13.30	6.23
13X-2, 95	114.55	29.40	5.09
13X-4, 95	117.55	12.80	6.29
13X-6, 95	120.55	18.90	5.73

Nannofossils, foraminifers, and micrite are the dominant sedimentary components throughout Subunit IIB. Nannofossils decrease in abundance from 65% to 10% downsection, whereas foraminiferal content increases downsection from near 0% to as much as 40%. The abundance of clay may also increase downsection. Siliceous microfossils occur mostly in trace amounts and rarely up to 2%.

Core 121-758A-32X, which contains the youngest Cretaceous sediments recovered at this site, is composed of mottled, very pale brown (10YR 8/3) calcareous nannofossil chalk. The core contains diffuse ash in Sections 1 through 4, a few shell fragments, and a microfault, with a 45° dip, at 70–75 cm in Section 1. The 2-cm displacement of a distinct burrow suggests that the fault is a reverse fault.

Lithologic Unit III

Unit III, which extends from 367.3 to 431.2 mbsf in Cores 121-758A-40X to 121-758A-48R (Table 2 and Fig. 5), consists of drilling biscuits and breccia of volcanic clay with foraminifers and nannofossils. The clay has camouflage-like varicolored, mottled greenish gray patches that range from light greenish gray (5G 7/1) to greenish gray (5G 5/1 and 5GY 5/1) to dark greenish gray (5G 4/1 and 5GY 4/1). Unlike the terrigenous clays encountered in Unit I, this clay is probably the degradation product of volcanic ash, encountered as tuff in the underlying unit below (see “Tephra” section, “Ninetyeast Ridge Sum-

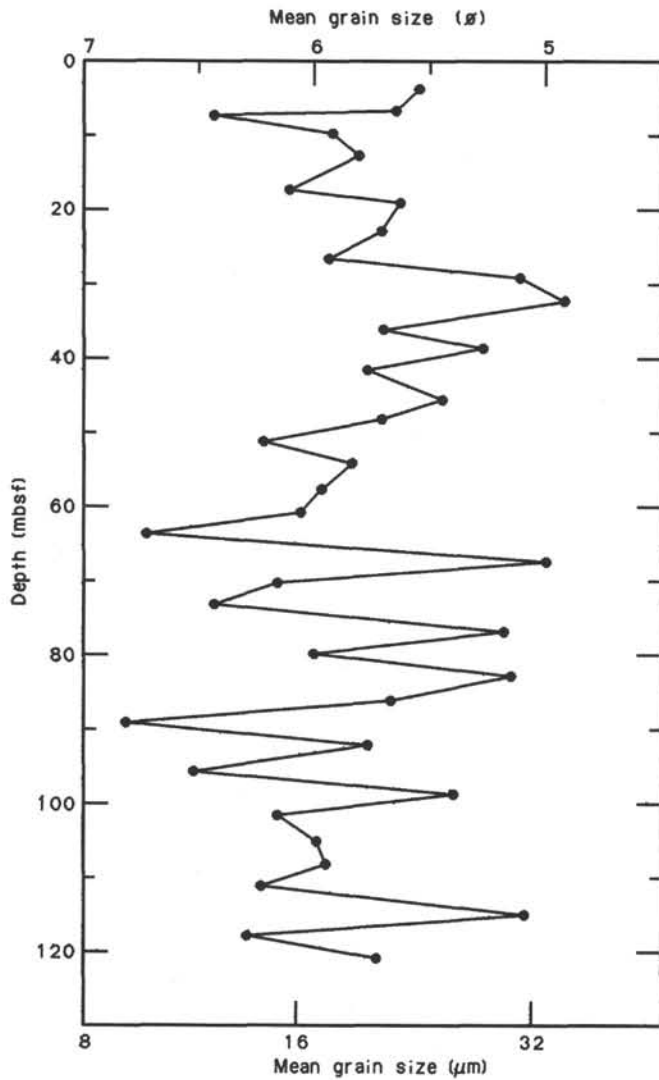


Figure 8. Mean grain size of the bulk sediment of lithologic Unit I, Hole 758A.

mary” chapter, this volume). Unit III has a mean calcium carbonate content of 31% (Table 16 and Fig. 6B) and contains several greenish gray (5GY 5/1) chert pebbles, dark ash layers, and porcellanite intervals up to 11 cm long. *Inoceramus* and other shell fragments are common throughout the unit.

Clay is the dominant component, making up 40% to 74% of the sediment. The nannofossil content is low, ranging between 10% to 20%. Foraminiferal concentrations decrease from 30% at the top of the unit to 3% at the bottom. Radiolarians average 6% in Cores 121-758A-40X and 121-758A-41X, but are essentially absent in the underlying cores.

Lithologic Unit IV

Unit IV, in the interval from Core 121-758A-49R to Section 121-758A-54R-CC (431.2–498.6 mbsf) (Table 2), consists of greenish gray (5G 5/1) tuff, with minor interbeds of ashy calcareous chalk, and partially indurated ash beds. The mottled and bioturbated tuff is in the form of drilling biscuits. It contains some pyrite in burrows, rounded basalt pebbles less than 1 cm in diameter, and shell fragments. Sedimentary structures include some sharp, scoured contacts, microfractures, and soft-sediment deformation. Six layers of sand- to lapilli-size lithic and

pumice fragments, which display graded bedding, are at 84–95 cm in Section 121-758A-54R-1 (Fig. 9).

Ash makes up more than 90% of the sediment in Cores 121-758A-48R to 121-758A-51R. In the calcareous sections within the tuff in Cores 121-758A-52R to 121-758A-54R, the micrite concentrations range from 25% to 57%. All microfossils occur in concentrations of 8% or less.

Lithologic Unit V

Unit V, in Section 121-758A-54R-CC to Core 121-758A-73R (498.6–676.8 mbsf) (Table 2), consists of basalt with minor interbeds of tuff and ash. The volcanic sediments, predominantly basaltic ashes, occur as thin, mostly fine-grained deposits between lava flows in Cores 121-758A-56R, 121-758A-57R, 121-758A-60R, 121-758A-65R, 121-758A-66R, and 121-758A-69R. The ashes in Cores 121-758A-56R and 121-758A-57R are bioturbated clayey tuffs and black (10GY 2.5/) to very dark greenish gray (10GY 3/1) volcanic sandstones. Glauconite grains were found in burrows less than 1 cm in diameter. The sedimentary structures observed in the sandstones include graded bedding and scoured contacts. The sandstones include small basalt pebbles and pumice fragments less than 0.5 cm in diameter. Most of the lithologic contacts between the basalt and the sediment, which is clearly water lain, are poorly preserved. Ankerite, identified by X-ray diffraction (XRD), occurs commonly in fractures near the contacts. A dark greenish gray (5G 4/1) ash bed, 10 cm thick, with white (10YR 8/1) calcareous (ankerite) infilling between small rounded basalt pebbles occurs in Section 121-758A-60R-1. The contacts with the basalt are well preserved, and the crevices in the basalt are filled with ash. The degree of alteration of the ash to clay increases toward contacts. Section 121-758A-65R-1 contains drilling biscuits of tuff that are very fine-grained and nearly devoid of carbonate material. The glass has been mostly altered to clay. The contact with the basalt is

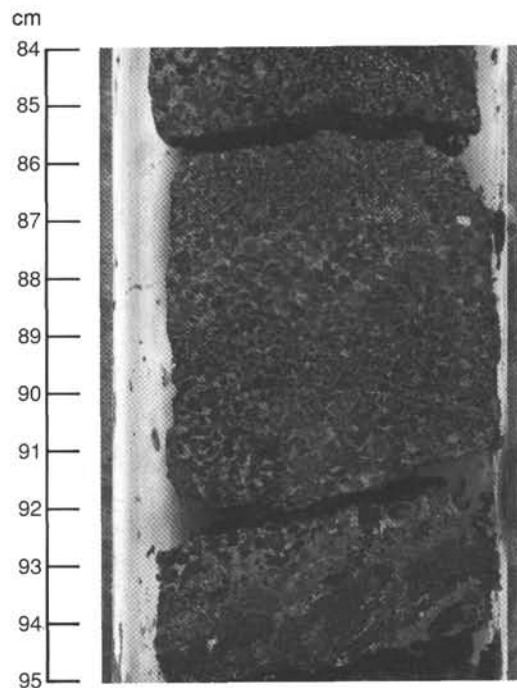


Figure 9. Beds of sand- to lapilli-size lithic and pumice fragments that display fining-upward graded bedding in lithologic Unit IV (Section 121-758A-54R-1, 84–95 cm).

well preserved, with ash filling the irregular convoluted surface of the basalt. Nannofossils were found in the ashes in Sections 121-758A-66R-1 and 121-758A-69R-1.

Correlation Among the Holes Drilled at Site 758

The three holes of Site 758 are on the southeastern edge of a high block on Ninetyeast Ridge. Hole 758A is 16 m north of Hole 758C, which, in turn, is 9.5 m north of Hole 758B. The top cores of Holes 758A and 758C obtained the mud line, which was not recognized in Core 121-758B-1H. The oozes of Unit I, which range in age from Holocene to middle Miocene, are characterized by long- and short-term changes identified by color variations, distinct tephra layers, calcium carbonate content, paleomagnetic stratigraphy, and volume magnetic susceptibility records. Stratigraphic correlation of these holes provides valuable information concerning missing sediment intervals within each hole. This information is crucial in investigating the paleomagnetic reversal history, tephrochronology, biostratigraphy, sediment-accumulation rates, or any other detailed or high-resolution study. Detailed correlations within lithologic Unit I at Site 758 are addressed in the "Paleomagnetism" section of this chapter.

Preliminary stratigraphic analysis suggests that 100% or more core recovery was achieved in all APC cores, with an average of 1 m of sediment missing between sequential full APC cores. Thus, adjacent APC holes are required to insure complete recovery of any sedimentary section.

Discussion

Sediments recovered at Site 758 reflect (1) the gradual tectonic subsidence of Ninetyeast Ridge, (2) the uplift and denudation of the Himalayas and the Tibetan Plateau, (3) changes in marine planktonic productivity and preservation, (4) the history of Indonesian Arc volcanic activity, and (5) migration of the drill site closer to Asia.

Unlike the subaerial basalt flows of Sites 757 and 756, those of the basal Unit V at Site 758 occurred in deep water (see "Igneous Petrology" section, this chapter). The oldest sedimentary unit, immediately overlying the basalt, consists of Campanian to Santonian(?) tuff with minor interbeds of ashy calcareous chalk. As the water deepened, the calcium carbonate content increased, and the ratio of molluscan macrofauna to pelagic microfauna decreased in the greenish gray chalks of Subunit IIB. The mollusks disappeared completely by the early Paleocene, in the pale white chalks of Subunit IIA. Deeper water pelagic sedimentation, interrupted by a 20-m.y. hiatus that spanned nearly the entire Eocene, continued through the Paleogene at a slow pace, which is typical for much of the eastern Indian Ocean. Minor amounts of Indonesian Arc volcanic ash formed the dominant nonpelagic sediment component until the middle to late Miocene, when the earliest recognized terrigenous sediments, related to the Himalayan uplift, reached Site 758. The long-term decrease in calcium carbonate content and increase in terrigenous clays suggest that the supply of terrigenous sediments increased from the Miocene to the Holocene, presumably in response to an increase in the uplift and denudation rates of the Himalayas and motion of the drill site closer to Asia. The number of ash deposits and the volume of ash per deposit increased from the early Pliocene to the Holocene. This change, which is only partially related to the northward motion of Site 758 toward the Indonesian Arc, may reflect an increase in late Pliocene and Pleistocene volcanic activity. The alternating beds of clay-rich and clay-poor nannofossil oozes in the Pliocene and Pleistocene may be related to glacial-interglacial cyclicity and/or changes in monsoonal climate regime.

BIOSTRATIGRAPHY

The objectives for drilling at Site 758 were to recover an expanded Cretaceous through Neogene section at the northern end of the north-south paleoceanographic/climatic transect in the eastern Indian Ocean and to recover a significant section of basalt from the northern end of the Ninetyeast Ridge for geochemical studies. In addition, we double APC cored the upper Neogene section in Holes 758A and 758B to ensure complete recovery of this sequence for detailed paleoclimatic studies and to develop a complete magnetic reversal stratigraphy for the last several million years.

Sediments at Site 758 include 122 m of middle Miocene to Holocene clay and foraminifer-rich nannofossil ooze, with decreasing clay content and increasing calcium carbonate content downhole. This upper sequence overlies 245 m of Maestrichtian to middle Miocene calcareous chalk and 132 m of Campanian tuff and ashy calcareous chalk.

Microfossil Abundance and Preservation

Calcareous nannofossils are abundant and well preserved in the Neogene sediments of Site 758. Preservation is very good in the middle Miocene to Pleistocene sequence, where the carbonate content in the sediment is diluted by a distinct terrigenous clay component. The effect of this dilution is to inhibit overgrowth of the discoasters, which was a constant nemesis in sediments from other Leg 121 sites.

In the Paleogene and Maestrichtian sequence, calcareous nannofossils are abundant and moderately to well preserved. Relative nannofossil frequency varies from few to abundant in the Campanian units, where the preservation is generally good. Diversity also varies throughout the Campanian sequence.

Planktonic foraminifers are abundant throughout the Neogene, but preservation tends to vary downhole, as a result of dissolution and breakage. Poor preservation due to dissolution is particularly noticeable in the early Pliocene to late Miocene age assemblages. Eocene planktonic foraminifers all occur in one core-catcher sample (121-758A-27X-CC); most are broken or dissolved, and some are filled with glauconite. Planktonic foraminifers are well preserved and abundant in nearly all of the core-catcher samples from the upper Paleocene to the lower Maestrichtian. Downward from the lower Maestrichtian, planktonic foraminifers become less abundant, but remain well preserved.

Benthic foraminifers are rare in Tertiary sediments, and few to common in the Upper Cretaceous sequences. Preservation is generally good in all samples examined.

Diatoms are common and moderately to well preserved in upper Pliocene to Holocene sediments. Specimens in the middle Miocene to middle Pliocene sections are rare and preservation is poor. Diatoms are common and moderately well preserved in the Oligocene and lower Miocene sediments. Common, moderately well-preserved specimens were also observed in the Campanian sediments recovered between Cores 121-758A-39X and 121-758A-40X.

A highly diverse and abundant, moderately preserved to well-preserved assemblage of radiolarians is found in samples of Oligocene to Holocene age. Cores 121-758A-38X to 121-758A-41X also contain common moderately well-preserved specimens. A few silicoflagellates and sponge spicules are found throughout the section.

Paleoenvironmental Analysis

Calcareous nannofossil, planktonic foraminifer, and diatom assemblages all indicate tropical conditions for the Neogene.

Highly diverse planktonic foraminifer and calcareous nannofossil assemblages of the uppermost Maestrichtian through the Paleogene are subtropical to tropical.

A transition from mid-latitude floral and faunal assemblages to subtropical to tropical assemblages apparently occurred sometime in the early Maestrichtian. This transition is noted between Cores 121-758A-33X and 121-758A-35X.

Planktonic foraminifers become less abundant downhole whereas benthic foraminifers occur in greater numbers, until they are about as abundant as planktonic foraminifers in Campanian sediments. The benthic foraminiferal assemblages at Site 758 indicate lower bathyal depths from the Campanian to the Oligocene and upper abyssal depths from the Miocene to the Holocene.

Biostratigraphy

Calcareous nannofossil, planktonic foraminifer, and diatom stratigraphy, as summarized in Figure 10, indicates the presence of a complete Neogene sequence at Site 758. However, several distinct disconformities are present in the Paleogene because the lowermost Oligocene, nearly all of the Eocene, and the lowermost Danian are missing. The Cretaceous/Tertiary boundary at this site is not complete. A good portion of the latest Maestrichtian calcareous nannofossil Zone CC26 and the planktonic foraminifer *Abathomphalus mayaroensis* Zone appear to be missing, as well as the early Danian calcareous nannofossil Subzone CP1a and planktonic foraminifer Zones P0 to P1b. The heavily bioturbated Cretaceous/Tertiary boundary is placed between Section 121-758A-31X-7 (295.25 mbsf) and Sample 121-758A-32X-1, 25–26 cm (295.85 mbsf), and probably lies within Section 121-758A-31X-CC.

Sediments from Cores 121-758A-32X to 121-758A-35X (295.63–334.3 mbsf) are dated as Maestrichtian based on the foraminifers, but because of possible problems with reworking, calcareous nannofossil data would place the Campanian/Maestrichtian boundary above Core 121-758A-35X. Sediments above basalt, in Sample 121-758X-57R-2, 26–27 cm (519.7 mbsf), are dated by calcareous nannofossils as early Campanian. A few recovered intervals of interbedded tuff containing calcareous nannofossils within the basalt could not be accurately dated.

A summary of sedimentation rates is presented in Figures 11 through 14. Calcareous nannofossil and diatom datum levels are given in Table 4.

Calcareous Nannofossils

Neogene

Neogene sediments from Site 758 contain abundant calcareous nannofossils that provide a complete redundant biostratigraphic zonation. The preservation is good, especially in the middle Miocene and younger sections. Terrigenous clay from the Bengal Fan dilutes the carbonate sediment, preventing overgrowth of the calcareous nannofossils and enhancing preservation. In the lower Miocene nannofossil chalks some of the nannofossils (especially discoasters) are slightly overgrown because this dilution effect is absent.

Neogene calcareous nannofossil assemblages at Site 758 are subtropical to tropical. All Neogene marker species used in the Okada and Bukry (1980) calcareous nannofossil zonation scheme were noted, except *Helicosphaera ampliaperita*.

Emiliania huxleyi, a Holocene marker species, is recorded in the upper 50 cm of Core 121-758C-1H. A detailed study using a scanning electron microscope (SEM) will be needed to delineate the Pleistocene/Holocene boundary at this site.

Pleistocene sediments are present down to Section 121-758A-4H-1 (25.2–27.7 mbsf) and to Sample 121-758B-4H-CC, where the last occurrence of *Discoaster brouweri* is noted. The low-lat-

itude assemblage includes abundant *Gephyrocapsa caribbeanica*, *Gephyrocapsa oceanica*, *Helicosphaera sellii*, common *Pseudoemiliania lacunosa*, and *Ceratolithus cristatus*. The last appearance of *P. lacunosa* is noted in Samples 121-758A-2H-1, 121-758B-1H-CC, and 121-758C-1H-5, 110 cm.

Pliocene sediment is present down to Samples 121-758A-8H-CC and 121-758B-8H-CC. The assemblage consists of abundant *D. brouweri*, *Discoaster pentaradiatus*, *Discoaster surculus*, *Reticulofenestra pseudoumbilica*, few *Ceratolithus acutus*, *Ceratolithus rugosus*, *Discoaster tamalis*, and *Discoaster variabilis*.

Late Miocene age assemblages are also marked by an abundance of discoasters, as recorded in Section 121-758A-8H-CC to Sample 121-758A-13X-CC and Samples 121-758B-9H-CC to 121-758B-10H-CC. *Discoaster quinqueramus*, *Discoaster bergrenii*, *Discoaster asymmetricus*, and *Discoaster neohamatus* are very common. A few *Discoaster hamatus* and *Amaurolithus primus* are present. The condensed middle Miocene section consists of *Catinaster coalithus*, *Discoaster kugleri*, and *Sphenolithus heteromorphus*. The occurrence of *C. acutus* is inconsistent in Section 121-758A-8H-CC. This makes the Miocene/Pliocene boundary delineation difficult. Considering the paleomagnetic and planktonic foraminifer data, the Miocene/Pliocene boundary could be in Section 121-758A-9H-CC. The presence of *Sphenolithus belemnus*, *Discoaster druggi*, *Triquetrorhabdulus carinatus*, and common *Cyclicargolithus floridanus* characterizes the lower Miocene section. The last occurrence of *Sphenolithus ciperoensis* in Section 121-758A-21X-5 (195.3–196.8 mbsf) is used to delineate the Oligocene/Miocene boundary at this site.

Paleogene

Calcareous nannofossils are abundant and moderately to well preserved in the Paleogene sediments of Hole 758A. A discontinuous section of approximately 107 m of lower Paleocene to upper Oligocene calcareous chalks was recovered. Missing are the lower Oligocene (Zone CP16), uppermost Eocene (Zone CP15b), middle and lower Eocene (Zones CP9–14), and the lowermost Paleocene (Zone CP1a). Zone CP3 also was not formally identified.

Paleocene nannofossil flora assemblages are typical of tropical environments, as indicated by abundant discoasters, diverse *Fasciculithus*, and the lack of abundant chiasmoliths. Oligocene assemblages consist of abundant and diverse sphenoliths and lack abundant reticulofenestrids in comparison with the high-latitude assemblages of this age on Broken Ridge.

The Oligocene sediments of Hole 758A contain common to abundant *Sphenolithus predistentus*, *Sphenolithus distentus*, *S. ciperoensis*, *C. floridanus*, and *Discoaster deflandrei*. The middle and late Oligocene age calcareous nannofossil Zones CP17–19 are assigned to sediments in the interval from Samples 121-758A-20X-CC to 121-758A-27X-CC, 29 cm (189.3–249.1 mbsf). A sharp contact is present at this level, separating this Oligocene section from the underlying upper Eocene sediments assigned to Zone CP15a.

Sediments of late Eocene age appear to be confined to the core catcher of Core 121-758A-27X. The assemblage includes abundant *Discoaster saipanensis*, *Discoaster barbadiensis*, *Bramletteius serraculoides*, *Reticulofenestra reticulata*, common *Sphenolithus pseudoradians*, *Coccolithus formosus*, and few *Reticulofenestra umbilica*. Reworked specimens of late Paleocene age are also common. A major disconformity lies between Cores 121-758A-27X and 121-758A-28X, separating the upper Eocene sediments from upper Paleocene strata.

Samples 121-758A-28X-1, 140–141 cm, to 121-758A-31X-3, 149–150 cm (258.3–290.4 mbsf), are placed in the late Paleocene age calcareous nannofossil Zones CP4–8. Sediments assigned to Zone CP8 contain common to abundant *Discoaster multiradia-*

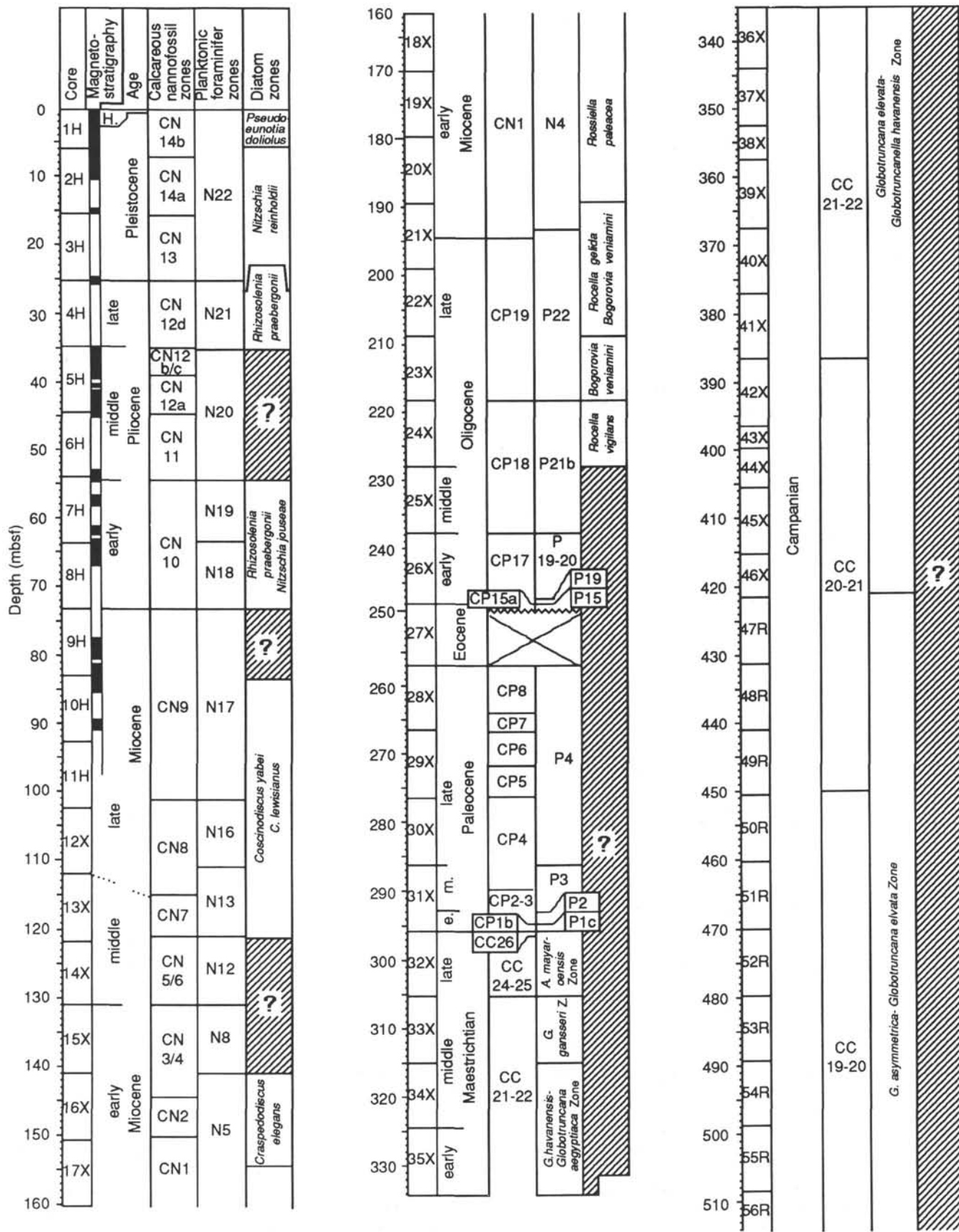


Figure 10. Calcareous nannofossil, planktonic foraminifer, and diatom zonations of Site 758. The top of the Campanian may be higher than shown (see text). The composite magnetostratigraphy for the upper 95 m of Holes 758A and 758B is given next to the ages.

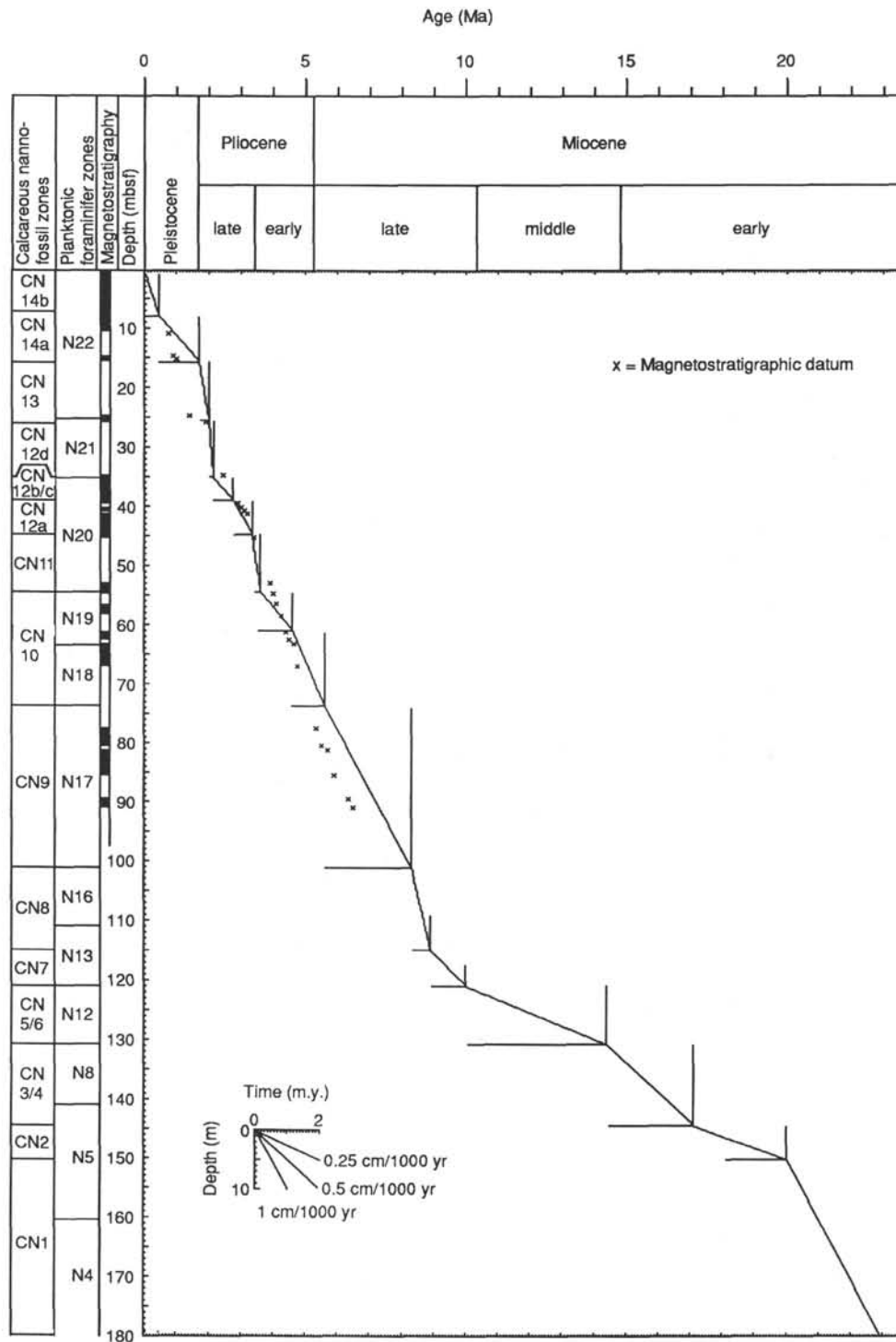


Figure 11. Age vs. depth plot of the Neogene at Site 758. Datums are based on the calcareous nannofossil zones of Figure 10. Uncertainty bars are given as the known age range of a given zone (horizontal) and its vertical range in the holes.

tus, *Discoaster mohleri*, and a diverse assemblage of species of the genus *Fasciculithus*.

Common to abundant *Discoaster okadai* are present in the samples placed in Zone CP7. This short-lived, large discoaster, which has five to seven long, tapering free rays, exhibits an experimental morphology not repeated until the Miocene and, to our knowledge, has not yet been reported from any Indian Ocean sites.

Samples assigned to Zones CP5 and CP6 contain abundant *Heliolithus kleinpellii*, *D. mohleri*, *Toweius eminens*, *Fasciculithus* sp., common *Chiasmolithus bidens*, *Chiasmolithus consuetus*, *Prinsius bisulcus*, and few *Discoasteroides bramlettei* and *Heliolithus cantabriae*. Assemblages of Zone CP4 consist of common *Cruciplacolithus tenuis*, *Chiasmolithus danicus*, *Elipsolithus macellus*, and the zonal marker *Fasciculithus tympaniformis*.

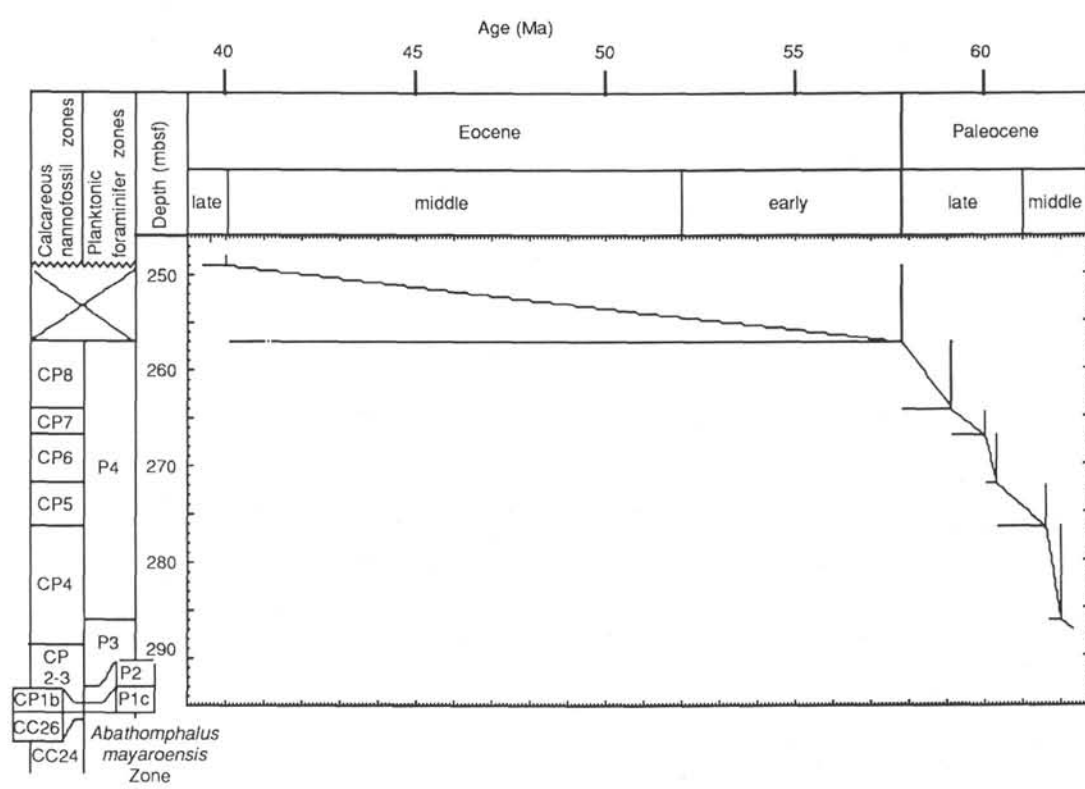
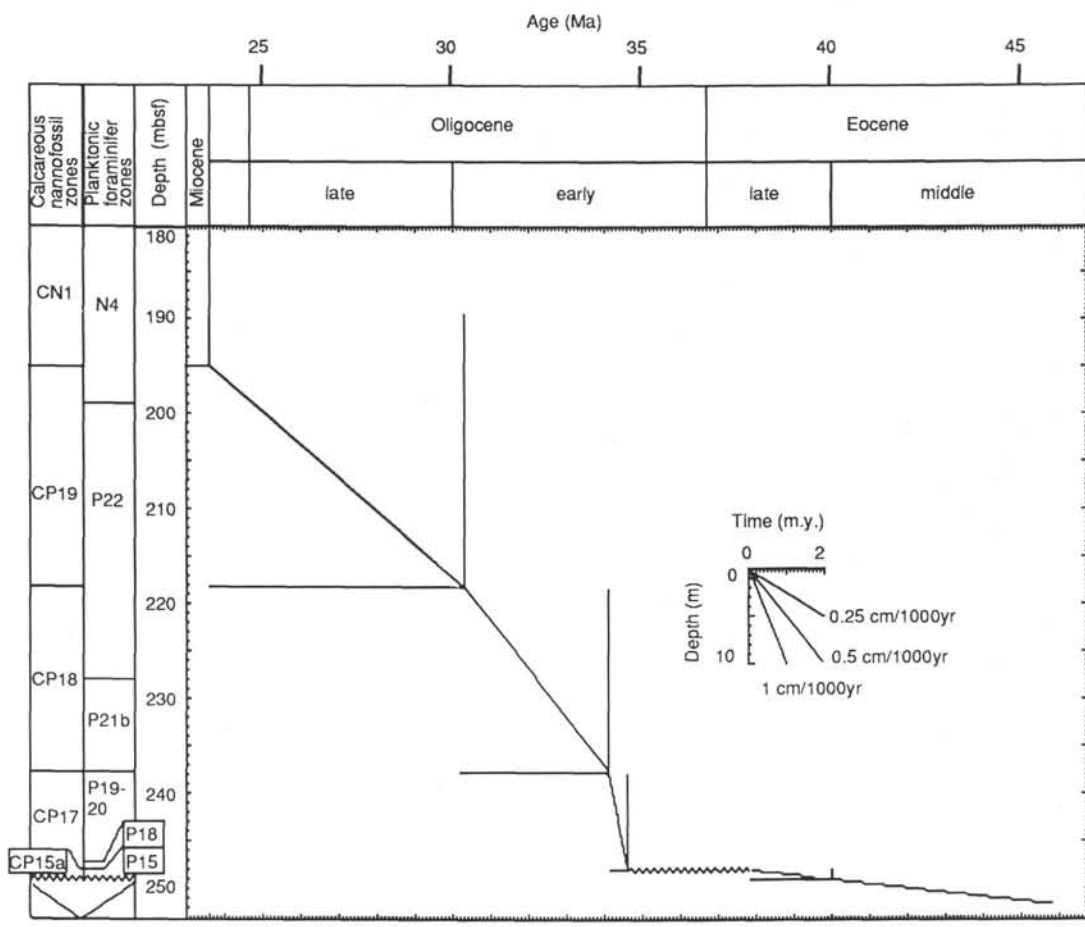


Figure 12. Age vs. depth plot of the Paleogene at Site 758. Error bars are as in Figure 11.

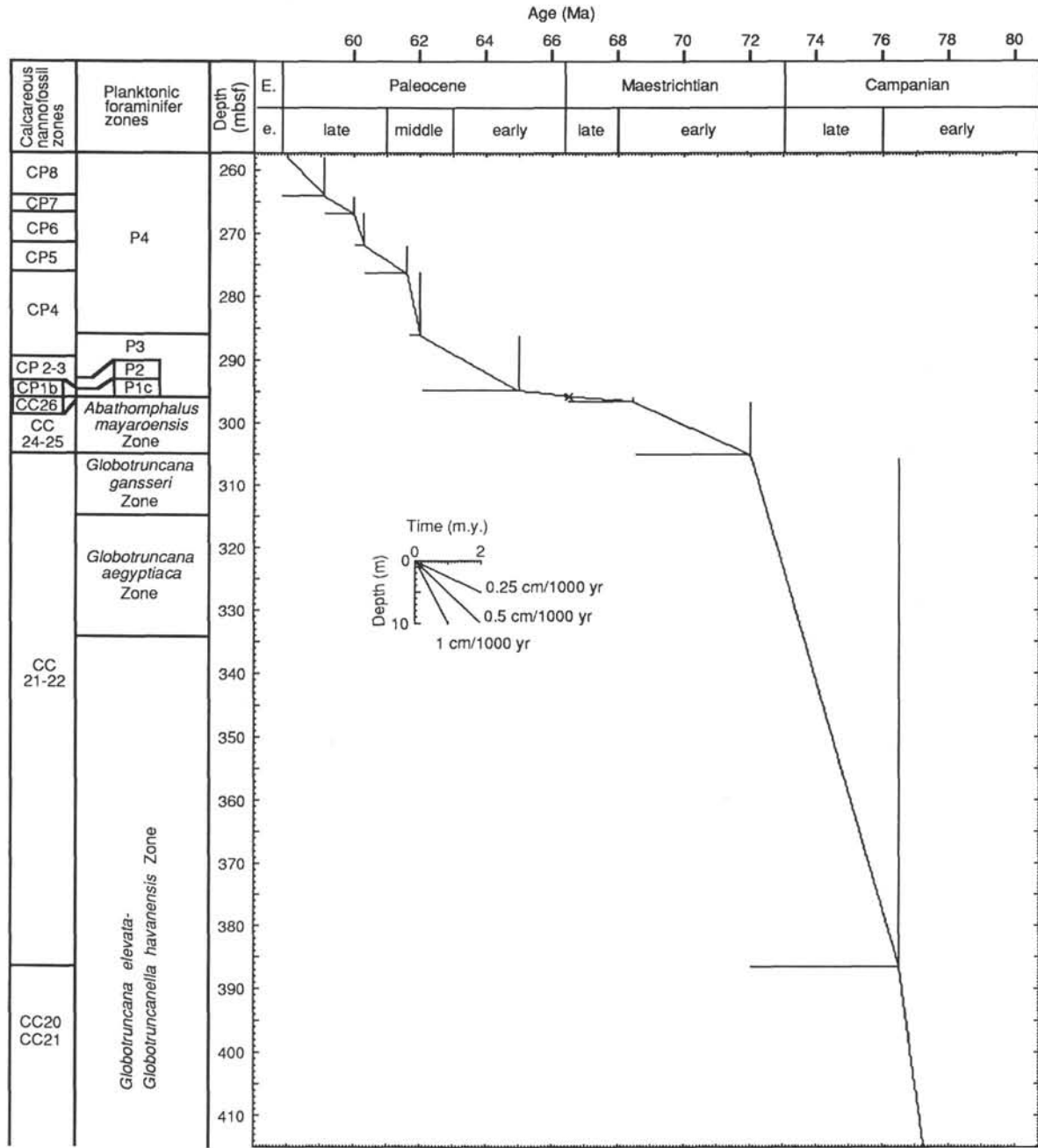


Figure 13. Age vs. depth plot of the Paleocene and Upper Cretaceous at Site 758. Error bars as in Figure 11.

The early Paleocene age Zone CP3 has not yet been delineated in the section at Site 758. Assuming the presence of a hiatus may be premature at this time though, because foraminiferal data would not agree with this interpretation. Zone CP2 is present within Core 121-758A-31X. The CP2 zonal marker *C. danicus* persists down to Sample 121-758A-31X-7, 24 cm (291.1 mbsf), but does not appear present in the lowermost samples containing Tertiary nannofossils. Core 121-758A-31X also contains reworked Cretaceous forms, which increase in abundance downcore.

A disconformity exists between Tertiary and Cretaceous strata as the lowermost Danian Subzone CP1a is not present. The Cretaceous/Tertiary boundary is presumed, at this time, to lie within the core catcher of Core 121-758A-31X. The Zone CP1b

marker species *C. tenuis* and other Tertiary species, such as *Coccolithus cavus*, are present at this level along with a highly diverse upper Maestrichtian assemblage. Tertiary specimens representative of Zone CP1b are interpreted to have been brought down as far as Sample 121-758A-32X-1, 25 cm, by bioturbation processes. Several burrows sampled in the interval from the base of Core 121-758A-31X to Sample 121-758-32X-1, 25 cm, were found to contain a high percentage of Tertiary forms in comparison with the surrounding matrix, which consists of only Cretaceous forms. No Tertiary forms were found below this level.

Cretaceous

Lower Campanian to upper Maestrichtian tuffs and calcareous chalks were recovered at Site 758. Calcareous nannofossils

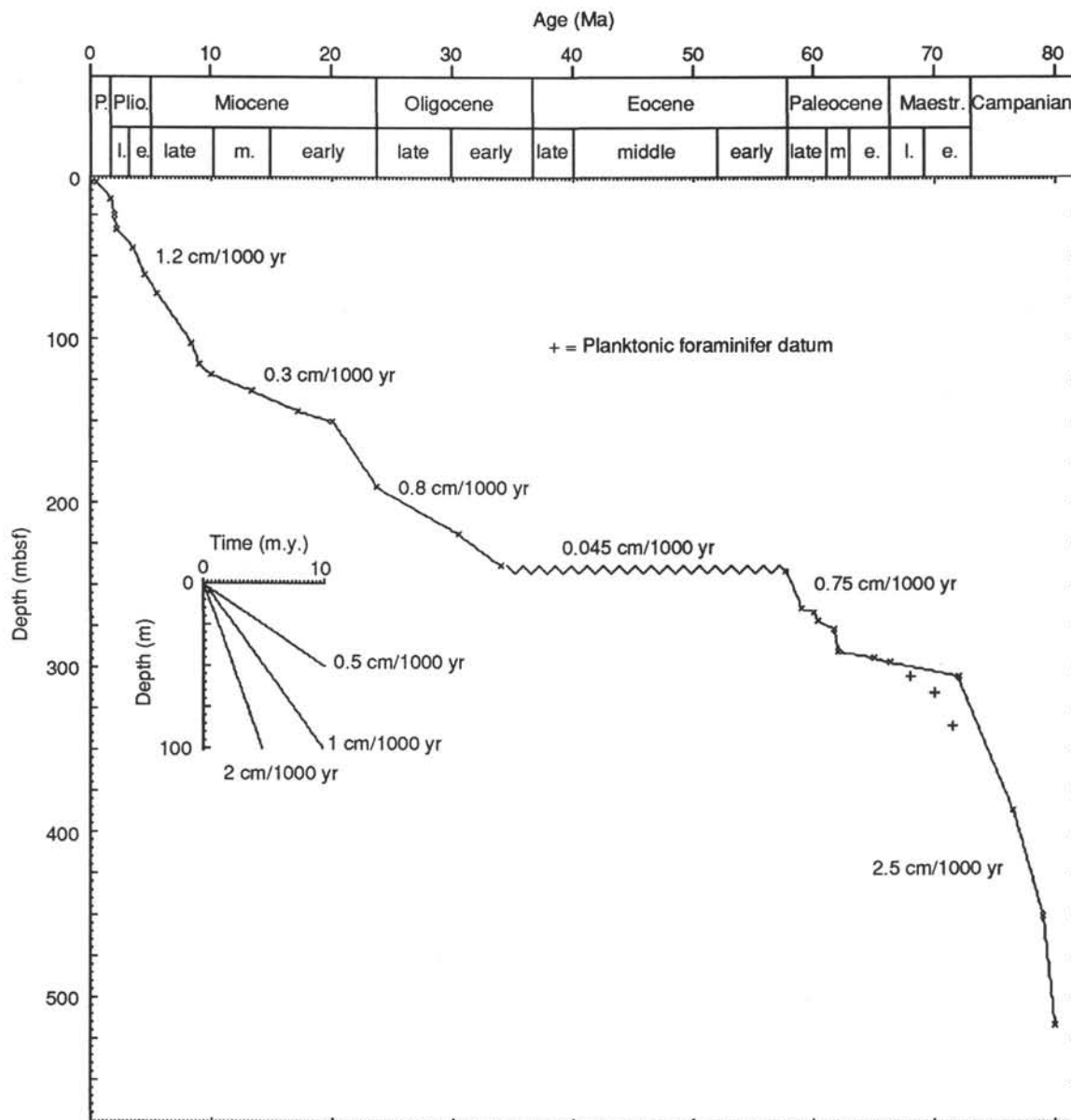


Figure 14. Composite age vs. depth plot for Site 758, based on calcareous nannofossil datums from Figure 10. Planktonic foraminifer datums are indicated where nannofossil control is lacking.

are common to abundant through most sections. Preservation is moderate in the Maestrichtian to upper Campanian sections and generally good through the remaining Campanian sequence.

A high-latitude assemblage similar to that found in the Cretaceous sediments of Broken Ridge is present in the Campanian sediments at Site 758. However, nannofossil assemblages were subtropical to tropical by late Maestrichtian time, reflecting the rapid northward movement of this site toward its present position north of the equator.

Upper Maestrichtian sediments, contained within Core 121-758A-32X, include abundant *Ceratolithus aculeus*, *Microrhabdulus decoratus*, *Micula decussata*, *Cretarhabdus* sp., *Arkhangelskiella cymbiformis*, and rare *Lithraphidites quadratus*. The late Maestrichtian marker species *Micula mura* has not yet been recognized. Reworked specimens of the Campanian marker *Aspidolithus parvus constrictus* were also found in Sample 121-758A-32X-CC.

Zones CC24 to CC25b of Sissingh (1977) are represented by the gap between the last occurrence of *Tranolithus phacelosus* and the first occurrence of *L. quadratus* within Core 121-758A-32X. Possible reworking may make the true last occurrence of *T. phacelosus* difficult to place.

The high-latitude forms *Biscutum magnum*, *Biscutum coronum*, *Nephrolithus corystus*, *Teichorhabdus ethmos*, and *Monomarginatus quaternarius* are present, though not in abundance, in the sediments of Cores 121-758A-33X to 121-758A-40X. Also present are common *Reinhardtites levis*, few *T. phacelosus*, and few to common specimens of *A. parvus constrictus*. The assemblage is typical of the upper Campanian (Zones CC22b-23a), although the upper part of this interval would be assigned to the Maestrichtian on the basis of planktonic foraminifers. The Campanian form *A. parvus constrictus* may be reworked in Cores 121-758A-33X and 121-758A-34X, but in Sample 121-758A-35X-CC the species is common. This species never reaches this

Table 4. Calcareous nannofossil and diatom datums, Site 758.

Species event ^a	Age (Ma)	Depth (mbsf)
Calcareous nannofossils		
LO <i>Pseudoemiliana lacunosa</i>	0.47	6.0–7.5
LO <i>Helicosphaera sellii</i>	1.37	15.6–17.1
LO <i>Discoaster brouweri</i>	1.90	25.2–26.7
LO <i>Discoaster pentaradiatus</i>	2.20	33.3–34.8
LO <i>Discoaster varibilis</i>	2.90	37.8–39.3
LO <i>Reticulofenestra pseudoumbilica</i>	3.50	44.4–45.9
FO <i>Discoaster tamalis</i>	3.80	57.0–58.5
LO <i>Discoaster quinqueramus</i>	5.60	69.7–71.2
FO <i>Amaurolithus primus</i>	6.50	83.1–84.6
FO <i>Discoaster quinqueramus</i>	8.20	102.4–103.9
LO <i>Discoaster hamatus</i>	8.85	116.6–118.1
LO <i>Sphenolithus belemnus</i>	17.4	144.0–145.5
LO <i>Sphenolithus ciperoensis</i>	25.2	195.3–196.8
FO <i>Sphenolithus ciperoensis</i>	30.2	218.3–219.8
FO <i>Sphenolithus distentus</i>	34.2	237.7–239.2
FO <i>Discoaster multiradiatus</i>	59.2	264.1–265.4
FO <i>Discoaster mohleri</i>	60.4	271.6–271.1
FO <i>Fasciculithus tympaniformis</i>	62.0	290.4–291.6
FO <i>Chiasmolithus danicus</i>	64.8	292.1–295.6
FO <i>Nephrolithus frequens</i>	69.0	295.8–295.9
^b Diatoms		
LO <i>Nitzschia reinholdii</i>	0.65	16.2–19.2
LO <i>Nitzschia fossilis</i>		3.6–6.0
LO <i>Rhizosolenia praebergonii</i> var. <i>robusta</i>	1.55	22.1–25.2
FO <i>Pseudoemotia doliolus</i>	1.8	25.2–25.8
LO <i>Rhizosolenia praebergonii</i> var. <i>praebergonii</i>	1.85	22.1–25.2
LO <i>Thalassiosira convexa</i>	2.1	31.8–34.8
FO <i>Thalassiosira fraga</i>	19.9	151.3–153.6
LO <i>Melosira architecturalis</i>	20.7	160.4–170.0
FO <i>Rossiella paleacea</i>	22.7	182.3–189.3
FO <i>Bogorovia veniamini</i>	26.5	208.7–218.3

^a FO = first occurrence; LO = last occurrence.

^b Equatorial Pacific diatom datums: Barron (1985a, 1985b) and Barron et al. (1985).

level of relative abundance in any of the samples below this depth and, thus, is interpreted as not being reworked in this sample.

Calcareous nannofossil assemblages change very little from Cores 121-758A-41X to 121-758A-57R, just above the basalt. Diversity is low for the most part, and species with stratigraphic ranges that cover most of the Campanian to early Maestrichtian are present, which makes precise zonation of the Campanian sediments difficult. The general assemblage includes *Aspidolithus parvus*, *A. parvus constrictus*, *Arkhangelskiella specillata*, *B. coronum*, *B. magnum*, *Tranolithus* sp., and *Reinhardtites anthophorus*. The entire interval can be assigned to the Campanian Zones CC19 to CC22. The presence of *A. specillata* and the lack of *A. parvus expansus* and *Marthasterites furcatus*, which were found on Broken Ridge, suggest that the lowermost early Campanian age Zones CC17 and CC18 were not reached.

Further detailed study through this interval should provide better stratigraphic resolution for the Campanian. Rare specimens of the late Campanian age species *Tetralithus gothicus* are present in Sample 121-758A-41X and if found with more consistency should allow for a more precise division of upper and lower Campanian stratigraphic units.

Planktonic Foraminifers

Neogene

Dominating the planktonic foraminifer assemblages are typical, warm subtropical to tropical faunas. Although planktonic foraminifers are abundant throughout, preservation tends to

vary downcore, as a result of dissolution and breakage. Poor preservation due to dissolution is particularly noticeable in the early Pliocene to late Miocene age assemblages.

Pleistocene. Pleistocene planktonic foraminifer assemblages were recovered from Samples 121-758A-1H-CC to 121-758A-3H-CC and 121-758B-1H-CC to 121-758B-3H-CC. Based on the presence of *Globorotalia truncatulinoides* and absence of *Globigerinoides obliquus extremus*, the faunas are assigned to the *Globorotalia truncatulinoides* Zone. Faunas are dominated by the tropical to warm subtropical species *Globigerinoides sacculifer*, *Globigerinoides conglobatus*, *Neogloboquadrina humerosa*, *Globorotalia menardii*, *Globorotalia tumida*, and *Pulleniatina obliquiloculata*. Also common throughout the interval is the ubiquitous species *Orbulina universa*. Although preservation is good in the >250 μ m fraction, extensive breakage occurs in fractions <250 μ m.

The co-occurrence of *Globorotalia tumida flexuosa* and *Globigerina calida calida* in Sample 121-758A-1H-CC assigns the assemblage to the *Globigerina calida calida* Subzone. Also present within this sample are common occurrences of *Sphaeroidinella dehiscentes excavata*, *Globorotalia unguolata*, and *Bolliella adamsi*. The absence of *Globorotalia tosaensis* indicates that this sample is younger than 0.6 Ma.

The first occurrence of *Pulleniatina finalis* without *Globigerinoides fistulosus* in Sample 121-758A-2H-CC indicates that the sediments are younger than 1.3 Ma. The last appearance of *G. fistulosus* in Sample 121-758A-3H-CC indicates the age of the sediments is 1.6 to 1.9 Ma. *Globorotalia crassaformis hessi* occurs in small numbers within this sample.

Pliocene. Pliocene planktonic foraminifer assemblages were recovered from Samples 121-758A-4H-CC to 121-758A-8H-CC and 121-758B-4H-CC to 121-758B-8H-CC. All of the zones from N21 to N18 are identified. Common throughout the Pliocene are the species *G. menardii*, *G. tumida*, *Globigerinoides ruber*, *G. sacculifer*, *Globorotalia limbata*, *Globigerinoides triloba*, *O. universa*, and *Sphaeroidinella dehiscentes*. Except for Samples 121-758A-4H-CC and 758B-4H-CC, preservation throughout this interval was extremely poor because of breakage and, more particularly, dissolution. This probably accounts for the low diversity in the assemblages from the lower Pliocene.

The presence of *Globorotalia multicamerata* and *G. tosaensis* without *Sphaeroidinellopsis seminulina* in Sample 121-758A-4H-CC indicates that the age of the assemblage is 2.9–3.1 Ma.

The last occurrence of *Globoquadrina dehiscentes* was noted in Sample 121-758A-6H-CC (Zone N20). The absence of *Globigerina nepenthes* in the same sample indicates that the assemblages are younger than 3.9 Ma. Therefore, the use of the last occurrence of *G. dehiscentes* as a marker of the Miocene/Pliocene boundary (Berggren, 1973) is questionable. The Miocene/Pliocene boundary is placed on the first occurrence of *G. tumida* and *S. dehiscentes*, between Samples 121-758A-8H-CC and 121-758A-9H-CC.

Miocene. Planktonic foraminifer assemblages of Miocene age were recovered from Samples 121-758A-9H-CC through 121-758A-20X-CC. Although extreme breakage and dissolution are apparent in Sample 121-758A-9H-CC, preservation throughout the Miocene is good.

Upper Miocene faunas are dominated by *G. dehiscentes*, *G. menardii*, *G. limbata*, *S. seminulina*, *Globoquadrina altispira altispira*, *Globoquadrina altispira globosa*, *G. nepenthes*, and *O. universa*.

The middle Miocene assemblages in Samples 121-758A-13X-CC and 121-758A-14X-CC are distinctive in that they exhibit low diversity and a very high proportion (up to 90%) of radiolarians occurs in the smaller fractions. Dominating the assemblages are *G. dehiscentes*, *Globorotalia siakensis*, *Globorotalia mayeri*, *Sphaeroidinellopsis multiloba*, and the subspecies of *G.*

altispira. Zonation of the assemblages, however, proved difficult because the subspecies of the *Globorotalia fohsi* lineage are very rare as a result of dissolution.

The lower Miocene/middle Miocene boundary is placed between Samples 121-758A-14X-CC and 121-758A-15X-CC, based on the development of *Orbulina suturalis* from *Praeorbulina glomerosa* and subspecies.

The early Miocene age assemblages proved difficult to assign to a planktonic foraminifer zone because the marker species are either rare or absent. Globoquadrinids dominate the early Miocene age faunas, particularly *G. dehiscens*, *Globoquadrina praede-hiscens*, *Globoquadrina baroemoensis*, *Globoquadrina venezuelana*, and the subspecies of *G. altispira*. Also common throughout are *G. siakensis* and *G. mayeri*.

The Miocene/Oligocene boundary was discerned between Samples 121-758A-20X-CC and 121-758A-21X-CC, based on the presence of *G. triloba*, *Globigerinoides primordius*, and *G. kugleri*.

Paleogene

Oligocene. Oligocene faunas were recovered from Samples 121-758A-21X-CC to 121-758A-27X-1, 79–81 cm. Although the planktonic foraminifer assemblages are well preserved throughout, the faunas are of low diversity. Common throughout the Oligocene is *Globorotalia opima nana* and *Globigerina tripartita*. The assemblages contain few marker species, and, therefore, zonation of these assemblages is tentative. The co-occurrence of *Pseudohastigerina micra* and *Globigerina selli* in the lowermost sample assigns the sediments to the early Oligocene age Zone P19 of Blow (1969).

Eocene. Planktonic foraminifers in the Eocene all occur only in Sample 121-758A-27X-CC. Most are broken or dissolved, and some are filled with glauconite. Section 121-758A-27X-CC consists of a foraminiferal sand (chalk) with pebbles in the interval between 30 and 48 cm.

Sample 121-758A-27X-CC contains reworked upper Paleocene forms such as *Morozovella oclusa* and *Morozovella simulatilis*; lower Eocene species such as *Morozovella formosa*, *Morozovella aragonensis*, *Morozovella caucasica*, *Acarinina soldadoensis*, and *Acarinina primitiva*; middle Eocene species such as *Acarinina bullbrooki*, *Truncorotaloides rohri*, *Truncorotaloides topilensis*, and *Globigerina senni*; and mostly middle Eocene representatives of the *Globigerinatheka* group, such as *Globigerinatheka subconglobata*. The age of the sample is difficult to determine, but a few fragments of *Turborotalia* aff. *cerroazulensis* indicate an latest middle Eocene to late Eocene age. Most of the specimens in this sample are encrusted or filled with glauconite, broken, and/or stained yellow or brown. Abraded bipyramidal quartz crystals with fluid inclusions are common. A few hundred fish teeth were found in the sample. The preservation of the foraminifers, the abundant fish teeth, and the fact that all substages of the Eocene are represented in the mixed assemblages suggest that the Eocene was a period of nondeposition (Fig. 14). Therefore, the alternative option of erosion of the uppermost Paleocene and Eocene sediments in the uppermost Eocene seems less probable.

Paleocene. A possibly complete but condensed Paleocene section was recovered from 256.9 to 294.6 mbsf. The well-preserved assemblages with almost no broken specimens and the abundance of low-latitude forms allow recognition of all of the foraminiferal Zones P4 through P1c (Toumarkine and Luterbacher, 1985). The uppermost Paleocene P5 Zone is missing, as are the P0–1a/1b Zones of the basal Danian (Smit, 1982). The P4 Zone (*Planorotalites pseudomenardii* Zone) is characterized by *Planorotalites pseudomenardii*, which has a well-developed imperforate keel in the assemblages of Samples 121-758A-28X-CC and 121-758A-29X-CC. Other species in the assemblages,

represented by robust, well-developed tropical forms, are *Morozovella velascoensis*, *Morozovella conicotruncata*, *M. simulatilis*, *M. oclusa*, *Morozovella aequa*, *Morozovella angulata*, *Morozovella kolchidica*, *Morozovella laevigata*, *Morozovella acuta*, and *Morozovella* aff. *pusilla*, along with *Globigerina linaperta* and *Globigerina velascoensis*. The acarininids are represented by *A. aff. soldadoensis* and *Acarinina mckannai*. The planktonic/benthic foraminiferal ratios are high (>20:1), indicating water depths in excess of 500 m (but see the following discussion of Campanian assemblages).

Sample 121-758A-30X-CC contains specimens transitional from *Planorotalites chapmani* to *P. pseudomenardii*. *M. angulata* and *Morozovella abundocamerata* are abundant, but only a few specimens of *M. velascoensis*, related to the four-chambered ancestral *M. acuta*, were found. Such an assemblage is typical for the very base of Zone P4 (*P. pseudomenardii* Zone). Commonly found in the coarse (>0.5 mm) fraction of Sample 121-758A-30X-CC is an unusual and atypically large species (up to 0.75 mm in size) (Fig. 15). This species has a low trochospiral test with five globular chambers in the last whorl. The umbilicus is open and contains apertural teeth. These forms can be best com-

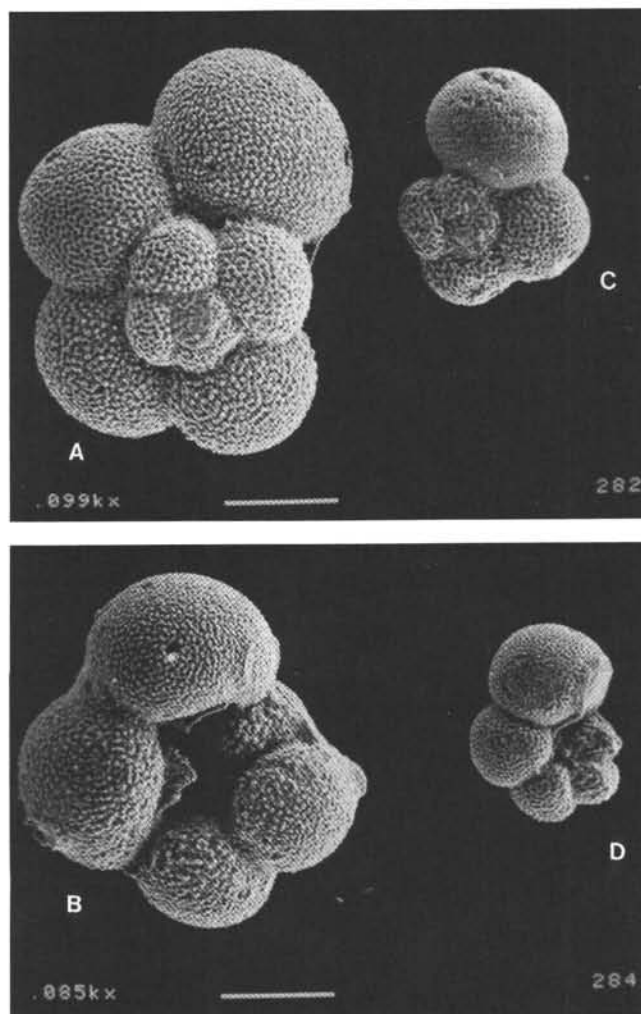


Figure 15. SEM photograph of an unknown species of planktonic foraminifer from the upper Paleocene P4 Zone (Sample 121-758A-30X-CC) of Hole 758A (A and B). For comparison, a large specimen of a similar species from the Danian (Sample 121-758A-31X-5, 115–120 cm), *Morozovella pseudobulloides*, is illustrated (C and D).

pared with *Morozovella trinidadensis*, *Morozovella pseudobulloides*, or *Morozovella inconstans*, although the range of those species is reportedly restricted to the P1-P2, and possibly the P3, Zones (Toumarkine and Luterbacher, 1985; Stainforth et al., 1975). In addition, the size (0.75 mm) of the specimens found is larger than the reported maximum size (0.4 mm; Stainforth et al., 1975) of the aforementioned species. Reworking is not likely, as specimens of these species found in the Danian are a little more than half the size of the specimens found here (Fig. 15).

The upper Danian P2 (*Morozovella uncinata*) Zone is found in Sample 121-758A-31X-5, 115–120 cm (293.1 mbsf), represented by *Morozovella uncinata*, *M. trinidadensis* (forms up to 0.4 mm), *Globigerina triloculinoides*, *M. pseudobulloides*, and *P. chapmani* or *Planorotalites compressa*. The lower Danian (but by no means the lowermost) P1c (*Morozovella trinidadensis*) Zone (close to the P2 Zone) is found in Sample 121-758A-31X-6, 115–120 cm (294.6 mbsf), about 1 m above the Cretaceous/Tertiary boundary and is represented by *G. triloculinoides*, *Globigerina edita*, *M. trinidadensis*, *M. pseudobulloides*, *Morozovella praecursoria*, and *P. compressa*. Specimens of *Globoconusa daubjergensis* are rare, which indicates that these assemblages are (sub)tropical, as *G. daubjergensis* is rare in low-latitude, but common in temperate, assemblages (Hansen, 1970).

Cretaceous/Tertiary Boundary

The Cretaceous/Tertiary boundary is located somewhere between Section 121-758A-31X-7 and Sample 121-758A-32X-1, 25–26 cm, or between 295.25 and 295.85 mbsf. Section 121-758A-31X-CC is a mixture of light yellow chalk with exclusively uppermost Maestrichtian fauna and darker yellow burrows(?) that contain still dominantly Cretaceous specimens (see the following text) but also (rare) representatives of Zone P1c, such as *M. pseudobulloides*, *M. trinidadensis*, and *P. compressa*. Zones P0 to P1b, or about 1.5 m.y. of the lower Paleocene, are missing. The uppermost Maestrichtian is probably not complete either. Sample 121-758A-32X-CC (305.3 mbsf) contains *Abathomphalus intermedius*, which is indicative of the basal part of the *Abathomphalus mayaroensis* Zone. This implies a thickness of only about 10 m for the *A. mayaroensis* Zone, which should have been about 50 m thick if the Campanian/early Maestrichtian sedimentation rates of 2.5 cm/1000 yr had prevailed at the end of the Cretaceous (Fig. 14).

Upper Cretaceous

Upper Cretaceous assemblages were found from 295.6 to 517.1 mbsf (Samples 121-758A-31X-CC to 121-758A-57R-CC). Most samples disintegrated well, in contrast to sediments of similar age and paleolatitude on Broken Ridge (Sites 752 and 754). The specimens are well preserved, even (or especially) in between ashes from 430 to 517.1 mbsf. The faunas of late Maestrichtian age (295.6–314.9 mbsf) are reasonably diverse, but from 314.9 to 517.1 mbsf only low-diversity faunas were found, similar in species composition to the planktonic faunas of Maestrichtian to Campanian age at Broken Ridge (Sites 752 and 754). Such faunas compare very well to other austral to transitional faunas found elsewhere in the Southern Hemisphere, such as at the Falkland Plateau (Sliter, 1975; Basov and Krashenninikov, 1983), Naturaliste Plateau (Herb, 1974), and Tasman Sea (Webb, 1973).

Upper Maestrichtian. The uppermost Maestrichtian was found only in Sample 121-758A-31X-CC, as previously mentioned, mixed with some Paleocene forms in burrows. *A. mayaroensis*, the namesake marker species for the uppermost Maestrichtian foraminiferal zone, occurs commonly in a well-preserved assemblage consisting of *Globotruncana arca*, rare *Globotruncana stuarti*, *Globotruncanella havanensis*, *Globotruncanella citae*,

Rugoglobigerina rotundata, *Rugoglobigerina rugosa*, *Globigerinelloides aspera*, *Globigerinelloides ehrenbergi*, *Heterohelix* spp., *Gublerina* sp., *Planoglobulina carseyae*, *Rugoglobigerina* aff. *scotti*, and *Racemiguembelina fructicosa*. This assemblage is transitional from tropical to austral faunas. The more tropical species are *R. fructicosa*, *R. scotti*, and *G. stuarti*. The scarcity of globotruncanids and the absence of large tropical forms, such as *Globotruncana contusa*, in combination with the abundance of *Globigerinelloides* and *Rugoglobigerina*, however, indicate close affinities with austral areas (Sliter, 1975). Sample 121-758A-32X-CC contains *A. aff. mayaroensis*, *A. intermedius*, *R. rugosa*, *R. rotundata*, rare *G. arca*, *G. havanensis*, *G. citae*, *Heterohelix* spp., and *Rugoglobigerina hexacamerata*, indicative of the basal part of the *A. mayaroensis* Zone. The transition from temperate, austral faunas to tropical faunas occurs just below the Cretaceous/Tertiary boundary, and the location of Site 758 probably moved northward across an important ecological boundary at that time.

Lower Maestrichtian to Campanian. Samples 121-758A-33X-CC, 121-758A-34X-CC, and 121-758A-35X-CC are characterized by low-diversity faunas dominated by species of *Rugoglobigerina* and *Globigerinelloides*. *R. hexacamerata* in combination with *Globotruncana linneana* indicates a middle to early Maestrichtian age. Other species include *G. havanensis*, *G. citae*, *Rugoglobigerina macrocephala*, *G. arca*, *Rugotruncana subpenyi*, and a few *Heterohelix* spp.

Keeled globotruncanids become increasingly scarce downhole, with the last specimen observed in Sample 121-758A-41X-CC. Below this sample, the faunas are of very low diversity, and long-ranging species of the genera *Globigerinelloides*, *Heterohelix*, *Rugoglobigerina*, or *Archaeoglobigerina* dominate the assemblages.

As at Broken Ridge, zonal assignments in the Campanian-Santonian age interval are difficult to make because of the complete absence of diagnostic species. Samples 121-758A-35X-CC to 121-758A-44X-CC are dominated by *R. rugosa*, *G. ehrenbergi*, *G. aspera*, and *Archaeoglobigerina blowi*, together with some specimens of *G. linneana* and *Globotruncana tricarinata*. All of these are long-ranging species with little biostratigraphic value.

The last *R. rugosa* was observed in Sample 121-758A-44X-CC (405.6 mbsf). In Samples 121-758A-46X-CC and 121-758A-47R-CC, assemblages are dominated by *Archaeoglobigerina*, such as *Archaeoglobigerina bosquensis*, the ancestral form of *Rugoglobigerina*, and a few transitional forms of *Archaeoglobigerina* to *Rugoglobigerina* occur as well. The occurrence of *Archaeoglobigerina*, in particular *A. bosquensis*, without rugoglobigerinids is generally taken as evidence for a Santonian age. *A. bosquensis* is reportedly restricted to the Santonian (Caron, 1985; Herb, 1974; Sliter, 1975; Basov and Krashenninikov, 1983). *A. bosquensis* is positively identified here, occurring commonly at Site 758 from 415.2 to 440.9 mbsf, which is dated as middle Campanian by means of nanofossils. *A. bosquensis* can be confused only with *R. rotundata*, but the latter species is restricted to the middle and upper Maestrichtian. Further analysis will probably show that the range of *A. bosquensis* has to be extended into the lower and middle Campanian, at least in temperate areas, which, unfortunately, serves to reduce its biostratigraphic value. Reworking is highly unlikely, considering the excellent preservation and abundance of the specimens of this species in Sample 121-758A-47X-CC.

Planktonic/benthic foraminiferal ratios drop downhole from 96% in the lower Paleocene to 70% in the upper Maestrichtian to less than 50% in most of the Campanian. Generally, this gives an indication of shallower depth. However, the benthic foraminiferal assemblages still indicate lower bathyal depths (see the following section).

Benthic Foraminifers

All core-catcher sediment samples from Hole 758A were examined for $> 125\mu\text{m}$ -sized foraminifers. Benthic foraminifers are rare in the Tertiary, but few to common in the Maestrichtian and Campanian. In Samples 121-758A-43X-CC, 121-758A-45X-CC, and 121-758A-51R-CC, foraminifers were not found. In general, benthic foraminifers are well preserved at Site 758. Water paleo-depth estimates using benthic foraminifer data are presented in Figure 16. The horizontal bars shown in this figure indicate the upper and lower depth limits of the respective faunas.

Pleistocene to Pliocene

Pleistocene to Pliocene faunas found in Samples 121-758A-1H-CC to 121-758A-8H-CC are characterized by the consistent occurrences of *Cibicidoides* spp., *Laticarinina pauperata*, *Favocassidulina favus*, *Oridorsalis umbonatus*, *Pyrgo murrhyna*, and *Uvigerina* spp. Particularly in the Pleistocene Samples 121-758A-1H-CC to 121-758A-3H-CC, *Uvigerina peregrina* and *Uvigerina proboscidea* are commonly found in association with *Epistominella exigua*. This faunal association indicates that the paleoenvironment was influenced by Indian Ocean Bottom Water, which is characterized by high temperature and salinity and low dissolved oxygen content (Corliss, 1979; Peterson, 1984).

Miocene

Upper Miocene faunas recovered in Samples 121-758A-9H-CC to 121-758A-12X-CC are similar to the Pliocene to Pleistocene faunas. In addition to the diagnostic taxa found in the Pliocene to Pleistocene, *Planulina wuellerstorfi* is a main element of the upper Miocene assemblage. Moreover, the species association *F. favus*, *Melonis pompilioides*, and *Nonion affine* is reported by Burke (1981) as characteristic of the lower slope of the Ontong

Java Plateau (2500–3000 m in depth). Therefore, the late Miocene water depth of upper abyssal is similar to the present depth.

In Samples 121-758A-13X-CC and 121-758A-14X-CC, middle Miocene faunas characterized by low diversity were found. They include lower bathyal to abyssal species such as *Anomalinoidea globulosus* and *L. pauperata*.

Lower Miocene faunas in Samples 121-758A-15X-CC to 121-758A-20X-CC are dominated by *Cibicidoides* spp., *Globocassidulina* spp., *Pleurostomella* spp., and *Stilostomella* spp. Based on the upper and lower depth limits of *Anomalinoidea semicribratus*, *Bulimina tuxpomensis*, *Cibicidoides havanensis*, and *Planulina costa*, the early Miocene water depth is assigned to the deeper part of the lower bathyal range (1500–2000 m).

Oligocene

Middle to upper Oligocene faunas are found in Samples 121-758A-21X-CC to 121-758A-26X-CC. Deep-water taxa such as *C. havanensis*, *Globocassidulina* spp., *Gyroidina soldanii*, *O. umbonatus*, and *Stilostomella* spp. were consistently found. Of the taxa examined, the Oligocene faunas somewhat resemble the early Miocene age faunas. However, deeper water taxa such as *Bulimina jarvisi* and *Cibicidoides grimsdalei* were rarely found in middle Oligocene Samples 121-758A-25X-CC and 121-758A-26X-CC. Taking the depth distribution of the species *B. tuxpomensis*, *Cibicidoides bradyi*, *C. havanensis*, *Hanzawaia amphora*, and *Planulina costa* into consideration, estimated water depths for the Oligocene show a wide variation from lower bathyal to upper abyssal depths (1000–3000 m).

Eocene

The upper Eocene faunas found in Sample 121-758A-27X-CC are characterized by low diversity and consist of lower bathyal

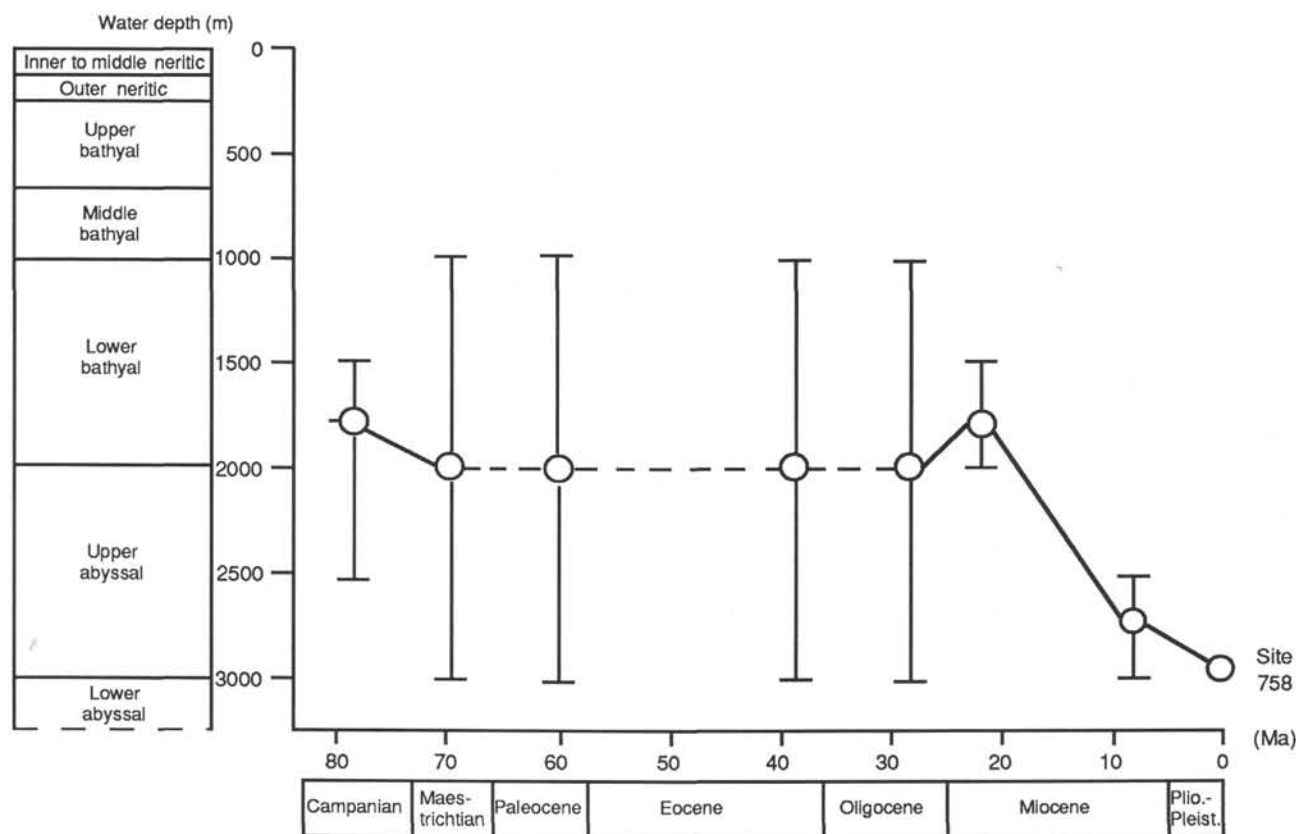


Figure 16. Age vs. water depth at Site 758, based on benthic foraminifers. Dotted lines indicate the inferred depth of missing strata.

to abyssal species such as *B. jarvisi*, *C. grimisdalei*, and *Nuttallides truempyi*.

Paleocene

The upper Paleocene faunas found in Samples 121-758A-28X-CC to 121-758A-30X-CC are characterized by the consistent occurrence of *Stensioina beccariiiformis*. The depth distribution of these faunas ranges from middle bathyal to abyssal depths, but the presence of *Bulimina velascoensis* in Sample 121-758A-29X-CC indicates that the upper Paleocene faunas are from lower bathyal to abyssal depths (1000–3000 m).

The lower Paleocene faunas in Sample 121-758A-31X-CC are dominated by *S. beccariiiformis* and *Coryphostoma incrassata*. *C. velascoensis* was also found frequently. These species indicate bathyal to abyssal depositional environments.

Maestrichtian

The species composition of the Maestrichtian fauna recovered in Sample 121-758A-32X-CC is similar to that of the early Paleocene age fauna and is dominated by the bathyal to abyssal species *S. beccariiiformis*, *Gyroidinoides globosus*, *Osangularia cordieriana*, and *Cibicidoides* spp.

Campanian

Compared with the Maestrichtian fauna, the Campanian benthic foraminifers found in Samples 121-758A-33X-CC to 121-758A-57R-CC are more diverse. Dominant in this fauna are *Cibicidoides dayi*, *C. velascoensis*, *C. incrassata*, *Gyroidina quadrata*, *G. globosus*, *Pyramidina* spp., and smaller-sized *S. beccariiiformis*. *Lenticulina* spp. were consistently found in all upper Campanian core-catcher samples. Thin-shaped *Gavelinella* sp. is dominant in Samples 121-758A-36X-CC to 121-758A-49R-CC.

These faunas are also characterized by the occurrence of *Osangularia cordieriana*, *Nuttallinella florealis*, and several species of the genera *Praebulimina*, *Pullenia*, *Dorothia*, *Quadrimorphina*, and *Ellipsoidella*. In Sample 121-758A-57R-CC, agglutinated forms such as *Cirbrostomoides* sp., *Rzehakina* sp., and *Tribrachia excavata* were frequently found. These faunas are similar to the Campanian fauna recovered in the South Atlantic Ocean (Sliter, 1977). The water depth indicated by these taxa is lower bathyal to upper abyssal and may fall within the upper part of the 1500- to 2500-m depth range.

Diatoms

Diatoms are present in most of the upper Oligocene through Holocene sediments recovered at Site 758. The assemblages are well preserved in the upper Pliocene to Holocene sediments (Cores 121-758A-1H to 121-758A-5H). Preservation is very poor in the lower Pliocene to middle Pliocene (Cores 121-758A-6H to 121-758A-15X), where only a few specimens were observed. The assemblages are moderately to well preserved in the upper Oligocene to lower Miocene sediments (Cores 121-758A-16X to 121-758A-24X). Diatoms were also observed in the Campanian sediments recovered between Cores 121-758A-39X and 121-758A-41X.

Neogene and Oligocene assemblages are typically tropical and are similar to those described in the tropical Indian Ocean (Schrader, 1974) and in the equatorial Pacific (e.g., Barron, 1985a). The Quaternary and Neogene low-latitude diatom zonation of Burckle (1972) and Barron (1985b) and the Eocene to Oligocene low-latitude diatom zonation of Fenner (1984) were used here.

The diatom zonation of Hole 758A is reported in Figure 10, and diatom datum levels used at this site are indicated in Table 4.

Neogene and Quaternary

Pleistocene. Based on the occurrence of *Pseudoeunotia doliolus* and the absence of *Nitzschia reinholdii* or *Nitzschia fossilis*, the *Pseudoeunotia doliolus* Zone is recognized between Samples 121-758A-1H-1, 63–65 cm, and 121-758A-1H-3, 63–65 cm. *N. reinholdii* is rare and was not found above Sample 121-758A-3H-3, 65–67 cm. Barron (1980) showed that the last occurrence in the eastern tropical Pacific of *N. fossilis* is slightly below the last occurrence of *N. reinholdii*. Therefore, we used here the last occurrence of *N. fossilis* to approximate the top of the *Nitzschia reinholdii* Zone. *N. fossilis* is first found in Sample 121-758A-1H-CC, and *Rhizosolenia praebergonii* var. *robusta* and var. *praebergonii* are first found in Sample 121-758A-3H-CC. Therefore, Subzone B of the *N. reinholdii* Zone is recognized between Samples 121-758A-1H-CC and 121-758A-3H-CC. The diatoms are abundant and well preserved. The assemblages are dominated by low-latitude species such as *Nitzschia marina*, *Azpeitia nodulifer*, *Thalassiosira oestrupii*, *Thalassionema nitzschioides*, *Hemidiscus cuneiformis*, and *Roperia tessellata*.

Pliocene. The first occurrence of *P. doliolus* in Sample 121-758A-4H-1, 65–67 cm, allows the interval between Samples 121-758A-3H-CC and 121-758A-4H-1, 65–67 cm, to be assigned to Subzone A of the *N. reinholdii* Zone. The *Rhizosolenia praebergonii* Zone is recognized between Samples 121-758A-4H-1, 65–67 cm, and 121-758A-4H-CC. Sample 121-758A-3H-CC is placed in Subzone C of this zone, based on the absence of *P. doliolus* and *Thalassiosira convexa*. Sample 121-758A-4H-CC, in which *Thalassiosira convexa* var. *aspinosa* was first found, is placed in Subzones A to B.

Lower Pliocene to Middle Miocene. Diatom preservation is very poor from Cores 121-758A-5H to 121-758A-15X, and most of the levels are barren of diatoms or contain only rare specimens that are generally not diagnostic for age. However, the occurrence of *Nitzschia jouseae* in Samples 121-758A-7H-CC and 121-758A-8H-CC allows the assignment of this interval to the Pliocene (*Nitzschia jouseae* Zone + *R. praebergonii* Subzone A).

Upper to middle Miocene sediments are recognized based on the occurrence of forms belonging to *Thalassiosira yabei* and *Thalassiosira grunowii* groups in Samples 121-758A-10H-CC and 121-758A-11H-CC and on the occurrence of *Denticulopsis hustedtii* in Sample 121-758A-13X-CC.

Samples 121-758A-14X-CC and 121-758A-15X-CC are totally barren of diatoms.

Lower Miocene. Poorly preserved to well-preserved diatom assemblages occur in the lower Miocene sediments, from Sections 121-758A-16X-CC to 121-758A-20X-CC. Although *Bogorovia veniamini* occurs between Samples 121-758A-16X-CC and 121-758A-17X-3, 65–67 cm, the presence of *Thalassiosira fraga* and *Coscinodiscus rhombicus* at these levels allows this interval to be assigned to the *Craspedodiscus elegans* Zone. Based on the occurrence of *B. veniamini* and *Rossiella paleacea*, the *Rossiella paleacea* Zone (lowermost Miocene) is recognized from Samples 121-758A-17X-CC to 121-758A-20X-CC. The most common species in the interval are *Synedra jouseana*, *C. rhombicus*, and *Rossiella symmetrica*. Other characteristic diatom taxa include *Coscinodiscus praenodulifer*, *C. elegans*, and *Asterolampra marylandica*. *Thalassiosira bukryi* was first found in Sample 121-758A-17X-1, 65–67 cm, and *Melosira architecturalis* was first found in Sample 121-758A-18X-CC.

Paleogene

Oligocene. The diatom flora is moderately to well preserved from Samples 121-758A-21X-1, 65–67 cm, to 121-758A-25X-CC. Because *Rocella gelida* was not found in the section, the

base of the *Rocella gelida* Zone was not recognized, and the *R. gelida* Zone (latest Oligocene to earliest Miocene) could not be separated from the *Bogorovia veniamini* Zone (late Oligocene).

The absence of *R. paleacea* in Sample 121-758A-21X-1, 65–67 cm, indicates that this level is older than the *R. paleacea* Zone and places this sample in either the *R. gelida* or *B. veniamini* Zones.

The occurrence of the Eocene-Oligocene restricted species *Thalassiosira mediaconvexa* (Fenner, 1981) in Sample 121-758A-21X-3, 65–67 cm, indicates an Oligocene age for this level. The assemblages are dominated by *S. jouseana* and *Rocella vigilans*. Other characteristic taxa include *C. rhombicus*, *Coscinodiscus oligocenicus*, *B. veniamini*, *R. symmetrica*, and *M. architecturalis*. Sample 121-758A-24X-CC contains a similar flora, with the exception of *B. veniamini*, which was last found in Sample 121-758A-23X-CC. Sample 121-758A-24X-CC is therefore placed in the *Rocella vigilans* Zone (late Oligocene).

Below Sample 121-758A-24X-CC, sediments are generally barren of diatoms.

Cretaceous

Diatoms were found from Samples 121-758A-39X-CC to 121-758A-40X-CC (Campanian). Sample 121-758A-40X-CC contains a moderately preserved diatom assemblage composed of species belonging to genera *Stephanopyxis*, *Biddulphia*, *Coscinodiscus*, and *Triceratium*.

Radiolarians

Most of the biogenic silica in the section is represented by radiolarians, which dominate the other siliceous microfossil groups (diatoms, silicoflagellates, and sponge spicules). Radiolarians are found in all core-catcher samples examined from Sections 121-758A-1H-CC to 121-758A-27X-CC (Oligocene to Holocene). The assemblages are moderately to well preserved and are highly diverse.

The preservation of radiolarians follows that of the diatoms. Thus, the best preserved assemblages are found in the upper Pliocene to Holocene and upper Oligocene to lower Miocene intervals. However, radiolarians occur in the middle Miocene to lower Pliocene sediments, where diatoms are not preserved. Sediments recovered below Sample 121-758A-27X-CC are barren of radiolarians, with the exception of Samples 121-758A-38X-CC to 121-758A-40X-CC (Campanian), which contain moderately preserved to well-preserved assemblages.

IGNEOUS PETROLOGY

Drilling at Hole 758A first encountered basaltic rock in the bottom of Core 121-758A-54R, which corresponds to a depth of 499 mbsf. The basalt underlies green and gray Campanian volcanic sediments. Drilling continued for a further 177.9 m, giving a total hole depth of 676.8 mbsf. A sequence of 29 basaltic units, with a total thickness of 118.54 m, and 5.3 m of interflow sediment, mainly tuffs and hyaloclastites, was recovered. The average basement recovery rate was 70% (Fig. 17).

A summary of the main features of each of the basaltic units is presented in Table 5. The units range in thickness from less than 2 m to more than 20 m; they are predominantly sheet flows or, in the case of the thicker units, possibly ponded flows. Four units in the lower part of the succession are pillow basalts. The flows are predominantly aphyric or sparsely plagioclase-phyric; two units are moderately plagioclase-phyric. The available data indicate that the flows were erupted in a deep-water environment.

Macroscopic Core Descriptions

The basalt units fall conveniently into three categories (see Table 5): (1) massive units with over 5 m of recovered core: flow Units 758A-F1 through 758A-F3, 758A-F7, 758A-F10, 758A-

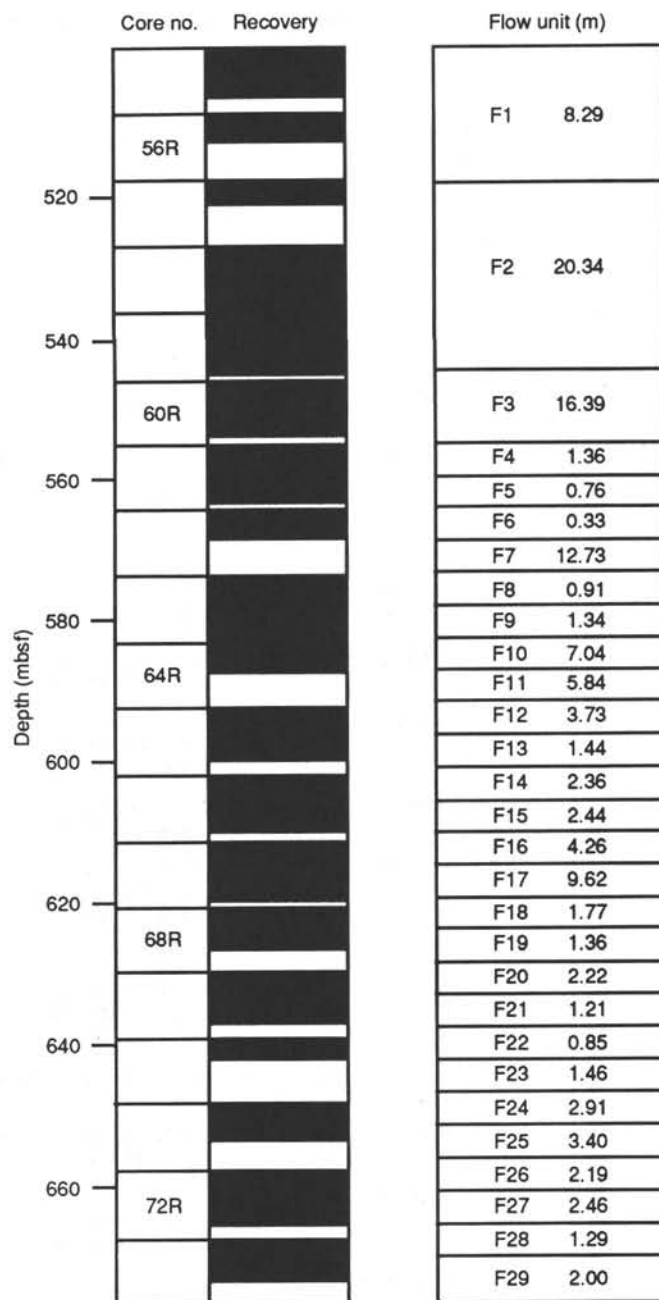


Figure 17. Distribution of recovered basalt, Hole 758A.

F11, and 758A-F17; (2) thin sheet flows (less than 5 m of recovered core): flow Units 758A-F4 through 758A-F6, 758A-F8, 758A-F9, 758A-F12 through 758A-F16, 758A-F18, 758A-F20, 758A-F22, 758A-F24, 758A-F26, and 758A-F27; and (3) pillow basalts: flow Units 758A-F19, 758A-F21, 758A-F23, and 758A-F25. In general terms, the thicker units of category (1) occur higher in the sequence, whereas the pillow basalts dominate in the lower part of the core. The depth vs. thickness plot, Figure 18, illustrates the change of unit thickness with depth.

Massive Basalt Units

These units are characterized by good recovery, in one instance exceeding 100%, with long, continuous core lengths (one length exceeded 3 m). Texturally, the basalts vary from cryptocrystalline near their margins, to medium grained, approaching

Table 5. Summary of basaltic lithologic units, Hole 758A.

Flow unit	Thickness ^a (m)	Core interval	Description	
			Macroscopic	Microscopic
758A-F1	8.92	54R-CC to -56R-1, 115 cm (Piece 7)	Sparsely plagioclase-phyric basalt with internal flow contacts	Aphyric to sparsely plagioclase-phyric basalt with a hyalophitic texture
Volcanic sandstones and tuffs 5.40				
758A-F2	20.34	57R-2, 114 cm (Piece 1), to -60R-1, 85 cm (Piece 2A)	Sparsely plagioclase-phyric basalt grading downunit to aphyric basalt	Aphyric to sparsely plagioclase-phyric basalt with hyalophitic texture
758A-F3	16.39	60R-1, 86 cm (Piece 2B), to -62R-3, 34 cm (Piece 3)	Aphyric basalt	Aphyric basalt with hyalophitic texture
758A-F4	3.05	62R-1, 36 cm (Piece 4A), to -62R-3, 50 cm (Piece 3)	Moderate to highly plagioclase-phyric basalt	Moderately plagioclase-phyric basalt with pseudomorphs after olivine phenocrysts (<1% at top of unit, 2%-3% near base) in rapidly cooled groundmass
758A-F5	0.60	62R-3, 50 cm (Piece 4), to -62R-3, 110 cm (Piece 9)	Sparsely plagioclase-phyric basalt	Not studied
758A-F6	0.33	62R-3, 110 cm (Piece 10), to -62R-4, 20 cm (Piece 3)	Aphyric basalt	Not studied
758A-F7	12.73	63R-1, 0 cm (Piece 1), to -64R-2, 149 cm (Piece 1B)	Sparsely plagioclase-phyric basalt grading to aphyric basalt	Aphyric basalt with a hyalophitic texture, and other parts of the unit are sparsely plagioclase-phyric
758A-F8	0.91	64R-3, 0 cm (Piece 1), to -64R-3, 91 cm (Piece 14)	Vesicular, aphyric basalt flow	Aphyric basalt; section studied is quench-textured
758A-F9	1.34	64R-3, 91 cm (Piece 15), to -64R-4, 79 cm (Piece 6)	Vesicular, aphyric basalt flow	Not studied
Volcanic tephra 0.40				
758A-F10	7.04	65R-1, 39 cm (Piece 5B), to -65R-6, 84 cm (Piece 1C)	Aphyric basalt	Aphyric basalt with a fine-grained hyalophitic texture
Fragments of volcanic tephra that probably fell into the hole 0.26				
758A-F11	5.84	66R-1 Piece 4 (26 cm), to -66R-5, 59 cm (Piece 1E)	Aphyric basalt (probably a continuation of 758A-F10)	Not studied
758A-F12	3.73	66R-5, 26 cm (Piece 1F), to -67R-1, 137 cm (Piece 4B)	Aphyric basalt	Not studied
Interflow carbonated sediment 0.13				
758A-F13	1.44	67R-2, 0 cm (Piece 1A), to -67R-2, 144 cm (Piece 1C)	Aphyric basalt flow (complete thickness of flow recovered)	Not studied
758A-F14	2.36	67R-3, 0 cm (Piece 1A), to -67R-4, 88 cm (Piece 3)	Aphyric basalt flow	Aphyric to sparsely plagioclase- and clinopyroxene-microphyric basalt
758A-F15	2.44	67R-4, 88 cm (Piece 4), to -67R-6, 60 cm (Piece 2)	Sparsely plagioclase- and pyroxene-phyric basalt flow	Sparsely plagioclase-clinopyroxene-phyric basalt
Thin band of interflow breccia or hyaloclastite 0.05				
758A-F16	4.26	67R-6, 65 cm (Piece 3), to -68R-3, 51 cm (Piece 4)	Vesicular, aphyric basalt flow	Aphyric basalt
758A-F17	9.62	68R-3, 51 cm (Piece 5), to -69R-5, 128 cm (Piece 1C)	Sparsely to moderately plagioclase-phyric basalt	Highly clinopyroxene-, moderately plagioclase-phyric basalt with a hyalophitic groundmass

Table 5 (continued).

Flow unit	Thickness ^a (m)	Core interval	Description	
			Macroscopic	Microscopic
Interflow layer of clayey tuff 0.08				
758A-F18	1.77	69R-6, 0 cm (Piece 1A), to -70R-1, 149 cm (Piece 11D)	Aphyric basalt sheet flow	Not studied
Interflow layer of altered hyaloclastite 0.16				
758A-F19	1.36	70R-2, 8 cm (Piece 2A), to -70R-2, 142 cm (Piece 7G)	Aphyric pillow basalt	Not studied
758A-F20	2.22	70R-2, 142 cm (Piece 8), to -71R-2, 34 cm (Piece 4)	Aphyric basalt sheet flow	Not studied
758A-F21	1.11	71R-2, 34 cm (Piece 5A), to -71R-3, 10 cm (Piece 13)	Aphyric pillow basalt	Not studied
758A-F22	0.85	71R-3, 10 cm (Piece 2), to -71R-3, 95 cm (Piece 3B)	Aphyric basalt sheet flow	Not studied
Carbonated hyaloclastite or basaltic breccia 0.02				
758A-F23	1.46	71R-3, 100 cm (Piece 5A), to -71R-4, 96 cm (Piece 6)	Aphyric pillow basalts	Not studied
758A-F24	2.91	71R-4, 96 cm (Piece 7), to -72R-2, 111 cm (Piece 1C)	Aphyric basalt sheet flow	Not studied
Fragment of interunit hyaloclastite or breccia				
758A-F25	3.40	72R-2, 116 cm (Piece 2B), to -72R-5, 18 cm (Piece 2)	Aphyric pillow and sheet flows	Not studied
758A-F26	2.19	72R-5, 18 cm (Piece 3), to -72R-6, 86 cm (Piece 5)	Aphyric to sparsely plagioclase-phyric basaltic sheet flow	Not studied
758A-F27	2.46	72R-6, 86 cm (Piece 6), to -73R-2, 82 cm (Piece 1C)	Aphyric basalt grading to sparsely plagioclase-phyric basalt in the lower part of the unit	Not studied
758A-F28	1.29	73R-2, 82 cm (Piece 1D), to -73R-3, 68 cm (Piece 4E)	Pillow breccia	Not studied
758A-F29	2.0	73R-3, 69 cm (Piece 4F), to -73R-4, 119 cm (Piece 9)	Sparsely plagioclase-phyric basaltic sheet flow	Not studied
Total recovered basalt 124.36				

^a Based on curated core.

doleritic, in their centers. The units have a mottled appearance, due to the presence of abundant mesostasis pockets between intergrowths of glomerophyric plagioclase and augite (hyalophitic texture); however, all of the mesostasis is now replaced by dark green or black smectites. The units comprise an aphyric to sparsely plagioclase-phyric basalt; in several instances (e.g., Units 758A-F2 and 758A-F7), individual units grade from plagioclase-phyric near the top to aphyric in the center and lower parts of the unit.

The contacts of the units, either with tuffaceous sediment or adjacent basalt units (Fig. 19), are commonly inclined and appear similar to the margins of basalt pillows. The contact zones show evidence of rapid cooling and, while there are no preserved glassy selvages or clay zones replacing selvages, the margins are commonly cryptocrystalline (Fig. 19). One upper contact shows a clear contact with bleached tuff (Fig. 20), which

appears to be the result of chemical, rather than thermal, induration. In thin section, this contact shows evidence of rapid quenching of the basalt magma against water. The units are sparsely vesicular, with vesicle zones adjacent to the contacts. These vesicles are often aligned and elongated normal to the flow margins, and in places develop into pipe vesicles several centimeters in length.

Thin, internal chill zones were observed in some of the massive units. These zones are approximately 3 cm across (Fig. 21) and are particularly common in flow Units 758A-F1 and 758A-F7. All of the studied internal chill zones show upwardly directed cooling, suggestive of heat loss through the top of the unit. The frequency of zones decreases toward the base of the flow. Our preliminary interpretation of these chill zones is that they result from successive injections of magma into the (rapidly) cooling flow body. The time interval between the succes-

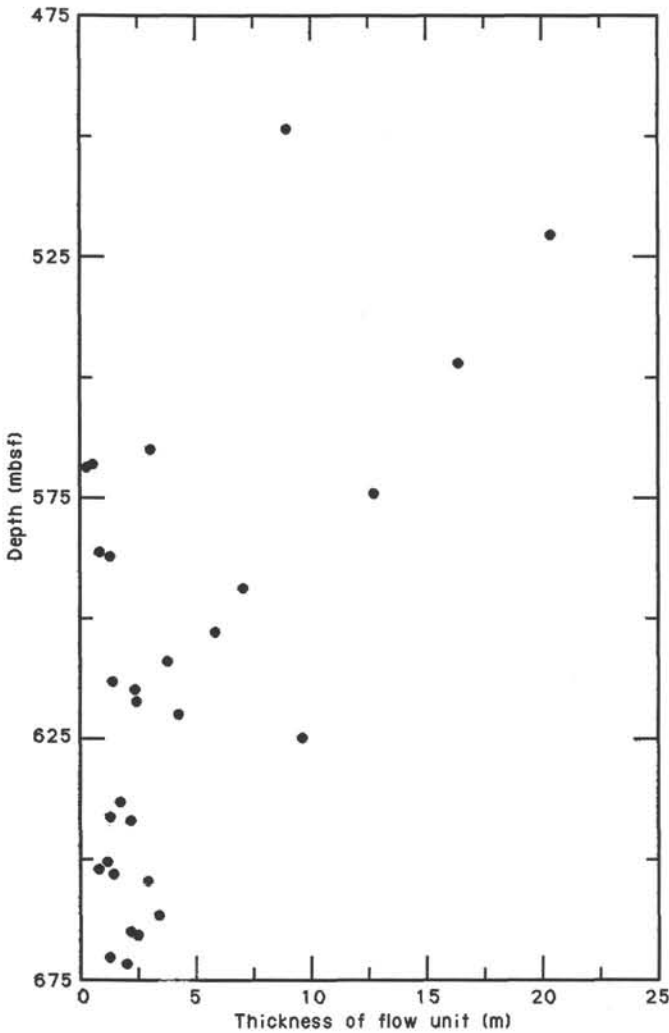


Figure 18. Plot of unit thickness vs. depth for the basaltic flows, Hole 758A.

sive magma batches is short, because the chilled zones are “welded” onto the pre-existing basalt; there is no evidence of fracturing along these zones.

The origin of these thick units is enigmatic. They may be intrusive bodies, but the absence of baked sediments against upper contacts or any other unequivocal evidence of thermal induration in the overlying tuff sequence mitigates against such an interpretation. Furthermore, the steeply inclined contacts do not indicate concordant sill emplacement. We prefer to interpret them as thick, submarine flows. Most submarine effusives are relatively thin (<5 m) sheet flows or pillow basalts; thick submarine flows are less common. Flows of up to 17.6 m thickness were recovered from DSDP Hole 417D in the western Atlantic (Donnelly et al., 1980); these flows also show the hyalophitic texture found in the Site 758 basalts (“ophimottled texture”; Donnelly et al., 1980).

The thick units do not show brecciated margins. Thick submarine flows may not show brecciation if their motion is rapidly arrested by the convective transfer of heat from their surface. Consequently, their surface could develop a ropy or pillowed structure, which could account for the high inclination of their margins. Further circumstantial evidence that these units are submarine effusives comes from their hyalophitic texture (i.e., the occurrence of considerable percentages of [originally glassy]

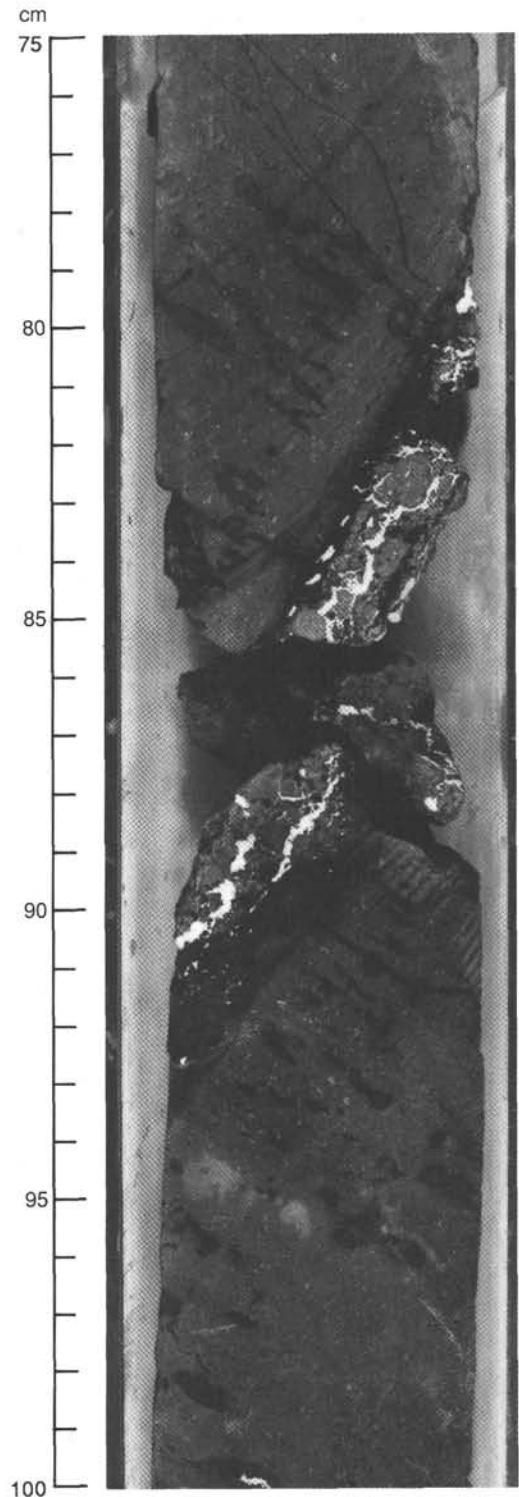


Figure 19. The contact between flow Units 758A-F2 and 758A-F3 (Section 121-758A-60R-1, 75–100 cm).

mesostasis surrounding the larger augite and plagioclase crystals) and the internal flow contacts. Both pieces of evidence point to rapid heat loss from the flow interiors.

Why are the flows so thick? Fluid submarine basaltic magma would be expected to rapidly disperse before solidifying. Possibly, the flows were ponded within a local basin. The pillow ba-

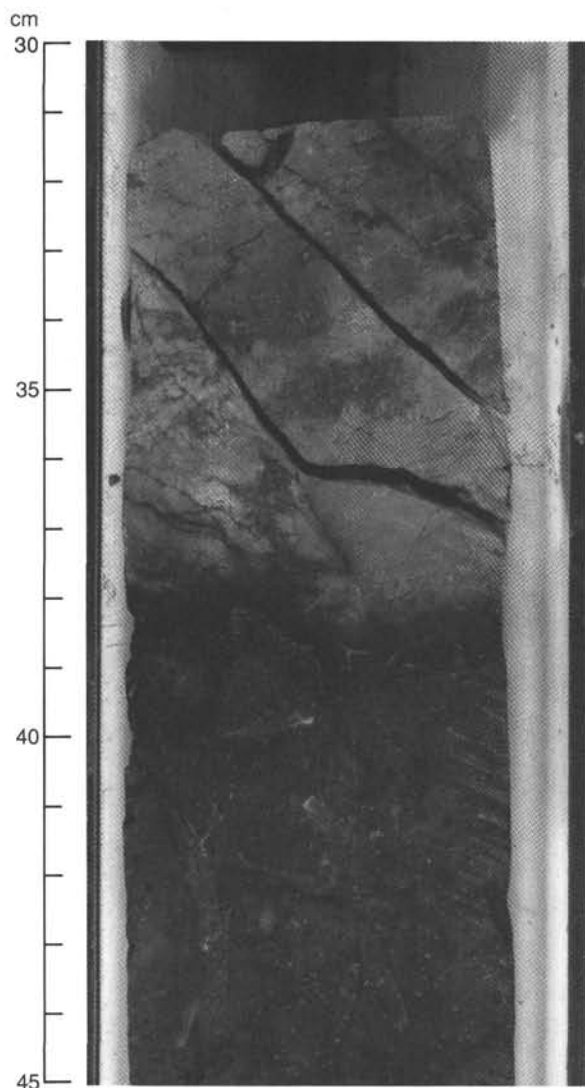


Figure 20. The upper contact of flow Unit 758A-F10 with bleached tuffaceous sediment (Section 121-758A-65R-1, 30-45 cm).

salt and thin sheet flows from deeper sections of the hole have a compositional similarity to the overlying thicker units, so there is no a priori reason to assume that the flows had a different viscosity or that the eruptive setting had changed dramatically.

Thin Sheet Flows and Pillow Basalts

These flows are morphologically similar to submarine basalts recovered from numerous sites on the ocean floor and show unequivocal evidence that the magmas were erupted into water beneath the depths at which phreatomagmatic activity is possible (>50 m?). A submarine environment for the entire basement section at Site 758 is consistent with the paleontological evidence, which indicates a bathyal environment for the oldest fossil assemblages ("Biostratigraphy" section), and the lithostratigraphy, which indicates deep-water deposition distal tephra.

Macroscopically, the sheet flows and pillow basalts both show evidence of quenching, in the form of glassy selvages (now replaced by black chloritic smectites). The sheet flows are approximately 1 to 3 m thick and are intercalated with the pillow basalts. Pillows vary from 15 to 80 cm across, with development of typical radially elongated, concentrically arranged vesicles

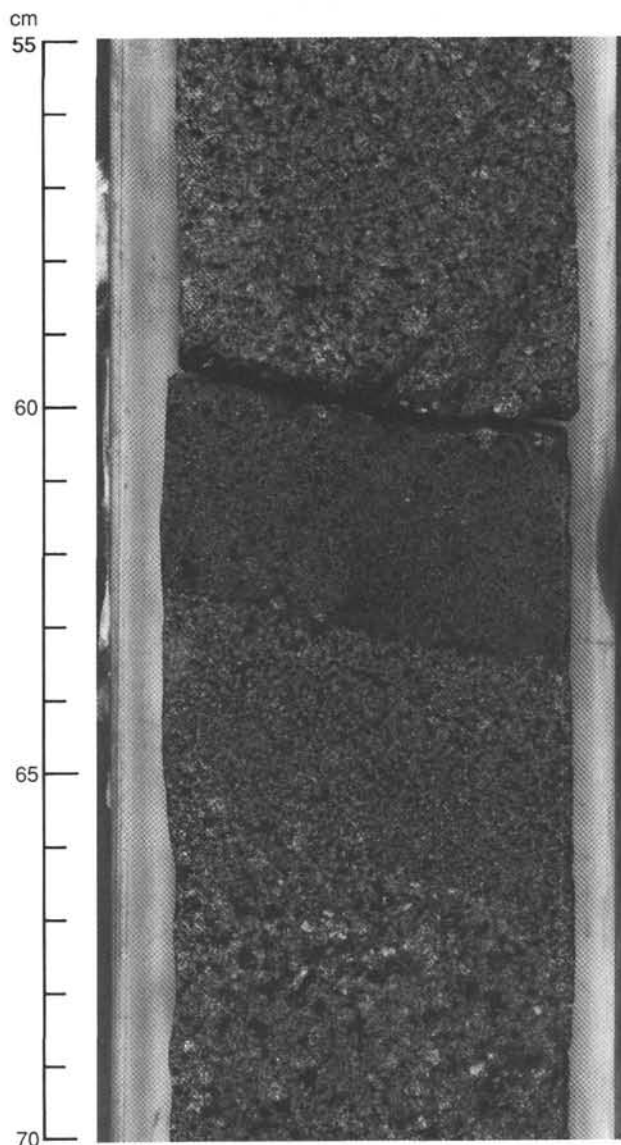


Figure 21. The thin internal contact within Unit 758A-F1 (Section 121-758A-55R-2, 55-70 cm).

(Fig. 22). The pillow basalt units are between 1 and 1.5 m thick. Mineralogically, the pillows and sheet flows are very similar to each other and, at least in terms of their phenocryst contents, to the overlying thicker flows. Most are aphyric, or they contain minor amounts of plagioclase or trace amounts of altered olivine phenocrysts.

All of the units from Hole 758A are pervasively altered, with replacement of groundmass mesostasis and infilling of vesicles and fractures by black, brown, and green smectites (Table 6). Small amounts of calcite occur in the basalts, but in much smaller proportions than in the basalts from Sites 756 and 757. Sulfide (iron pyrite) is a ubiquitous phase in the Site 758 basalts: trace amounts occur in both the groundmass and vesicles. In the latter, it is frequently embedded in dark-colored smectite. No zeolites were seen, nor were any oxidative alteration or oxidized flow tops observed. Although most of the units recovered at Site 758 are vesicular, the frequency of large cavities is much lower than in the basalts from Sites 756 and 757, which is again consistent with emplacement of the magma in a deep-water environment.

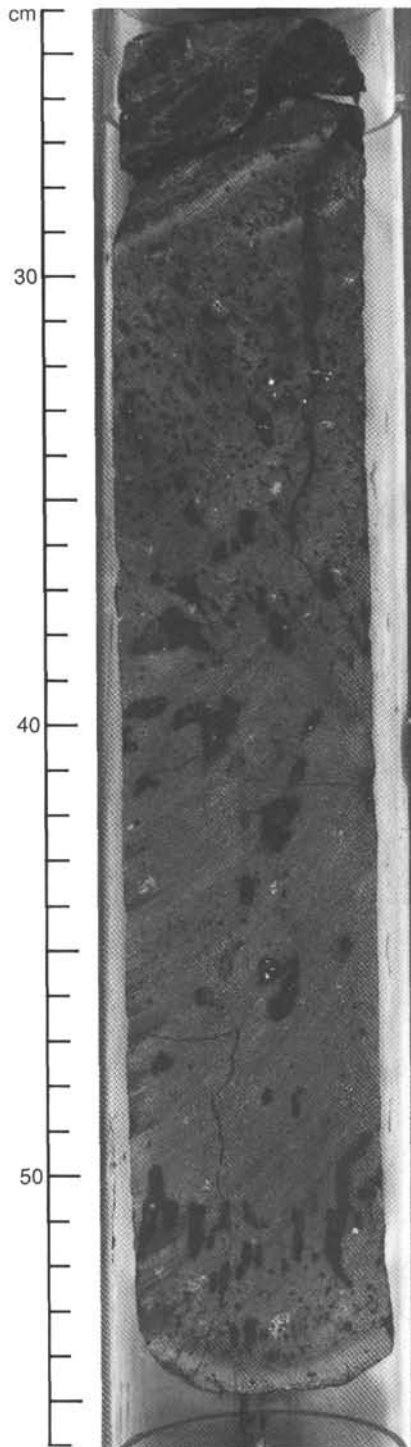


Figure 22. Part of a small pillow of basalt in Unit 758A-F23, with two selvages at 29 and 53 cm and zones of radially-arranged vesicles (Section 121-758A-71R-4, 24–56 cm).

Petrography

Over 20 thin sections of basalts from Site 758 were made; this account presents a preliminary survey of 16. A summary of the petrologic characteristics of each unit is included in Table 5; the modal data are summarized in Table 7.

Table 6. XRD secondary mineral determinations, Hole 758A.

Core, section, interval (cm)	Shipboard data-base file number	Location	XRD determination
55R-1, 72–73	252UBN.RD 259UBG.RD	Vein	Saponite or nontronite calcite, quartz
55R-6, 47–48	251UBN.RD 258UBG.RD	Fracture	Saponite, calcite
57R-3, 6–7	255UBN.RD 265UBG.RD	Vein	Chlorite/smectite, opal
58R-2, 48–49	253UBN.RD 260UBG.RD	Vein	Chlorite/smectite
58R-4, 110–111	254UBN.RD 261UBG.RD	Fragments of vein	Chlorite-smectite
59R-5, 74–75	268UBN.RD 269UBG.RD	Thick vein	Quartz, chlorite-smectite
60R-1, 88–89	256UBW.RD 266UBG.RD	Flow contact	Saponite, calcite
61R-3, 82–83	257UBN.RD 267UBG.RD	Vein	Chlorite-smectite, quartz
62R-1, 108–109	262UBN.RD 270UBG.RD	Cavity filling	Ankerite
62R-2, 16–17	263UBN.RD 271UBG.RD	Thick vein	Chlorite-smectite
62R-2, 53–54	264UBN.RD 272UBG.RD	Thick vein	Chlorite-smectite, quartz, calcite
66R-6, 95–96	281UBN.RD	Vein fragments	Chlorite-smectite, plagioclase
70R-2, 31–32	283UBN.RD	Altered selvage	Chlorite-smectite, plagioclase
71R-2, 90–91	284UBN.RD	Altered selvage	Smectite-chlorite
71R-2, 93–94	285UBN.RD	Altered selvage	Smectite-chlorite, quartz

Primary Igneous Mineralogy

Massive Flow Units

The upper flows from Hole 758A are predominantly aphyric or sparsely plagioclase-phyric. In some of these units, internal chilled contacts have clear textural evidence of quenching. There are variations in the abundances of the phenocrysts across these contacts. For example, Figure 23 shows that the coarse facies is plagioclase-phyric, while the finer-grained, chilled facies is aphyric. This suggests that the chill contacts separate truly distinct magma batches. The massive units appear to be olivine free, but more detailed studies will be required to ascertain this. Flow Unit 758A-F17 is highly clinopyroxene-plagioclase-phyric, with approximately 20% pale green-brown pleochroic clinopyroxene phenocrysts.

The massive flows have an unusual texture, consisting of stellate glomerocrysts over 2 mm across in a very fine-grained, probably originally glassy, mesostasis. The proportion of mesostasis can be as high as 70%, although in all of the studied samples, the mesostasis is now replaced by smectite. The glomerocrysts are aggregates of augite and plagioclase, with intergranular opaques that commonly show skeletal overgrowths. The association of relatively coarsely crystalline doleritic glomerocrysts in such a glassy groundmass (hyalophitic texture) presumably reflects rapid cooling during the final stages of emplacement of the magma. Toward the margins of the units, and within the thin internal chill zones, the crystal size distinctively decreases to fine grained and even cryptocrystalline.

The massive units are sparsely vesicular; the vesicles are usually located in the mesostasis.

Sheet Flows and Pillow Basalts

Flow Unit 758A-F4 is highly plagioclase-phyric, with over 10% plagioclase phenocrysts, but the majority of the units are aphyric or contain small amounts of olivine and/or clinopyroxene phenocrysts. Several units have trace amounts of olivine

phenocrysts (now completely replaced by green smectite), but the olivine is subordinate in abundance to the plagioclase. Pyroxene-phyric units appear to be restricted to flow Unit 758A-F14 and below (cf. flow Unit 758A-F17), as mentioned previously.

The groundmass textures of these units reflect rapid cooling: granular through variolitic to spherulitic, showing a range of quench textures typical of submarine basalts. Skeletal plagioclase microlites and plumose clinopyroxene are common. Mesostasis is usually replaced by brown and green clays.

The sheet flows and pillow basalts are variably vesicular. The proportion of vesicles is as much as 20%, but is usually much less.

Secondary Mineralogy

All of the basalts from Hole 758A show evidence of alteration. The massive units are pervasively altered, showing total replacement of mesostasis by brown and olive-green smectites. The original igneous mineralogy of augite, plagioclase, and opaques is only slightly affected by this alteration, with only minor replacement of the plagioclase cores by clays. The vesicles are filled with black, brown, or green smectites, or more rarely by calcite.

The more rapidly quenched pillow basalts and sheet flows show a similar secondary mineralogy, suggesting that there is no significant downhole variation in the alteration profile. In this and other respects, the alteration history of Site 758 is different than that of Sites 756 and 757. For example, no zeolites are found at Site 758, although more detailed studies are required to confirm this. The majority of the fractures and vesicles are filled with soft brown and green smectites and fibrous chlorite-smectites (Table 6), and calcite also occurs. Late-stage oxidative alteration associated with calcite veins, as observed at Sites 756 and 757, is not seen. All of the units studied contain sulfide (iron pyrite?) phases.

The alteration of the basalts from Site 758 has apparently caused a decrease in their seismic velocity, in comparison with the values from Sites 756 and 757 ("Physical Properties" section, this chapter). The relatively decreased seismic velocity is probably related to the high proportion of clays in the Site 758 samples. At one stage during the visual core description, we noticed that the ends of long, continuous core sections bowed upward by 1–2 cm. Again, this was attributed to the drying out of the clay minerals.

Geochemistry

Nineteen basalts were analyzed for major and trace elements by X-ray fluorescence (XRF) (Table 8). As at the other Ninetyeast Ridge sites, basement basalts from this site have distinctive geochemical characteristics that require different parental magma compositions. The deeper penetration at Site 758 also demonstrates significant downhole variability in composition. These different parental magma compositions may require compositionally distinct sources, but this requires confirmation by shorebased isotopic analyses.

The basalts are tholeiitic, with 48% to 50% SiO₂, and only one sample contains more than 1.52% TiO₂. Although there are no systematic geochemical trends as a function of depth (Fig. 24), several distinct compositions occur in the recovered core. The uppermost flow units, 758A-F1 through 758A-F3, which form massive flows (Table 5), are relatively evolved as measured by the FeO*/MgO ratio (Fig. 25), but they do not have higher abundances of Ti, Zr, and Nb (Figs. 26 and 27). These massive basalts also have unusually low Na₂O contents (1.83% to 2.05%; Fig. 28).

Plagioclase-rich flow Unit 758A-F4 has a high Al₂O₃ content (~19.7%), which may reflect accumulation of plagioclase. However, these lavas have high Cr and Ni contents (e.g., Fig. 29) that

are not explainable by plagioclase accumulation alone. Apparently, this unit formed from a compositionally distinct parental magma.

Flow units 758A-F7 through 758A-F27 have relatively high MgO contents (8.65% to 11.28%), which are higher than any basalts from Sites 756 and 757 (Fig. 28). These high MgO contents are not accompanied by a high Ni content (maximum of 123 ppm). The lack of a MgO-Ni correlation (Fig. 29) indicates that olivine fractionation was not a major process in generating these lavas. The pillow lava Units 758A-F19, 758A-F21, and 758A-F25 are not compositionally distinct (Table 8) from the nonpillowed flows. Flow Units 758A-F14 and 758A-F17, however, have distinctive compositions (e.g., Fig. 28).

In several trace element abundance characteristics, Site 758 lavas fill in the gap between basement basalts from Sites 756 and 757 (e.g., Figs. 26 and 27). However, they extend the V-Nb trend of Site 757 basalts (Fig. 30). The Zr/Nb ratios in Site 758 basalts are intermediate between basalts from Sites 756 and 757, but Site 758 basalts define a different Y/Nb-Zr/Nb trend than that of the Site 757 basalts (Fig. 31). This difference could reflect different end-member compositions on the mixing trend of mid-oceanic ridge basalt (MORB) to ocean island basalt (Fig. 32), or Y/Nb may have been affected by crustal processes such as clinopyroxene fractionation.

Relative to estimates of primitive mantle composition, basalts from Site 758 are depleted in highly incompatible elements (Fig. 32). Relative to most ocean island basalt compositions, several Site 758 basalts have very high K/Rb ratios (>1000), seven samples have <0.5 ppm Rb, and seven have atypically low K₂O/P₂O₅ (<1) (Table 8). These low abundances of highly incompatible elements may reflect the depleted nature of the MORB mantle component, but the low concentrations of large-ion lithophile elements could result from alkali loss during secondary alteration.

Twelve samples from the bedded ash units, overlying the lavas, were analyzed for trace elements. The results (Table 9) must be interpreted with caution because the ash layers are altered and diluted by unknown amounts of biogenic carbonate and silica. Nevertheless, we conclude that the ashes are dominantly basaltic and thus similar to ashes from other sites on Ninetyeast Ridge. The trace element ratios, Y/Nb and Zr/Nb, of the ashes were probably unmodified by alteration and dilution by biogenic material. These ratios in the ashes at Site 758 differ significantly from the ratios of Site 758 basalts; specifically, most of the ashes have lower values for Y/Nb and Zr/Nb (Fig. 33). Similar differences were noted at Site 757 (see "Igneous Petrology" section, "Site 757" chapter, this volume). The ashes are probably the result of phreatic activity in a shallow-water environment, perhaps at some distance (at least 10 km) from the location of Site 758. These results indicate that the magma compositions in these two environments were significantly different.

Conclusions

1. Drilling at Site 758 penetrated 177.9 m of basaltic and minor interbedded tephra. The basaltic sequence is subdivided into 29 lithologic units; three tephra horizons were identified.
2. The basalt units represent submarine flows, ranging in thickness from less than 1 to over 20 m. Morphologically they encompass pillow basalts (near the bottom of the cored sequence), thin sheet flows, and massive sheet flows.
3. The basalts are either aphyric, plagioclase-phyric, or clinopyroxene- and plagioclase-phyric. In the thin sections studied, olivine is a rare phenocryst phase and does not occur in the massive flow units.
4. Geochemically, the Site 758 basalts show no systematic downhole variations. Flow Units 758A-F4 and 758A-F17 are geochemically distinct and also mineralogically distinct. Flow

Table 7. Modal analyses of basalt thin sections, Hole 758A.

	55R-2, 69-73 cm (Piece 1E) ^a	55R-3, 25-27 cm (Piece 1B)	58R-7, 32-36 cm (Piece 1)	59R-7, 52-56 cm (Piece 2)	60R-2, 22-24 cm (Piece 1)	60R-4, 58-62 cm (Piece 1C)	61R-4, 28-33 cm (Piece 1)
Flow unit	758A-F1	758A-F1	758A-F2	758A-F2	758A-F3	758A-F3	758A-F3
Phenocrysts							
Plagioclase (%)	0	10	2-3	<2	tr	<2	<2
diameter (mm)	—	1-2	1-3	0.5	1	1-3	1-3
Clinopyroxene (%)	0	0	0	0	0	0	0
diameter (mm)	—	—	—	—	—	—	—
Groundmass							
Plagioclase (%)	25	35	30	25	30	35	35
length (mm)	0.3-1.0	0.2-1.0	0.5-2.0	0.1-2.0	0.2-0.5	0.5-1.0	0.5-1.0
Clinopyroxene (%)	15	30	20	20	20-25	20	20
diameter (mm)	0.2-0.4	0.2-0.4	0.3-0.5	0.1-1.0	0.2-0.3	0.5	0.5
Opakes (%)	<5	2-5	<5	5	5	5-10	5-10
Secondary minerals							
Smectite after mesostasis	60	20	50	50	40-50	>20	>30
^b Smectite after olivine	0	0	0	0	0	0	0
Vesicles (%)	<1	0	2	0	0	0	0
Alteration (%)	60	20	50	50	40-50	>20	30

Note: tr = trace; * = groundmass phases are too small to distinguish accurately.

^a Fine-grained part of an internal chill contact.

^b Mainly olivine phenocrysts and microphenocrysts.

Unit 758A-F4, for example, is plagioclase rich and has a high Al₂O₃ content.

5. The trace element data indicate that the Site 758 basalts fall within the broad field of other Ninetyeast Ridge basalts, indicating an origin from a source with both MORB and ocean island basalt components.

6. The tephra from Site 758 are compositionally distinct from the underlying basalts. This may reflect the different magmatic environments sampled by the tephra (subaerial/phreatic) and the lavas (submarine).

PALEOMAGNETICS

Susceptibility

The susceptibility data from Site 758 (Fig. 34) show very distinctive variations at both long and short wavelengths. The short-wavelength data from the APC-cored sequences (Cores 121-758A-1H to 121-758A-11H, 0-102.6 mbsf; 121-758B-1H to 121-758B-10H, 0-96 mbsf; and 121-758C-1H, 0-9.4 mbsf) were useful in correlating cores from the three holes. This correlation is discussed separately in this section. Here, we discuss the more general features of the susceptibility data from Hole 758A.

The base level of susceptibility starts at around 10⁻⁵ cgs units and rises slightly to a maximum at about 10 mbsf and then falls to a minimum (about 5 × 10⁻⁶ cgs units) at about 30 mbsf. There is a second slight maximum around 60 mbsf and then a drop to consistently low values (below 5 × 10⁻⁶ cgs units) at 80 mbsf. Superimposed on this base level are numerous short-wavelength features. Some of these can be ascribed to ash layers, but most are apparently the result of subtle lithologic variations that are not as yet understood. Susceptibility values remain low to about 110 mbsf. This behavior is puzzling because the bottom of this unit corresponds to an increase in the sedimentation rate ("Biostratigraphy" section). If this increase in sedimentation was caused by an increase in terrigenous input, an increase in susceptibility would be expected instead of a min-

imum. There is no evidence, however, for an increase in biogenic sedimentation, which would tend to reduce the susceptibility. The matter remains unresolved for the present.

The interval from 100 to about 280 mbsf, corresponding to the lower part of lithologic Subunit IB and the upper part of Subunit IIA (nannofossil ooze and chalk), has generally higher susceptibility values (from 2 × 10⁻⁶ to 15 × 10⁻⁶ cgs units), with spikes as high as 50 × 10⁻⁶ cgs units. From 280 to 325 mbsf (calcareous chalks of the lower part of lithologic Subunit IIA and the upper part of Subunit IIB), base levels are higher and more variable (5 × 10⁻⁶ to 5 × 10⁻⁵ cgs units), with spikes as high as 2 × 10⁻⁴ cgs units. The calcareous clays and tuffs of the lower part of lithologic Subunit IIB and Units III and IV (325-498.6 mbsf) show a very irregular susceptibility pattern. Base levels are higher (2 × 10⁻⁵ to 10⁻⁴ cgs units) than in the overlying sequence and increase downward. Spikes are as high as 3.5 × 10⁻⁴ cgs units. The exceptionally high peak at 465.5 mbsf may be due to drilling contamination.

The lowermost lithologic Subunit V (498.6-676.8 mbsf) basalts of Campanian age have susceptibility values varying irregularly between 10⁻³ and 5 × 10⁻³ cgs units. Many of the apparently low values on the susceptibility profile (Fig. 34) correspond to gaps between individual basalt pieces and do not represent true susceptibility. A markedly low susceptibility interval in the upper part of Unit V (510-520 mbsf) corresponds to an interbedded clayey tuff with micrite.

Remanence

Sediments

The natural remanent magnetization (NRM) of all but the most disturbed archive-half cores from Hole 758A, down to Core 121-758A-51R (460.2-469.9 mbsf), and all of the cores from Holes 758B and 758C was measured with the cryogenic magnetometer. Cores below 121-758A-51R could not be measured with this instrument because the high remanent intensities were well above its dynamic range.

Table 7 (continued).

62R-1, 44-48 cm (Piece 4A)	62R-3, 8-13 cm (Piece 2)	63R-6, 44-48 cm (Piece 1B)	64R-3, 37-38 cm (Piece 6)	65R-3, 52-57 cm (Piece 1A)	67R-4, 84-88 cm (Piece 3)	67R-4, 106-110 cm (Piece 4)	68R-1, 51-54 cm (Piece 4)	69R-4, 43-46 cm (Piece 1C)
758A-F4	758A-F4	758A-F7	758A-F8	758A-F10	758A-F14	758A-F15	758A-F16	758A-F17
10	10	0	0	tr	10	10	0	5
1-4	2-6	—	—	4	<1	0.5-3	—	1-3
0	0	0	0	0	<5	0.5-2	0	20
—	—	—	—	—	0.1	5	1-3	—
40	30	40	30	40	*	*	40	30
<0.2	1-2	1-2	0.1-0.5	0.5-1.0	*	*	0.1-1.0	0.5-1.0
30	40	40	30	15	*	*	15	15
<0.1	<4.0	1.0	0.5	0.2	*	*	<0.5	<0.5
2-3	2-3	<5	2	<5	*	*	2-3	5
10-20	5	10-15	30	30	*	*	40	20
1	2-5	0	0	0	*	*	0	0
5	0	5-10	15	0	0	>10	15	0
10-25	50	15	30	30	>10	>10	40	20

Variations in NRM intensity after alternating field (AF) demagnetization at 9 mT in lithologic Unit I (0-121.7 mbsf) clearly reflect variations in susceptibility. NRM intensity varies gradually throughout this unit over nearly three orders of magnitude, from 10^{-2} to 10 mA/m (Fig. 35). This is in marked contrast with the underlying sedimentary sequence (Fig. 36). Throughout lithologic Units II and III (121.7-431.2 mbsf) the remanent intensity after 9-mT AF demagnetization shows a remarkably stable base level, which increases slowly and gradually from about 1 mA/m at the top of Unit II to 120 mA/m at the base of Unit III. In contrast to Unit I, the remanent intensity pattern of Units II and III does not follow the main variations in the susceptibility pattern, other than a general increase in intensity with depth. The interval between 310 and 320 mbsf is the only exception. A susceptibility spike flanked by susceptibility lows is reflected in remanence lows down from 10 to 0.1 mA/m. The lows correlate with the presence of cherty zones. Intensities throughout Unit IV (431.2-498.6 mbsf) increase downward from 50 to 3000 mA/m at 465 mbsf, the lowest core (121-758A-51R) measurable on the cryogenic magnetometer.

The polarity record of lithologic Unit I is exceptionally good and is discussed in detail in the following. At this stage the polarity record for the remainder of the sedimentary section is poor and cannot be confidently correlated to the geomagnetic reversal time scale (GRTS). This is due partly to poor recovery and drilling disturbance (Cores 121-758A-27X to 121-758A-29X, 121-758A-37X, 121-758A-40X, 121-758A-46X, and 121-758A-49R) and partly to the absence, at present, of detailed biostratigraphic control and discrete sample demagnetization data. Detailed interpretation awaits further shorebased studies, but some general observations can be made.

The Oligocene to lower Miocene sequence appears to have predominantly reversed polarities in the interval 170 to 235 mbsf, apart from a short normal polarity sequence at 182 to 183 mbsf. This sequence cannot be interpreted in terms of the GRTS (Berggren et al., 1985), apart from representing an interval or intervals, between Chrons C12 and C6C (Fig. 36). Reversed polarity intervals in the reduced Paleocene sequence (277-296 mbsf) cannot be identified more precisely than Chron C27R and/or C28R (Fig. 36). Likewise, the normal/reversed sequence in the

uppermost Maestrichtian (296-305 mbsf) cannot be defined more precisely than Chron C30 or C31. The presence of a short normal polarity interval (296-297.5 mbsf) suggests that Chron C29R occurs within the hiatus at the Cretaceous/Tertiary boundary interval.

Only the underlying sequence (305-465 mbsf) can be identified with reasonable certainty as Chrons C31R to C33N (Fig. 36), with Chron C33N covering a long interval between 340 and 465 mbsf. Current paleontological control suggests absence of the lowermost Campanian. This is consistent with the absence of Chron C33R in the section down to 465 mbsf (Core 121-758A-51R).

Basalts

The initial remanence of 170 basalt samples from Cores 121-758A-55R to 121-758A-73R (498.9-676.8 mbsf) was measured with the Molspin magnetometer. In addition, five samples were AF demagnetized in seven to nine steps up to 12 to 16 mT. Initial remanent intensities of the samples ranged from 500 to more than 1000 mA/m (Fig. 37). The average intensity (arithmetic mean = 4.7A/m) for the Site 758 basalts is higher than that of the basalts from either Site 756 (2.1 A/m) or 757 (1.2 A/m). AF demagnetization studies showed very low median destructive field (MDF) values varying from 2 to 8 mT. A univectorial component above 6 mT was obtained in four of the five samples (Fig. 38). The exception, Sample 121-758A-61R-2, 99-101 cm (Fig. 38B), showed a gradual steepening of the magnetization vector up to 10 mT. The demagnetized samples had a stable magnetization vector of normal polarity with two prevalent inclination ranges. Samples 121-758A-55R-2, 108-110 cm, and 121-758A-61R-2, 99-101 cm, showed inclinations higher than -70° , whereas Samples 121-758A-58R-2, 116-118 cm, 121-758A-59R-2, 98-100 cm, and 121-758A-60R-2, 94-96 cm, showed inclinations in the -55° to -61° range. The few samples measured obviously do not allow averaging out of secular variation on a statistical basis. Nevertheless, a discussion of some apparent trends in paleolatitudes serves to illustrate some of the problems that may be faced upon interpretation of more detailed studies.

Corresponding paleolatitudes for the steep inclination group range from 57° to 59° S. This may represent a primary basement

Table 8. XRD analyses of basalts, Hole 758A.

	55R-3, 29–32 cm (Piece 1B)	58R-7, 32–36 cm (Piece 1)	59R-7, 52–56 cm (Piece 1A)	60R-4, 58–62 cm (Piece 1C)	61R-4, 28–32 cm (Piece 1)	62R-1, 44–48 cm (Piece 4A)	62R-3, 8–13 cm (Piece 2)	63R-6, 44–48 cm (Piece 1A)	64R-3, 37–41 cm (Piece 6)
Flow unit	758A-F1	758A-F2	758A-F2	758A-F3	758A-F3	758A-F4	758A-F4	758A-F7	758A-F8
Major elements (wt%)									
SiO ₂	48.99	49.40	49.62	49.70	49.28	48.06	48.47	49.36	49.07
TiO ₂	1.05	1.30	1.17	1.39	1.31	0.96	0.93	1.51	1.50
Al ₂ O ₃	16.09	14.13	14.01	14.13	13.81	19.70	19.75	13.97	15.54
^a Fe ₂ O ₃	11.39	12.77	12.76	12.66	12.80	9.31	8.26	12.66	12.52
MnO	0.14	0.17	0.18	0.16	0.16	0.19	0.16	0.17	0.21
MgO	7.76	8.07	9.26	9.09	8.62	8.66	6.63	8.83	10.46
CaO	11.94	11.37	10.24	10.49	11.13	10.79	13.07	10.65	8.42
Na ₂ O	1.83	1.89	2.05	1.95	1.88	1.82	1.72	1.96	2.20
K ₂ O	0.06	0.11	0.14	0.12	0.12	0.22	0.20	0.11	0.14
P ₂ O ₅	0.07	0.10	0.09	0.10	0.09	0.05	0.06	0.10	0.10
	99.35	99.29	99.50	99.79	99.17	99.76	99.25	99.32	100.13
CaCO ₃	0.08	0.08	0.17	0.42	0.08	0.67	0.67	0.17	0.33
Loss on ignition	0.74	0.90	0.95	2.73	2.38	2.38	1.69	1.30	1.75
^b FeO/MgO	1.32	1.58	1.24	1.25	0.97	0.97	1.12	1.29	1.08
CIPW norms									
Quartz	0.00	0.00	0.00	0.18	0.17	0.00	0.00	0.22	0.00
Orthoclase	0.48	0.66	0.84	0.72	0.72	1.31	1.20	0.66	0.84
Albite	15.72	16.26	17.60	16.70	16.20	15.54	14.75	16.86	18.77
Anorthite	36.00	30.25	29.04	29.80	29.39	45.35	46.20	29.48	32.37
Diopside	19.47	21.78	18.00	18.22	21.52	6.86	15.66	19.35	7.48
Hypersthene	23.70	25.06	27.80	28.93	26.66	20.43	17.67	27.71	28.91
Olivine	0.14	0.00	1.70	0.00	0.00	6.68	0.92	0.00	6.02
Apatite	0.16	0.22	0.20	0.22	0.20	0.11	0.13	0.22	0.22
Ilmenite	2.03	2.51	2.24	2.68	2.54	1.84	1.79	2.92	2.88
Magnetite	2.30	2.59	2.58	2.55	2.60	1.87	1.67	2.56	2.51
Trace elements (ppm)									
Rb	1	2	2	2	<1	2	2	1	<1
Sr	123	135	132	141	129	142	144	134	148
Ba	22	29	29	22	27	20	19	25	18
V	315	356	312	349	323	263	229	351	373
Cr	130	68	59	125	155	330	250	140	216
Ni	73	75	70	75	79	115	123	75	80
Cu	123	163	145	131	130	86	88	130	134
Zn	80	87	73	87	109	66	64	85	85
Y	21	26	23	26	25	14	15	27	20
Zr	54	75	68	77	75	51	50	82	78
Nb	3.5	4.9	4.4	4.6	4.6	3.3	2.8	5.2	5.2
Ce	8	9	12	13	16	5	4	17	9

^a Total iron as Fe₂O₃.^b Total iron as FeO.

magnetization. The sampled basalt sequence cannot be precisely dated at this stage; however, biostratigraphic and magnetostratigraphic evidence suggests a correlation with Chron C33N or possibly with Chron C34N. Based on the present position of Site 758 and the absolute position of the Indian plate within a hot-spot reference frame (Morgan, 1983; Patriat and Achache, 1984; Klootwijk et al., 1985), the expected paleolatitude during the Campanian/Santonian is about 55°S (Fig. 39). Following the same reasoning, the 36° to 42°S paleolatitude range for the latter group suggests acquisition of the magnetization between 60 and 70 Ma. Such low paleolatitudes may be interpreted either as a primary magnetization of a sill emplaced during this time or as a secondary magnetization. Macroscopic examination indicates that the basalts are flows, rather than sills. Pending further studies, it is suggested that these lower inclination components may have been acquired in the same time interval as the extrusion of the Deccan Traps, during a time of increased tectonic activity on the Indian plate. Widespread remagnetization of that age has been established within the Indian subcontinent

(Klootwijk, 1979) and may have occurred in other tectonically active regions of the Indian plate.

Correlation of the APC Sequences in Holes 758A, 758B, and 758C

A major goal of this site was recovery of a complete Holocene to Miocene-Pliocene sequence for paleoclimatic study. Very good recovery with the APC was possible because of the substantial clay content of the Holocene to upper Miocene ooze of lithologic Unit I (0–121.7 mbsf). Eleven APC cores were taken from Hole 758A (0–102 mbsf) and 10 from Hole 758B (0–96 mbsf). Unequivocal mud-line cores were obtained from Holes 758A and 758C. As gaps in core recovery normally occur between successive APC cores, cores in Holes 758A and 758B were staggered in depth with respect to each other. Although cored sequences can be assigned nominal depths from drilling records, these are not sufficiently accurate for high-resolution correlation. At Site 758 it was possible to provide between-hole correlation with a precision of a few centimeters by using a combina-

Table 8 (continued).

65R-3, 52-57 cm (Piece 1A)	67R-4, 69-72 cm (Piece 2)	67R-4, 106-110 cm (Piece 4)	68R-1, 51-54 cm (Piece 1C)	69R-4, 43-46 cm (Piece 1C)	70R-2, 121-124 cm (Piece 7F)	71R-1, 84-88 cm (Piece 13)	71R-3, 116-119 cm (Piece 5A)	72R-3, 48-51 cm (Piece 2)	73R-1, 113-116 cm (Piece 7E)
758A-F10	758A-F14	758A-F15	758A-F16	758A-F17	758A-F19	758A-F20	758A-F23	758A-F25	758A-F27
49.73	49.93	48.50	47.82	49.00	48.45	49.21	48.86	48.74	48.73
1.41	1.92	1.35	1.52	1.25	1.35	1.51	1.27	1.32	1.20
15.39	15.52	15.64	14.59	13.89	15.12	15.54	15.09	15.74	15.59
11.88	12.24	12.75	12.65	12.17	11.97	11.98	11.72	11.45	11.48
0.18	0.28	0.18	0.23	0.20	0.23	0.26	0.22	0.24	0.23
9.77	8.65	10.73	10.64	9.81	10.75	11.28	10.27	9.60	9.34
9.66	9.21	8.53	9.17	11.54	9.44	7.60	9.66	9.74	10.56
2.10	2.41	2.10	2.25	1.67	2.08	2.35	2.04	2.20	1.98
0.06	0.14	0.07	0.09	0.11	0.07	0.23	0.07	0.06	0.05
0.25	0.13	0.10	0.12	0.08	0.10	0.11	0.09	0.09	0.08
100.42	100.44	99.84	99.07	99.71	99.66	100.04	99.28	99.18	99.21
0.17	0.42	0.58	3.08	0.17	0.75	0.50	0.67	0.33	0.33
1.49	1.42	1.70	2.85	1.56	1.94	2.15	1.74	1.46	1.20
1.09	1.13	1.07	1.07	1.12	1.00	0.96	1.03	1.07	1.11
0.00	0.00	0.00	0.00	0.00	0.0	0.0	0.0	0.0	0.0
0.36	0.83	0.42	0.5	0.7	0.4	1.4	0.4	0.4	0.3
17.85	20.49	17.95	19.4	14.3	17.8	20.0	17.5	18.9	17.0
32.54	31.27	33.39	30.0	30.4	32.2	31.5	32.3	33.5	34.0
11.53	11.36	7.18	12.8	22.0	12.0	4.8	12.9	12.4	15.3
30.65	29.42	27.86	12.3	24.6	24.0	28.5	26.5	24.1	24.4
1.44	0.21	7.82	11.2	2.9	8.4	8.3	5.3	5.7	4.1
0.55	0.29	0.22	0.27	0.18	0.22	0.25	0.20	0.20	0.18
2.69	3.67	2.59	2.95	2.41	2.58	2.88	2.46	2.55	2.32
2.38	2.45	2.57	2.57	2.45	2.42	2.41	2.37	2.32	2.32
<1	<1	<1	<1	<1	<1	2	<1	1	<1
144	155	138	136	120	127	138	125	130	121
19	26	15	16	27	13	37	17	12	8
354	417	337	363	299	358	368	344	361	351
215	97	191	111	226	180	185	200	217	130
85	74	72	64	113	76	76	79	80	76
127	171	119	134	119	134	123	122	130	135
66	92	86	93	80	99	89	91	102	83
21	26	20	22	22	20	20	20	20	20
74	102	70	79	68	73	77	69	72	66
3.7	6.2	4.4	5.4	4.1	4.8	4.7	4.8	4.3	3.8
4	14	9	8	6	6	8	10	10	8

tion of magnetic remanence, susceptibility, and distinct lithologic markers such as ash layers (Fig. 40 and backpocket Fig. 41 and Tables 10 through 12). Complete coverage of the Holocene to Miocene-Pliocene sequence was obtained from the combined record of Holes 758A and 758B.

Polarity Record

The magnetostratigraphic record of Holes 758A and 758B is of exceptionally high quality. A complete record of virtually all chrons and events from the Brunhes Chron to Chron 6 (terminology of Berggren et al., 1985) was established for both holes. Only the two Reunion Subchrons were not unequivocally identified from whole-core measurements. A search will be made with a detailed discrete sample study of Hole 758B.

Most boundaries between normal and reversed polarity intervals are sharp and can be located to within about 20 cm (Fig. 40), although some transitions are more prolonged (e.g., subchrons in the Gauss Chron of Hole 758B). A detailed study of several polarity transition records is planned using U-channel sampling of Hole 758B.

The quality of the record enables correlation between both holes (Table 10) with a precision in the order of one or two mea-

surement intervals (10-20 cm). This correlation shows gaps in coverage of individual holes as large as 1 to more than 2 m (Table 12). The most obvious consequence of these gaps is the loss of records of the Olduvai and the Cochiti Subchrons in Hole 758A. These subchrons, however, are recovered in Hole 758B (Fig. 40).

Susceptibility Record

The primary magnetic measurement used for correlation of Holes 758A, 758B, and 758C is the volume susceptibility. This parameter is controlled by the mineralogy, grain size, and concentration of magnetic carriers in the sedimentary sequence. At Site 758, the primary control on susceptibility in lithologic Unit I appears to be the amount of magnetic material present, as suggested by the good correlation between variations in susceptibility and remanence intensity (Fig. 35). The amount of magnetic material, in turn, is probably controlled primarily by the ratio of terrestrial influx to biogenic carbonate production. Further study is required to clearly establish the origin of the susceptibility variations. Susceptibility can be correlated very well between Holes 758A and 758B. The base-level changes are modulated by variations of much shorter wavelength as well as sev-

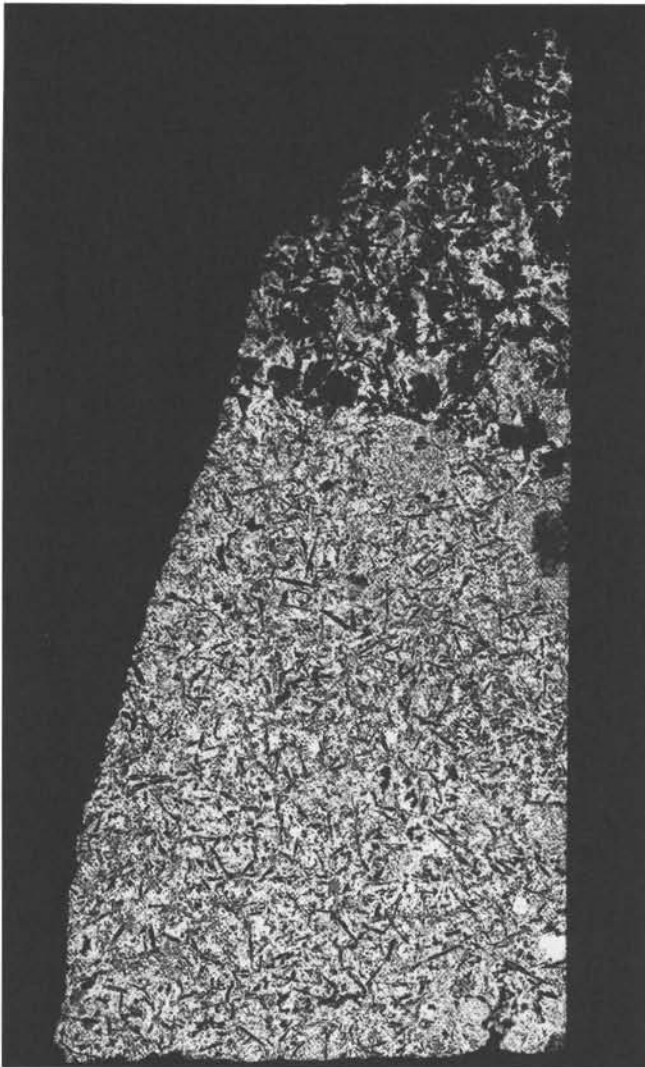


Figure 23. Negative photograph of thin-section Sample 121-758A-55R-2, 69-73 cm, showing fine-grained aphyric basalt chilled against porphyritic medium-grained basalt. This chill zone is an internal contact within flow Unit 758A-F1.

eral large distinctive spikes where ash layers are intercalated with the clayey oozes (Table 11, see also "Lithostratigraphy and Sedimentology" section). The latter two features form the basis for a very detailed correlation between Holes 758A and 758B (Fig. 41, backpocket) and provide a resolution in the order of the measurement interval (3 cm). Corresponding cores in both holes are tied at least at one point, with some at more than 20. In the few cases where the susceptibility record lacked distinctive features (Cores 121-758A-9H to 121-758A-10H, 74-92.8 mbsf, and 121-758B-9H and 121-758B-10H, 74-92 mbsf), the polarity record provided adequate correlation.

Although gaps of up to 2.6 m occur between successive cores, none of these gaps overlap between the two holes. Thus, the combined record of both holes provides continuous coverage of the sedimentary sequence. This record clearly illustrates the necessity of duplicate or triplicate APC coring to obtain a continuous record and the value of such a record for high-resolution studies, as shown by comparison of the susceptibility record of Cores 121-758A-1H, 121-758B-1H (Fig. 41), and 121-758C-1H (not shown here). A curious feature of the susceptibil-

ity record is the double peak found from 2.5 to 3 mbsf in Holes 758A and 758C which is not present in Hole 758B. About 1 m of sediment is apparently missing from Hole 758B. At present, no explanation can be put forward, either in terms of coring or sedimentology.

Eastman-Whipstock Multishot Core Orientation Tool

Although the orientation data from the Multishot were sufficient to aid in polarity determination (Table 13), reversed polarity intervals in the corrected data show a gradual change in declination values with depth (Fig. 40). This drift amounts to 80° clockwise extrapolated over a 100-m interval of Hole 758A and to 80° counterclockwise extrapolated over a 100-m interval of Hole 758B. The pattern is more consistent at Hole 758B than at Hole 758A, where Cores 121-758A-4H and possibly 121-758A-8H do not follow the trend. The drift is not obvious in the normal polarity intervals. The reason for this difference is not clear. This discrepancy may result from incomplete removal of an overprint after 9-mT demagnetization, but it is uncertain whether the reversed or normal intervals maintain the original direction. No explanation can be given at present for the observed sense and magnitude of drift in the two holes. Holes 758A and 758B were drilled in succession with the same drill string. The opposing drift sense in the two holes is not expected if the drift is caused by twisting of the drill string between the Multishot measurement series and pressurizing of the drill string prior to APC shooting.

INORGANIC GEOCHEMISTRY

A major objective of the chemical measurements on pore waters from Leg 121 was to determine the horizontal uniformity of the chemical gradients in the pore fluids. Lateral changes in pore-water chemistry can be related to lithologic changes in the sediments or basalts, structural features of the basement, or the convection of fluids in the basement and possibly even sediments. For more detail see the "Inorganic Geochemistry" section of the "Site 756" chapter. A summary of the overall inorganic geochemistry results is in the "Ninetyeast Ridge Summary" chapter.

Results

Site 758 is at a latitude of about 5°N on Ninetyeast Ridge. The topography is smooth in comparison with that of Sites 756 and 757, although relatively recent deformation affects the whole area (for more detail, see the "Ninetyeast Ridge Underway Geophysics" chapter, this volume). A sediment cap about 500 m thick that consists of 370 m of carbonate-rich sediments and 140 m of calcareous clay and ash overlies a sequence of volcanic units, which consists of thick basalt layers and thin tuffs. This entire sequence, in turn, overlies basaltic basement.

The chemical compositions of the pore fluids from Site 758 are given in Table 14. The alkalinities, magnesium and calcium concentrations, and chloride ion and sulfate ion concentrations from Holes 758A and 758B are plotted as a function of depth in Figure 42.

Changes in pore-water chemistry with depth are moderate at Site 758 in comparison with previously studied DSDP sites (Lawrence and Gieskes, 1981). Calcium ion concentrations increase with depth to 520 mbsf. Distinct increases in the calcium ion gradient were observed at about 330 and 510 mbsf. Magnesium ion concentrations decrease with depth and generally mirror the changes in calcium (see Fig. 42). Alkalinities decrease with depth, with the largest change at about 330 mbsf. Sulfate ion concentrations decrease with depth, with the largest change seen in the deepest sample interval. Chlorinities increase gradually with depth.

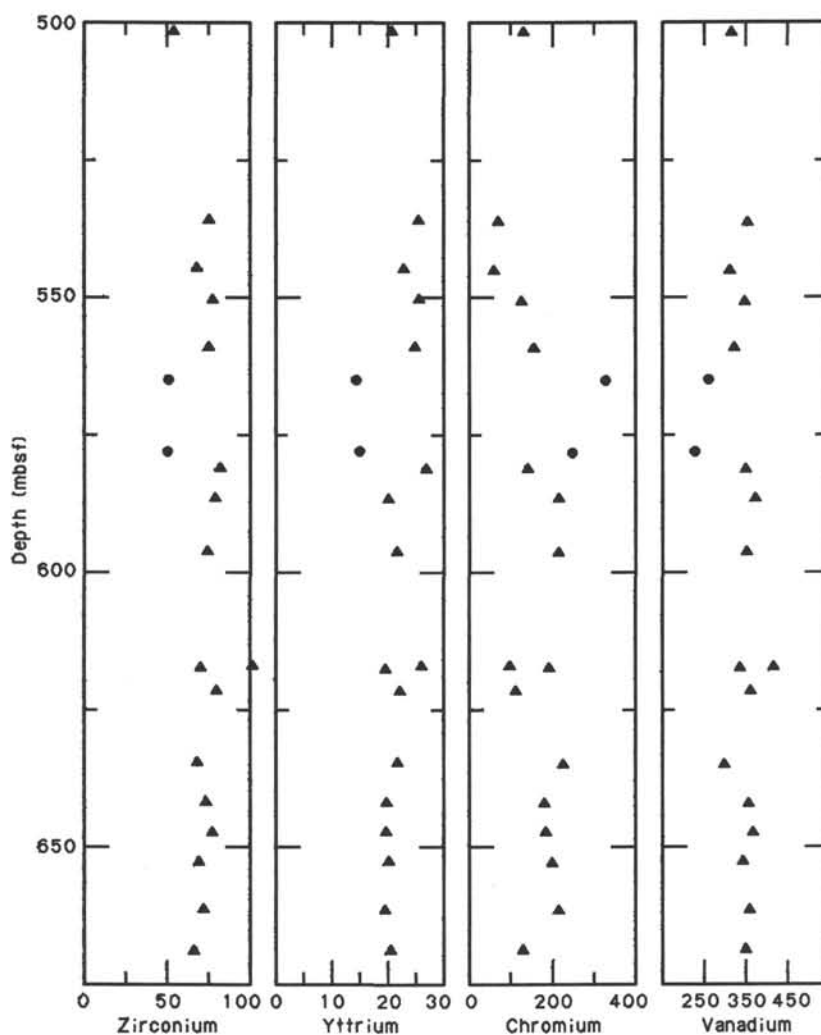


Figure 24. Plot of Zr, Y, Cr, and V abundances in Site 758 basalts as a function of depth. Although there are no systematic trends, there are distinctive compositional units within the core (e.g., the solid circles highlight flow Unit 758A-F4).

Discussion

The gradual increase in calcium and decrease in magnesium ion concentrations with depth is a reflection of the alteration of volcanic ash and basalt (Lawrence and Gieskes, 1981). Both the ash and the basalt are altered to clay minerals (see "Lithostratigraphy and Sedimentology" and "Igneous Petrology" sections). The marked increase in calcium and decrease in magnesium ion concentrations at 330 and 500 mbsf (see Fig. 42) are probably related to lithologic changes in the sediments. A simple interpretation relates steeper chemical gradients to lower diffusivities. For Site 758 this means lower diffusivity below 320 mbsf than above this level. No marked change in physical properties was noted at 320 mbsf; however, a physical-properties boundary at 345 mbsf marks the transition from lower density, higher water content sediments below to higher densities above (see "Physical Properties" section). The chert pebbles and porcellanite layers found below this depth would impede diffusion and thereby increase the chemical gradients. Apparently these materials were not sampled for physical properties. Below 500 mbsf basalt layers occur where another increase in gradient was observed. If the basalt layers are not highly fractured, they may serve to impede diffusion and increase the chemical gradients.

The decrease in alkalinity and sulfate ion concentrations and increase in chlorinities with depth are probably related to the increase in calcium ion concentration that is caused by the alteration of ash. As calcium ion concentration increases, alkalinity decreases as a result of the supersaturation with respect to calcium carbonate. The decrease in sulfate ion concentration with depth may be due to pore-water supersaturation with respect to gypsum at depths beyond the total penetration. The lowermost sample has a markedly lower sulfate concentration than the sample just above it (see Fig. 42). The actual zone of sulfate supersaturation, although not reached at Site 758, was reached at Site 757 (see Table 13 of the "Site 757" chapter).

The increase in chlorinity with depth at Site 758 is most probably a result of water uptake when clay minerals form from the alteration of volcanic material. The marked decrease in chlorinity at 452 mbsf is probably due to analytical error, as indicated by the fact that the salinity at that depth shows no corresponding decrease (see Table 14).

No significant differences were found between the chemical analyses of Holes 758A and 758B, unlike the results from Sites 756 and 757. The separation of the two holes at Site 758 is only 30 m, much less than the separation of 200 m at Sites 756 and 757. In addition, the sedimentary section at Site 758 is much

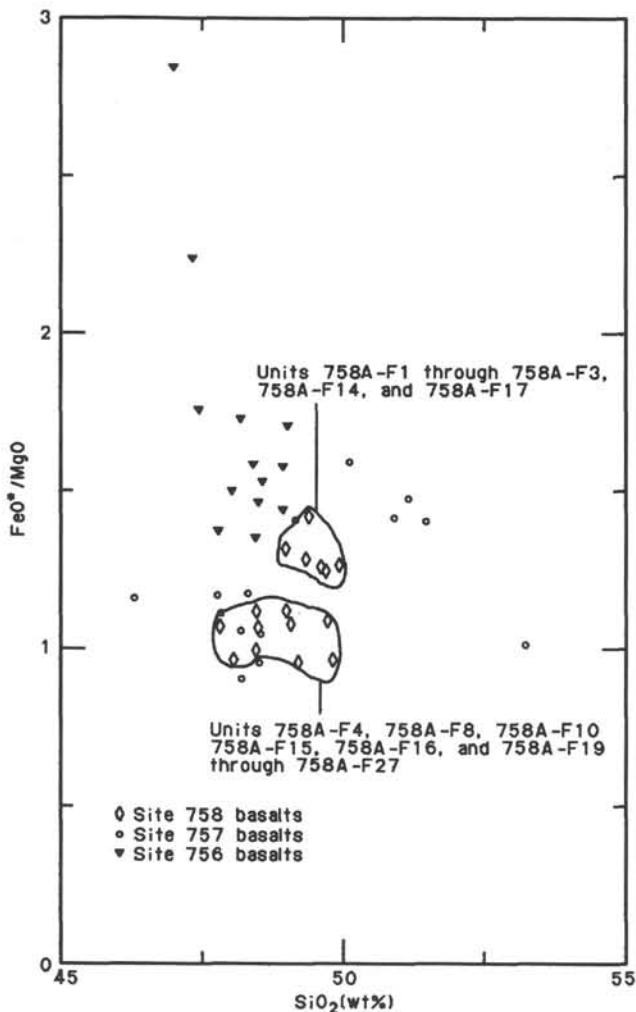


Figure 25. Plot of FeO^* (as total iron)/MgO vs. SiO_2 content illustrating that most of the lowermost flow units at Site 758 are relatively undifferentiated (i.e., $\text{FeO}^*/\text{MgO} < 1.12$). Data for Leg 121 Sites 756 and 757 in this and subsequent figures are from the "Igneous Petrology" sections of those site chapters (this volume).

thicker than at Sites 756 and 757. Lateral changes in water chemistry may exist in the Site 758 area, but they are probably more gradual.

ORGANIC GEOCHEMISTRY

At Site 758 on Ninetyeast Ridge, measurements of hydrocarbon gas concentrations, quantities of total carbon and carbonate carbon, and the bulk geochemical composition of the organic matter by Rock-Eval pyrolysis were performed (see "Explanatory Notes" chapter, this volume, and the "Organic Geochemistry" section, "Site 752" chapter, for analytical details). The Pleistocene to Miocene sections of Holes 758A, 758B, and 758C were studied in more detail in order to obtain data about small-scale variations in calcite percentages. Such variations are probably due to temporal changes in the quantity of terrestrial deposition on the distal southern Bengal fan and might reflect climatic changes (see "Lithostratigraphy and Sedimentology" section).

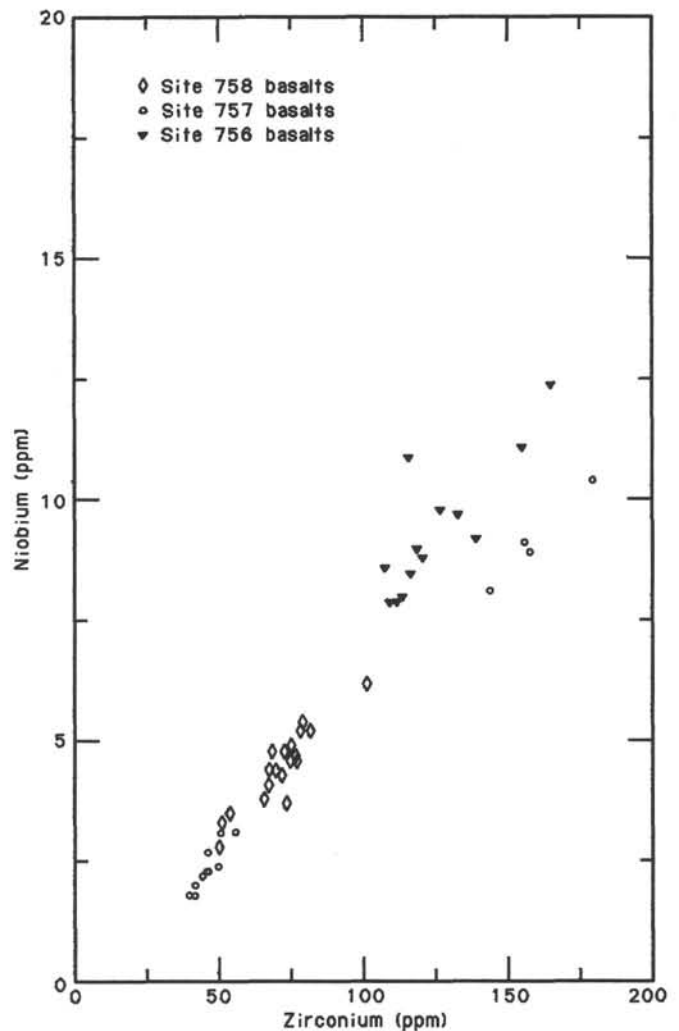


Figure 26. Abundances of Nb vs. Zr in basement basalts from Leg 121 sites. In the linear trend over a large range in abundances Site 758 basalts fill the gap between basalts from Sites 756 and 757.

Gas Analyses

Concentrations of methane in the headspace gases did not exceed 9 ppm. Ethane was detected in only one headspace gas sample (Table 15), and no propane was found.

Organic Carbon

Organic matter occurs mainly in the upper 20 m and below 400 mbsf, but percentages of organic carbon do not exceed 0.9%. The highest amounts of organic matter were found in the uppermost Pleistocene sediments directly below the sediment/water interface (Table 16 and Figs. 43 through 46). The organic matter below 400 mbsf comes from the Upper Cretaceous section. Similar percentages of organic matter were found at Broken Ridge in the lower Maestrichtian and the Turonian to Santonian sections of Sites 754 and 755, respectively.

The hydrogen content of the organic matter, as revealed by Rock-Eval pyrolysis, is low (i.e., less than 140 mg hydrocarbons/g organic carbon was produced during Rock-Eval pyrolysis). Hydrogen contents are slightly higher in the Cretaceous organic matter than those in the Pleistocene (Table 17). The

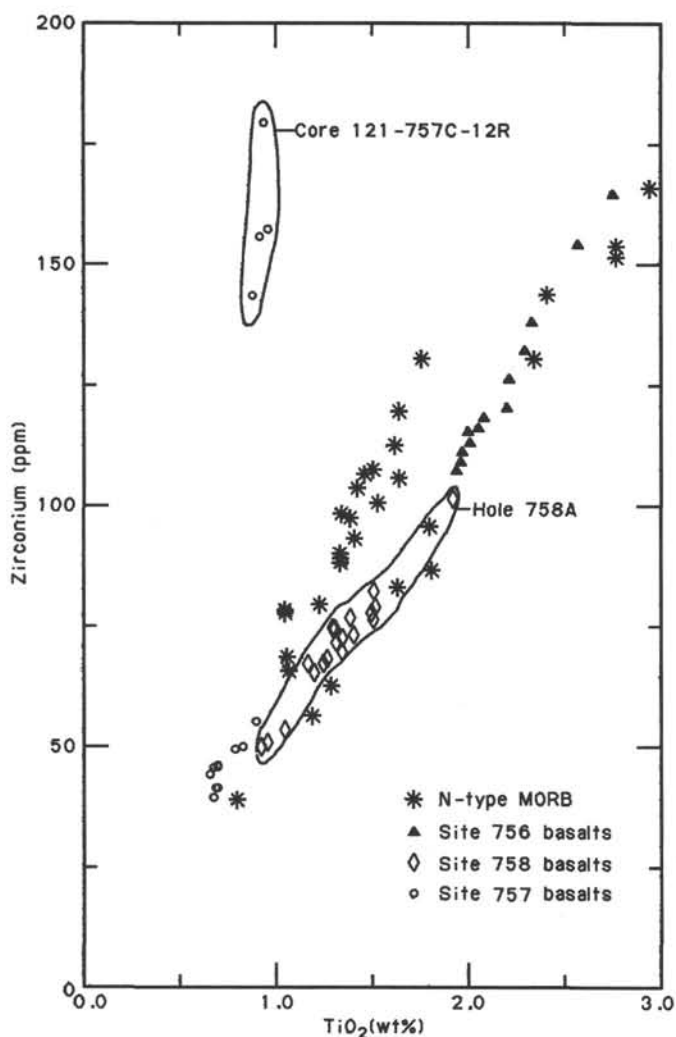


Figure 27. Abundances of Zr vs. TiO_2 in basement basalts from Leg 121. Basalts from each site define a linear trend, with Site 758 lavas filling the gap between the lavas of Sites 756 and 757. Basalts from Core 121-757C-12R have much lower TiO_2/Zr and do not lie on this trend.

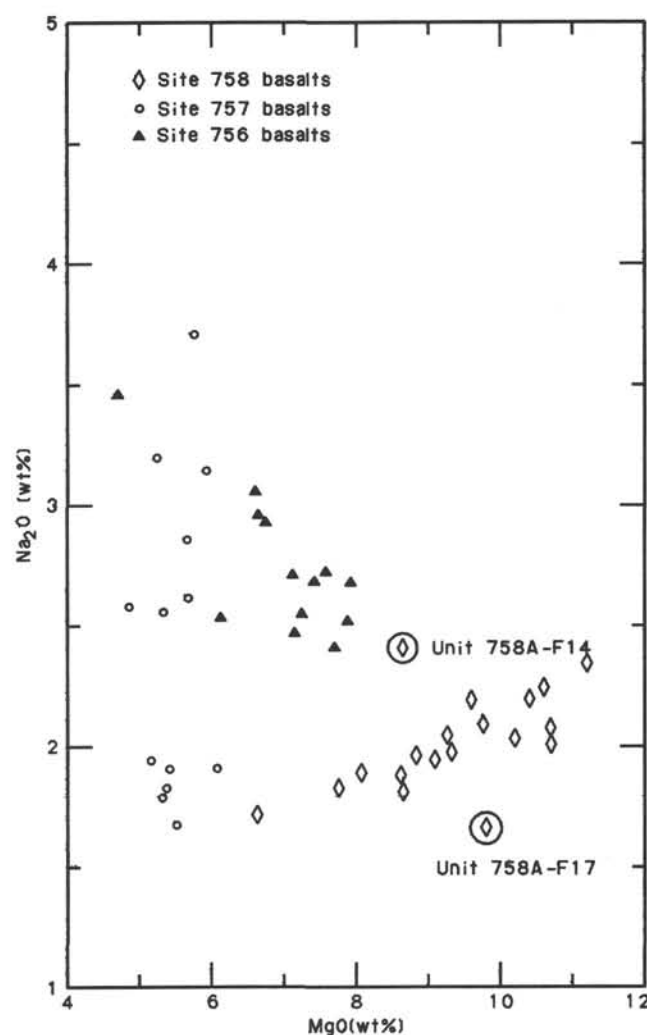


Figure 28. Abundances of Na_2O vs. MgO in basement basalts from Leg 121 sites. Flow Units 758A-F14 and 758A-F17 deviate from the trend defined by the other Site 758 lavas and are also compositionally distinct in other geochemical parameters.

present data indicate deposition of terrestrial rather than marine organic matter in both intervals (see "Geochemistry" section, "Broken Ridge Summary" chapter, this volume; Kemp and Harris, 1975). The high organic carbon content directly below the sediment/water interface points toward an increasing influence of Bengal Fan terrestrial deposition on the northern Ninetyeast Ridge.

Carbonate Carbon

Carbonate contents in the Tertiary sediments at Site 758 are generally lower than those at Sites 757 and 756. From the Pleistocene to Miocene carbonate percentages increase to about 90% (Table 16 and Figs. 43-46). Whereas the general downhole increase of carbonate percentages is quite continuous in the Holocene to middle Miocene interval, there are major fluctuations in the middle to upper Miocene (125-145 mbsf) and in the Pleistocene (0-30 mbsf). The former may be attributed to the initial phase of the hard collision between India and Asia (Klootwijk et al., 1985) and the latter to differences between glacial and interglacial times. Further studies are necessary to test these hypotheses. In the underlying upper Eocene to middle Miocene in-

terval (between 250 and 145 mbsf), carbonate content is almost consistently 87%.

Multiple unconformities in the interval from 260 to 295 mbsf separate the Paleocene section from overlying Oligocene and younger rocks. In the Paleocene, carbonate percentages average 95%. Environmental conditions during the deposition of this facies may have been similar to those in the Neogene at Sites 752-757, indicating nearly exclusive deposition of carbonate at that time. On the other hand, the composition of the Paleocene section at Site 758 differs considerably from the Paleocene drilled at Broken Ridge, where biogenic opal and volcanic ash are major constituents of the sediments.

In the Maestrichtian to Campanian sediments drilled between 300 and 400 mbsf, carbonate percentages decrease downhole from 95% to 15%, reflecting higher proportions of biogenic silica and volcanic ash in the older sediments. The fact that ash contents in the upper Maestrichtian to Paleocene section are much lower than in the same interval on Broken Ridge might suggest that the source of the ash on Broken Ridge was much closer to Broken Ridge than to Ninetyeast Ridge (Kerguelen?) at that time and only of local importance (i.e., Site 758

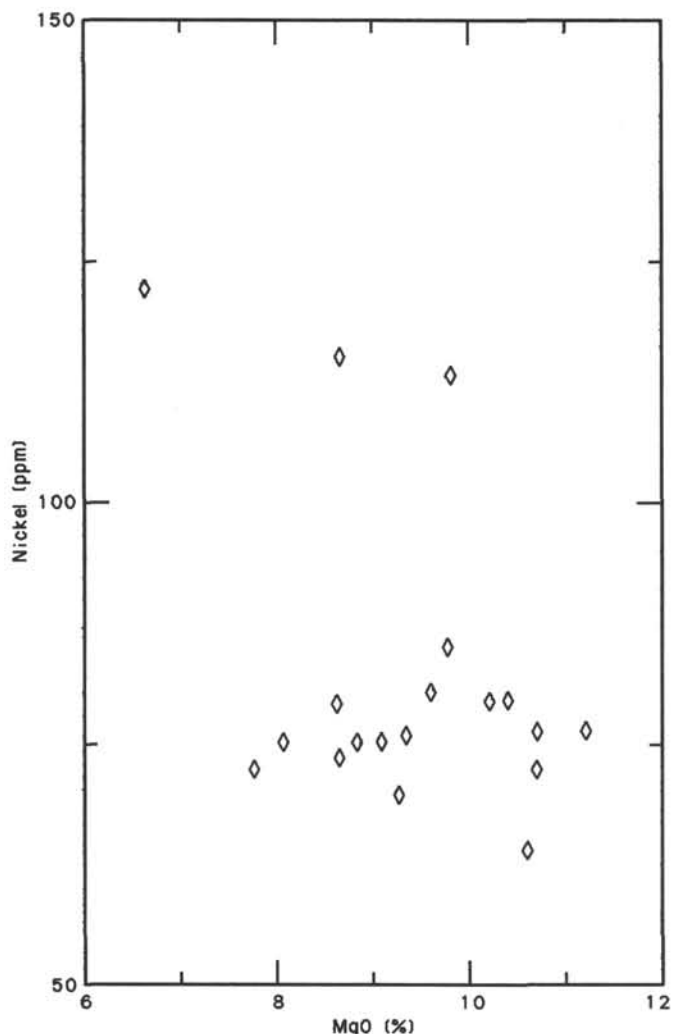


Figure 29. Abundances of Ni vs. MgO in Leg 121 basalts from Site 758. In contrast to many basaltic suites there is no positive correlation between Ni and MgO content. Units 758A-F4 and 758A-F17 have significantly higher Ni contents.

was distal and Broken Ridge was more proximal to the hot spot at that time). On the other hand, the high content of biogenic silica in the Cretaceous and its absence in the Paleocene (see "Biostratigraphy" section, "Site 752" chapter) probably reflect the rapid northward movement of Site 758 out of the silica-favorable higher latitudes.

PHYSICAL PROPERTIES

Three holes (758A, 758B, and 758C) were cored at Site 758. Hole 758A was reentered to achieve the deepest penetration of Leg 121, with a depth of 677 mbsf. Holes 758A and 758B constitute a double-APC sequence to 96 mbsf. Most of the double APC-cored section of Hole 758A (0-72 mbsf) and all of Hole 758B were densely sampled (one to two samples per section) for index properties to provide information about bulk sediment flux into this sedimentary column. Hole 758C is a mud-line core that was not used for the study of physical properties.

Results

Index Properties

Water content (expressed as water weight relative to wet sample weight), porosity, bulk density, dry-bulk density, and grain

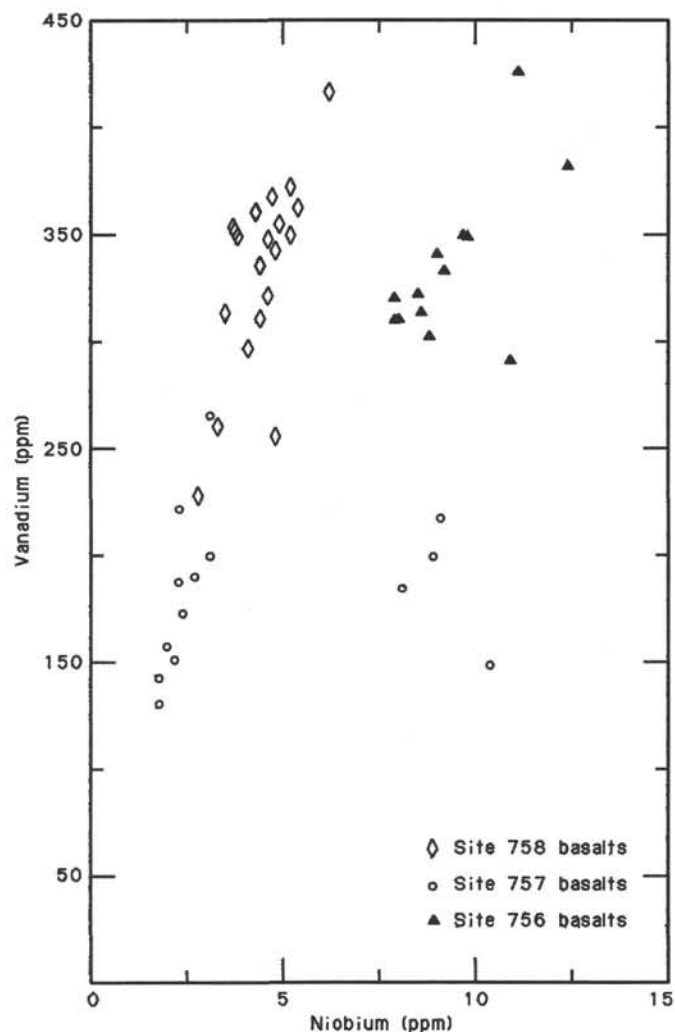


Figure 30. Abundances of V vs. Nb in basement basalts from Leg 121 sites. Each site defines a distinct field; however, basalts from Site 758 extend the trend of the uppermost lavas from Site 757.

(or matrix) density of the samples from Holes 758A and 758B are listed in Table 18 and plotted relative to depth in Figures 47 and 48. GRAPE bulk densities of both Holes 758A and 758B are in good agreement with each other as well as with the wet-bulk densities measured from the laboratory samples (Fig. 48).

Four units are identified in terms of physical properties: unit A (0-247 mbsf), unit B (247-345 mbsf), unit C (345-499 mbsf), and unit D (499-677 mbsf). The boundaries do not coincide with lithologic unit boundaries except for the boundary between units C and D. This latter boundary corresponds to the top of basalt flows at the boundary between lithologic Units IV and V (see "Lithostratigraphy and Sedimentology" section).

Physical-properties unit A is characterized by gradual down-hole increases of wet- and dry-bulk densities and a gradual decrease of water content. The bulk density in unit A increases with depth from 1.45 to 1.75 g/cm³, and the gradient decreases with depth. The gradient of index properties in the upper 5 m of the section is especially high.

A distinct bulk density increase from 1.75 to 2.0 g/cm³ at 247 mbsf marks the boundary with the underlying unit B. Although this boundary does not coincide with that of the lithologic units, the 17.7% recovery of Core 121-758A-27X was unusually poor, perhaps reflecting the change of physical properties at this horizon. Unit B is characterized by constant index

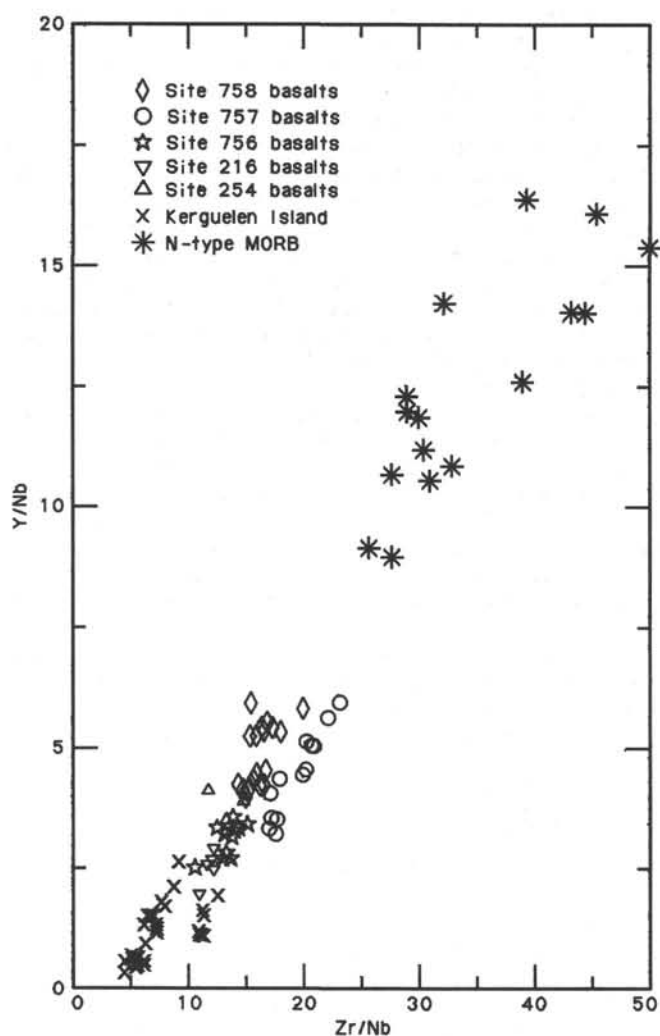


Figure 31. Y/Nb vs. Zr/Nb in basement basalts from Ninetyeast Ridge. The basalts from Sites 757 and 758 overlap in Zr/Nb, but the Site 758 basalts are offset to higher Y/Nb. All the data form an elongated trend between the MORB and Kerguelen fields, but they do not define a single mixing line. Data sources for DSDP Sites 216 and 254, MORB, and Kerguelen are Storey et al. (1988, unpubl. data), Price et al. (1986), Bougault et al. (1979), and Saunders (1983).

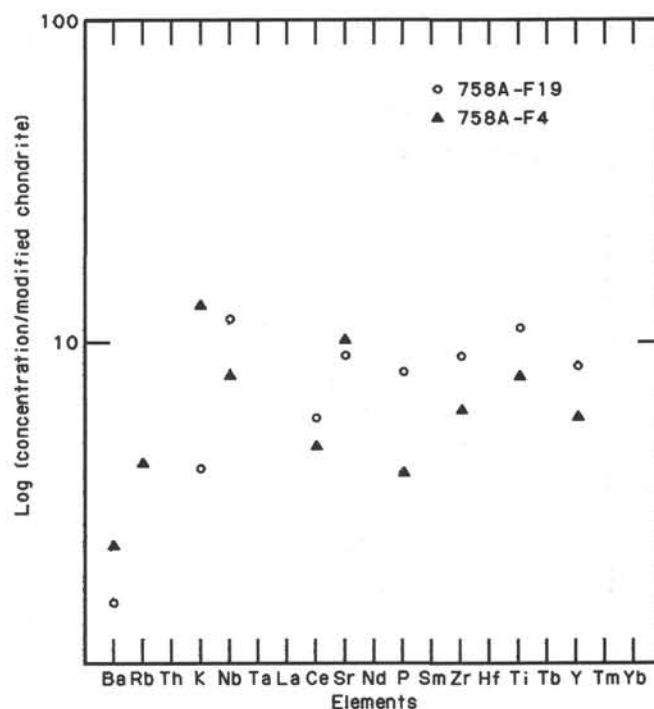


Figure 32. Abundances of incompatible elements in flow Units 758A-F4 and 758A-F19 normalized to chondritic abundances (except for alkali metals and phosphorus). The Rb value is not plotted for Unit 758A-F19 because the Rb content is only 0.3 ppm. Normalizing values from Sun and McDonough (in press).

properties. The mean wet-bulk density in unit B is $1.92 \text{ g/cm}^3 \pm 0.04 \text{ g/cm}^3$.

Unit C shows a large variation of index properties in contrast with unit B. The boundary between units B and C at 345 mbsf is also in a section with unusually poor core recovery (Core 121-758A-37X, 8.3%) and does not coincide with a lithologic boundary. The index properties of unit C are highly variable, especially in the upper half (345–400 mbsf). The bulk density varies between 1.5 and 2.4 g/cm^3 in unit C. The upper part of unit C (345–400 mbsf) has highly variable index properties and is in good correlation with a zone of high magnetic susceptibility (see "Paleomagnetism" section). This correlation suggests that the variation of index properties in unit C may reflect the variation of ash content in chalk (no samples for index properties were taken from the dense ash layers in unit C).

Table 9. XRF analyses of ashes, Hole 758A.

	39X-1, 84–87 cm	40X-2, 60–63 cm	40X-2, 65–68 cm	41X-2, 114–118 cm	41X-5, 22–23 cm	41X-5, 24–26 cm	42X-2, 53–56 cm	48R-3, 80–83 cm	49R-1, 42–44 cm	51R-4, 75–78 cm	51R-4, 90–93 cm	51R-4, 110–113 cm
CaCO ₃ (wt%)	17.91	18.74	15.49	24.66	11.25	16.99	10.16	2.5	1.92	0.33	5.58	9.25
Trace elements (ppm)												
Rb	14	17	12	18	14	14	10	2	4	26	4	8
Sr	384	399	359	460	291	336	500	149	209	141	133	160
Ba	413	476	389	612	419	514	373	38	61	76	166	188
V	294	260	305	214	286	248	347	309	283	401	92	139
Cr	58	42	23	24	33	29	107	146	174	16	16	31
Ni	60	44	58	42	46	44	91	84	54	39	24	31
Cu	135	120	153	86	114	99	143	102	103	59	27	28
Zn	112	96	123	71	145	126	84	57	69	250	60	64
Y	27	24	28	24	21	21	7	28	13	32	12	16
Zr	111	91	99	94	90	92	101	61	67	166	47	55
Nb	9.1	7.7	8.6	8.5	8.8	8.8	6.9	4.6	4.8	13.0	5.7	6.1
Ce	11	8	9	12	6	9	2	10	4	22	9	10

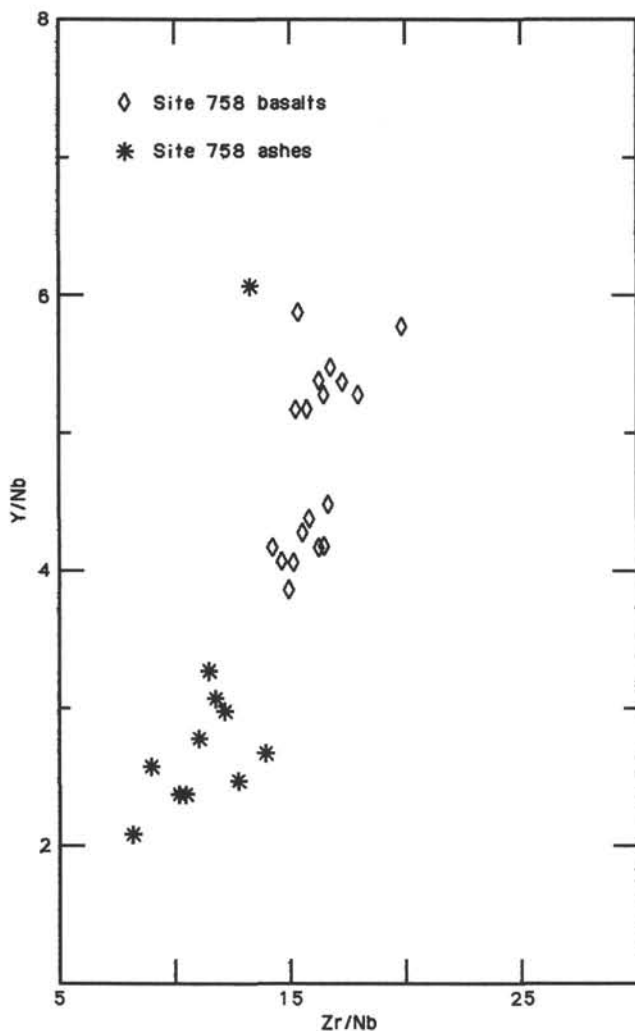


Figure 33. Y/Nb vs. Zr/Nb in basement basalts and the overlying ashes from Site 758.

Unit D corresponds to lithologic Unit V, which contains basalts with interbedded tuff. The low densities of 1.8–2.0 g/cm³ between 500 and 525 mbsf are due to the interbedded tuff layers. The mean value of the basalt bulk densities at this site is 2.66 ± 0.11 g/cm³. The bulk density of basalts decreases with depth (Fig. 47). This variation may reflect lithologic changes from upper massive basalts to lower pillow basalts.

Compressional-Wave Velocity

Compressional-wave velocity data obtained from laboratory samples are listed in Table 19 and displayed in Figures 47 and 48, with the *P*-wave-logger data. Compressional-wave velocity anisotropy was examined by measuring velocities in three directions of propagation. Only velocity A, corresponding to the vertical direction, is displayed in Figures 47 and 48. Acoustic impedance logs, computed from GRAPE and *P*-wave-logger data in the upper part of the hole and from bulk-density and compressional-wave velocity data (velocity A) in the lower part, are displayed in Figures 47 and 48.

P-wave-logger velocities of Holes 758A and 758B are between 1450 and 1580 m/s (Fig. 48). The data from both APC holes do not exhibit the same trends, whereas the GRAPE density data show good agreement. The *P*-wave-logger data of Hole 758A, however, show good agreement with velocity data mea-

sured by using Hamilton Frame. The mismatch of the *P*-wave-logger data of the double APC-cored section may be the result of some mechanical distortion of the cores after their recovery.

The overall velocity variation in Hole 758A shows good correlation with the classification of units based on index properties (Fig. 47). Velocities increase continuously with depth through physical-properties unit A from about 1500 to 1680 m/s. The velocity in unit B shows a small variation between 1600 and 1900 m/s, and velocity in unit C shows a large variation between 1700 and 3600 m/s. The variation of velocity in unit C may reflect the ash content of the chalk, in the same way as the index properties. Velocities measured in the laboratory appear to be lower than those expected from seismic correlation (see "Seismic Stratigraphy" section). The reason for this discrepancy is a matter of debate.

High velocities in unit D represent basalts (3700–6000 m/s), and low velocities are intercalated tuffs (1700–1900 m/s) (Figs. 47 and 49). The mean velocity in the basalts is 4370 ± 470 m/s for 43 samples, which is lower than comparable data for the basalts from Sites 756 (5130 ± 420 m/s for 14 samples) and 757 (4950 ± 390 m/s for 13 samples), even suggesting a gradual velocity decrease to the north.³ This probably results from the more altered nature of the basalts at Site 758 than those at Sites 756 and 757. Figure 49 shows the velocity decrease with depth. This variation may reflect the lithologic change from upper massive basalts to lower pillow basalts, similar to the corresponding decrease of bulk density with depth.

No systematic velocity anisotropy was observed (Fig. 49).

Vane Shear Strength

Records of torque vs. vane rotation were obtained for measurements of vane shear strength in the Hole 758A sediments. The results are shown in Table 20 and Figure 50. The vane shear strength is much higher at Site 758, with a maximum value of 104 kPa at 82 mbsf, in comparison with Sites 756 and 757 on southern and central Ninetyeast Ridge, where the values are generally less than 20 kPa. Shear strength rapidly increases from 17 kPa at 2 mbsf to 104 kPa at 82 mbsf. Below 82 mbsf, shear strengths decrease with depth to 40 kPa at 120 mbsf. The sediments are too stiff to measure vane shear strength between 120 and 250 mbsf, but become soft enough to measure the vane shear strength between 250 and 280 mbsf. The mean strength between 250 and 280 mbsf, 23 ± 10 kPa, is anomalously low compared with the value measured between 0 and 120 mbsf, 63 ± 21 kPa.

The high values of vane shear strength in the upper section reflect the terrigenous clay content in the sediments. The unusual decrease of vane shear strength with depth below 82 mbsf may be due to the smaller terrigenous fraction in the sediments because it matches a downhole calcium carbonate increase (see "Organic Geochemistry" section). The zone of low shear strength below 250 mbsf, first thought to be core disturbance, may indeed have abnormally low strength, as lithologic descriptions suggest that the interval is not disturbed (see "Lithostratigraphy and Sedimentology" section).

Formation Factor

Formation factor was obtained by comparing the electrical resistance of a probe in soft sediment against resistance of the same probe immersed in seawater. The results are shown in Table 21 and Figure 50. Data are lacking between 200 and 260

³ The basement basalts at DSDP Site 254 on the southernmost part of Ninetyeast Ridge have a mean velocity of 4750 m/s for seven samples (Davies, Luyendyk, et al., 1974). Poor penetration and recovery into basement during previous DSDP drilling on Ninetyeast Ridge resulted in a lack of velocity data for basement basalts at other sites.

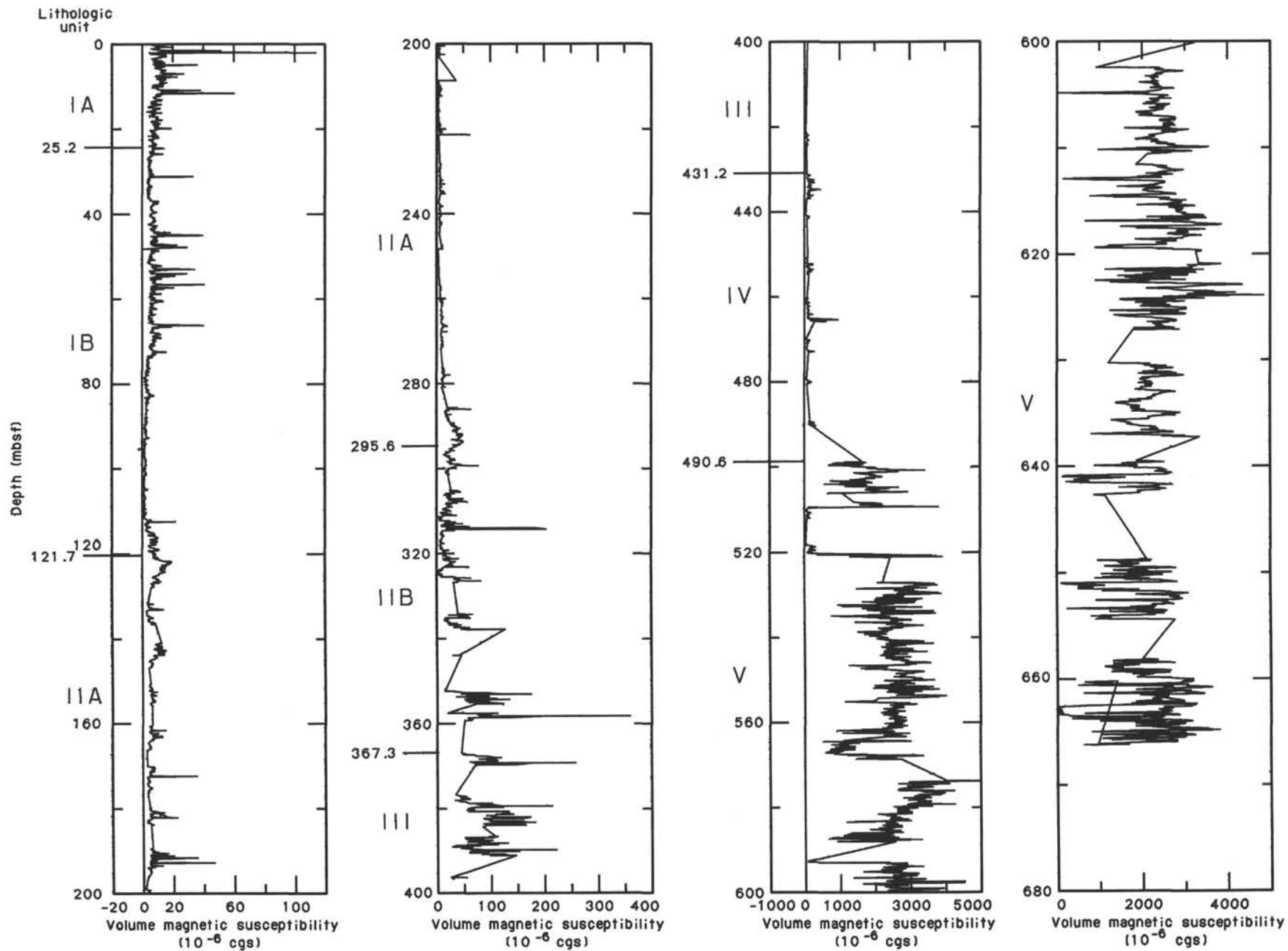


Figure 34. Volume magnetic susceptibility profile for Hole 758A.

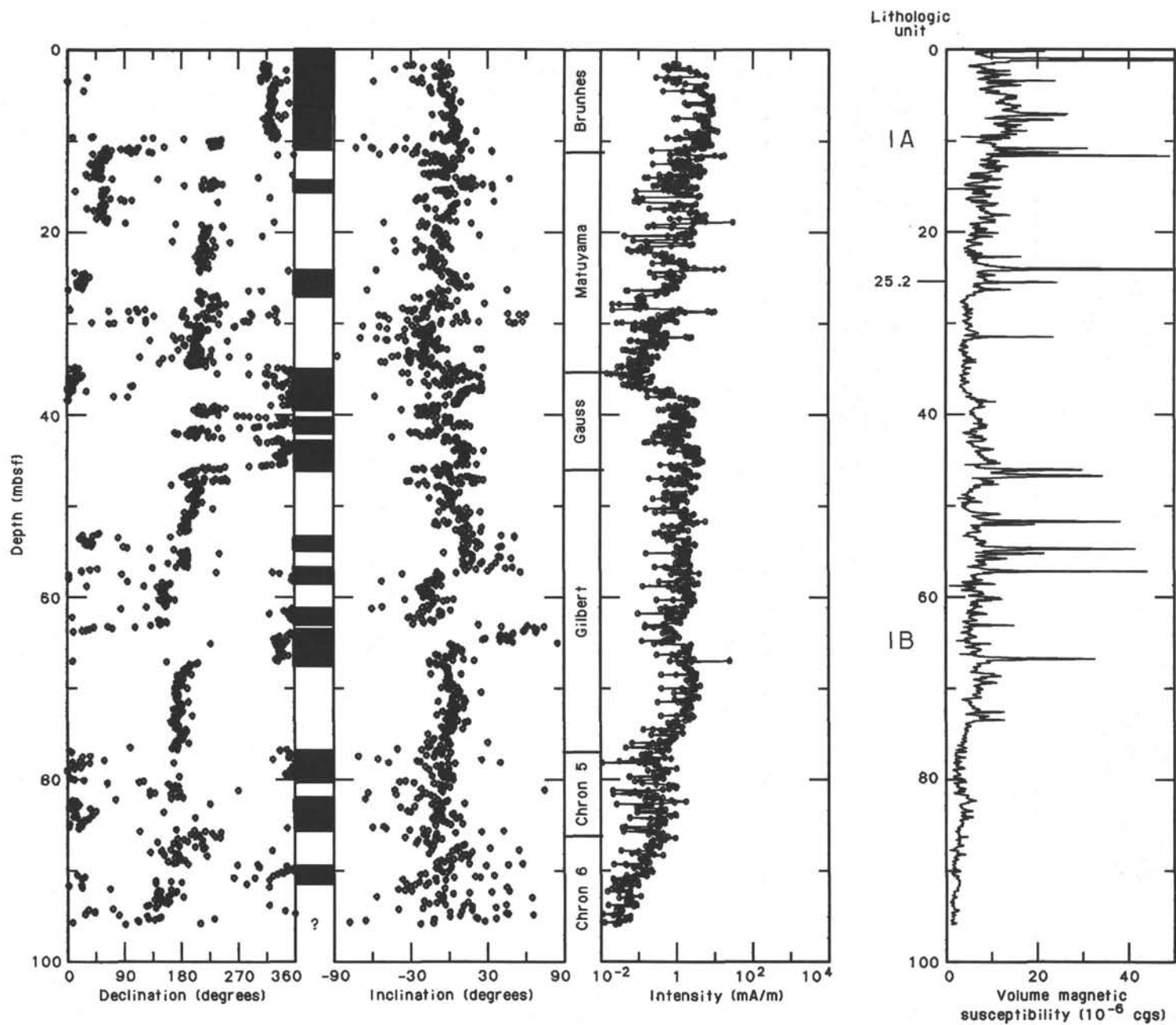


Figure 35. Comparison of susceptibility and remanent intensity after 9-mT AF demagnetization for Hole 758B. Cores 121-758B-1H and 121-758B-2H (0-18.9 mbsf) are not azimuthally oriented.

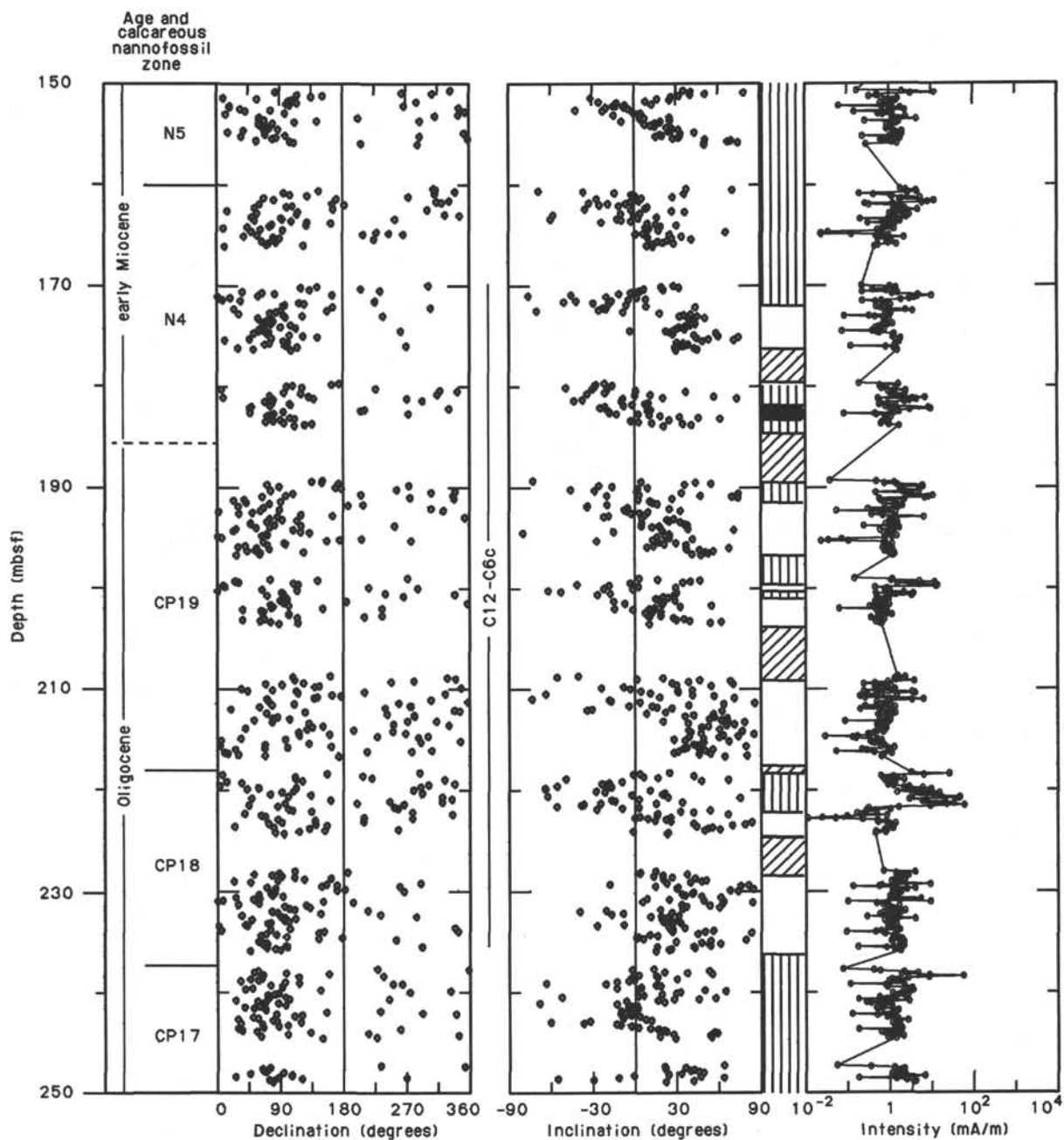


Figure 36. Magnetostratigraphy of Hole 758A below 150 mbsf. Vertical hatching indicates an uninterpretable magnetic remanence signal, normal (reversed) intervals are indicated by black (white), and inclined hatching indicates no recovery or a disturbed section for which remanence was not measured. Possible correlations to the GRTS are shown in the center column.

mbsf because the sediments are too consolidated for probe insertion. However, soft sediments between 260 and 300 mbsf allowed us to resume measuring.

The formation factor of the sediments, 1.3–2.1, is slightly lower at Site 758 than for sediments at Sites 756 (1.3–2.4) and 757 (1.5–2.8) and does not significantly increase with depth, as do the formation factors of Sites 756 and 757.

Thermal Conductivity

Thermal conductivities are reported in Table 22 and displayed in Figure 51. The measurements were done for both sediments and basaltic rocks. Thermal conductivity values continu-

ously increase with depth from less than 1.0 W/m°C at 2 mbsf to 1.8 W/m°C at 670 mbsf. The thermal conductivity vs. depth gradient is steepest in the upper 100 m of the hole, and a simple linear regression that worked at Sites 756 and 757 does not fit the data distribution at this site. The difference may be due to the high clay content of the Site 758 sediments.

Summary

Four physical-properties units, A through D, are identified on the basis of differences in index properties and compressional-wave velocities. The boundaries of units A/B (247 mbsf) and B/C (345 mbsf) are not coincident with those of the litho-

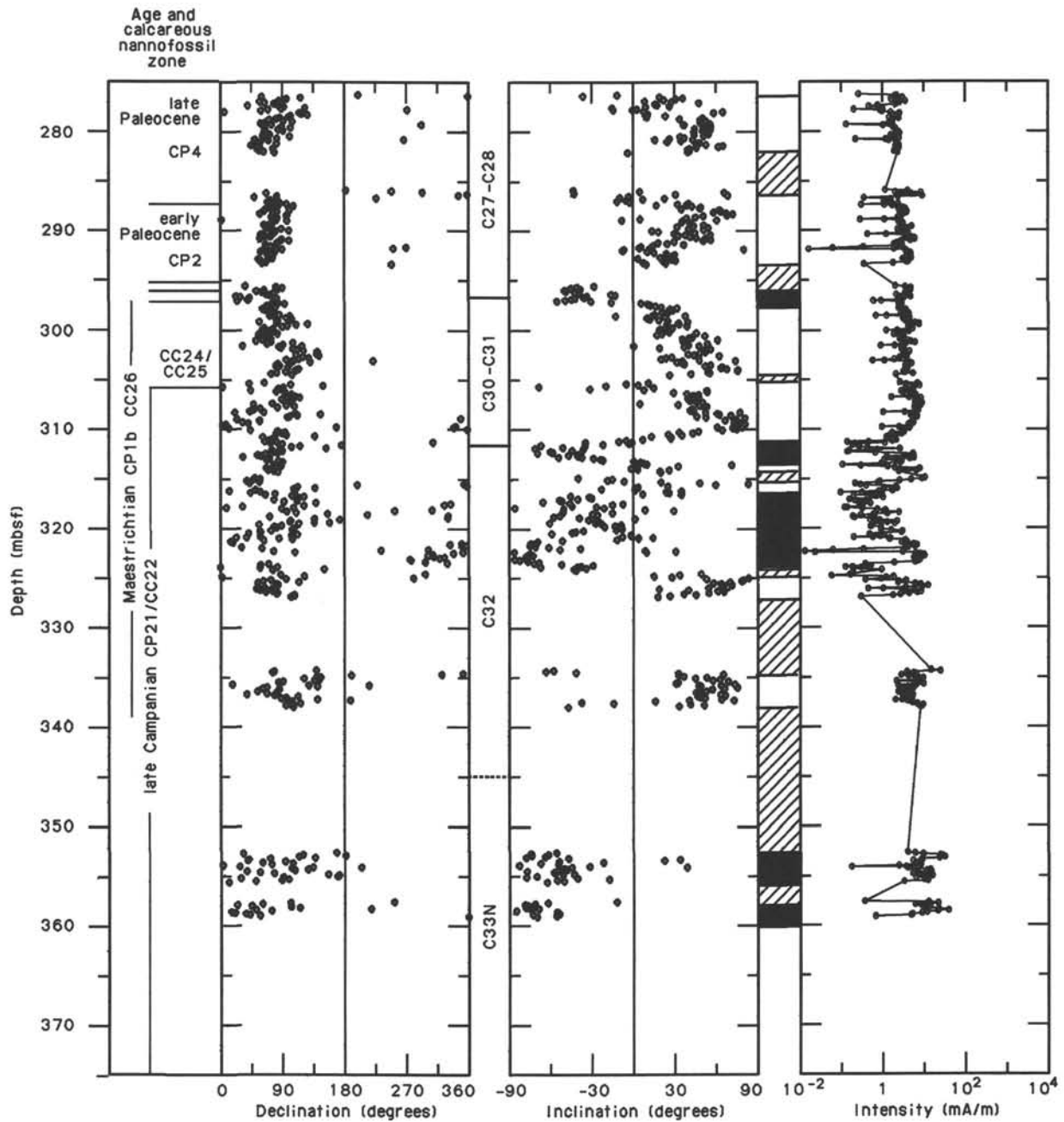


Figure 36 (continued).

logic units. Unusually poor core recoveries at these boundaries suggest that significant changes of physical properties occur at these horizons. The boundary of units C/D (499 mbsf), however, coincides well with the boundary between lithologic Units IV and V.

The variations of vane shear strength, formation factor, and thermal conductivity are different from those of Sites 756 and 757. Vane shear strength, generally higher than the values measured at Sites 756 and 757, shows an unusual decrease with depth between 82 and 125 mbsf and a zone of unusually low shear strength at 260–290 mbsf. The increase of formation factor with depth is lower than that at Sites 756 and 757. The mean velocity of basalts, 4370 ± 470 m/s, is the lowest measured at

the three Ninetyeast Ridge sites (Site 756 = 5130 ± 420 m/s and Site 757 = 4950 ± 390 m/s).

The index properties of the Site 758 sediments reflect the lithologic changes related to a history of prolonged northward travel of the site from high southern latitudes to an equatorial area close to modern volcanic arcs and to the Himalayan orogeny.

GEOPHYSICAL WELL LOGGING

The logging plan at Site 758 included four tool strings: the seismic stratigraphic, the lithoporosity, the geochemical, and the borehole televiewer (BHTV) (see "Explanatory Notes" chapter). Water depth at Site 758 is 2924 m, and hole depth is 677

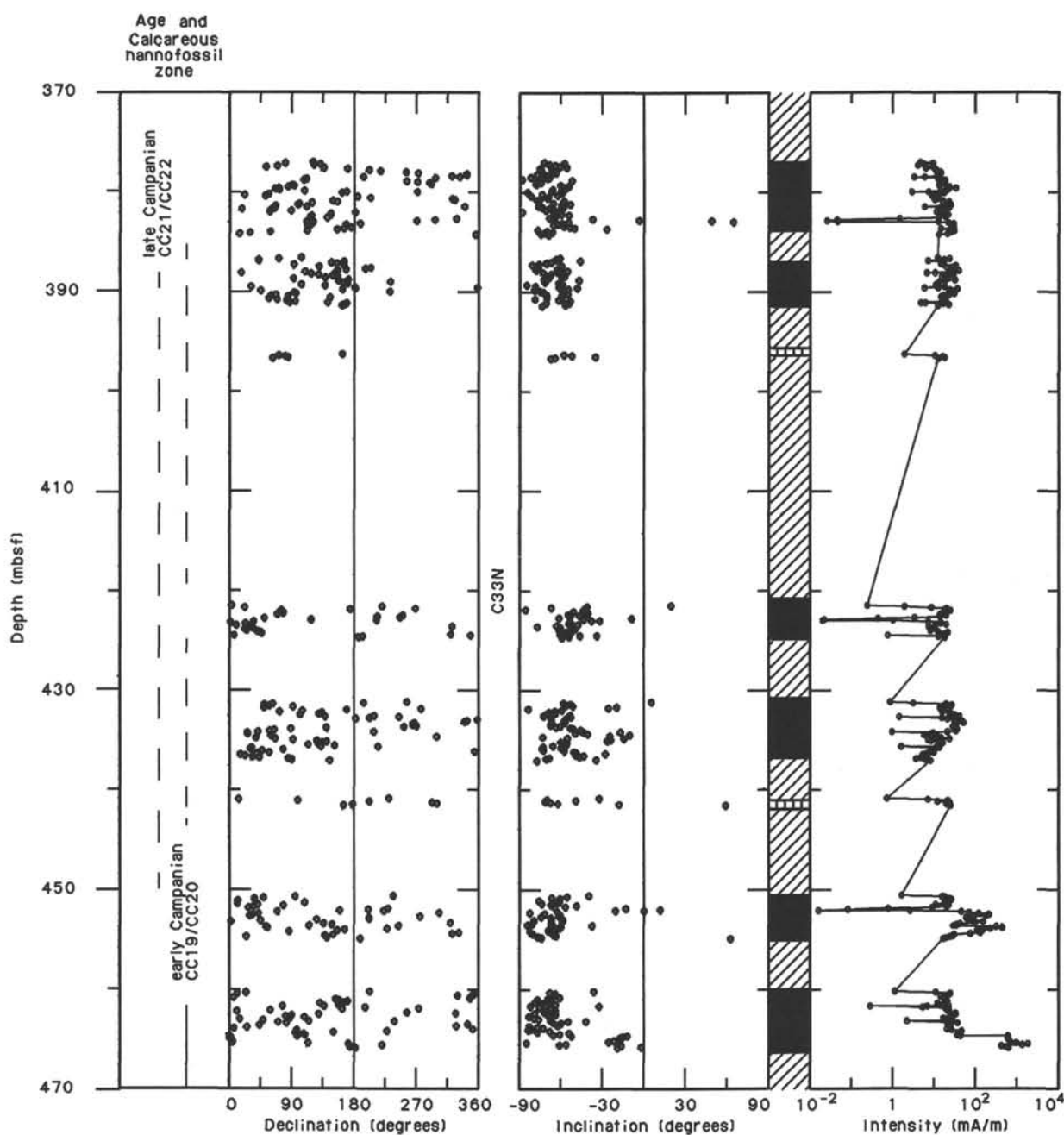


Figure 36 (continued).

mbsf. The drill pipe was set at 42 mbsf for the first run of the seismic stratigraphic string. Because the tool would not pass below a bridge at 405 mbsf, only the interval above this depth was logged.

The seismic stratigraphic string provided downhole and uphole recordings from 42 to 405 mbsf and 405 to 0 mbsf (42–0 mbsf through pipe), respectively. Data quality is good from 40 to 375 mbsf for the natural gamma, resistivity, and sonic slow-speed curves.

The geochemical string provided a downhole recording from 0 to 95 mbsf (0–42 mbsf through pipe) and an uphole recording from 395 to 0 mbsf (42–0 mbsf through pipe). The data quality is good in the open-hole interval from 40 to 395 mbsf for elemental yields of sulfur, iron, chlorine, hydrogen, aluminum,

calcium, and silicon, as well as capture cross section, total gamma radiation, and uranium, potassium, and thorium percentages. Post-cruise processing will begin with a normalization procedure in order to obtain dry-weight percentages for Ca, Si, Fe, S, Ti, K, Gd, Mg, and Al. This procedure is followed by processing to obtain an estimate of mineralogy.

Despite hole conditioning (including KCl added to the mud to suppress clay swelling) and wiper trips, bridges (constrictions in the borehole) formed rapidly between 405 and 625 mbsf (intervals with clay, ash, and basalt). Some of the bridges appear to have formed as a result of material falling downhole, as they occurred within massive basalt units where core recovery was nearly 90%. Because of time constraints, we decided to run the BHTV with the pipe set at 553 mbsf after another wiper trip.

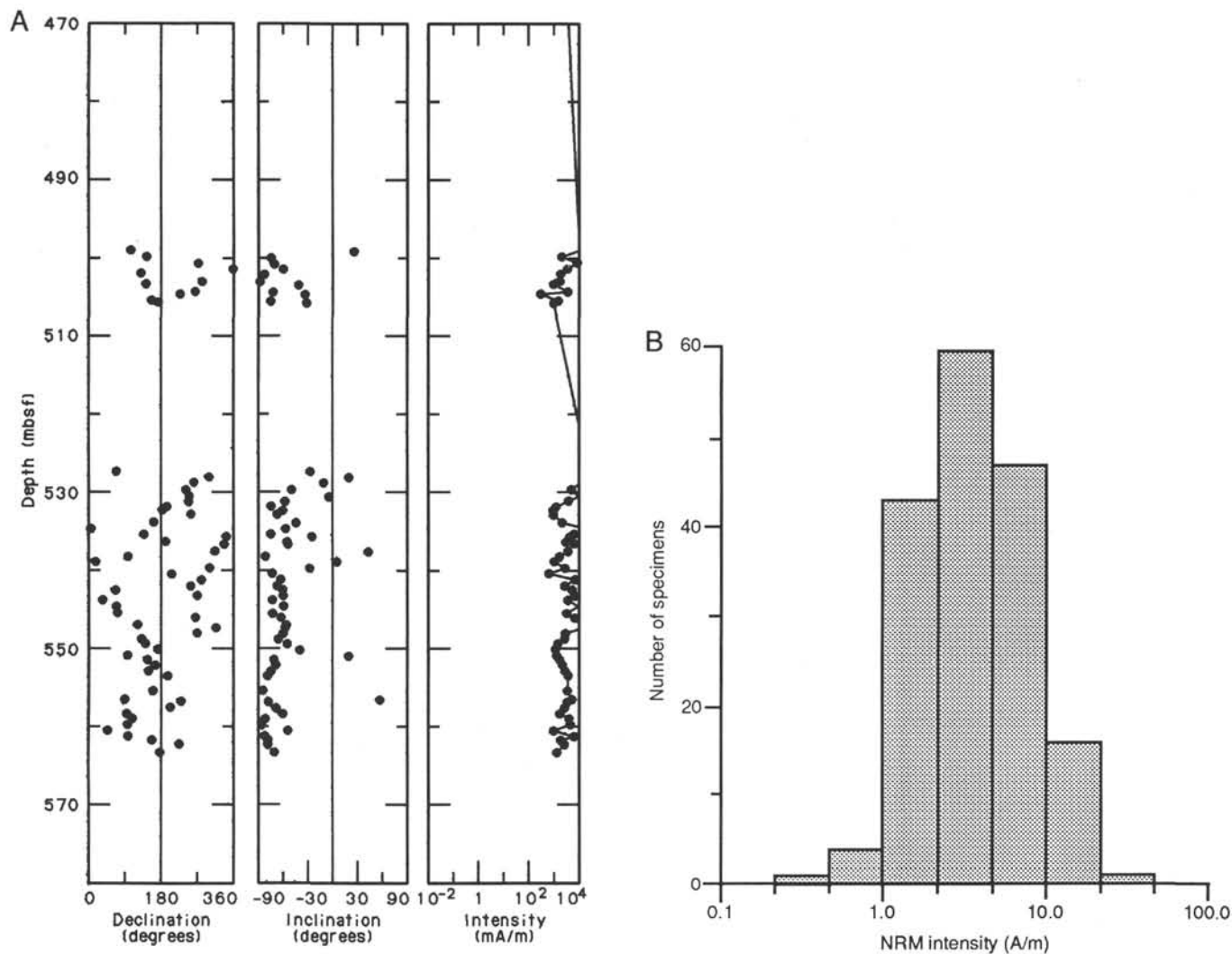


Figure 37. **A.** NRM of basalt samples from Cores 121-758A-55R to 121-758A-61R. **B.** Histogram of NRM intensities for basalts from Cores 121-758A-55R to 121-758A-72R.

The BHTV made two uphole recordings in the basalts, from 610 to 550 mbsf and 555 to 525 mbsf. The quality of the data is good, despite poor hole conditions and irregularities in the tool's compass firing.

Interpretation

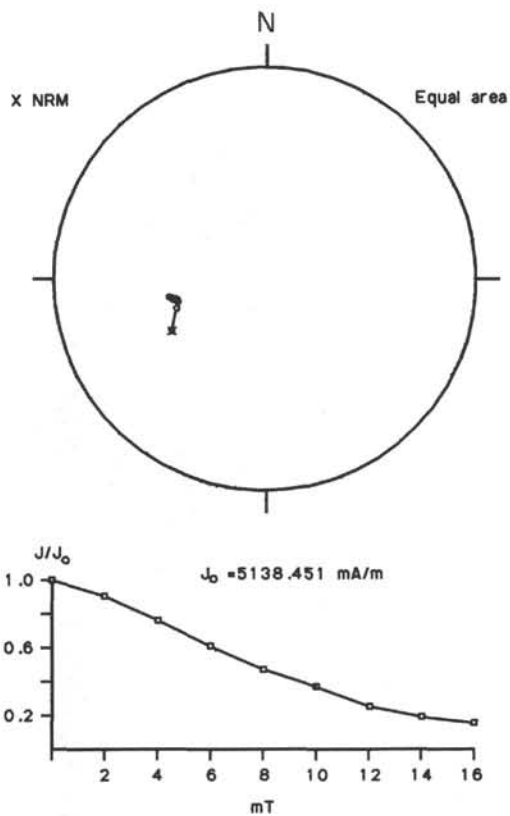
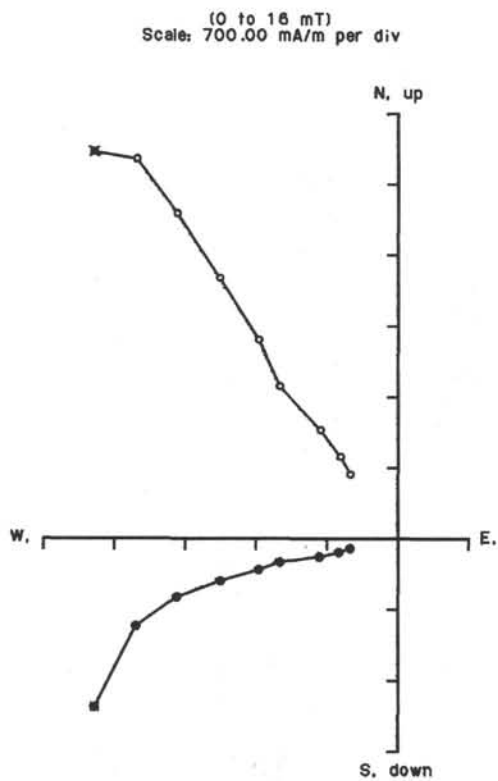
Decreasing clay content downward from 50 to 122 mbsf in lithologic Subunit IB is evident on the gamma, thorium, and potassium logs (arrow 1, Fig. 52) and on the aluminum log (Fig. 53). The calcareous nanofossil chalks in the interval from 127 to 146 mbsf (arrow 2, Fig. 52) show a decrease in sonic slowness (increase in sonic velocity) coupled with an increase in resistivity. A sharp decrease in slowness (increase in sonic velocity) and an increase in resistivity and gamma values (caused primarily by an increase in thorium) occur in the interval at 249–257 mbsf (arrow 3, Fig. 52). A decrease in the aluminum and hydrogen yields is also seen at this depth (Fig. 53). This interval marks the Eocene hiatus as well as a change in bulk density from an average of 1.7 g/cm³ above 250 mbsf (in physical-properties unit A) to an average of 1.9 g/cm³ below 260 mbsf (in physical-properties unit B) (see Fig. 47).

Increasing clay content and decreasing carbonate content from 296 mbsf down to the end of the logged interval at 375 mbsf are evident as an increase in silicon and aluminum yields

and a decrease in calcium yield in Figure 53 and an increase in gamma radiation in Figure 52. The interval of higher resistivities and variable slowness from 310 to 360 mbsf (arrow 4, Fig. 52) corresponds to the occurrence of porcellanite and chert in the chalks of lithologic Subunit IIB. Below 360 mbsf and to the end of the logged interval at 375 mbsf (arrow 5, Fig. 52), an interval of high slowness and low resistivity corresponds to the uppermost section of volcanic clays in lithologic Subunit III. Because the core recovery through this interval is low (21.9%–64.0%), it is not surprising that the boundary between lithologic Units II and III was placed 7 m higher than the logging determination. The agreement between velocity values determined from logging and those used in seismic stratigraphic modeling is good (see Fig. 58).

The BHTV produced good quality data in the interval from 540 to 610 mbsf. Although no indications of wellbore breakouts or fractures are apparent in the photographic records, post-cruise processing of the video record reveals a zone of breakouts in a small interval from 550 to 560 mbsf, which indicates that the maximum horizontal compressive stress is in a north-south direction (Fig. 54). Methods of enhancing these images are being investigated. Analyses of borehole ellipticity will provide an indication of *in-situ* stress even where no detectable breakouts have developed. In addition to providing information about

A



B

(0 to 14 mT)
Scale: 500.00 mA/m per div

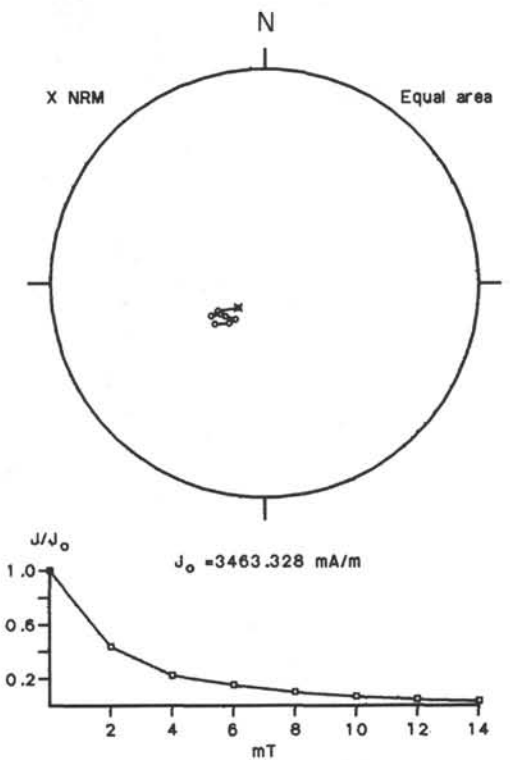
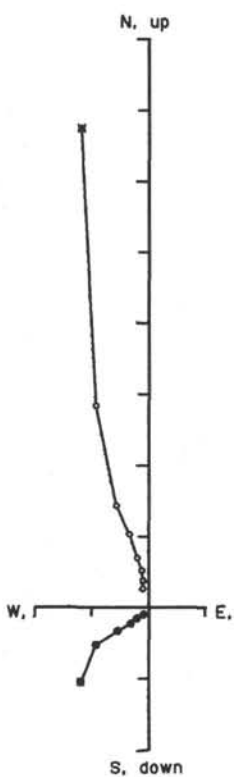


Figure 38. Zijderveld, equal area, and intensity decay plots for basalt samples from Hole 758A, lithologic Unit V. **A.** Sample 121-758A-58R-2, 116-118 cm. **B.** Sample 121-758A-61R-2, 99-101 cm.

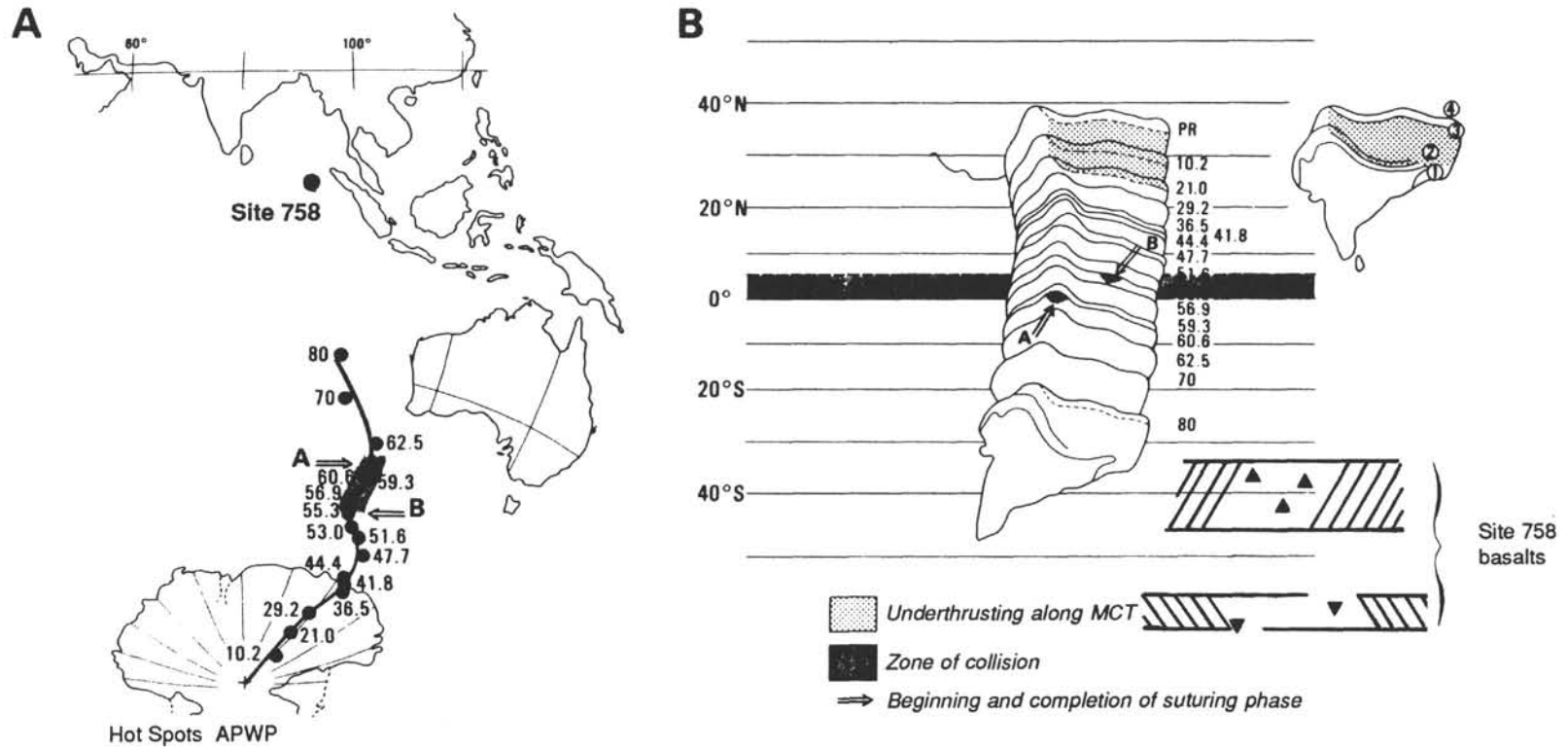


Figure 39. Comparison of the expected paleolatitude of Site 758 according to (A) a simulated apparent polar wander path (APWP) for the Indian Plate and (B) paleolatitudes corresponding with the inclination of the stable magnetization component in five basalt samples. In both diagrams, note the coincidence between the onset (arrow A) and end (arrow B) of the first phase of counterclockwise rotation and the passage of Greater India's northern boundary through the paleolatitude belt defined by collision-related secondary magnetization components. Numbers give the chronology in Ma; PR = present day; MCT = Main Central Thrust. Modified after Klootwijk et al. (1985).

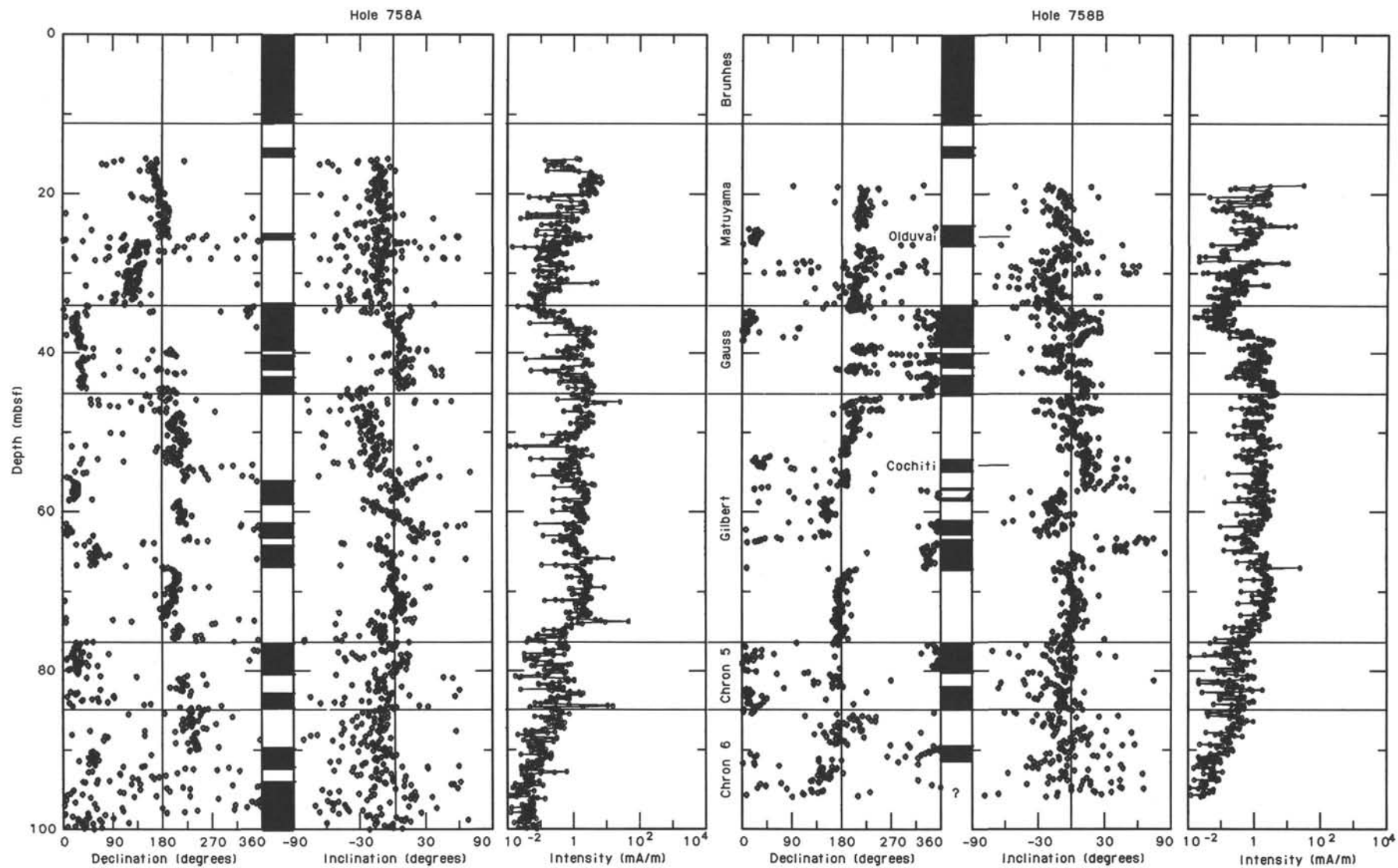


Figure 40. Magnetostratigraphy and mean declination drift pattern of oriented APC-cored Holocene to Miocene-Pliocene sequences of Holes 758A and 758B after 9-mT demagnetization. Data from Cores 121-758B-1H and 121-758B-2H (unoriented) are shown in Figure 35.

Table 10. Transition ages and depths for Holes 758A and 758B.

Depth (mbsf)		Transition	Type	Age (Ma)
Hole 758A	Hole 758B			
10.9	10.7	Brunhes/Matuyama	N-R	0.73
14.2	14.25	Upper Jaramillo	R-N	0.91
15.3	15.25	Lower Jaramillo	N-R	0.98
^a	24.3	Upper Olduvai	R-N	1.66
26.0	26.4	Lower Olduvai	N-R	1.88
34.2	34.75	Matuyama/Gauss	R-N	2.47
39.5	39.0	Upper Kaena	N-R	2.92
40.5	40.25	Lower Kaena	R-N	2.99
41.9	41.4	Upper Mammoth	N-R	3.08
42.9	42.6	Lower Mammoth	R-N	3.18
^a	45.7	Gauss/Gilbert	N-R	3.40
^a	53.0	Upper Cochiti	R-N	3.88
^a	54.5	Lower Cochiti	N-R	3.97
56.2	56.8	Upper Nunivak	R-N	4.10
58.7	58.3	Lower Nunivak	N-R	4.24
61.5	61.1	Upper Sidufjall	R-N	4.40
63.05	62.4	Lower Sidufjall	N-R	4.47
^b 64.0	63.2	Upper Thvera	R-N	4.57
66.7	^a	Lower Thvera	N-R	4.77
76.4	^a	Gilbert/Chron 5	R-N	5.35
80.5	80.4		N-R	5.53
82.7	82.2		R-N	5.68
84.3	85.4	Chron 5/Chron 6	N-R	5.89
90.2	89.4		R-N	6.37
92.1	91.0		N-R	6.50

^a Transition in unrecovered interval.

^b Susceptibility correlations suggest transition may be within unrecovered interval.

stress directions, the BHTV record shows the locations of many of the boundaries between the tuffs and massive flows in the logged interval.

Summary

Geophysical well logging at Site 758 has provided a BHTV determination of the orientation of maximum horizontal compressive stress, confirmation of lithostratigraphic boundaries, and delineation of the properties of strata in poorly recovered intervals. Logging sonic velocities agree with velocities used in the seismic stratigraphic model to get the two-way traveltime to match the cored recovery. Because of the rapidly deteriorating hole conditions, much of the logging planned for this site could not be conducted.

SEISMIC STRATIGRAPHY

General Setting

Site 758 is at 5°23.05' N, 90°21.67' E, on the northern part of Ninetyeast Ridge (Fig. 55). The site is on the southeast side of one of the large en echelon blocks that characterize this part of the ridge. RC2705 surveyed the site area in June 1986. The area is heavily faulted and at least some of the faults have been recently active (see "Ninetyeast Ridge Underway Geophysics" chapter).

Site Survey

The *JOIDES Resolution* site survey was performed using an echo-sounder and two 80-in.³ water guns as a seismic source for a digital single-channel recording system. The records were filtered at 65–160- and 40–160-Hz filter settings and plotted at horizontal scale rates of 75 and 50 lines/in., respectively. The analog record made with the 65–160-Hz filter seems to be of a better quality and was used for interpretation. The seismic profile crossing the site (dip line) and the strike line that crosses the

dip line approximately 600 m northwest of the site location are shown in Figures 56 and 57. The complete reprocessed versions of the same lines are shown in backpocket Figure 17 of the "Ninetyeast Ridge Underway Geophysics" chapter.

JOIDES Resolution approached the site from the southeast and shot three dip lines and one strike line to obtain a better appreciation of the environment of the drill site. Unfortunately, the survey was performed outside of the GPS window, and as a result, the quality of the navigation is poor compared with previous Leg 121 site surveys. Although the navigation is good by other standards, we did not locate Site 758 at the intersection of the dip and strike lines.

Correlation between Seismic Stratigraphy and Lithostratigraphy

Lithostratigraphy

The lithologic sequence is divided into five units and several subunits (see "Lithostratigraphy and Sedimentology" section). Unit I (0–121.7 mbsf) is a Holocene to middle Miocene nannofossil ooze, divided into Subunits IA (0–25.2 mbsf) and IB (25.2–121.7 mbsf). The calcium carbonate content in Subunit IB is higher than in Subunit IA and increases downcore as clay content decreases.

Unit II (121.7–367.3 mbsf) is also divided into two subunits. Subunit IIA (121.7–295.6 mbsf) consists of middle Miocene to lower Paleocene nannofossil chalk. A major unconformity is at 249 mbsf in this subunit, and most of the Eocene section is missing (see "Biostratigraphy" section). This unconformity correlates to the P-unconformity of Curray et al. (1982). The Cretaceous/Tertiary boundary (and a stratigraphic hiatus) occur between Subunits IIA and IIB. Subunit IIB (295.6–367.3 mbsf) is an upper Maestrichtian to upper Campanian calcareous chalk.

Unit III (367.3–431.2 mbsf) is a Campanian calcareous clay. Unit IV (431.2–495 mbsf—where hard drilling was encountered) is a greenish gray Campanian tuff. These two sedimentary units overlie submarine basaltic sheet flows and some pillow lavas.

Velocities

Velocities measured from core samples using the *P*-wave logger and on a Hamilton Frame velocimeter were used as a guideline for seismic model velocities because sonic log velocities were not available for interpretation at the time. However, the sonic log velocities can be used to check the sample velocities and to refine the velocity model. The model velocities were derived by matching reflectors (Table 23) to lithologic boundaries and to impedance contrasts. Especially important are the reflectors matched to the ooze/chalk contact at 122 mbsf and the sediment/basalt contact, estimated from a marked decrease in the drill penetration rate during the drilling of Core 121-758-54R, at 493 mbsf. A major unconformity at 256 mbsf was used to check the validity of the aforementioned match (by calculating the depth of its reflection using the velocity derived from the match of reflectors above and below and only then matching this depth to the unconformity depth as drilled). Model velocities were kept close to the velocities measured on core samples (Fig. 58).

The seismic model velocities are listed in Table 24 and plotted together with the measured velocities in Figure 58. The model and measured velocities agree very well, except in the interval from 296 to 367 mbsf, where the measurements are lower (by approximately 300 m/s) than the model velocity. Most of the measured velocities from 122 to 296 mbsf are also lower, apparently because the velocity measurements in this interval were performed on samples that were more disturbed by drilling. Sharp velocity peaks in the interval from 367 to 431 mbsf were not considered in the estimate of velocities for the seismic model.

Table 11. Correlation of massive ash layers and zones of concentrated ash blebs (from 2 to 34 cm thick) between holes at Site 758.

Ash layer	Magnetic susceptibility peak	Hole 758A			Hole 758B			Hole 758C			Comment
		Core, section, interval (cm)	Depth (mbsf)	Ash thickness	Core, section, interval (cm)	Depth (mbsf)	Ash thickness	Core, section, interval (cm)	Depth (mbsf)	Ash thickness	
A	3	1H-2, 0-34	1.50-1.84	34	1H-1, ? (soupy)			1H-2, 8-34	1.58-1.84	26	Probably Toba ash, 75,000 yr Mysterious black ash only in 758A coarser than overlying ash "A"
B	3a	1H-2, 44-57	1.94-2.07	13	?		?				
C	21	2H-1, 110-116	7.10-7.16	6	1H-5, 117-123	7.17-7.23	6	1H-6, 147.5, to 1-7, 4		6.5	Light gray, with white and pink hue; 2-cm-long spindle (?) in ash of 758B
D	35	2H-4, 30-43	10.80-10.93	13	2H-1, 123-137	10.73-10.87	14				Just below Brunhes/Matuyama boundary
E	39	2H-4, 112-117	11.62-11.67	5	2H-2, 60-64	11.60-11.64	4				Extremely abrupt basal contact
F	67	3H-3, 122-128	19.82-19.88	6	Not recovered						
G	85	Not recovered			3H-4, 63-73	24.03-24.13	10				
H	105	4H-5, 0-5	31.20-31.25	5	4H-3, 9-13						
I	below 165	6H-5, 43-48	50.83-50.88	5	6H-2, 41-48	49.61-49.68	7				Concentration of pumice blebs, not a true massive ash layer
J	187	7H-2, 117-122	56.67-56.72	5	6H-7, 43-54	57.13-57.24	11				Dark ash with sharp basal contact
K	211	Not recovered			7H-4, 130-133	63.10-63.13	3				
L	217	?			7H-6, 28-33	65.08-65.13	5				Ash only in half of core liner in 758B
M	223	8H-2, 146-150	66.66-66.70	4	7H-CC, 13-16	67.14-67.17	3				Ash in core catcher of Core 758B-7H
N	239	8H-6, 138-140	72.58-72.60	2	8H-4, 111-113	72.61-72.63	2				Zone of smeared ash layers and blebs within 758B-8H-4, 88-134 cm, is not a distinct massive ash layer

Note: Ash thickness is from visual core description.

Table 12. Apparent gaps between cores and patches with cores from adjacent holes based on the magnetic susceptibility, Site 758.

Core no.	Depth (mbsf)	Length		Recovery (%)	Magnetic susceptibility interval (mbsf)	Core catcher length (m)	Core breaks	Magnetic susceptibility gap (m)	Points not used in correlation
		cored (m)	recovered (m)						
121-758A-									
1H	0.0-6.0	6.0	6.11	101.8	0.03-5.70	0.30			
2H	6.0-15.6	9.6	10.02	104.4	6.03-15.98	0.21	1H-2H	1.74	0
3H	15.6-25.2	9.6	10.00	104.2	15.63-25.29	0.29	2H-3H	0.48	0
4H	25.2-34.8	9.6	10.05	104.7	25.23-34.92	0.23	3H-4H	2.28	1
5H	34.8-44.4	9.6	9.98	104.0	34.83-44.49	0.24	4H-5H	0.66	0
6H	44.4-54.0	9.6	9.97	103.9	44.43-54.09	0.26	5H-6H	2.22	0
7H	54.0-63.7	9.7	10.02	103.3	54.03-63.69	0.25	6H-7H	1.68	0
8H	63.7-73.4	9.7	9.94	102.5	63.73-73.33	0.32	7H-8H	1.17	0
9H	73.4-83.1	9.7	9.95	102.6	73.43-83.03	0.20	8H-9H	0.39	6
10H	83.1-92.8	9.7	9.97	102.8	83.13-92.76	0.23	9H-10H	1.71	27
11H	92.8-102.4	9.6	9.99	104.1	92.85-102.45	0.23	10H-11H	1.59	3
12X	102.4-112.1	9.7	9.55	98.5			11H-12X		
Sum and mean recovery of APC cores			106.00	103.5			Sum of magnetic susceptibility gaps	13.92	Sum of sediment gaps
							Mean magnetic susceptibility gaps	1.39	Mean sediment gaps
121-758B-									
1H	0.0-9.5	9.5	9.88	104.0	0.03-9.72	0.09			
2H	9.5-18.9	9.4	9.59	102.0	9.53-18.89	0.11	1H-2H	-0.36	NA
3H	18.9-28.4	9.5	9.95	104.7	18.93-28.53	0.22	2H-3H	1.44	0
4H	28.4-38.0	9.6	9.71	101.1	28.43-37.82	0.23	3H-4H	0.57	0
5H	38.0-47.7	9.7	9.94	102.5	38.03-47.66	0.20	4H-5H	1.89	0
6H	47.7-57.3	9.6	9.83	102.4	47.73-57.33	0.12	5H-6H	2.88	0
7H	57.3-67.0	9.7	9.99	103.0	57.33-66.99	0.23	6H-7H	0.84	0
8H	67.0-76.7	9.7	10.04	103.5	67.03-76.69	0.25	7H-8H	0.24	2
9H	76.7-86.3	9.6	9.91	103.2	76.73-86.30	0.22	8H-9H	0.63	0
10H	86.3-96.0	9.7	9.84	101.4	86.33-95.93	0.17	9H-10H	1.80	1
Sum and mean recovery of APC cores			98.68	102.8			Sum of magnetic susceptibility gaps	9.93	Sum of sediment gaps
							Mean magnetic susceptibility gaps	1.10	Mean sediment gaps
121-758C-									
1H	0.0-9.4	9.4	9.40	100.0	0.03-8.97	0.15			

Acoustic Impedance

Acoustic impedance was calculated throughout the section (see "Physical Properties" section).

The impedance gradually increases over the interval from 0 to about 340 mbsf from approximately 2260 to 4000 Mg/m²s,

with several minor peaks. The impedance is fairly constant (ranging from 3700 to 4000 Mg/m²s) from about 350 to 493 mbsf, with several major peaks (Fig. 58). Below this interval, impedance values increase to an average of 13,000 Mg/m²s in the basalt flows. The numerous peak values are caused by the widely differing densities and seismic velocities in basalt.

Table 12 (continued).

Core gap (m)	Top of patch interval from 758B (m)	Bottom of patch interval from 758B (m)	Patch interval thickness (m)	Comments
1.44	4.32	6.06	1.74	Comparison to Hole 758C gives 1.41-m core gap
0.27	15.65	16.13	0.48	Core catcher magnetic susceptibility was measured
1.99	23.37	25.68	2.31	
0.43	35.42	36.08	0.66	
1.98	43.94	46.16	2.22	
1.42	52.80	54.48	1.68	
0.92	63.03	64.20	1.17	
0.07	73.18	73.75	0.57	
1.51	82.58	85.10	2.52	
1.36	91.58	93.26	1.68	
11.39				
1.14				
	Top of patch interval from 758A (m)	Bottom of patch interval from 758A (m)		
-0.45	Overlap, thus NA			Overpenetrated core, top 1.5 m soupy An overlap of section, not a gap First correlatable point (at 1.56 m) in Hole 758B suggests that 1.8 m is missing from the top of the core
1.33	18.81	20.25	1.44	
0.35	27.93	28.50	0.57	
1.66	36.57	38.46	1.89	
2.68	45.99	48.87	2.88	
0.72	56.76	57.60	0.84	
0.01	66.49	66.79	0.30	Ash layer "M" in core catcher
0.38	76.37	77.00	0.63	
1.58	85.17	87.00	1.83	
8.26				
0.92				
Section 7 not measured, contains ash "C"				

Reflectors

Ten reflectors, numbered from 1 to 10 in Figures 56 through 58, were used to interpret the stratigraphy at Site 758. The sediment/water interface is reflector 1 and is followed by a group of

reflectors that appear to be sea-surface reflections of the outgoing pulse of the water gun ("ghosts"). The distance to the sea-floor reflector is 2925 uncorrected m, which agrees with the depth determined from the drill pipe. The two-way traveltimes, depths, and seismic velocities are shown in Table 24.

Table 13. Multishot core orientation data, Site 758.

Core	Drift (degrees)	Direction of drift (degrees)	Declination (degrees)	Shot rate (min)	Half-hour delay	Instrument number
121-758A-						
3H	9.0	30	350	1.0	N	EW40649
4H	3.2	47	312	1.0	N	EW40649
5H	3.4	47	320	1.0	N	EW40649
6H	3.6	47	350	1.0	N	1606
7H	3.4	47	244	1.0	N	1606
8H	3.5	49	55	1.0	N	1606
9H	3.6	52	250	1.0	N	EW40649
10H	3.3	52	330	1.0	N	EW40649
11H	3.2	55	322	1.0	N	EW40649
121-758B-						
3H	1.3	290	236	1.0	N	1606
4H	5.2	308	200	1.0	N	1606
5H	5.5	305	146	1.0	N	1606
6H	5.8	305	45	1.0	N	EW40649
7H	5.2	310	274	1.0	N	EW40649
8H	5.8	305	58	1.0	N	EW40649
9H	5.4	310	302	1.0	N	1606
10H	5.1	312	10	1.0	N	1606

Correlation

Correlation of seismic reflectors with the impedance and lithology is shown in Figure 58. The velocity structure in Table 24 was used for the interpretation. Reflectors based on this model show good correlation with lithologic units, unconformities, and downhole acoustic impedance.

Reflector 2 (40 mbsf) is the uppermost reflector below the seafloor reflectors. It correlates with an increase in bulk density and velocity. Reflector 2 does not correspond to an abrupt lithologic change.

Reflector 3 (122 mbsf) marks a change from ooze to chalk (see "Lithostratigraphy and Sedimentology" section). This reflector also marks a boundary from layers with less to more seismic stratification. It can be correlated with a small increase in density and with a large increase in sediment strength. Vane shear measurements were stopped for an interval below this point because of the increased sediment strength.

Reflector 4 (232 mbsf) is a strong southeasterly-dipping reflector. It is correlated with a slight decrease in bulk density. More importantly, we can see stratigraphic onlap above this reflector marking a seismic sequence boundary. Supportive evidence in the biostratigraphy data suggests reworking of the sediment in this depth range (see "Biostratigraphy" section), with perhaps a stratigraphic hiatus and a reflective surface as a consequence.

Reflector 5 (256 mbsf) is correlated with an increase in bulk density, a decrease in water content, and a marked hiatus or very condensed section in sedimentation (see "Biostratigraphy" section) from the lower Oligocene to the disconformity between the Eocene and Paleocene. This reflector also matches a peak in the impedance.

Reflector 6 (296 mbsf) does not correlate with any of the physical properties, except to a further decrease downsection in water content. However, it marks the lithologic change from Subunits IIA to IIB (see "Lithostratigraphy and Sedimentol-

Table 14. Site 758 interstitial-water geochemical data.

Sample (interval in cm)	Depth (mbsf)	Volume (mL)	pH	Alkalinity (mmol/L)	Salinity (g/kg)	Magnesium (mmol/L)	Calcium (mmol/L)	Chloride (mmol/L)	Sulfate (mmol/L)	Phosphate (μ mol/L)	Ammonia (μ mol/L)	Mg^{2+}/Ca^{2+}
758A-1H-3, 145-150	4.45	56	7.60	3.690	36.0	51.70	10.70	547.00	26.90	4.00	22	4.83
758B-1H-6, 40-44	7.90	7			36.0	50.30	10.80	542.00	26.70	2.00	52	4.66
758A-3H-6, 145-150	24.55	63	7.50	3.930	36.0	50.30	12.30	558.00	27.20	1.00	69	4.09
758B-3H-6, 40-44	26.80	9			36.0	49.60	12.20	550.00	26.30	1.00	81	4.07
758B-5H-6, 62-68	46.12	8			36.0	48.60	13.30	547.00	25.50	1.00	77	3.65
758A-6H-6, 145-150	53.35	55	7.40	3.750	36.0	48.50	14.30	563.00	25.30	0.00	74	3.39
758B-7H-6, 63-69	65.43	10			36.0	47.40	14.60	548.00	24.40	1.00	77	3.25
758A-9H-6, 145-150	82.35	50	7.40	3.670	36.0	47.20	16.00	554.00	25.20	0.00	84	2.95
758B-9H-6, 63-69	84.83	10			36.0	46.60	15.50	543.00	24.00	1.00	77	3.01
758A-12X-5, 145-150	109.85	50	7.30	3.620	36.0	46.10	17.50	549.00	24.50	1.00	63	2.63
758A-15X-2, 145-150	134.35	30	7.50	3.690	36.0	45.30	20.00	555.00	24.20	0.00	58	2.27
758A-18X-3, 145-150	164.85	30	7.40	3.270	36.0	44.20	21.80	548.00	24.10	0.00	43	2.03
758A-21X-4, 145-150	195.25	30	7.40	3.210	36.5	43.50	23.40	558.00	24.90	1.00	41	1.86
758A-24X-3, 145-150	222.75	30	7.20	2.930	36.0	42.50	25.30	555.00	23.70	1.00	35	1.68
758A-28X-5, 145-150	264.35	16	7.40	2.640	36.0	40.80	28.10	555.00	23.50	0.00	32	1.45
758A-31X-5, 145-150	293.35	18	7.30	2.330	36.3	39.70	30.70	556.00	23.50		27	1.29
758A-34X-5, 145-150	322.35	27	8.00	2.170	36.0	37.90	33.50	563.00	22.90	0.00	24	1.13
758A-38X-1, 145-150	354.05	10	7.60	0.910	39.5	31.90	42.50					0.75
758A-41X-4, 140-150	382.90	25	7.80	0.710	36.5	30.60	46.00	566.00	23.40	0.00	7	0.67
758A-46X-CC, 33-40	415.53	12	8.10	0.680	38.0	30.60	52.40	569.00	23.70	0.00	3	0.58
^a 758A-47R-1, 140-150	422.90	4			35.0	31.70	44.40	533.00	22.60	0.00	13	0.71
758A-50R-1, 140-150	452.00	15	7.90	0.940	38.0	26.00	55.00	548.00	22.60	0.00	0	0.47
758A-54R-1, 140-150	490.60	25	7.90	0.640	38.0	25.80	57.70	574.00	22.70	0.00	3	0.45
758A-57R-1, 140-150	519.30	10			38.5	18.70	76.30	585.00	19.80	0.00	9	0.25

^a Apparently contaminated with seawater.

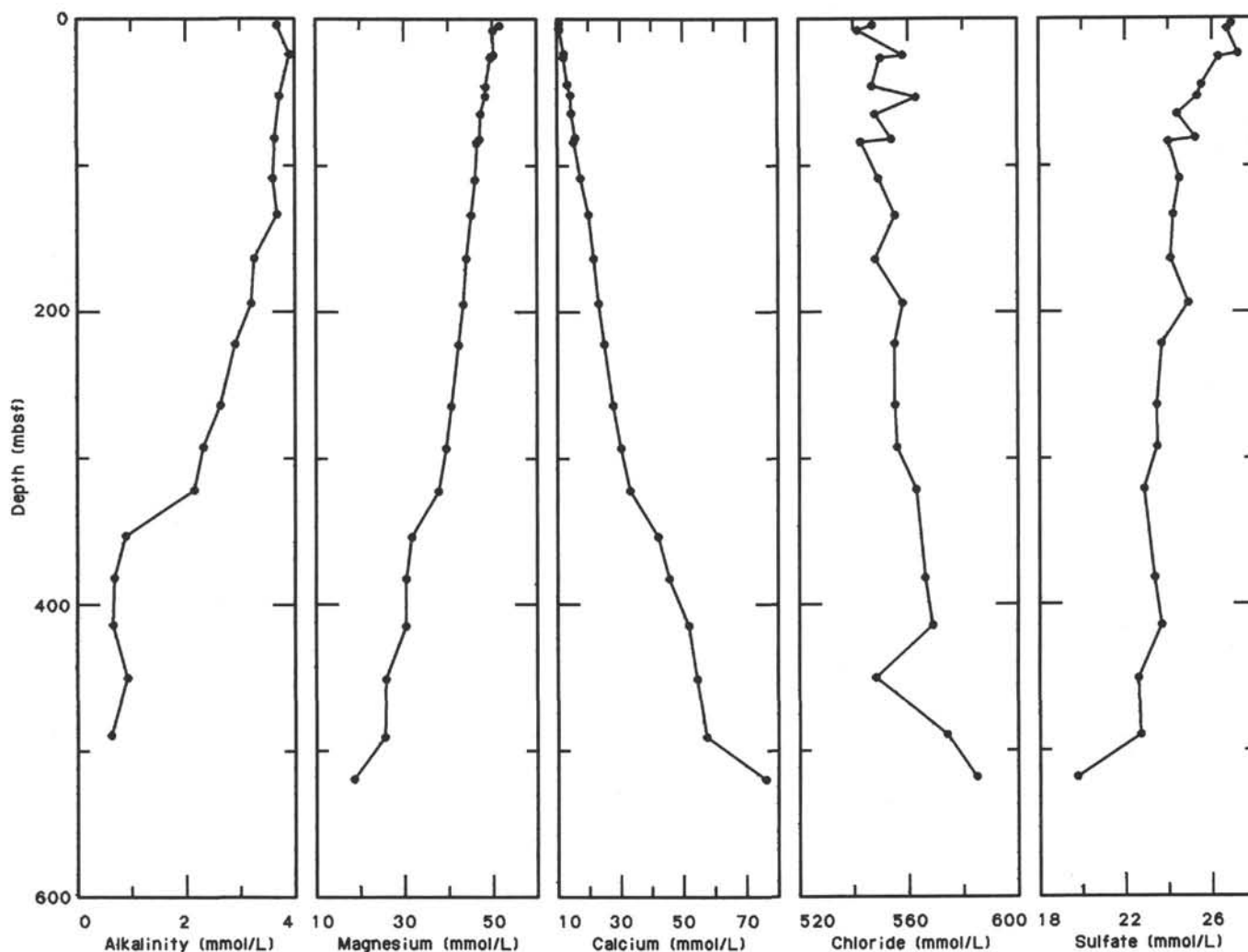


Figure 42. Interstitial-water profiles, Site 758.

Table 15. Concentration of methane (C_1) and ethane (C_2) in samples from Hole 758A.

Core, section, interval (cm)	Depth (mbsf)	C_1 ($\mu\text{L/L}$)	C_2 ($\mu\text{L/L}$)
1H-4, 0-3	4.50	3.0	
3H-7, 0-3	24.60	3.0	
6H-7, 0-3	53.40	3.0	
9H-6, 0-3	80.90	3.0	
12X-6, 0-3	109.90	4.0	
15X-3, 0-3	134.40	4.0	
18X-4, 0-1	164.90	4.0	
21X-4, 119-120	194.99	3.0	
24X-3, 145-150	222.75	5.0	
28X-5, 145-150	264.35	5.0	
31X-5, 0-3	291.90	4.0	
33X-6, 0-3	312.80	5.0	
38X-1, 142-145	354.02	6.0	
41X-2, 142-145	379.92	9.0	0.4
47R-1, 140-150	422.90	3.0	
48R-2, 0-5	432.70	2.0	
50R-1, 140-150	452.00	3.0	
57R-1, 137-140	519.27	2.0	

ogy" section). Reflector 6 coincides with a stratigraphic hiatus around the Cretaceous/Tertiary boundary (see "Biostratigraphy" section).

Reflector 7 (367 mbsf) is a lithostratigraphic boundary between Subunit IIB (chalk) and Unit III (calcareous clay with ash). It corresponds to changes in all measured physical properties and marks the beginning of widely variable values of bulk density, velocity, and grain density.

Reflector 8 (431 mbsf) is a very strong reflector correlated with a lithologic change between Campanian clay and tuff. Small increases in seismic velocity and impedance and a marked increase in water content occur at this depth.

Reflector 9 (493 mbsf) marks a lithologic change between Campanian tuff and the underlying basalt flows and ties to changes in all physical-property measurements.

Reflector 10 (682? mbsf) is the last interpretable reflector and marks "seismic basement." We believe that reflector 9 is a correct representation of the top of the basalt flows, although we did not drill through any lithologic change that can be correlated with the top of seismic basement. This implies that the velocity needed to calculate the depth of reflector 10 must be in excess of 4600 m/s, which seems high in comparison with velocities measured on basalt samples. However, when we tried to match this reflector to pillow lava basalts at 640 mbsf, in order to explain this reflector as a lithologic change, the resultant velocity was 3600 m/s. This velocity seems too low, even in making allowances for the presence of low-velocity tuffs between the ashes. This lower reflector also could be some complex multiple generated within the intercalated basalts and tuffs. Unfortu-

Table 16. Percentages of total carbon, inorganic carbon, organic carbon, and calcium carbonate in samples from Site 758.

Core, section, interval (cm)	Depth (mbsf)	Total carbon (%)	Inorganic carbon (%)	Organic carbon (%)	CaCO ₃ (%)
121-758A-					
1H-1, 28-30	0.28	8.07	7.18	0.89	59.8
1H-1, 125-127	1.25	7.06	6.65	0.41	55.4
1H-2, 65-67	2.15	7.80	7.42	0.38	61.8
1H-2, 125-127	2.75	6.45	6.08	0.37	50.7
1H-3, 26-28	3.26	6.77	6.63	0.14	55.2
1H-3, 126-128	4.26		7.11		59.2
1H-4, 65-67	5.15		7.07		58.9
1H-4, 116-118	5.66	8.51	8.33	0.18	69.4
2H-1, 35-37	6.35	7.06	6.70	0.36	55.8
2H-1, 136-138	7.36		6.66		55.5
2H-2, 65-67	8.15		7.96		66.3
2H-2, 125-127	8.75	6.94	6.53	0.41	54.4
2H-3, 65-67	9.65	8.40	8.38	0.02	69.8
2H-3, 116-118	10.16		7.87		65.6
2H-4, 65-67	11.15		6.68		55.6
2H-4, 106-108	11.56	5.86	5.68	0.18	47.3
2H-5, 18-20	12.18		6.60		55.0
2H-5, 106-108	13.06		7.49		62.4
2H-6, 65-67	14.15		7.12		59.3
2H-6, 116-118	14.66		7.96		66.3
3H-1, 25-27	15.85	7.92	7.81	0.11	65.1
3H-1, 126-128	16.86		8.37		69.7
3H-2, 65-67	17.75		7.28		60.6
3H-2, 125-127	18.35		8.08		67.3
3H-3, 25-27	18.85	7.93	7.91	0.02	65.9
3H-3, 125-127	19.85		7.80		65.0
3H-4, 25-27	20.35		7.93		66.1
3H-4, 125-127	21.35	8.01	7.72	0.29	64.3
3H-5, 25-27	21.85		7.33		61.1
3H-5, 125-127	22.85		7.75		64.6
3H-6, 25-27	23.35		7.24		60.3
3H-6, 116-118	24.26	6.70	6.48	0.22	54.0
3H-7, 25-27	24.85		7.55		62.9
4H-1, 54-56	25.74		8.52		71.0
4H-1, 125-127	26.45		8.15		67.9
4H-2, 25-27	26.95		8.28		69.0
4H-2, 125-127	27.95		7.64		63.6
4H-3, 25-27	28.45	8.11	7.86	0.25	65.5
4H-3, 125-127	29.45		7.74		64.5
4H-4, 25-27	29.95		8.18		68.1
4H-4, 125-127	30.95		8.15		67.9
4H-5, 25-27	31.45		8.51		70.9
4H-5, 125-127	32.45		8.78		73.1
4H-6, 26-28	32.96		8.28		69.0
4H-6, 125-127	33.95		8.28		69.0
4H-7, 25-27	34.45	8.09	8.03	0.06	66.9
5H-1, 25-27	35.05		8.79		73.2
5H-1, 125-127	36.05		8.92		74.3
5H-2, 25-27	36.55		8.19		68.2
5H-2, 125-127	37.55		8.80		73.3
5H-3, 125-127	39.05		8.36		69.6
5H-4, 25-27	39.55		7.71		64.2
5H-4, 125-127	40.55		8.78		73.1
5H-5, 25-27	41.05		8.18		68.1
5H-5, 125-127	42.05		8.41		70.1
5H-6, 25-27	42.55	8.09	7.94	0.15	66.1
5H-6, 125-127	43.55		8.55		71.2
5H-7, 25-27	44.05		8.35		69.6
6H-1, 25-27	44.65		8.23		68.6
6H-1, 125-127	45.65	8.26	8.24	0.02	68.6
6H-2, 125-127	47.15	8.26	8.24	0.02	68.6
6H-3, 25-27	47.65		8.64		72.0
6H-3, 125-127	48.65		8.92		74.3
6H-4, 25-27	49.15		8.46		70.5
6H-4, 125-127	50.15		9.24		77.0
6H-5, 25-27	50.65		8.66		72.1
6H-5, 125-127	51.65		8.48		70.6
6H-6, 25-27	52.15	7.57	7.40	0.17	61.6
6H-6, 125-127	53.15	9.15	9.07	0.08	75.6
6H-7, 25-27	53.65		9.15		76.2
7H-1, 125-127	55.25		7.33		61.1
7H-2, 125-127	56.75		9.07		75.6
7H-3, 125-127	58.25		9.02		75.1
7H-4, 125-127	59.75		8.94		74.5

Table 16 (continued).

Core, section, interval (cm)	Depth (mbsf)	Total carbon (%)	Inorganic carbon (%)	Organic carbon (%)	CaCO ₃ (%)
121-758A- (Cont.)					
7H-5, 125-127	61.25		9.34		77.8
7H-6, 125-127	62.75		9.58		79.8
8H-1, 125-127	64.95		9.87		82.2
8H-2, 125-127	66.45		8.95		74.6
8H-3, 125-127	67.95		9.64		80.3
8H-4, 125-127	69.45	9.39	9.33	0.06	77.7
8H-5, 125-127	70.95		8.83		73.6
8H-6, 125-127	72.45		8.21		68.4
9H-2, 125-127	76.15	8.29	8.24	0.05	68.6
9H-4, 125-127	79.15	9.04	8.97	0.07	74.7
9H-6, 125-127	82.15		9.54		79.5
10H-2, 89-91	85.49		9.86		82.1
10H-4, 94-97	88.54	10.23	10.23	0.00	85.2
10H-6, 95-98	91.55		9.94		82.8
11H-2, 95-97	95.25		10.27		85.6
11H-4, 95-97	98.25	9.64	9.48	0.16	79.0
11H-6, 95-97	101.25		9.62		80.1
12X-2, 95-97	104.85	7.78	7.72	0.06	64.3
12X-4, 95-97	107.85	10.24	10.27	0.00	85.6
12X-6, 95-97	110.85		9.81		81.7
13X-2, 95-97	114.55		9.61		80.1
13X-4, 95-97	117.55	8.95	9.09	0.00	75.7
13X-6, 95-97	120.55		8.56		71.3
14X-2, 70-72	123.90	9.14	9.23	0.00	76.9
14X-4, 70-72	126.90		10.18		84.8
15X-2, 72-74	133.62	10.64	10.83	0.00	90.2
16X-2, 70-72	143.20	9.50	9.51	0.00	79.2
16X-4, 70-72	146.20		10.51		87.6
17X-2, 72-74	152.92	10.22	10.15	0.07	84.6
17X-4, 72-74	155.92		10.12		84.3
18X-2, 71-73	162.61	9.97	9.99	0.00	83.2
18X-4, 69-71	165.59		10.24		85.3
19X-2, 71-73	172.21	10.59	10.49	0.10	87.4
19X-4, 70-72	175.20		9.94		82.8
20X-2, 70-72	181.90	10.09	10.13	0.00	84.4
21X-2, 67-69	191.47	10.27	10.24	0.03	85.3
21X-4, 64-66	194.44		10.02		83.5
22X-2, 91-93	201.41	10.83	10.68	0.15	89.0
22X-CC, 29-31	204.01	10.54	10.56	0.00	88.0
23X-2, 102-104	211.22		10.45		87.1
23X-4, 100-102	214.20	10.63	10.66	0.00	88.8
24X-2, 95-97	220.75		10.61		88.4
24X-4, 97-99	223.77	10.42	10.36	0.06	86.3
25X-2, 95-97	230.45		10.29		85.7
25X-4, 95-97	233.45	10.48	10.44	0.04	87.0
25X-6, 36-38	235.86		10.31		85.9
26X-2, 95-97	240.15	10.45	10.46	0.00	87.1
26X-4, 95-97	243.15		10.66		88.8
27X-1, 95-97	248.25	10.72	10.77	0.00	89.7
28X-2, 59-61	258.99		11.49		95.7
28X-4, 93-95	262.33		11.49		95.7
28X-6, 93-95	265.33	11.33	11.35	0.00	94.6
29X-2, 94-96	269.04		11.46		95.5
29X-4, 62-64	271.72	11.38	11.45	0.00	95.4
30X-2, 95-97	278.75		11.29		94.1
30X-4, 95-97	281.75	11.50	11.39	0.11	94.9
31X-2, 95-97	288.35		11.07		92.2
31X-4, 95-97	291.35		11.13		92.7
31X-6, 95-97	294.35	10.46	10.51	0.00	87.6
31X-CC, 31-33	295.52		9.82		81.8
33X-2, 72-74	307.52		9.27		77.2
33X-4, 72-74	310.52		10.54		87.8
33X-6, 72-74	313.52	8.76	8.80	0.00	73.3
34X-2, 70-72	317.10	9.97	9.92	0.05	82.6
34X-2, 73-75	317.13		8.95		74.6
34X-6, 80-82	323.20		9.06		75.5
35X-2, 60-62	326.70	8.79	8.70	0.09	72.5
36X-2, 60-62	336.40	9.70	9.70	0.00	80.8
37X-CC, 16-17	344.37	9.67	9.82	0.00	81.8
38X-2, 145-147	355.55	6.63	6.60	0.03	55.0
39X-1, 84-87	358.44		2.15		17.9
39X-1, 124-126	358.84	8.86	8.80	0.06	73.3
40X-2, 41-43	369.21	5.41	5.28	0.13	44.0
40X-2, 60-63	369.40		2.25		18.7

Table 16 (continued).

Core, section, interval (cm)	Depth (mbsf)	Total carbon (%)	Inorganic carbon (%)	Organic carbon (%)	CaCO ₃ (%)
121-758A- (Cont.)					
40X-2, 65-68	369.45		1.86		15.5
41X-2, 70-72	379.20	4.12	3.97	0.15	33.1
41X-2, 114-118	379.64		2.96		24.7
41X-5, 22-23	383.22		1.35		11.3
41X-5, 24-26	383.24		2.04		17.0
42X-2, 53-56	388.63		1.22		10.2
42X-2, 86-88	388.96	3.43	3.44	0.00	28.7
42X-3, 31-33	389.91		4.89		40.7
43X-1, 44-46	396.74	4.32	4.22	0.10	35.2
44X-CC, 29-31	399.89	4.39	4.20	0.19	35.0
45X-CC, 0-2	405.60	1.21	1.13	0.08	9.4
46X-CC, 38-40	415.58	5.11	4.68	0.43	39.0
47R-2, 110-117	424.10	2.32	2.15	0.17	17.9
48R-2, 71-73	433.41		0.34		2.8
48R-3, 80-83	435.00		0.30		2.5
48R-4, 108-110	436.78	1.37	1.24	0.13	10.3
49R-1, 42-44	441.32		0.23		1.9
49R-1, 65-66	441.55		0.57		4.8
50R-1, 96-98	451.56	1.43	1.39	0.04	11.6
50R-3, 33-34	453.93		0.07		0.6
51R-2, 73-75	462.43		0.56		4.7
51R-4, 74-76	465.44		0.04		0.3
51R-4, 75-78	465.45		0.04		0.3
51R-4, 90-98	465.60		0.67		5.6
51R-4, 110-113	465.80		1.11		9.3
52R-1, 90-92	470.80	3.47	3.30	0.17	27.5
52R-2, 90-92	472.30	1.84	1.61	0.23	13.4
53R-1, 62-64	480.22		0.76		6.3
54R-1, 34-36	489.54	1.45	1.27	0.18	10.6
55R-3, 29-32	502.03		0.01		0.1
56R-2, 78-80	510.68	0.78	0.63	0.15	5.3
57R-1, 20-22	518.10		0.05		0.4
57R-2, 82-84	520.22	2.88	2.80	0.08	23.3
58R-7, 32-36	535.94		0.01		0.1
59R-7, 52-56	544.84		0.02		0.2
60R-4, 58-62	550.52		0.05		0.4
61R-4, 28-33	559.11		0.01		0.1
62R-1, 44-48	564.74		0.08		0.7
62R-3, 8-13	567.29		0.08		0.7
63R-6, 44-48	580.82		0.02		0.2
121-758B-					
1H-1, 125-127	1.25		7.33		61.1
1H-2, 128-130	2.78		7.16		59.6
1H-3, 128-130	4.28		8.81		73.4
1H-4, 129-131	5.79		6.13		51.1
1H-5, 130-132	7.30		6.92		57.6
1H-6, 130-132	8.80		6.23		51.9
1H-7, 25-27	9.25		6.84		57.0
2H-2, 90-92	11.90		7.73		64.4
2H-3, 90-92	13.40		7.06		58.8
2H-5, 90-92	16.40		7.78		64.8
2H-6, 90-92	17.90		7.26		60.5
2H-7, 38-40	18.88		6.87		57.2
3H-1, 125-127	20.15		8.22		68.5
3H-2, 125-127	21.65		7.28		60.6
3H-3, 125-127	23.15		7.98		66.5
3H-4, 125-127	24.65		7.93		66.1
3H-5, 125-127	26.15		7.99		66.6
3H-6, 125-127	27.65		8.20		68.3
3H-7, 55-57	28.45		7.78		64.8
4H-1, 125-127	29.65		8.21		68.4
4H-2, 125-127	31.15		8.18		68.1
4H-3, 125-127	32.65		8.40		70.0
4H-4, 125-127	34.15		8.18		68.1
4H-5, 125-127	35.65		8.31		69.2
4H-6, 125-127	37.15		8.47		70.6
4H-7, 34-36	37.74		8.58		71.5
5H-4, 125-127	43.75		7.18		59.8
5H-5, 125-127	45.25		8.84		73.6
5H-6, 125-127	46.75		8.24		68.6
5H-7, 55-57	47.55		9.23		76.9
6H-1, 125-127	48.95		9.20		76.6
6H-2, 125-127	50.45		8.78		73.1

Table 16 (continued).

Core, section, interval (cm)	Depth (mbsf)	Total carbon (%)	Inorganic carbon (%)	Organic carbon (%)	CaCO ₃ (%)
121-758B- (Cont.)					
6H-3, 125-127	51.95		7.87		65.6
6H-4, 125-127	53.45		9.11		75.9
6H-5, 125-127	54.95		8.06		67.1
6H-6, 125-127	56.45		8.37		69.7
6H-7, 55-57	57.25		8.58		71.5
7H-1, 55-57	57.85		8.81		73.4
7H-2, 55-57	59.35		9.35		77.9
7H-3, 55-57	60.85		9.68		80.6
7H-4, 55-57	62.35		9.32		77.6
7H-5, 55-57	63.85		9.86		82.1
7H-6, 55-57	65.35		9.26		77.1
7H-7, 55-57	66.85		8.79		73.2
8H-1, 55-57	67.55		9.18		76.5
8H-4, 55-57	72.05		9.36		78.0
8H-5, 55-57	73.55		8.82		73.5
8H-6, 55-57	75.05		9.30		77.5
8H-7, 55-57	76.55		9.02		75.1
9H-1, 55-57	77.25		9.39		78.2
9H-2, 55-57	78.75		9.10		75.8
9H-3, 55-57	80.25		8.85		73.7
9H-4, 55-57	81.75		9.10		75.8
9H-5, 55-57	83.25		9.44		78.6
9H-6, 55-57	84.75		9.78		81.5
9H-7, 55-57	86.25		9.58		79.8
10H-1, 55-57	86.85		9.78		81.5
10H-2, 55-57	88.35		9.73		81.1
10H-3, 55-57	89.85		10.17		84.7
10H-4, 55-57	91.35		9.34		77.8
10H-5, 55-57	92.85		9.83		81.9
10H-6, 55-57	94.35		9.49		79.1
10H-7, 55-57	95.85		9.96		83.0
121-758C-					
1H-1, 45-47	0.45	7.77	6.97	0.80	58.1
1H-1, 115-117	1.15	7.66	7.38	0.28	61.5
1H-2, 45-47	1.95		7.71		64.2
1H-2, 115-117	2.65		7.08		59.0
1H-3, 45-47	3.45	7.62	7.35	0.27	61.2
1H-3, 115-117	4.15		6.88		57.3
1H-4, 45-47	4.95		7.64		63.6
1H-4, 115-117	5.65		6.26		52.2
1H-5, 45-47	6.45		7.51		62.6
1H-5, 115-117	7.15		7.12		59.3
1H-6, 45-47	7.95		7.66		63.8
1H-6, 115-117	8.65		7.05		58.7

nately, no sonic log was run over this interval because of hole problems. At this time, we do not have a satisfactory explanation for the seismic basement reflector.

Seismic Stratigraphy Interpretation

The basaltic flows found at the base of Hole 758A (493-676.8 mbsf) dip to the east on the seismic sections. The reverberating or "ringing" reflectors within the flows are probably caused by alternating flows and tuff, flow internal structures (changes in porosity, for instance), or by alteration that changes the physical properties of the flows. The amount of tephra and thickness of the flows decrease with depth (see "Igneous Petrology" section).

The sedimentary layers dip gently to the east and are parallel to each other. This particular sedimentary pattern does not extend beyond the immediate vicinity of the drill site. Farther away, the layers dip in various directions and are broken by faults. The layers (Oligocene-Miocene chalk) above the unconformity at 256 mbsf onlap from the southeast, which signifies the presence of a time gap that increases in the upslope direction. The sedimentary layers above the unconformity are more hummocky in appearance than the layers below.

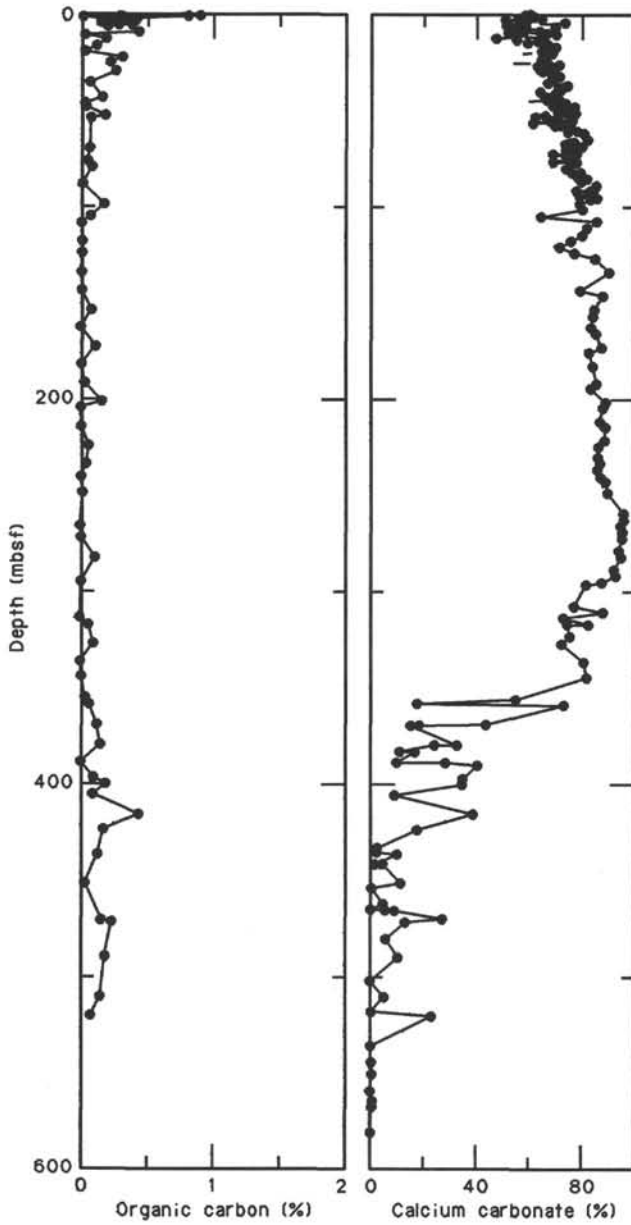


Figure 43. Organic carbon content and calcium carbonate content in samples from Site 758.

The most important reflectors, the Eocene unconformity and the seismic basement, can be followed throughout most of the survey area (see "Ninetyeast Ridge Underway Geophysics" chapter). While the thickness of the sediments and basalt flows beneath the unconformity seems almost constant, the thickness of the sediment above is highly variable. The sediment above the unconformity is thickest on the crest of the ridge. The hummocky appearance (unless it is fault induced) of the sediments above the unconformity points to a more energetic environment at that time. Such an environment would help to create an uneven sediment distribution, especially along the slopes of the ridge. The tectonic deformation, which may be inferred from the change in the sedimentation, began in the Eocene (the time of the unconformity) and may be connected to an intraplate deformation of the Indian plate, which started sometime after the collision of India with Asia. In addition, the ridge underwent recent tectonic activity, as may be judged from a number of

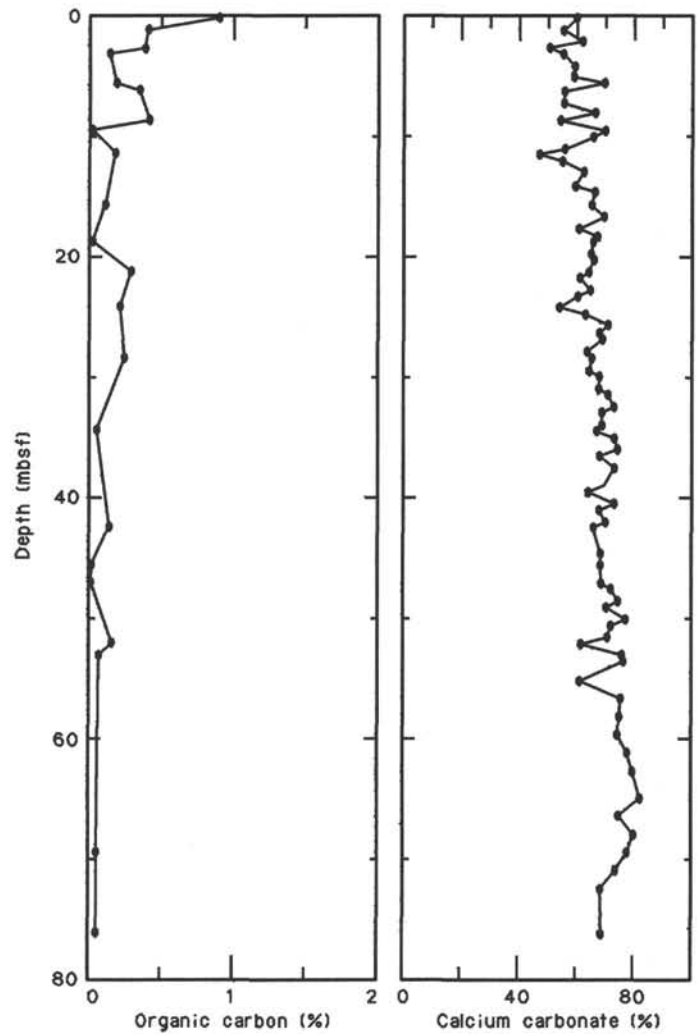


Figure 44. Organic carbon content and calcium carbonate content in samples from the upper Miocene to Pleistocene interval in Hole 758A.

faults that continue to surface. The flat top of the ridge was uplifted, while slopes on the sides of the ridge became steeper.

Conclusions

The nature of the seismic basement at Site 758 remains unresolved. We drilled through several submarine lava flows with spectacular basalt recovery, but did not reach the interpreted seismic basement. The lava flows seem to be the cause of the particular ringing reflector seismic signature. It is not clear that the ringing reflector/seismic basement interface represents a real change in lithology.

The sedimentary layers above the basalt flows are interesting from a seismic stratigraphic point of view. We recognize two main seismic units: lithologic Unit II below the Eocene unconformity and Unit I above the unconformity. The thickness of Unit II is practically constant throughout the area. The geologic evidence points to quiet deposition following the submarine volcanism as the ridge slowly subsided.

The picture changed in the early Eocene at the time of unconformity. After the collision of India with Asia, the ridge faults were apparently reactivated. This led to steepening of the ridge slopes and the variable thickness of sediments above the unconformity. The length of the stratigraphic hiatus associated

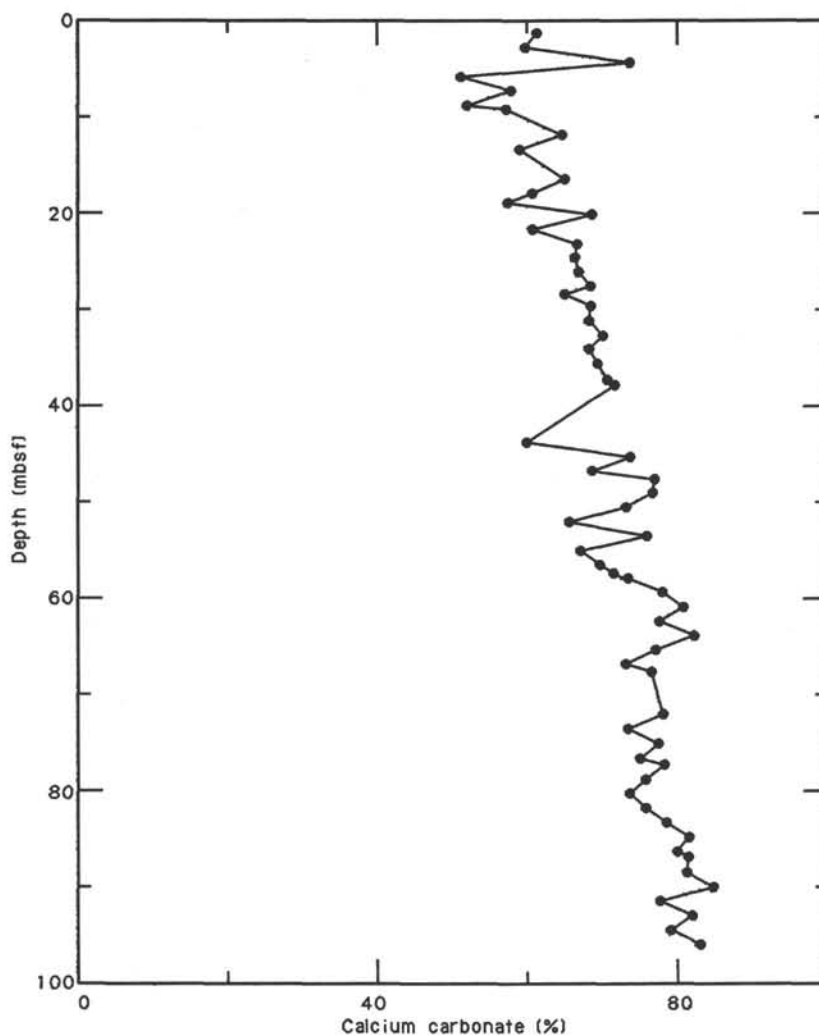


Figure 45. Calcium carbonate content in samples from the upper Miocene to Pleistocene interval in Hole 758B.

with the unconformity varies considerably throughout the survey area.

The reflectors at Site 758 tie very well with lithologic and sedimentary horizons at this site. We were able to recognize all of the major lithologic divisions (see the preceding correlation) and also several hiatuses in sedimentation. Especially important are the recognition of a large stratigraphic hiatus at 256 mbsf (Eocene unconformity) and the hiatus at the Cretaceous/Tertiary boundary.

SPECULATIVE CORRELATION BETWEEN THE NEOGENE SUSCEPTIBILITY PROFILE OF SITE 758 AND EVOLUTION OF THE INDIA-ASIA CONVERGENCE ZONE

The volume magnetic susceptibility profile at Site 758 shows characteristic patterns in base-level trends and spikes on which a tentative subdivision of the profile into susceptibility (K-) units is based (Figs. 59 and 60). A tentative correlation of these units with phases in the tectonic evolution of the India-Asia convergence zone is presented. Further studies of Site 758 material may well show that paleoclimatic and paleoceanographic changes have also made significant contributions to changes in sediment influx at this location. Pending the outcome of such studies and the determination of their effects on the susceptibility record (either on primary origin of K-unit boundaries or just modulat-

ing effects within a K-unit), it is still useful to document apparent correlations between major breaks in the Neogene susceptibility profile of Site 758 with constraints on timing of major phases in the Himalayan orogeny.

Definition of Susceptibility Units

The proposed susceptibility units (K1 to K9) are not necessarily related to the five lithologic units (I to V) or the physical-properties units (A to D) recognized at Site 758, although common boundaries do occur. The K-units are defined in terms of depth intervals with respect to Hole 758A (Table 25). Their relationship to the lithologic units ("Lithostratigraphy and Sedimentology" section) and physical-properties units ("Physical Properties" section) within Hole 758A is shown in Figure 59.

Base-level susceptibilities of units K1-K4 (Holocene to upper Miocene ooze of Subunits IA and IB) either vary per unit between 5×10^{-6} and 15×10^{-6} cgs units (K1 and K3) or are less than 5×10^{-6} (K2 and K4). Susceptibility spikes up to 40×10^{-6} to 60×10^{-6} cgs units occur throughout units K1 to K3, with a particularly large spike (about 10^{-4} cgs units) at the very top of unit K1. The spikes represent ash layers (see Figs. 35 and 40 and Table 11 in the "Paleomagnetism" section).

The susceptibility of unit K5 (nanofossil ooze and chalk of Subunits IB and IIA) is markedly higher than that of unit K4 and varies from 5×10^{-6} to 20×10^{-6} cgs units. The boundary

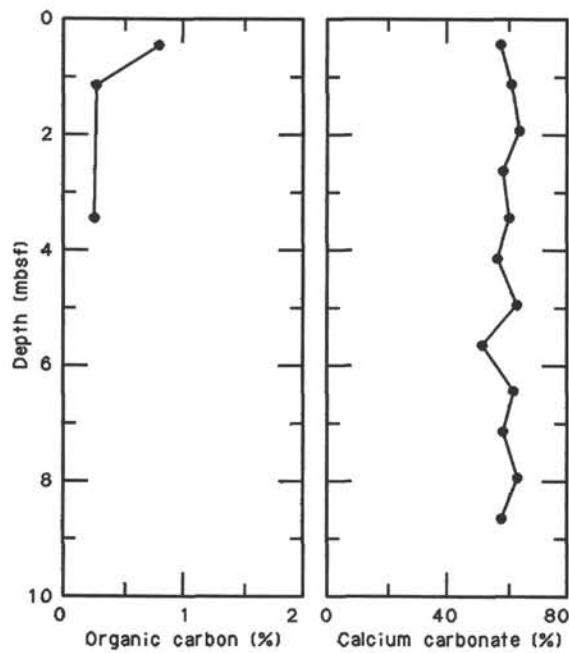


Figure 46. Organic carbon content and calcium carbonate content in samples from the Pleistocene to Holocene interval in Hole 758C.

between units K5 and K6 cannot be more closely placed than somewhere in the interval from 144 to 151 mbsf because of a gap in core recovery (147–151 mbsf). Unit K6 (nanofossil and calcareous nanofossil chalk of Subunit IIA) is characterized by a rather stable base-level susceptibility that varies gradually between 2×10^{-6} and 15×10^{-6} cgs units, with some spikes up to 50×10^{-6} cgs units.

The underlying unit K7 (mainly calcareous chalk of Subunits IIA and IIB) has markedly higher and more variable base-level susceptibilities of between 5×10^{-6} and 50×10^{-6} cgs units, with spikes from 10^{-4} to 2×10^{-4} cgs units. The calcareous clays and tuffs of unit K8 show a very irregular susceptibility pattern. Base-level susceptibility is higher (2×10^{-5} to 10^{-4} cgs units) than in the overlying unit K6 and increases downward. This unit is characterized by susceptibility spikes of up to 4.5×10^{-4} cgs units. The lowermost unit, K9, is equivalent to lithologic Unit V (Campanian and older basalts). This unit is characterized by susceptibility values varying irregularly from 10^{-3} to 5×10^{-3} cgs units. A remarkably low susceptibility interval (10^{-4} to 3×10^{-4} cgs units) between 510 and 520 mbsf represents an interbedded clayey tuff with micrite.

Neogene Susceptibility Record at Site 758 and the Himalayan Orogeny

It has been argued (“Paleomagnetism” section) that the sharp breaks in susceptibility between units K1, K2, K3, and K4 may represent abrupt changes in influx of terrigenous material. This interpretation is extended to the distinct break between units K4 and K5 and the less distinct break between units K5 and K6. These sharp changes can be dated through the Neogene age vs. depth plot for Site 758 (Fig. 61; see also “Biostratigraphy” section) as follows:

Break	Age (Ma)
K1/K2	~2
K2/K3	~2.5
K3/K4	5–6
K4/K5	9
K5/K6	15–20

The age ranges for the K3/K4 break and the K5/K6 break reflect the uncertainty in biostratigraphic control (5–6 and 15–17 Ma, respectively) and the lack of core recovery (17–20 Ma; 147–151 mbsf). This first-order dating attempt will be fine-tuned for the APC-cored Holocene to Miocene-Pliocene sequence by a very detailed correlation of its susceptibility profile with the GRTS (Fig. 40 and “Paleomagnetism” section).

The influx of terrigenous material at Site 758 on the northern end of Ninetyeast Ridge results, for the most part, from runoff of the Ganges and Brahmaputra river systems. Therefore, these abrupt susceptibility changes probably reflect major changes in the tectonic regime of the Himalaya–southeastern Tibetan region. The magnetostratigraphic and susceptibility record of the Holocene to upper Miocene sequence at Site 758 is of exceptional quality, and the paleomagnetic and biostratigraphic record of the Miocene sequence is of high quality. Such changes in the tectonic regime may be possibly dated with a precision that is probably not obtainable from onshore geological observations.

It may be argued that deepening of the northern part of Ninetyeast Ridge during the Neogene, as determined from benthic foraminiferal assemblages (Fig. 16 in the “Biostratigraphy” section), may have led to local increases only in terrigenous influx from a closer association of Site 758 with the Bengal Sea Fan sedimentation system. Such a mechanism may be advanced for the conspicuous upward increase in clay content from the upper part of Core 121-758A-13X at 115 mbsf, which correlates with the K4/K5 break at 9 Ma (Fig. 61) and corresponds closely with the boundary at 121.7 mbsf between lithologic Units I and II. However, the gradual decline in CaCO₃ percentages from the

Table 17. Results of Rock-Eval pyrolysis of samples from Site 758.

Sample (interval in cm)	Depth (mbsf)	Weight (mg)	T _{max} (°C)	S1 (mg HC/g rock)	S2 (mg HC/g rock)	S3 (mg HC/g rock)	Productivity index	S2/S3	Pyrolyzied carbon (0.083 [S1+S2])	Total organic carbon (wt%)	Hydrogen index (mg HC/g C _{org})	Oxygen index (mg CO ₂ /g C _{org})
121-758A-1H-1, 28–30	0.28	99.6	427	0.13	0.12	2.57	0.54	0.04	0.02	0.89	13	288
121-758A-1H-1, 125–127	1.25	96.4	387	0.17	0.32	2.18	0.35	0.14	0.04	0.41	78	531
121-758A-1H-2, 65–67	2.15	93.1	375	0.11	0.18	1.84	0.39	0.09	0.02	0.38	47	484
121-758A-1H-2, 125–127	2.75	91.2	378	0.15	0.19	1.84	0.44	0.10	0.02	0.37	51	497
121-758A-2H-1, 35–37	6.35	87.2	395	0.16	0.26	2.06	0.38	0.12	0.03	0.36	72	572
121-758A-2H-2, 125–127	8.75	91.1	318	0.07	0.09	1.90	0.44	0.04	0.01	0.41	21	463
121-758A-3H-4, 125–127	21.35	90.6	338	0.09	0.11	1.64	0.45	0.06	0.01	0.29	37	565
121-758A-4H-3, 25–27	28.45	94.1	336	0.07	0.10	1.50	0.44	0.06	0.01	0.25	40	600
121-758A-41X-2, 70–72	379.20	97.7	338	0.12	0.12	1.48	0.50	0.08	0.02	0.15	80	986
121-758A-44X-CC, 29–31	399.89	111.3	404	0.14	0.25	0.72	0.37	0.34	0.03	0.19	131	378
121-758A-46X-CC, 38–40	415.58	98.8	394	0.15	0.24	0.95	0.39	0.25	0.03	0.43	55	220
121-758A-52R-2, 90–92	472.30	92.4	414	0.22	0.27	0.93	0.46	0.29	0.04	0.23	117	404
121-758C-1H-1, 45–47	0.45	85.7	427	0.08	0.12	2.29	0.40	0.05	0.01	0.80	15	286
121-758C-1H-1, 115–117	1.15	97.6	379	0.21	0.26	2.28	0.46	0.11	0.03	0.28	92	814

Table 18. Index properties of samples from Holes 758A and 758B.

Core, section, interval (cm)	Depth (mbsf)	Water content (%)	Porosity (%)	Density (g/cm ³)		
				wet bulk	dry bulk	grain
121-758A-						
1H-1, 28	0.28	55.77	76.82	1.43	0.63	2.65
1H-1, 125	1.25	54.58	75.49	1.44	0.65	2.58
1H-2, 65	2.15	51.54	73.50	1.47	0.71	2.63
1H-2, 125	2.75	52.07	74.04	1.48	0.71	2.65
1H-3, 26	3.26	50.75	73.31	1.69	0.83	2.69
1H-3, 126	4.26	50.99	73.85	1.51	0.74	2.74
1H-4, 65	5.15	49.56	72.19	1.51	0.76	2.67
1H-4, 116	5.66	47.32	70.42	1.55	0.81	2.68
2H-1, 35	6.35	50.85	73.59	1.50	0.74	2.72
2H-1, 136	7.36	51.17	73.52	1.50	0.73	2.67
2H-2, 65	8.15	48.22	70.49	1.52	0.79	2.59
2H-2, 125	8.75	51.57	73.21	1.48	0.72	2.59
2H-3, 65	9.65	48.84	71.88	1.53	0.78	2.71
2H-3, 116	10.16	48.78	71.34	1.52	0.78	2.64
2H-4, 65	11.15	49.49	72.68	1.52	0.77	2.74
2H-4, 106	11.56	46.67	69.39	1.54	0.82	2.62
2H-5, 18	12.18	48.84	71.82	1.53	0.78	2.70
2H-5, 106	13.06	46.57	70.18	1.58	0.84	2.73
2H-6, 65	14.15	48.61	71.73	1.54	0.79	2.71
2H-6, 116	14.66	47.47	70.75	1.55	0.81	2.70
3H-1, 25	15.85	48.16	72.04	1.56	0.81	2.80
3H-1, 126	16.86	48.32	70.77	1.54	0.80	2.62
3H-2, 65	17.75	49.15	71.95	1.55	0.79	2.68
3H-2, 125	18.35	48.39	72.08	1.60	0.82	2.78
3H-3, 25	18.85	50.03	72.71	1.51	0.76	2.69
3H-3, 125	19.85	49.57	72.48	1.54	0.78	2.71
3H-4, 25	20.35	47.10	70.40	1.55	0.82	2.70
3H-4, 125	21.35	46.13	70.46	1.59	0.85	2.82
3H-5, 25	21.85	48.16	71.12	1.55	0.80	2.68
3H-5, 125	22.85	47.60	71.59	1.58	0.83	2.80
3H-6, 25	23.35	46.26	68.66	1.55	0.83	2.57
3H-6, 116	24.26	45.27	68.35	1.57	0.86	2.64
3H-7, 25	24.85	45.78	69.66	1.58	0.86	2.75
4H-1, 54	25.74	43.58	67.22	1.61	0.91	2.68
4H-1, 125	26.45	44.46	68.37	1.60	0.89	2.73
4H-2, 25	26.95	46.31	69.43	1.56	0.84	2.66
4H-2, 125	27.95	43.23	67.47	1.63	0.93	2.75
4H-3, 25	28.45	43.19	67.41	1.62	0.92	2.75
4H-3, 125	29.45	41.97	65.84	1.63	0.94	2.70
4H-4, 25	29.95	40.74	64.49	1.64	0.97	2.67
4H-4, 125	30.95	43.92	66.92	1.59	0.89	2.61
4H-5, 25	31.45	42.21	66.29	1.62	0.94	2.72
4H-5, 125	32.45	44.34	68.46	1.61	0.90	2.76
4H-6, 26	32.96	45.17	68.87	1.58	0.87	2.71
4H-6, 125	33.95	42.39	66.99	1.63	0.94	2.79
4H-7, 25	34.45	42.46	66.28	1.62	0.93	2.70
5H-1, 25	35.05	43.21	66.24	1.59	0.90	2.61
5H-1, 125	36.05	45.36	68.36	1.57	0.86	2.63
5H-2, 25	36.55	44.43	67.65	1.58	0.88	2.64
5H-2, 125	37.55	45.61	69.08	1.58	0.86	2.69
5H-3, 25	38.05	45.48	68.81	1.57	0.86	2.67
5H-3, 125	39.05	44.43	69.12	1.61	0.89	2.83
5H-4, 25	39.55	44.63	68.04	1.58	0.87	2.67
5H-4, 125	40.55	45.64	69.09	1.57	0.85	2.69
5H-5, 25	41.05	44.68	68.61	1.59	0.88	2.74
5H-5, 125	42.05	45.33	68.84	1.58	0.86	2.69
5H-6, 25	42.55	42.61	65.77	1.60	0.92	2.62
5H-6, 125	43.55	42.58	66.41	1.62	0.93	2.70
5H-7, 25	44.05	43.55	66.87	1.59	0.90	2.65
6H-1, 25	44.65	45.47	69.35	1.58	0.86	2.74
6H-1, 125	45.65	40.94	65.38	1.65	0.98	2.76
6H-2, 125	47.15	44.61	68.70	1.56	0.86	2.76
6H-3, 25	47.65	44.50	68.07	1.59	0.88	2.69
6H-3, 125	48.65	43.86	67.41	1.59	0.89	2.68
6H-4, 25	49.15	42.22	66.50	1.64	0.95	2.75
6H-4, 125	50.15	44.38	67.74	1.59	0.88	2.66
6H-5, 25	50.65	43.69	67.56	1.60	0.90	2.71
6H-5, 125	51.65	43.28	67.42	1.61	0.91	2.74
6H-6, 25	52.15	42.75	66.61	1.60	0.92	2.70
6H-6, 125	53.15	42.06	66.32	1.65	0.95	2.74
6H-7, 25	53.65	42.48	67.67	1.64	0.94	2.87
7H-1, 125	55.25	35.08	59.19	1.80	1.17	2.72
7H-2, 125	56.75	43.78	67.60	1.61	0.91	2.71
7H-3, 125	58.25	44.36	68.69	1.61	0.89	2.78
7H-4, 125	59.75	43.08	68.00	1.65	0.94	2.84

Table 18 (continued).

Core, section, interval (cm)	Depth (mbsf)	Water content (%)	Porosity (%)	Density (g/cm ³)		
				wet bulk	dry bulk	grain
121-758A- (Cont.)						
7H-5, 125	61.25	41.71	65.45	1.63	0.95	2.68
7H-6, 125	62.75	41.63	65.46	1.63	0.95	2.69
8H-1, 125	64.95	38.53	63.50	1.64	1.01	2.81
8H-2, 125	66.45	41.81	65.85	1.64	0.95	2.72
8H-3, 125	67.95	42.76	66.24	1.61	0.92	2.66
8H-4, 125	69.45	39.42	63.16	1.67	1.01	2.67
8H-5, 125	70.95	41.42	65.95	1.65	0.97	2.77
8H-6, 125	72.45	40.95	64.27	1.62	0.96	2.62
9H-2, 125	76.15	41.53	65.95	1.65	0.97	2.76
9H-4, 125	79.15	41.84	66.15	1.64	0.96	2.75
9H-6, 125	82.15	40.11	64.36	1.66	0.99	2.73
10H-2, 90	85.50	40.56	65.05	1.67	0.99	2.76
10H-4, 95	88.55	36.21	60.57	1.73	1.11	2.74
10H-6, 95	91.55	39.55	63.33	1.67	1.01	2.67
11H-2, 95	95.25	37.31	61.29	1.73	1.08	2.69
11H-4, 95	98.25	38.23	63.44	1.75	1.08	2.84
11H-6, 95	101.25	39.55	63.79	1.68	1.01	2.73
12X-2, 95	104.85	37.98	61.21	1.69	1.05	2.61
12X-4, 95	107.85	39.01	62.99	1.69	1.03	2.69
12X-6, 95	110.85	38.80	62.28	1.67	1.02	2.64
13X-2, 95	114.55	39.06	62.55	1.67	1.02	2.64
13X-4, 95	117.55	38.82	62.93	1.71	1.04	2.71
13X-6, 95	120.55	42.04	66.21	1.64	0.95	2.73
14X-2, 70	123.90	37.09	60.68	1.70	1.07	2.65
14X-4, 70	126.90	37.63	62.03	1.71	1.07	2.74
15X-2, 72	133.62	40.42	64.22	1.67	0.99	2.68
16X-2, 70	143.20	39.98	63.78	1.66	1.00	2.68
16X-4, 70	146.20	42.11	65.55	1.62	0.94	2.65
17X-2, 72	159.92	41.03	65.48	1.66	0.98	2.76
17X-4, 72	155.92	39.26	62.52	1.66	1.01	2.61
18X-2, 71	162.61	39.53	62.98	1.67	1.01	2.63
18X-4, 69	165.59	39.76	63.43	1.66	1.00	2.66
19X-2, 71	172.21	38.16	61.98	1.69	1.04	2.68
19X-4, 70	175.20	37.29	60.86	1.70	1.07	2.65
20X-2, 70	181.90	41.55	64.91	1.63	0.95	2.63
21X-2, 67	191.47	38.66	61.86	1.66	1.02	2.60
21X-4, 64	194.44	39.85	63.48	1.65	0.99	2.65
22X-2, 91	201.41	36.75	60.55	1.70	1.07	2.67
22X-CC, 29	204.01	37.05	61.03	1.71	1.07	2.69
23X-2, 102	211.22	37.69	61.72	1.74	1.08	2.70
23X-4, 100	214.20	37.35	61.03	1.71	1.07	2.66
24X-2, 95	220.75	37.85	62.93	1.76	1.09	2.82
24X-4, 97	223.77	37.33	61.49	1.77	1.11	2.71
25X-2, 95	230.45	37.02	60.25	1.72	1.08	2.61
25X-4, 95	233.45	39.84	63.63	1.69	1.02	2.67
25X-6, 36	235.86	37.59	60.87	1.74	1.09	2.61
26X-2, 95	240.15	34.51	57.95	1.78	1.16	2.65
26X-4, 95	243.15	38.10	62.55	1.74	1.08	2.75
27X-1, 95	248.25	25.60	47.22	1.99	1.48	2.64
28X-2, 59	258.99	28.45	52.65	1.93	1.38	2.84
28X-4, 93	262.33	28.16	51.34	1.91	1.37	2.73
28X-6, 93	265.33	30.27	53.76	1.87	1.30	2.72
29X-2, 94	269.04	29.14	52.71	1.89	1.34	2.75
29X-4, 62	271.72	30.30	53.79	1.87	1.30	2.71
30X-2, 95	278.75	29.27	52.59	1.93	1.36	2.72
30X-4, 95	281.75	27.05	49.51	1.94	1.42	2.68
31X-2, 95	288.35	28.71	52.25	1.95	1.39	2.75
31X-4, 95	291.35	28.16	51.26	1.95	1.40	2.72
31X-6, 95	294.35	33.22	56.64	1.83	1.22	2.66
31X-CC, 31	295.52	31.54	56.32	1.90	1.30	2.84
33X-2, 72	307.52	25.29	47.33	1.96	1.46	2.69
33X-4, 72	310.52	27.82	51.10	1.93	1.39	2.75
33X-6, 72	313.52	28.43	51.66	1.91	1.37	2.73
34X-2, 70	317.10	28.74	51.74	1.89	1.34	2.69
34X-4, 73	320.13	26.00	48.20	1.97	1.45	2.69
34X-6, 80	323.20	28.61	52.21	1.90	1.36	2.76
35X-2, 60	326.70	26.64	48.86	1.92	1.41	2.67
36X-2, 59	336.39	27.74	51.17	1.92	1.39	2.77
37X-2, 16	344.37	24.86	46.69	1.99	1.49	2.68
38X-2, 145	355.55	44.55	67.34	1.58	0.88	2.59
39X-1, 124	358.84	27.08	49.74	1.95	1.42	2.70
40X-2, 41	369.21	5.92	12.49	2.38	2.23	2.30
41X-2, 70	379.20	49.15	70.37	1.53	0.78	2.48
41X-4, 77	382.27	52.98	75.17	1.49	0.70	2.71
42X-2, 86	388.96	44.34	68.20	1.62	0.90	2.72

Table 18 (continued).

Core, section, interval (cm)	Depth (mbsf)	Water content (%)	Porosity (%)	Density (g/cm ³)		
				wet bulk	dry bulk	grain
121-758A- (Cont.)						
42X-3, 31	389.91	33.93	57.81	1.78	1.18	2.70
43X-1, 44	396.74	10.05	20.96	2.29	2.06	2.41
44X-CC, 29	399.89	10.97	22.87	2.23	1.98	2.44
45X-CC, 0	405.60	16.79	29.91	2.00	1.66	2.14
46X-CC, 38	415.58	32.13	53.82	1.88	1.28	2.49
47R-2, 73	423.73	36.54	60.15	1.78	1.13	2.65
48R-2, 71	433.41	39.19	57.47	1.77	1.07	2.12
48R-4, 108	436.78	39.88	64.19	1.73	1.04	2.74
49R-1, 65	441.55	46.79	69.61	1.62	0.86	2.63
50R-1, 96	451.56	44.23	67.82	1.64	0.92	2.69
50R-3, 33	453.93	28.59	49.11	1.97	1.41	2.44
51R-2, 73	462.43	40.04	64.78	1.76	1.06	2.79
51R-4, 74	465.44	27.58	50.51	2.03	1.47	2.72
52R-1, 90	470.80	31.97	54.85	1.83	1.25	2.62
52R-2, 90	472.30	35.22	56.87	1.74	1.13	2.45
53R-1, 62	480.22	37.19	62.94	1.86	1.17	2.91
54R-1, 34	489.54	22.23	42.63	2.02	1.57	2.64
55R-1, 94	499.84	4.05	10.39	2.71	2.60	2.79
55R-3, 25	501.99	2.42	6.75	2.80	2.73	2.97
55R-5, 86	505.46	2.81	7.85	2.74	2.67	3.00
56R-1, 69	509.09	3.07	8.10	2.68	2.60	2.83
56R-2, 78	510.68	31.50	53.50	1.78	1.22	2.54
57R-1, 20	518.10	19.06	36.62	1.97	1.59	2.49
57R-2, 82	520.22	28.22	51.14	1.85	1.33	2.70
57R-3, 15	520.76	5.30	13.05	2.50	2.36	2.73
58R-2, 15	528.71	6.91	17.11	2.60	2.42	2.82
58R-4, 14	531.70	5.56	14.55	2.71	2.56	2.94
58R-6, 137	535.58	3.26	8.85	2.82	2.73	2.93
59R-1, 136	537.86	3.66	9.91	2.80	2.70	2.94
59R-6, 65	544.23	4.21	11.11	2.76	2.64	2.89
60R-2, 12	547.29	3.68	9.32	2.68	2.58	2.74
60R-4, 109	551.03	3.72	9.75	2.70	2.60	2.85
60R-6, 108	553.76	4.53	11.55	2.66	2.54	2.80
61R-1, 36	555.46	3.49	9.42	2.69	2.59	2.92
61R-3, 98	558.40	3.11	9.03	2.73	2.65	3.14
61R-5, 19	560.51	2.79	7.50	2.74	2.66	2.87
61R-7, 12	563.03	5.00	13.24	2.64	2.50	2.95
62R-1, 25	564.55	7.80	18.73	2.46	2.27	2.77
62R-2, 125	567.01	2.73	7.15	2.73	2.66	2.79
63R-2, 114	576.26	5.92	15.04	2.62	2.47	2.86
63R-4, 129	579.06	6.71	16.91	2.60	2.43	2.88
63R-6, 133	581.88	3.47	9.22	2.75	2.66	2.87
64R-1, 123	584.43	4.58	11.70	2.67	2.55	2.81
64R-3, 114	587.12	8.31	19.22	2.75	2.52	2.67
65R-1, 62	593.32	6.49	15.64	2.48	2.32	2.71
65R-3, 24	595.45	4.33	11.26	2.64	2.52	2.85
65R-5, 96	598.98	4.91	12.71	2.62	2.49	2.87
66R-2, 110	604.69	3.85	9.84	2.68	2.57	2.77
66R-4, 123	607.42	5.43	13.22	2.53	2.39	2.70
66R-6, 55	609.64	2.57	6.93	2.75	2.68	2.87
67R-1, 87	612.37	0.88	2.48	2.91	2.89	2.91
67R-3, 80	615.25	4.15	10.46	2.50	2.39	2.75
67R-5, 37	617.78	5.29	13.39	2.54	2.40	2.82
68R-2, 123	623.52	7.61	18.68	2.50	2.31	2.83
68R-4, 33	625.43	4.97	12.70	2.59	2.46	2.82
69R-2, 109	632.66	2.95	7.90	2.77	2.69	2.87
69R-4, 58	634.78	3.49	9.31	2.76	2.66	2.89
70R-1, 74	640.14	6.14	15.11	2.55	2.39	2.77
71R-1, 89	649.49	12.08	26.73	2.55	2.24	2.70
71R-3, 121	652.77	5.25	12.84	2.61	2.48	2.70
72R-1, 91	658.91	5.39	13.09	2.54	2.40	2.69
73R-1, 121	668.81	3.84	10.02	2.66	2.56	2.84
73R-3, 102	671.55	5.47	13.14	2.51	2.37	2.66

121-758B-

1H-1, 125	1.25	52.70	74.65	1.47	0.70	2.67
1H-2, 125	2.75	49.79	72.00	1.49	0.75	2.62
1H-3, 125	4.25	47.25	69.74	1.53	0.81	2.60
1H-4, 125	5.75	47.82	70.67	1.54	0.81	2.66
1H-5, 125	7.25	49.16	72.75	1.53	0.78	2.79
1H-6, 125	8.75	50.21	72.47	1.49	0.74	2.64
1H-7, 25	9.25	47.71	70.50	1.54	0.80	2.65
2H-2, 90	11.90	50.31	73.00	1.50	0.74	2.70
2H-3, 90	13.40	49.28	72.09	1.52	0.77	2.68

Table 18 (continued).

Core, section, interval (cm)	Depth (mbsf)	Water content (%)	Porosity (%)	Density (g/cm ³)		
				wet bulk	dry bulk	grain
121-758B- (Cont.)						
2H-5, 90	16.40	48.64	71.17	1.54	0.79	2.63
2H-6, 90	17.90	50.26	72.94	1.55	0.77	2.69
2H-7, 38	18.88	46.52	69.26	1.56	0.83	2.62
3H-1, 125	20.15	48.81	72.13	1.53	0.78	2.74
3H-2, 125	21.65	46.52	69.35	1.54	0.82	2.63
3H-3, 125	23.15	46.80	70.65	1.56	0.83	2.77
3H-4, 125	24.65	42.22	66.07	1.63	0.94	2.70
3H-5, 125	26.15	44.07	67.39	1.60	0.89	2.65
3H-6, 125	27.65	46.37	70.36	1.58	0.85	2.78
3H-7, 55	28.45	45.24	69.35	1.60	0.87	2.77
4H-1, 125	29.65	43.72	67.62	1.60	0.90	2.72
4H-2, 125	31.15	45.78	69.53	1.58	0.85	2.73
4H-3, 125	32.65	44.08	68.13	1.61	0.90	2.74
4H-4, 125	34.15	43.97	67.73	1.60	0.90	2.71
4H-5, 125	35.65	42.43	65.94	1.62	0.93	2.66
4H-6, 125	37.15	43.06	66.87	1.61	0.92	2.70
4H-7, 35	37.75	43.94	67.76	1.60	0.90	2.71
5H-4, 125	43.75	45.06	68.82	1.59	0.88	2.72
5H-5, 125	45.25	42.95	67.46	1.63	0.93	2.79
5H-6, 125	46.75	44.45	67.61	1.59	0.88	2.64
5H-7, 36	47.36	43.20	66.98	1.61	0.91	2.70
6H-1, 125	48.95	45.65	68.50	1.59	0.86	2.62
6H-2, 125	50.45	43.41	67.02	1.60	0.91	2.68
6H-3, 125	51.95	43.66	67.31	1.61	0.91	2.69
6H-4, 125	53.45	40.71	64.92	1.65	0.98	2.73
6H-5, 125	54.95	44.14	67.88	1.59	0.89	2.71
6H-6, 125	56.45	42.47	66.39	1.63	0.94	2.71
6H-7, 55	57.25	42.74	65.84	1.60	0.91	2.61
7H-1, 55	57.85	44.24	67.89	1.60	0.89	2.69
7H-2, 55	59.35	44.07	67.93	1.60	0.90	2.72
7H-3, 55	60.85	42.97	66.46	1.61	0.92	2.66
7H-4, 55	62.35	41.97	66.21	1.62	0.94	2.74
7H-5, 55	63.85	40.41	65.20	1.69	1.00	2.80
7H-6, 55	65.35	41.74	66.31	1.65	0.96	2.78
7H-7, 55	66.85	43.83	67.44	1.59	0.89	2.68
8H-1, 55	67.55	42.68	66.29	1.61	0.92	2.67
8H-2, 55	69.05	41.49	65.09	1.62	0.95	2.66
8H-3, 55	70.55	41.62	65.31	1.62	0.95	2.67
8H-4, 55	72.05	42.04	66.58	1.65	0.96	2.78
8H-5, 55	73.55	40.67	64.44	1.65	0.98	2.68
8H-6, 55	75.05	41.47	65.47	1.63	0.95	2.71
8H-7, 55	76.55	42.26	65.72	1.62	0.94	2.65
9H-1, 55	77.25	41.76	66.29	1.67	0.97	2.78
9H-2, 55	78.75	40.91	64.88	1.65	0.98	2.70
9H-3, 55	80.25	41.50	65.30	1.62	0.95	2.68
9H-4, 55	81.75	40.75	64.70	1.65	0.98	2.70
9H-5, 55	83.25	40.47	65.13	1.66	0.99	2.78
9H-6, 55	84.75	39.59	63.59	1.68	1.01	2.70
9H-7, 55	86.25	40.45	64.56	1.66	0.99	2.71
10H-1, 55	86.85	37.20	60.70	1.69	1.06	2.64
10H-2, 55	88.35	38.49	63.08	1.70	1.05	2.77
10H-3, 55	89.85	36.10	60.60	1.76	1.13	2.76
10H-4, 55	91.35	38.04	62.56	1.70	1.05	2.76
10H-5, 55	92.85	34.77	59.04	1.76	1.15	2.74
10H-6, 55	94.35	33.94	57.63	1.76	1.16	2.68
10H-7, 55	95.85	38.38	62.44	1.69	1.04	2.70

middle Miocene (Fig. 43, "Organic Geochemistry" section) indicates that depth increased gradually. Such a gradual deepening process cannot be related to the sudden susceptibility changes.

A comparison of susceptibility unit boundaries at Site 758 with the susceptibility units defined at Sites 717 and 719 on the Bengal Sea Fan (Cochran, Stow, et al., 1989) shows that the K2/K3 and the K3/K4 breaks can be correlated with susceptibility breaks identified in Holes 717C (250 and 480 mbsf, respectively) and 719A (Fig. 62). This correlation strongly supports the conclusion drawn from the Site 758 susceptibility record that the susceptibility breaks may reflect phases in Himalayan tectonics. Such a conclusion, however, was not explicitly drawn by the Leg

116 Shipboard Scientific Party from the Hole 717 and 719 susceptibility records.

Numerous models for the evolution of the India-Asia convergence zone have been proposed. Although such models vary widely, there is general consensus on the timing of major tectonic events. For our present purpose it is adequate to illustrate timing of tectonic changes using one of the more recent and representative tectonic syntheses (Klootwijk et al., 1985). Whatever deficiencies this particular model may prove to contain as new field observations become available, it is presently the only evolutionary model that accounts for the oroclinal bending of the Himalayan Arc.

The model from Klootwijk et al. (1985) is summarized in Figure 63. Interpretation of the marked breaks between susceptibility units K1 to K6 is confined to the Neogene part of the model (i.e., stages C to E).

K5/K6 Break (15–20 Ma)

The K5/K6 break is the least conspicuous break. Its late early Miocene timing relates to an initial uplift phase of the Higher Himalaya, shortly after the latest Oligocene to early Miocene initiation of intracontinental underthrusting along the Main Central Thrust. At that time the Indian shield started to subduct below its choked-off northern margin (stage C, Fig. 63). This uplift is a Himalayan-wide event that is well dated around 17 Ma, from $^{40}\text{Ar}/^{39}\text{Ar}$ studies in the Everest region (17 Ma; Kaneoka and Kono, 1981) and Gangdese Belt (17–20 Ma; Copeland et al., 1987) and fission track studies of the northwest Himalayan Syntaxis (just prior to 15 Ma; Zeitler et al., 1982). Results from recent drilling on the Bengal Sea Fan (Cochran, Stow, et al., 1989) indicate that this phase was already well established at 17 Ma.

K4/K5 Break (9 Ma)

The K4/K5 break is reflected in a sharp increase in the sedimentation rate. It agrees closely in timing with initiation of the Middle Siwaliks sedimentation (10 Ma; Johnson et al., 1982; Mascle and Herail, 1982), which reflects increased uplift of the Higher Himalaya. It is possible that the marked increase in sedimentation rate in the Hole 758A record (Fig. 61), which continues until the present, reflects the onset of a change from compressional tectonism to an extensional regime in southern Tibet (10–5 Ma; Mercier et al., 1987).

K3/K4 Break (5–6 Ma)

This phase can be related to the initiation of major extensional tectonism in southern Tibet (4 Ma; Tapponnier et al., 1982, 1986). This extension may have already started in the latest Miocene, as suggested by a basal sedimentary sequence of that age in the Kali Gandaki graben of the Nepal Himalaya (Colchen et al., 1980). This extensional tectonism has been related, causally and in timing, to oroclinal bending of the Himalayan Arc (Klootwijk et al., 1985; stage E, Fig. 63). This phase is also expressed in the onset of Upper Siwaliks sedimentation (5 Ma; Johnson et al., 1982; Mascle and Herail, 1982), which reflects increased topographic relief, and coincides in timing with a major tectonic change in the Northwestern Himalayan Syntaxis (4–5 Ma; Burbank, 1983; Burbank and Reynolds, 1984).

K2/K3 (2.5 Ma) and K1/K2 Breaks (2 Ma)

The K2/K3 and K1/K2 breaks can be related to major pulses of uplift at about 2 Ma in the Northwestern Himalayan Syntaxis (Burbank and Reynolds, 1984) and in the Higher Himalaya (Zhang et al., 1980; Fort et al., 1982; Mercier et al., 1987).

REFERENCES

- Barron, J. A., 1980. Upper Pliocene and Quaternary diatom biostratigraphy of Deep Sea Drilling Project Leg 54, tropical eastern Pacific. In Rosendahl, B. R., Hekinian R., et al., *Init. Repts. DSDP*, 54: Washington (U.S. Govt. Printing Office), 455–485.
- , 1985a. Late Eocene to Holocene diatom stratigraphy of the equatorial Pacific Ocean, Deep Sea Drilling Project Leg 85. In Mayer, L., Theyer, F., Thomas, E., et al., *Init. Repts. DSDP*, 85: Washington (U.S. Govt. Printing Office), 413–456.
- , 1985b. Miocene to Holocene planktic diatoms. In Bolli, H. M., Saunders, J. G., and Perch-Nielsen, K. (Eds.), *Plankton Stratigraphy*: Cambridge (Cambridge Univ. Press), 763–810.
- Barron, J. A., Nigrini, C. A., Pujos, A., Saito, T., Theyer, F., Thomas, E., and Weinreich, N., 1985. Synthesis of biostratigraphy, central equatorial Pacific, Deep Sea Drilling Project Leg 85: refinement of Oligocene to Quaternary biochronology. In Mayer, L., Theyer, F., Thomas, E., et al., *Init. Repts. DSDP*, 85: Washington (U.S. Govt. Printing Office), 905–934.
- Basov, I. A., and Krashennnikov, V. A., 1983. Stratigraphy of Cretaceous sediments of the Falkland Plateau based on planktonic foraminifers, Deep Sea Drilling Project, Leg 71. In Ludwig, W. J., Krashennnikov, V. A., et al., *Init. Repts. DSDP*, 71: Washington (U.S. Govt. Printing Office), 745–771.
- Berggren, W. A., 1973. The Pliocene time-scale: calibration of planktonic foraminiferal and calcareous nannoplankton zones. *Nature*, 243:391–397.
- Berggren, W. A., Kent, D. V., Flynn, J. J., and Van Couvering, J. A., 1985. Cenozoic geochronology. *Geol. Soc. Am. Bull.*, 96:1407–1418.
- Blow, W. H., 1969. Late middle Eocene to Recent planktonic biostratigraphy. In Bronnimann, P., and Renz, H. H. (Eds.), *Proc. Int. Conf. Planktonic Microfossils, 1st, Geneva, 1967*, 1:199–421.
- Bolli, H. M., Saunders, J. B., and Perch-Nielsen, K. (Eds.), 1985. *Plankton Stratigraphy*: Cambridge (Cambridge Univ. Press).
- Bougault, H., Treuil, M., and Joron, J.-L., 1979. Trace elements in basalts from 23°N and 36°N in the Atlantic Ocean: fractional crystallization, partial melting, and heterogeneity of the upper mantle. In Melson, W. G., Rabinowitz, P. D., et al., *Init. Repts. DSDP*, 45: Washington (U.S. Govt. Printing Office), 493–506.
- Burbank, D. W., 1983. The chronology of intermontane-basin development in the Northwestern Himalaya and the evolution of the Northwest Syntaxis. *Earth Planet. Sci. Lett.*, 64:77–92.
- Burbank, D. W., and Reynolds, R.G.H., 1984. Sequential late Cenozoic structural disruption of the northern Himalayan foredeep. *Nature*, 34:114–118.
- Burckle, L. H., 1972. Late Cenozoic planktonic diatom zones from the eastern equatorial Pacific. *Nova Hedwigia*, 39:217–246.
- Burke, S. C., 1981. Recent benthic foraminifera of the Ontong Java Plateau. *J. Foraminiferal Res.*, 11:1–19.
- Caron, M., 1985. Cretaceous planktic foraminifera. In Bolli, H. M., Saunders, J. B., and Perch-Nielsen, K. (Eds.), *Plankton Stratigraphy*: Cambridge (Cambridge Univ. Press), 713–762.
- Cochran, J. R., Stow, D.A.V., et al., 1989. *Proc. ODP, Init. Repts.*, 116: College Station, TX (Ocean Drilling Program).
- Cochran, J. R., Stow, D.A.V., and Leg 116 Shipboard Scientific Party, 1987. Collision in the Indian Ocean. *Nature*, 330:519–521.
- Colchen, M., Fort, M., and Freydet, P., 1980. Evolution paléogéographique et structurale du fossé de la Thakkhola-Mustang (Himalaya du Nepal): implications sur l'histoire récente de la chaîne Himalayenne. *C. R. Acad. Sci. Ser. 2*, 290:314–317.
- Copeland, P., Harrison, T. M., Kidd, W.S.F., Xu Ronghua, and Zhang Yuquan, 1987. Rapid early Miocene acceleration of uplift in the Gangdese Belt, Xizang (southern Tibet), and its bearing on accommodation mechanisms of the India-Asia collision. *Earth Planet. Sci. Lett.*, 86:240–252.
- Corliss, B. H., 1979. Recent deep-sea benthonic foraminiferal distribution in the southeast Indian Ocean: inferred bottom-water routes and ecological implications. *Mar. Geol.*, 31:115–138.
- Curry, J. R., Emmel, F. J., Moore, D. G., and Raitt, R. W., 1982. Structure, tectonics and geological history of the northeastern Indian Ocean. In Nairn, A.E.M., and Stehli, F. G. (Eds.), *The Indian Ocean*: New York (Plenum), 399–450.

- Davies, T. A., Luyendyk, B. P., et al., 1974. *Init. Repts. DSDP*, 26: Washington (U.S. Govt. Printing Office).
- Donnelly, T., Francheteau, J., Bryan, W., Robinson, P., Flower, M., Salisbury, M., et al., 1980. *Init. Repts. DSDP*, 51, 52, 53: Washington (U.S. Govt. Printing Office).
- Duncan, R. A., 1978. Geochronology of basalts from the Ninetyeast Ridge and continental dispersion in the eastern Indian Ocean. *J. Volcanol. Geotherm. Res.*, 4:283-305.
- Duncan, R. A., Backman, J., Macdonald, A., et al., in press. Réunion hotspot activity through Tertiary time: initial results from the Ocean Drilling Program, Leg 115. *J. Volcanol. Geotherm. Res.*
- Fenner, J., 1981. Diatoms in the Eocene and Oligocene sediments off northwest Africa, their stratigraphic and paleogeographic occurrences [Ph.D. dissert.]. Univ. Kiel.
- _____, 1984. Eocene-Oligocene planktic diatom stratigraphy in the low latitudes and in the high southern latitudes. *Micropaleontology*, 30:319-442.
- Fort, M., Freyret, P., and Colchen, M., 1982. Structural and sedimentological evolution of the Thakkhola-Mustang graben (Nepal Himalayas). *Z. Geomorphol. Suppl.*, 42:75-98.
- Hansen, H. J., 1970. Biometric studies on the stratigraphic evolution of *Globoconusa daubjergensis* (Bronniman) from the Danian of Denmark. *Dan. Geol. Foren. Medd.*, 19:314-360.
- Harland, W. B., Cox, A. V., Llewellyn, P. G., Pickton, C.A.G., Smith, A. G., and Walters, R., 1982. *A Geologic Time Scale*: Cambridge (Cambridge Univ. Press).
- Herb, R., 1974. Cretaceous planktonic foraminifera from the eastern Indian Ocean. In Davies, T. A., Luyendyk, B. P., et al., *Init. Repts. DSDP*, 26: Washington (U.S. Govt. Printing Office), 745-771.
- Johnson, N. M., Opdyke, N. P., Johnson, G. D., Lindsay, E. H., and Tahirkheli, R.A.K., 1982. A time framework based on magnetostratigraphy for the Siwaliks sediments of the Kaur area (Peshawar, Pakistan). *Paleoclimatol. Paleocenoogr. Paleocol.*, 37:17-42.
- Kaneoka, I., and Kono, M., 1981. $^{40}\text{Ar}/^{39}\text{Ar}$ dating of Himalayan rocks from the Mount Everest region. *J. Geophys.*, 49:207-211.
- Klootwijk, C. T., 1979. A review of palaeomagnetic data from the Indian fragment of Gondwanaland. In Farah, A., and De Jong, K. A. (Eds.), *Geodynamics of Pakistan*: Quetta (Geol. Surv. Pakistan), 41-80.
- Klootwijk, C. T., Conaghan, P. J., and Powell, C. McA., 1985. The Himalayan Arc: large-scale continental subduction, oroclinal bending and back-arc spreading. *Earth Planet. Sci. Lett.*, 75:167-183.
- Lawrence, J. R., and Gieskes, J. M., 1981. Constraints on water transport and alteration in the oceanic crust from the isotopic composition of pore water. *J. Geophys. Res.*, 86:7924-7934.
- Masclé, G., and Herail, G., 1982. Les Siwaliks: le prisme d'accrétion tectonique associée à la subduction intracontinentale himalayenne. *Geol. Alpine*, 58:95-103.
- Mercier, J. L., Armijo, R., Tapponnier, P., Carey-Gailhardis, E., and Han Tong Lin, 1987. Change from late Tertiary compression to Quaternary extension in southern Tibet during the India-Asia collision. *Tectonics*, 6:275-304.
- Molnar, P., and Tapponnier, P., 1975. Cenozoic tectonics of Asia: effects of a continental collision. *Science*, 189:419-426.
- Morgan, W. J., 1983. Hotspot tracks and the early rifting of the Atlantic. *Tectonophysics*, 94:123-139.
- Ninkovich, D., Shackleton, N. J., Abdel-Monem, A. A., Obradovich, J. D., and Izett, G., 1978. K-Ar age of the late Pleistocene eruption of Toba, North Sumatra. *Nature*, 276:574-577.
- Okada, H., and Bukry, D., 1980. Supplementary modification and introduction of code numbers to the low latitude coccolith biostratigraphy (Bukry, 1973; 1975). In Haq, B. U. (Ed.), *Nannofossil Biostratigraphy*: Stroudsburg, PA (Hutchison Ross), 321-377.
- Patriat, P., and Achache, J., 1984. India-Eurasia collision chronology has implications for crustal shortening and driving mechanism of plates. *Nature*, 311:615-621.
- Pearce, J. W., 1978. The northward motion of India since the Late Cretaceous. *Geophys. J. R. Astron. Soc.*, 52:277-312.
- Peterson, L. C., 1984. Recent abyssal benthic foraminiferal biofacies of the eastern equatorial Indian Ocean. *Mar. Micropaleontol.*, 8:479-579.
- Prell, W. L., Niitsuma, N., et al., 1989. *Proc. ODP, Init. Repts.*, 117: College Station, TX (Ocean Drilling Program).
- Price, R. C., Kennedy, A. K., Riggs-Sneeringer, M., and Frey, F. A., 1986. Geochemistry of basalts from the Indian Ocean triple junction: implications for the generation and evolution of Indian Ocean Ridge basalts. *Earth Planet. Sci. Lett.*, 78:379-396.
- Rea, D. K., Leinen, M., and Janecek, T. R., 1985. Geologic approach to the long-term history of atmospheric circulation. *Science*, 227: 721-725.
- Royer, J.-Y., Sclater, J. G., and Sandwell, D. T., in press. A preliminary tectonic chart of the Indian Ocean. *Proc. Indian Acad. Sci., Earth Planet. Sci.*
- Saunders, A. D., 1983. Geochemistry of basalts recovered from the Gulf of California during Leg 65 of the Deep Sea Drilling Project. In Lewis, B.T.R., Robinson, P., et al., *Init. Repts. DSDP*, 65: Washington (U.S. Govt. Printing Office), 591-622.
- Schrader, H.-J., 1974. Cenozoic marine planktonic diatom stratigraphy of the tropical Indian Ocean. In Fisher, R. L., Bunce, E. T., et al., *Init. Repts. DSDP*, 24: Washington (U.S. Govt. Printing Office), 887-967.
- Seeber, L., Armbruster, J. G., and Quittmeyer, R. C., 1981. Seismicity and continental subduction in the Himalayan Arc. In Gupta, H. K., and Delany, F. M. (Eds.), *Zagros, Hindu Kush, Himalaya Geodynamic Evolution*: Washington (Am. Geophys. Union), 215-242.
- Sissingh, W., 1977. Biostratigraphy of Cretaceous calcareous nannoplankton. In Haq, B. U. (Ed.), *Nannofossil Biostratigraphy*: Stroudsburg, PA (Hutchinson Ross), 129-144.
- Sliter, W. V., 1975. Cretaceous foraminifers from the southwestern Atlantic Ocean, Leg 36, Deep Sea Drilling Project. In Barker, P., Dalziel, I.W.D., et al., *Init. Repts. DSDP*, 36: Washington (U.S. Govt. Printing Office), 519-574.
- _____, 1977. Cretaceous benthic foraminifers from the western South Atlantic Leg 39, Deep Sea Drilling Project. In Perch-Nielsen, K., Supko, P. R., et al., *Init. Repts. DSDP*, 39: Washington (U.S. Govt. Printing Office), 657-697.
- Smit, J., 1982. Extinction and evolution of planktonic foraminifera at the Cretaceous/Tertiary boundary. In Silver, L. T., and Schultz, P. H. (Eds.), *Geological Implications of Impacts of Large Asteroids and Comets on the Earth*: Spec. Pap. Geol. Soc. Am., 190:329-353.
- Srivastava, S. P., Arthur, M. A., et al., 1987. *Proc. ODP, Init. Repts.*, 105: College Station, TX (Ocean Drilling Program).
- Stainforth, R. M., Lamb, J. L., Luterbacher, H. P., Beard, J. H., and Jeffords, R. M., 1975. Cenozoic planktonic foraminiferal zonation and characteristics of index forms. *Univ. Kans. Paleontol. Contrib. Pap.*, 62.
- Stein, S., and Okal, E., 1978. Seismicity and tectonics of the Ninetyeast Ridge area: evidence for internal deformation of the Indian plate. *J. Geophys. Res.*, 83:2233-245.
- Storey, M., Saunders, A. D., Tosney, J., Leak, P., Thrillwall, M. F., Thompson, R. N., Menzies, M. A., and Marriner, G. F., 1988. Geochemical evidence for plume-mantle interactions beneath Kerguelen and Heard islands, Indian Ocean. *Nature*, 336:371-374.
- Sun, S. S., and McDonough, W. F., in press. Chemical and isotopic systematics of oceanic basalts: implications for mantle composition and processes. In Saunders, A. D., and Norry, M. J. (Eds.), *Magma-tism in Ocean Basins*: Spec. Publ. Geol. Soc. London.
- Tapponnier, P., Peltzer, G., and Armijo, R., 1986. On the mechanics of the collision tectonics between India and Asia. In Coward, M. P., and Rees, A. C. (Eds.), *Collision Tectonics*: Spec. Publ. Geol. Soc. London, 19:115-157.
- Tapponnier, P., Peltzer, G., Le Dain, A. Y., Armijo, R., and Cobbold, P., 1982. Propagating extrusion tectonics in Asia: new insights from simple experiments with plasticine. *Geology*, 10:611-616.
- Toumarkine, M., and Luterbacher, H., 1985. Paleocene and Eocene planktic foraminifera. In Bolli, H. M., Saunders, J. B., Perch-Nielsen, K. (Eds.), *Plankton Stratigraphy*: Cambridge (Cambridge Univ. Press), 87-154.
- Webb, P. N., 1973. Upper Cretaceous-Paleocene foraminifera from Site 208 (Lord Howe Rise, Tasman Sea), DSDP Leg 21. In Burns, R. E., Andrews, J. E., et al., *Init. Repts. DSDP*, 21: Washington (U.S. Govt. Printing Office), 541-573.
- Zeitler, P. K., Tahirkheli, R.A.K., Naeser, C. W., and Johnson, N. M., 1982. Unroofing the history of a suture zone in the Himalaya of Pakistan by means of fission-track annealing ages. *Earth Planet. Sci. Lett.*, 57:227-240.
- Zhang, R.-Z., et al., 1980. *A Scientific Guide Book to South Xizang (Tibet), June 2—June 14, 1980*: Beijing (Acad. Sinica).

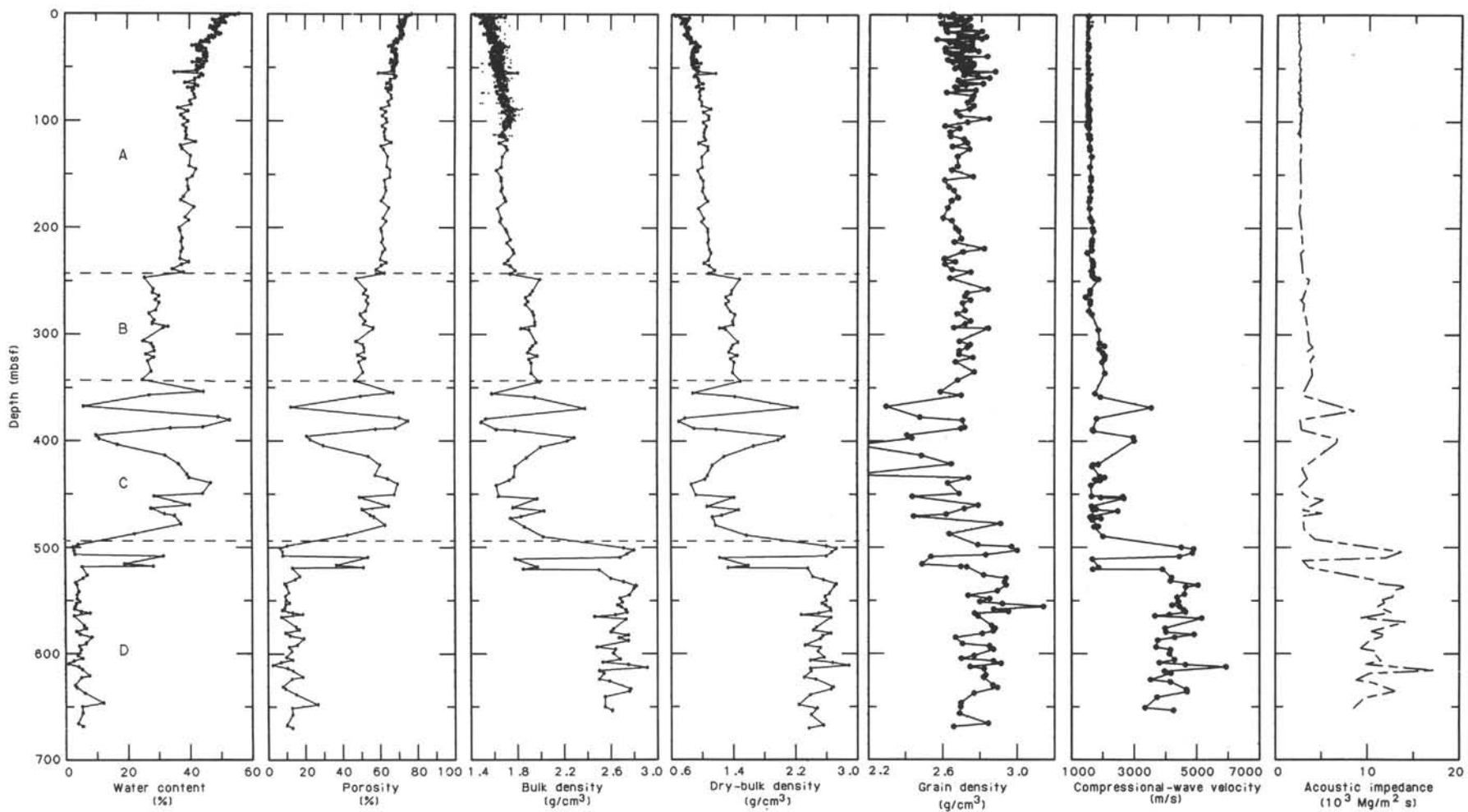


Figure 47. Water content, porosity, bulk density, dry-bulk density, grain density, compressional-wave velocity, and acoustic impedance profiles of samples from Hole 758A.

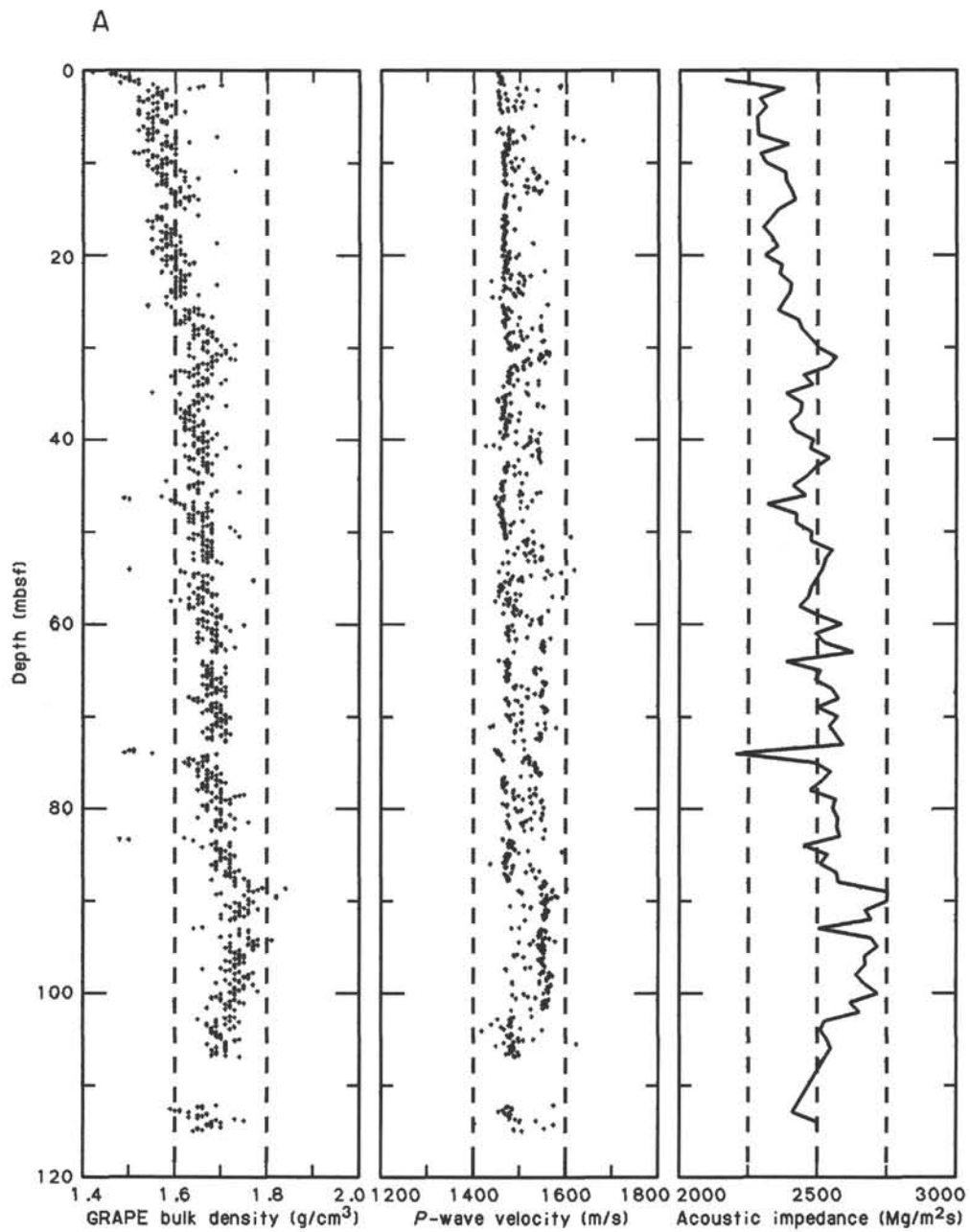


Figure 48. **A.** GRAPE densities, *P*-wave-logger velocities, and acoustic impedance profiles from Hole 758A. **B.** GRAPE densities, *P*-wave-logger velocities, and acoustic impedance profiles from Hole 758B.

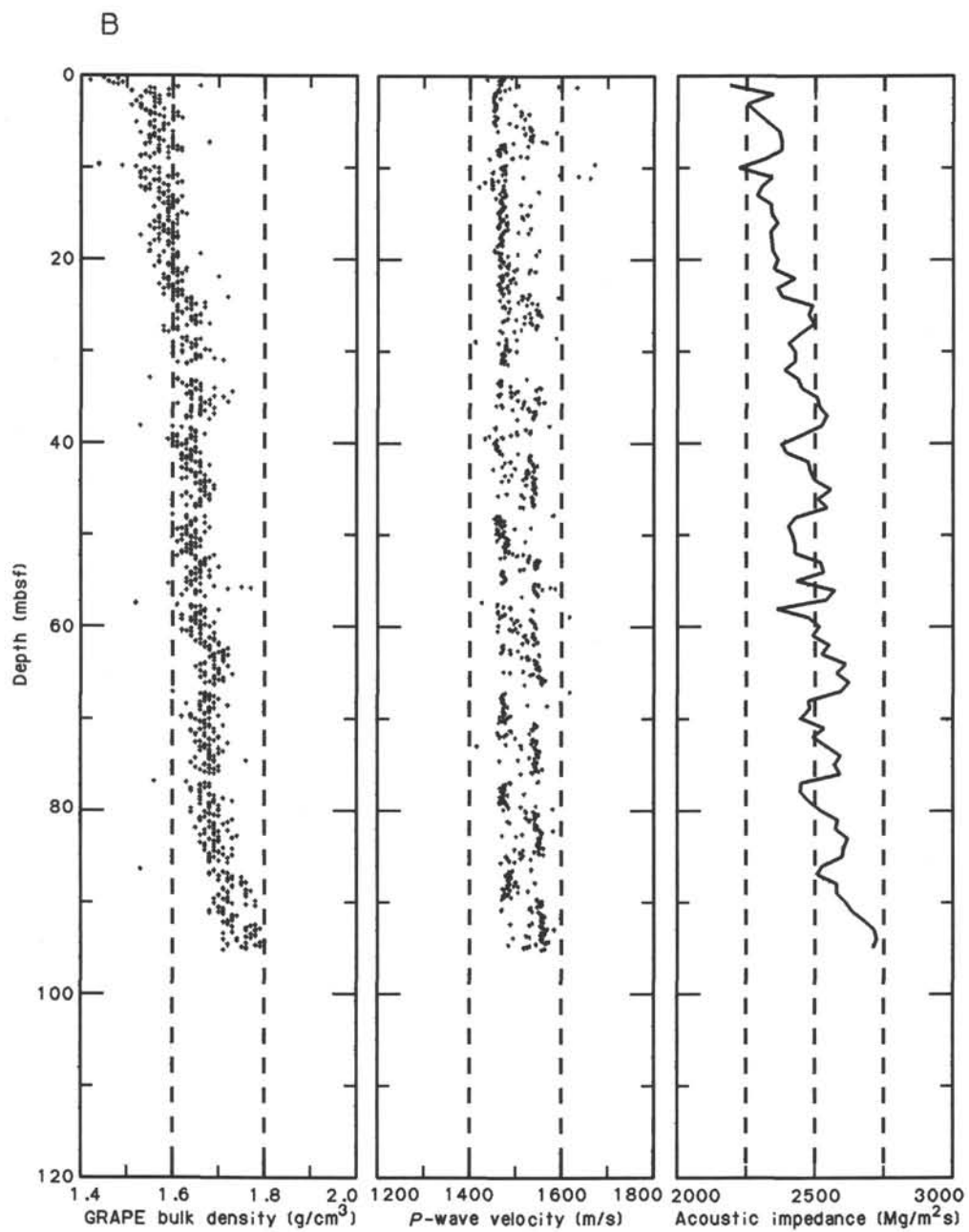


Figure 48 (continued).

Table 19. Compressional-wave velocity of samples from Hole 758A.

Core, section, interval (cm)	Depth (mbsf)	Direction ^a	Compressional-wave velocity (m/s)
8H-4, 125	69.45	C	1560.8
9H-2, 10	75.00	C	1472.8
9H-4, 7	77.97	C	1481.7
9H-6, 13	81.03	C	1524.1
10H-2, 21	84.81	C	1509.2
10H-4, 12	87.72	C	1511.2
10H-6, 11	90.71	C	1548.6
11H-2, 16	94.46	C	1530.2
11H-6, 13	100.43	C	1538.1
12X-2, 12	104.02	C	1501.2
12X-4, 24	107.14	C	1539.8
13X-2, 11	113.71	C	1554.0
13X-4, 11	116.71	C	1576.3
14X-2, 65	123.85	C	1562.3
14X-4, 65	126.85	C	1567.3
15X-2, 70	133.60	C	1628.7
16X-2, 75	143.25	C	1572.7
17X-2, 80	153.00	C	1612.3
17X-4, 67	155.87	C	1631.9
18X-2, 90	162.80	C	1592.2
18X-4, 60	165.50	C	1618.8
19X-2, 55	172.05	C	1590.3
19X-4, 65	175.15	C	1576.1
20X-2, 70	181.90	C	1590.0
21X-2, 67	191.47	C	1599.8
21X-4, 64	194.44	C	1669.5
22X-2, 91	201.41	C	1677.0
22X-CC, 29	204.01	C	1713.5
23X-2, 138	211.58	C	1660.3
23X-4, 42	213.62	C	1658.1
23X-CC, 28	217.05	C	1644.2
24X-2, 93	220.73	C	1667.6
24X-4, 118	223.98	C	1521.3
25X-2, 146	230.96	C	1681.8
25X-4, 87	233.37	C	1699.0
25X-6, 34	235.84	C	1706.1
26X-2, 142	240.62	C	1646.4
26X-4, 42	242.62	C	1669.3
26X-CC, 40	245.06	C	1678.2
27X-1, 5	247.35	C	1751.2
27X-1, 95	248.25	C	1898.2
28X-2, 14	258.54	C	1614.3
28X-4, 16	261.56	C	1611.9
28X-6, 21	264.61	C	1452.0
29X-2, 13	268.23	C	1617.6
29X-4, 12	271.22	C	1611.5
30X-2, 10	277.90	C	1565.4
30X-4, 21	281.01	C	1673.0
31X-2, 133	288.73	C	1632.4
31X-4, 7	290.47	C	1694.5
31X-6, 11	293.51	C	1768.0
31X-CC, 31	295.52	A	1884.2
31X-CC, 31	295.52	B	1894.8
33X-2, 72	307.52	C	1924.3
33X-2, 72	307.52	A	1932.8
33X-2, 72	307.52	B	1950.5
33X-4, 72	310.52	A	2089.8
33X-4, 72	310.52	B	2051.7
33X-4, 72	310.52	C	2113.9
33X-6, 72	313.52	A	1900.5
33X-6, 72	313.52	B	1958.4
33X-6, 72	313.52	C	1985.0
34X-2, 70	317.10	C	2069.6
34X-2, 70	317.10	A	2026.6
34X-2, 70	317.10	B	2039.2
34X-4, 73	320.13	A	2122.6
34X-4, 73	320.13	C	2184.3
34X-4, 73	320.13	B	2238.2
34X-6, 80	323.20	C	2114.2
34X-6, 80	323.20	B	2055.1
34X-6, 80	323.20	A	2105.1
35X-2, 60	326.70	C	2103.4
35X-2, 60	326.70	B	2113.2
35X-2, 60	326.70	A	2017.0
36X-2, 59	336.39	C	2128.0
36X-2, 59	336.39	B	2135.0

Table 19 (continued).

Core, section, interval (cm)	Depth (mbsf)	Direction ^a	Compressional-wave velocity (m/s)
36X-2, 59	336.39	A	2119.8
37X-CC, 16	344.37	C	2162.8
37X-CC, 16	344.37	B	2153.0
38X-2, 145	355.55	C	1898.8
38X-2, 145	355.55	B	1880.5
38X-2, 145	355.55	A	1792.4
39X-1, 124	358.84	C	2081.1
39X-1, 124	358.84	B	2048.1
39X-1, 124	358.84	A	1974.9
40X-2, 41	369.21	A	3597.6
41X-2, 70	379.20	C	1962.3
41X-2, 70	379.20	B	1878.3
41X-2, 70	379.20	A	1861.5
41X-4, 77	382.27	C	1917.9
41X-4, 77	382.27	B	1924.3
42X-2, 86	388.96	C	1808.8
42X-2, 86	388.96	B	1813.8
42X-2, 86	388.96	A	1727.5
42X-3, 31	389.91	A	1746.4
42X-3, 31	389.91	B	1855.9
42X-3, 31	389.91	C	1857.5
43X-1, 44	396.74	A	3015.4
43X-1, 44	396.74	B	3265.8
44X-CC, 29	399.89	A	3048.6
44X-CC, 29	399.89	C	3283.1
44X-CC, 29	399.89	B	3331.3
47R-1, 43	421.93	A	1904.9
47R-1, 56	422.06	A	1736.5
47R-2, 73	423.73	A	1724.5
47R-2, 76	423.76	A	1697.7
47R-2, 76	423.76	B	1762.9
47R-2, 76	423.76	C	1794.1
48R-2, 41	433.11	A	1977.4
48R-2, 71	433.41	A	1958.1
48R-2, 71	433.41	C	1972.0
48R-2, 71	433.41	B	1976.6
48R-2, 138	434.08	A	2109.6
48R-3, 110	435.30	A	1926.7
48R-4, 41	436.11	A	1817.0
48R-4, 108	436.78	A	1973.9
49R-1, 66	441.56	B	1804.8
49R-1, 66	441.56	C	1796.1
49R-1, 66	441.56	A	1675.3
50R-1, 96	451.56	A	1696.6
50R-1, 96	451.56	C	1793.1
50R-2, 15	452.25	A	2694.6
50R-2, 71	452.81	A	1993.6
50R-3, 34	453.94	C	2810.3
50R-3, 34	453.94	A	2736.9
51R-1, 53	460.73	A	1700.2
51R-1, 53	460.73	C	1805.5
51R-2, 14	461.84	C	1804.6
51R-2, 14	461.84	A	1705.6
51R-2, 135	463.05	A	1839.8
51R-3, 94	464.14	C	1798.9
51R-3, 94	464.14	A	1742.6
51R-4, 78	465.48	A	2530.6
51R-4, 78	464.48	C	2446.2
52R-1, 22	470.12	A	1725.8
52R-1, 96	470.86	A	1661.8
52R-2, 131	472.71	C	2170.0
52R-2, 131	472.71	A	2010.1
52R-3, 36	473.26	A	1712.4
53R-1, 35	479.95	A	1919.5
53R-1, 66	480.26	A	1787.7
54R-1, 34	489.54	A	2069.3
54R-1, 34	489.54	C	2337.9
54R-1, 34	489.54	B	2256.5
55R-1, 94	499.84	C	4681.0
55R-1, 94	499.84	B	4529.3
55R-1, 94	499.84	A	4574.2
55R-3, 25	501.99	C	5082.4
55R-3, 25	501.99	B	4947.2
55R-3, 25	501.99	A	4976.9
55R-5, 86	505.46	C	4931.4
55R-5, 86	505.46	B	4924.5
55R-5, 86	505.46	A	4922.2

Table 19 (continued).

Core, section, interval (cm)	Depth (mbsf)	Direction ^a	Compressional-wave velocity (m/s)
56R-1, 69	509.09	B	4481.3
56R-1, 69	509.09	A	4511.6
56R-1, 69	509.09	C	4586.9
56R-2, 78	510.68	C	1758.0
56R-2, 78	510.68	B	1750.6
56R-2, 78	510.68	A	1715.1
57R-1, 20	518.10	A	1924.9
57R-1, 20	518.10	C	2657.6
57R-1, 20	518.10	B	2584.3
57R-2, 82	520.22	A	1738.5
57R-2, 82	520.22	C	1827.0
57R-2, 82	520.22	B	1839.3
57R-3, 15	520.76	B	4013.1
57R-3, 15	520.76	C	3913.2
57R-3, 15	520.76	A	3950.2
58R-2, 15	528.71	B	4260.3
58R-2, 15	528.71	C	4278.8
58R-2, 15	528.71	A	4253.9
58R-4, 14	531.70	A	4214.4
58R-4, 14	531.70	B	4332.0
58R-4, 14	531.70	C	4406.1
58R-6, 137	535.58	B	5105.6
58R-6, 137	535.58	A	5108.0
58R-6, 137	535.58	C	5131.1
59R-1, 136	537.86	B	4785.9
59R-1, 136	537.86	A	4709.3
59R-1, 136	537.86	C	4801.7
59R-6, 56	544.14	C	4565.5
59R-6, 56	544.14	A	4676.7
59R-6, 56	544.14	B	4807.1
60R-2, 12	547.29	A	4420.1
60R-2, 12	547.29	C	4420.1
60R-2, 12	547.29	B	4402.0
60R-4, 109	551.03	B	4357.6
60R-4, 109	551.03	A	4463.8
60R-4, 109	551.03	C	4543.0
60R-6, 108	553.76	C	4512.6
60R-6, 108	553.76	B	4296.8
60R-6, 108	553.76	A	4259.9
61R-1, 36	555.46	B	4503.1
61R-1, 36	555.46	A	4512.6
61R-1, 36	555.46	C	4541.1
61R-3, 98	558.40	B	4709.0
61R-3, 98	558.40	A	4650.1
61R-3, 98	558.40	C	4742.3
61R-5, 19	560.51	C	4783.7
61R-5, 19	560.51	B	4740.1
61R-5, 19	560.51	A	4697.4
61R-7, 12	563.03	C	4130.8
61R-7, 12	563.03	B	4126.9
61R-7, 12	563.03	A	4167.0
62R-1, 25	564.55	A	3709.1
62R-1, 25	564.55	B	3672.3
62R-1, 25	564.55	C	3791.3
62R-2, 125	567.01	B	5314.5
62R-2, 125	567.01	C	5160.8
62R-2, 125	567.01	A	5227.1
63R-2, 114	576.26	A	4035.4
63R-2, 114	576.26	B	4247.6
63R-2, 114	576.26	C	4178.5
63R-4, 129	579.06	B	4029.6
63R-4, 129	579.06	A	4065.7
63R-4, 129	579.06	C	4143.4
63R-6, 133	581.71	B	4990.8
63R-6, 133	581.71	C	4988.5
63R-6, 133	581.71	A	4974.8
64R-1, 123	584.43	A	4344.0
64R-1, 123	584.43	C	4279.3
64R-1, 123	584.43	B	4329.3
64R-3, 114	587.12	A	3794.7
64R-3, 114	587.12	C	3760.8
64R-3, 114	587.12	B	3850.8
65R-1, 62	593.32	A	3756.5
65R-1, 62	593.32	C	3791.6
65R-1, 62	593.32	B	3785.0
65R-3, 24	595.45	A	4212.1
65R-3, 24	595.45	C	4253.4

Table 19 (continued).

Core, section, interval (cm)	Depth (mbsf)	Direction ^a	Compressional-wave velocity (m/s)
65R-3, 24	595.45	B	4262.3
65R-5, 96	598.98	B	4220.3
65R-5, 96	598.98	A	4172.1
65R-5, 96	598.98	C	4236.8
66R-2, 110	604.69	A	4344.8
66R-2, 110	604.69	B	4321.4
66R-2, 110	604.69	C	4455.9
66R-4, 123	607.42	B	3898.9
66R-4, 123	607.42	A	3862.3
66R-4, 123	607.42	C	3891.9
66R-6, 55	609.64	B	4705.9
66R-6, 55	609.64	A	4695.7
66R-6, 55	609.64	C	4832.2
67R-1, 87	612.37	A	6005.5
67R-1, 87	612.37	B	6078.4
67R-3, 80	615.25	C	4033.3
67R-3, 80	615.25	A	4014.8
67R-3, 80	615.25	B	4067.3
67R-5, 37	617.78	A	4222.7
67R-5, 37	617.78	B	4113.6
67R-5, 37	617.78	C	4213.1
68R-2, 123	623.52	C	3667.8
68R-2, 123	623.52	B	3600.3
68R-2, 123	623.52	A	3580.0
68R-4, 33	625.43	B	4304.6
68R-4, 33	625.43	A	4220.0
68R-4, 33	625.43	C	4406.6
69R-2, 109	632.66	C	4853.9
69R-2, 109	632.66	B	4684.8
69R-2, 109	632.66	A	4727.5
69R-4, 58	634.78	B	4566.9
69R-4, 58	634.78	C	4680.4
69R-4, 58	634.78	A	4747.2
70R-1, 74	640.14	C	3814.2
70R-1, 74	640.14	A	3783.5
70R-1, 74	640.14	B	3824.5
71R-1, 89	649.49	B	3372.7
71R-1, 89	649.49	A	3385.0
71R-3, 121	652.77	C	4418.8
71R-3, 121	652.77	A	4308.3
71R-3, 121	652.77	B	4053.9
72R-1, 91	658.91	C	3987.0
72R-1, 91	658.91	B	4058.5
72R-1, 91	658.91	A	3944.9
73R-1, 121	668.81	C	4374.5
73R-1, 121	668.81	B	4284.9
73R-1, 121	668.81	A	4300.6
73R-3, 102	671.55	C	3849.3
73R-3, 102	671.55	B	3847.7
73R-3, 102	671.55	A	3878.6

^a A = vertical propagation; B = propagation perpendicular to the split-core face; C = propagation parallel to the split-core face.

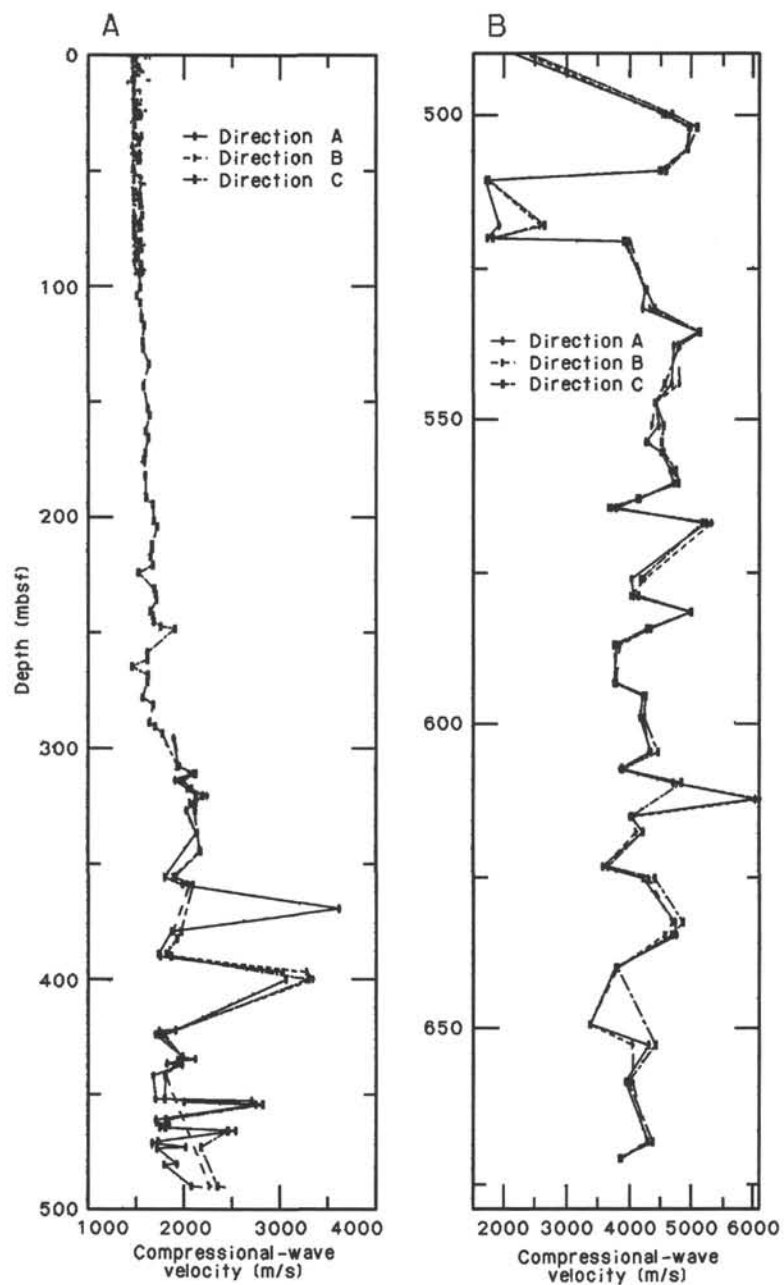


Figure 49. Compressional-wave velocity of samples from Hole 758A. Direction A is a velocity of vertical propagation. Directions B and C are velocities of horizontal propagation, where velocity B is perpendicular to the split-core surface of the sample and velocity C is parallel to it. **A.** 0 to 490 mbsf. **B.** 490 to 670 mbsf. Note scale change from Figure 49A.

Table 20. Vane shear strength of samples from Hole 758A.

Core, section, interval (cm)	Depth (mbsf)	Undrained shear strength (kPa)
1H-2, 65	2.15	16.9
1H-4, 65	5.15	42.1
2H-2, 65	8.15	36.2
2H-4, 107	11.57	47.7
2H-6, 65	14.15	67.5
3H-2, 65	17.75	54.1
3H-4, 137	21.47	52.9
3H-6, 137	24.47	50.5
4H-2, 126	27.96	73.6
4H-4, 126	30.96	77.1
4H-6, 126	33.96	83.7
5H-2, 126	37.56	54.5
5H-4, 126	40.56	57.9
5H-6, 125	43.55	61.3
6H-2, 125	47.15	40.8
6H-4, 125	50.15	56.1
6H-6, 125	53.15	65.8
7H-2, 125	56.75	40.8
7H-4, 125	59.75	96.4
7H-6, 129	62.79	72.6
8H-2, 126	66.46	66.9
8H-4, 125	69.45	77.2
8H-6, 122	72.42	81.7
9H-2, 125	76.15	97.6
9H-4, 125	79.15	102.1
9H-6, 125	82.15	104.4
10H-2, 90	85.50	54.5
10H-4, 95	88.55	82.8
10H-6, 95	91.55	61.3
11H-2, 95	95.25	52.2
11H-4, 95	98.25	82.8
11H-6, 95	101.25	80.6
12X-2, 95	104.85	38.6
12X-4, 95	107.85	42.0
12X-6, 95	110.85	34.0
13X-2, 95	114.55	61.3
13X-4, 95	117.55	72.6
13X-6, 95	120.55	42.0
28X-2, 88	259.28	9.8
28X-4, 107	262.47	17.9
28X-6, 129	265.69	24.5
29X-2, 95	269.05	12.6
29X-4, 63	271.73	35.2
30X-2, 95	278.75	26.1
30X-4, 95	281.75	32.9

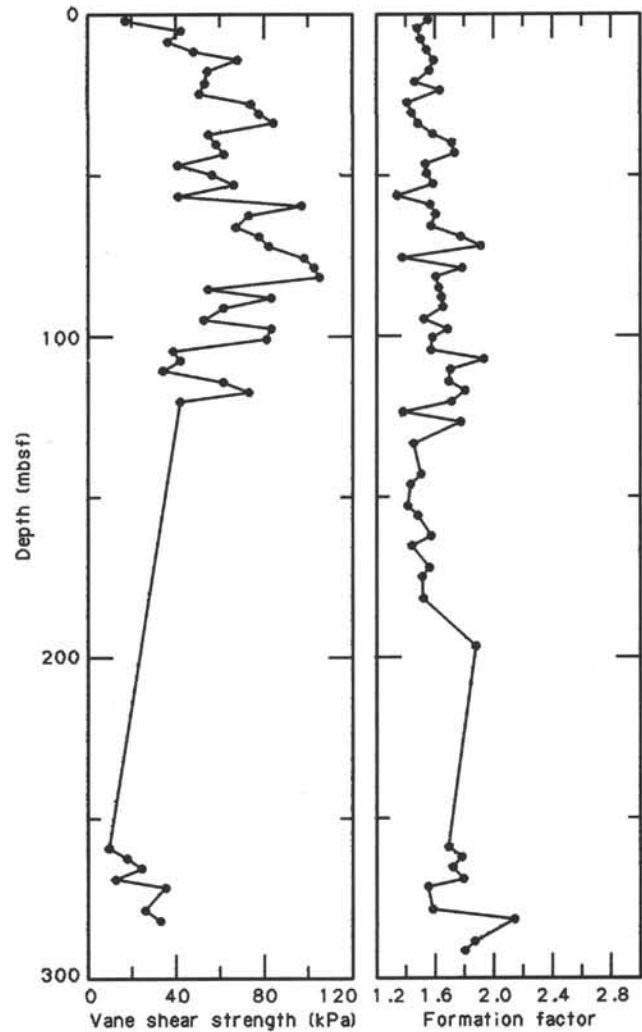


Figure 50. Vane shear strength and formation factor of sediments from Hole 758A.

Table 21. Formation factor of samples from Hole 758A.

Core, section, interval (cm)	Depth (mbsf)	Formation factor
1H-2, 67	2.17	1.55
1H-4, 58	5.08	1.48
2H-2, 64	8.14	1.50
2H-4, 98	11.48	1.54
2H-6, 108	14.58	1.59
3H-2, 64	17.74	1.56
3H-4, 106	21.16	1.46
3H-6, 96	24.06	1.63
4H-2, 121	27.91	1.41
4H-4, 121	30.91	1.44
4H-6, 136	34.06	1.48
5H-2, 126	37.56	1.58
5H-4, 125	40.55	1.71
5H-6, 125	43.55	1.73
6H-2, 124	47.14	1.53
6H-4, 127	50.17	1.54
6H-6, 121	53.11	1.58
7H-2, 132	56.82	1.34
7H-4, 120	59.70	1.56
7H-6, 122	62.72	1.60
8H-2, 111	66.31	1.57
8H-4, 124	69.44	1.77
8H-6, 115	72.35	1.91
9H-2, 112	76.02	1.37
9H-4, 123	79.13	1.78
9H-6, 123	82.13	1.60
10H-2, 96	85.56	1.62
10H-4, 90	88.50	1.64
10H-6, 91	91.51	1.65
11H-2, 92	95.22	1.52
11H-4, 90	98.20	1.68
11H-6, 90	101.20	1.58
12X-2, 88	104.78	1.57
12X-4, 86	107.76	1.93
12X-6, 88	110.78	1.70
13X-2, 90	114.50	1.69
13X-4, 85	117.45	1.80
13X-6, 104	120.64	1.71
14X-2, 70	123.90	1.38
14X-4, 70	126.90	1.77
15X-2, 70	133.60	1.45
16X-2, 70	143.20	1.50
16X-4, 70	146.20	1.43
17X-2, 75	152.95	1.41
17X-4, 65	155.85	1.48
18X-2, 70	162.60	1.57
18X-4, 70	165.60	1.44
19X-2, 70	172.20	1.56
19X-4, 70	175.20	1.51
20X-2, 70	181.90	1.52
21X-CC, 7	196.84	1.88
28X-2, 83	259.23	1.69
28X-4, 82	262.22	1.78
28X-6, 104	265.44	1.72
29X-2, 88	268.98	1.79
29X-4, 57	271.67	1.55
30X-2, 84	278.64	1.58
30X-4, 81	281.61	2.14
31X-2, 89	288.29	1.87
31X-4, 88	291.28	1.80

Table 22. Thermal conductivity of samples from Hole 758A.

Core, section, interval (cm)	Depth (mbsf)	Thermal conductivity (W/m°C)
1H-2, 80	2.30	0.957
1H-4, 80	5.30	1.135
2H-2, 80	8.30	1.063
2H-4, 80	11.30	1.097
2H-6, 80	14.30	1.310
3H-2, 80	17.90	1.166
3H-4, 80	20.90	1.206
3H-6, 80	23.90	1.187
4H-2, 80	27.50	1.202
4H-4, 80	30.50	1.289
4H-6, 80	33.50	1.362
5H-2, 80	37.10	1.225
5H-4, 80	40.10	1.243
5H-6, 80	43.10	1.204
6H-2, 80	46.70	1.268
6H-4, 80	49.70	1.272
6H-6, 80	52.70	1.275
7H-2, 80	56.30	1.324
7H-4, 80	59.30	1.328
7H-6, 80	62.30	1.324
8H-2, 80	66.00	1.276
8H-4, 80	69.00	1.285
8H-6, 80	72.00	1.286
9H-2, 80	75.70	1.304
9H-4, 80	78.70	1.289
9H-6, 80	81.70	1.325
10H-2, 80	85.40	1.447
10H-4, 80	88.40	1.401
10H-6, 80	91.40	1.482
11H-2, 80	95.10	1.369
11H-4, 80	98.10	1.337
11H-6, 80	101.10	1.310
12X-2, 80	104.70	1.420
12X-4, 80	107.70	1.486
12X-6, 80	110.70	1.534
13X-2, 80	114.40	1.330
13X-4, 80	117.40	1.384
13X-6, 80	120.40	1.325
14X-2, 80	124.00	1.384
14X-4, 80	127.00	1.327
15X-2, 80	133.70	1.354
16X-2, 80	143.30	1.398
16X-4, 80	146.30	1.319
17X-2, 80	153.00	1.324
17X-4, 50	155.70	1.368
18X-2, 80	162.70	1.466
19X-2, 80	172.30	1.480
19X-4, 80	175.30	1.454
20X-2, 80	182.00	1.327
21X-2, 80	191.60	1.368
21X-4, 80	194.60	1.332
22X-2, 80	201.30	1.409
23X-2, 80	211.00	1.406
23X-4, 80	214.00	1.390
24X-2, 80	220.60	1.422
24X-4, 80	223.60	1.369
25X-2, 80	230.30	1.448
25X-4, 80	233.30	1.374
26X-2, 80	240.00	1.307
26X-4, 80	243.00	1.442
27X-1, 80	248.10	1.629
28X-2, 80	259.20	1.028
28X-4, 80	262.20	1.689
28X-6, 80	265.20	1.401
29X-2, 80	268.90	1.697
29X-4, 70	271.80	1.815
30X-2, 80	278.60	1.684
30X-4, 70	281.50	1.718
31X-CC, 27	295.48	1.550
33X-2, 111	307.91	1.580
34X-2, 40	316.80	1.580
35X-2, 56	326.66	1.750
36X-2, 57	336.37	1.440
37X-CC, 13	344.34	1.350
38X-2, 142	355.52	1.340

Table 22 (continued).

Core, section, interval (cm)	Depth (mbsf)	Thermal conductivity (W/m°C)
39X-1, 119	358.79	1.610
41X-2, 89	379.39	0.580
42X-2, 76	388.86	1.540
44X-CC, 27	399.87	2.070
47R-2, 110	424.10	1.330
48R-1, 133	432.53	1.300
50R-3, 120	454.80	1.370
51R-1, 72	460.92	1.330
52R-1, 125	471.15	1.270
53R-1, 82	480.42	1.080
54R-1, 26	489.46	1.620
55R-2, 113	501.41	1.130
56R-1, 87	509.27	1.730
56R-1, 135	509.75	1.340
57R-1, 77	518.67	1.420
58R-1, 13	527.23	1.780
59R-6, 58	544.16	1.780
60R-1, 74	546.64	1.650
61R-1, 27	555.37	1.850
62R-2, 121	566.97	1.720
63R-6, 123	581.61	1.710
64R-3, 60	586.58	1.580
65R-1, 59	593.29	1.570
66R-2, 101	604.60	1.920
67R-3, 77	615.22	1.470
68R-4, 25	625.35	1.720
69R-1, 127	631.47	1.780
70R-1, 68	640.08	1.840
71R-2, 135	651.45	1.620
72R-1, 107	659.07	1.660

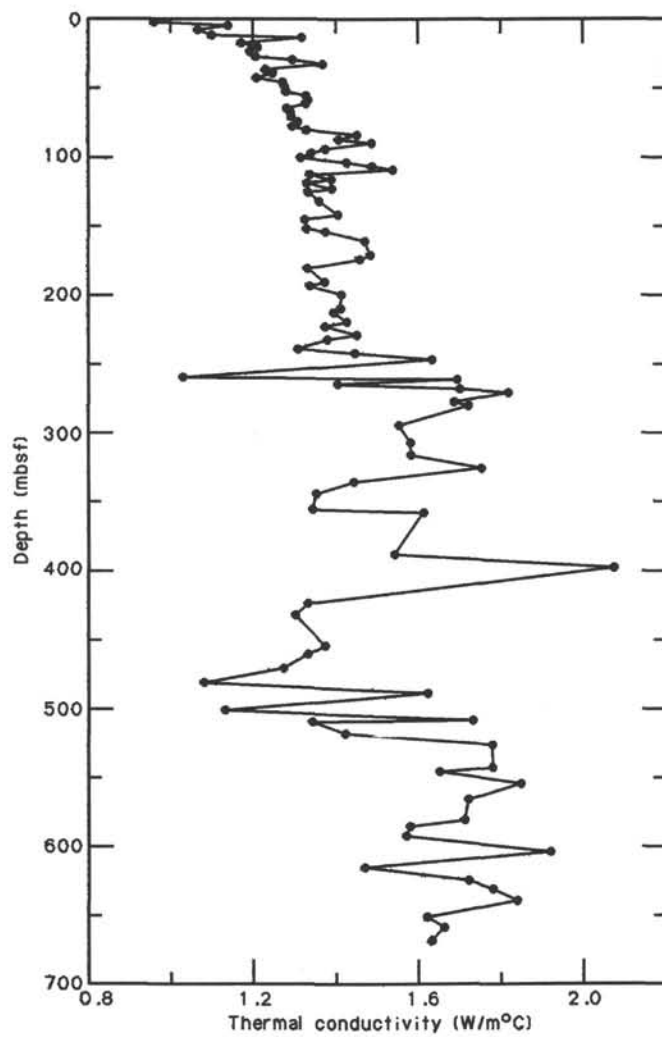


Figure 51. Thermal conductivity for Hole 758A.

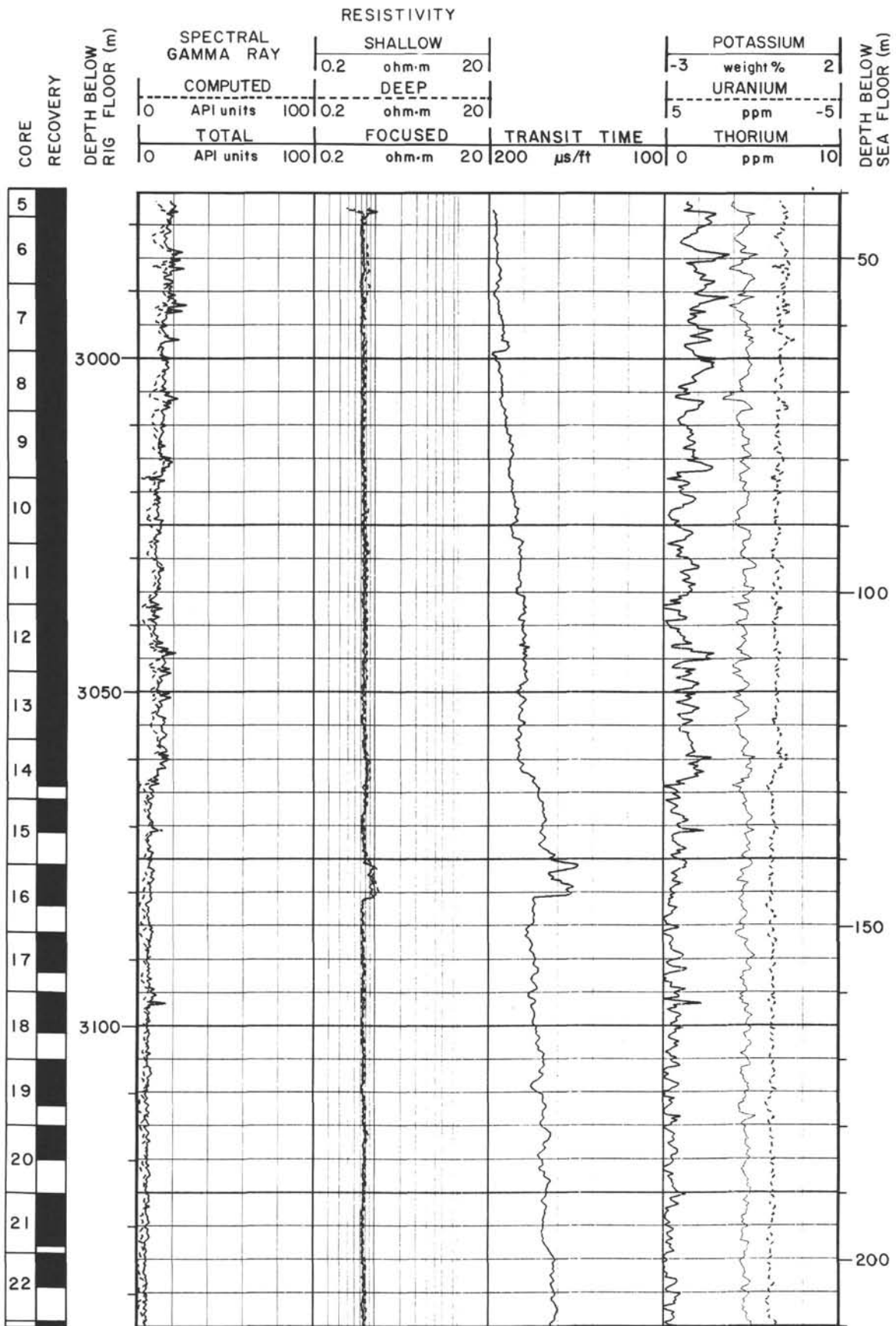


Figure 52. Core recovery; computed and total spectral gamma ray; shallow, deep, and focused resistivity; long-spacing transit time; and potassium, uranium, and thorium logs in Hole 758A, 40-375 mbsf.

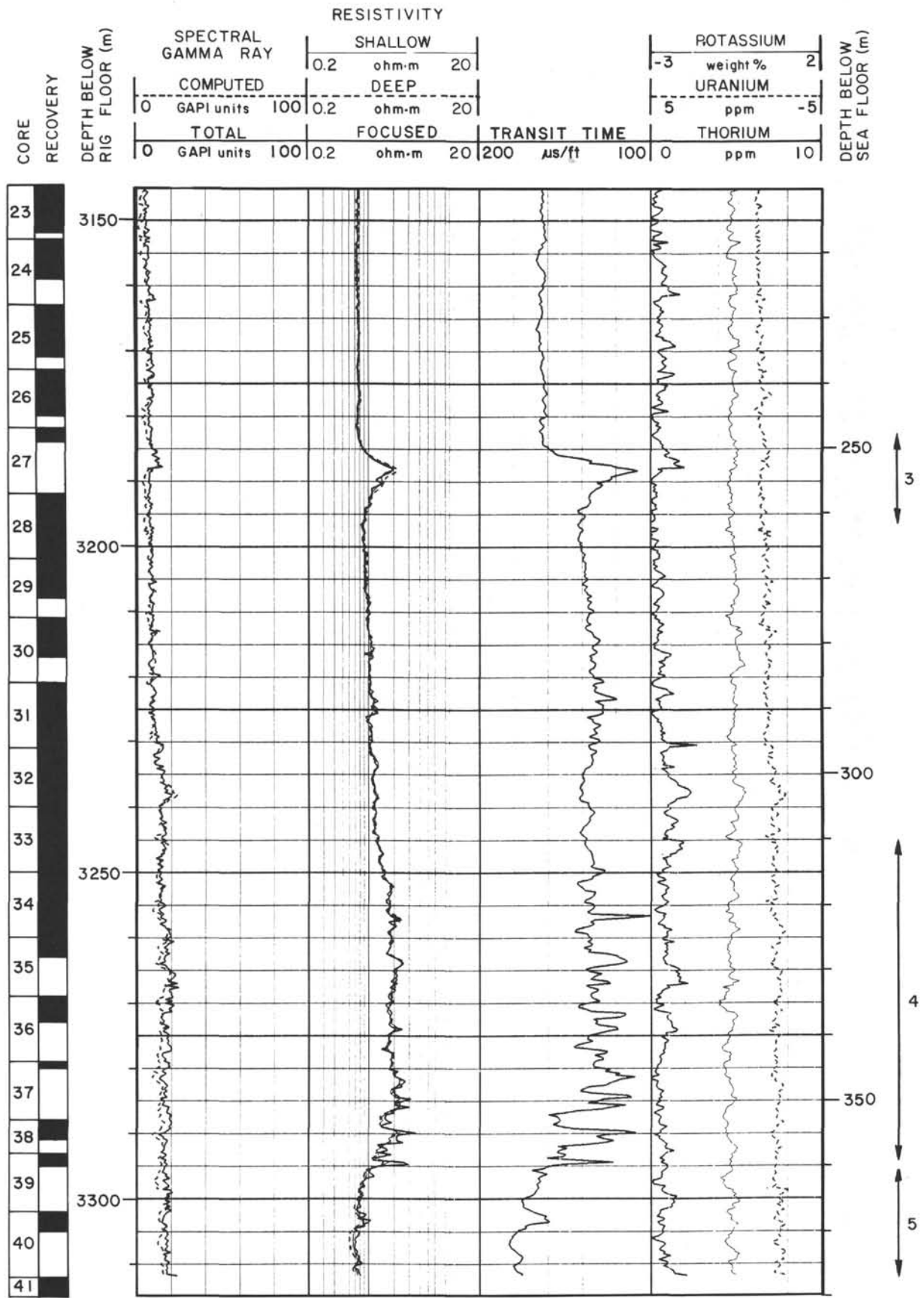


Figure 52 (continued).

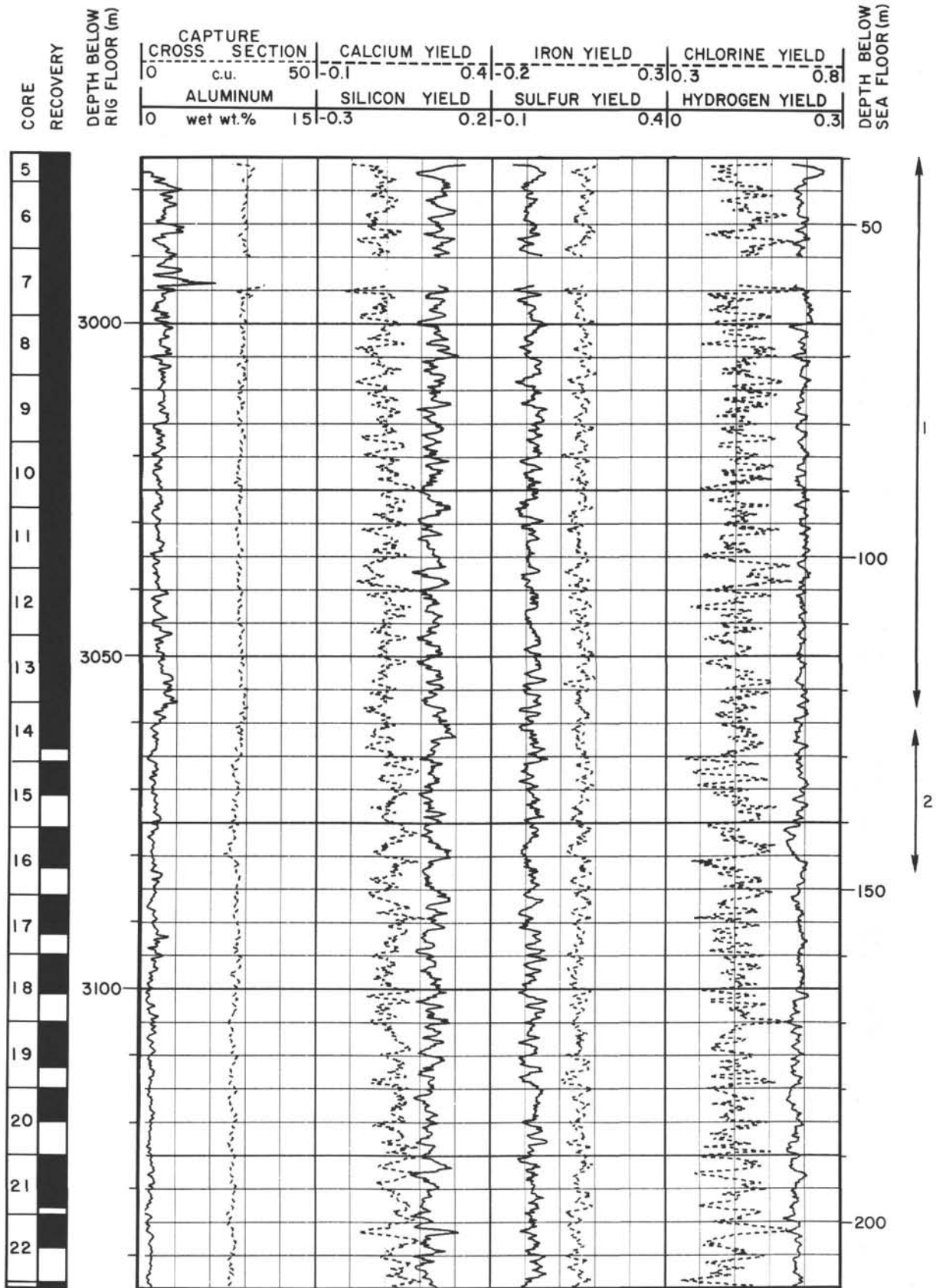


Figure 53. Core recovery, capture cross section, aluminum, and yields of calcium, silicon, iron, sulfur, chlorine, and hydrogen of logs in Hole 758A, 40-395 mbsf.

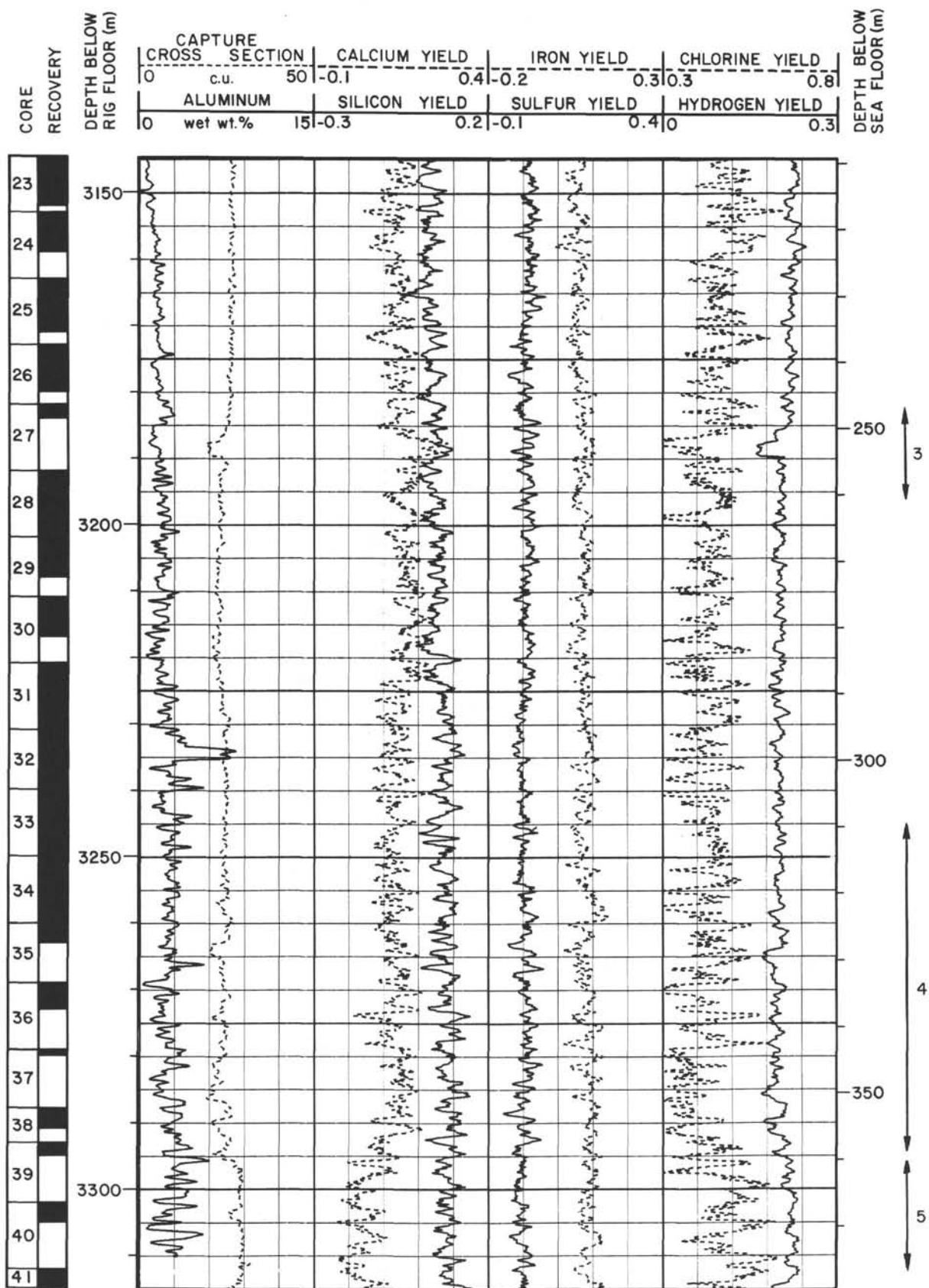


Figure 53 (continued).

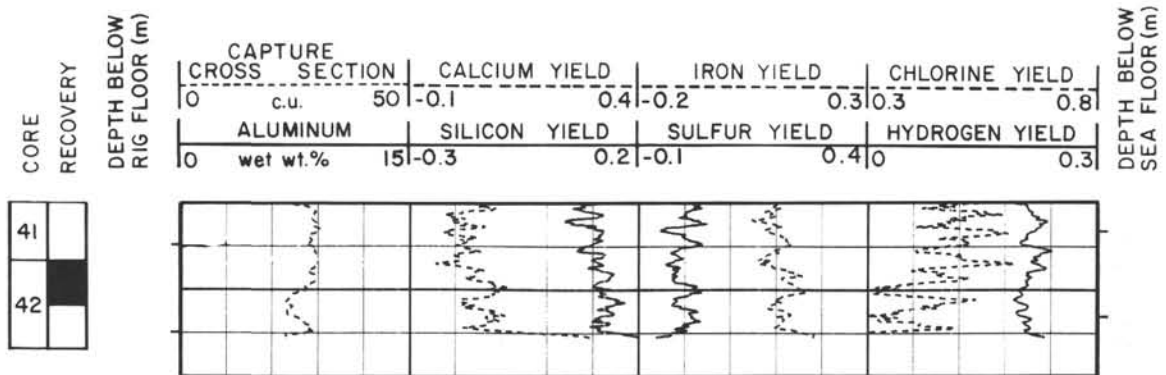


Figure 53 (continued).

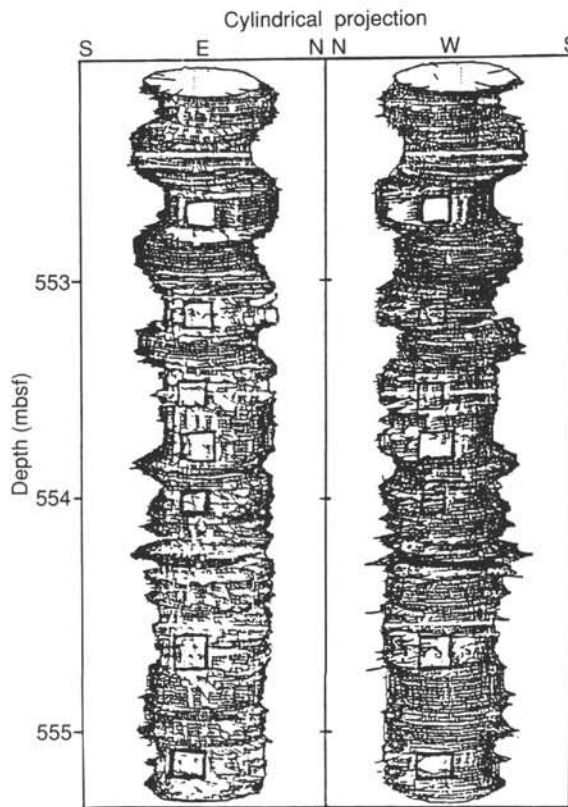


Figure 54. Cylindrical projection of the BHTV log showing breakouts (outlined by square markers) in Hole 758A, 553-556 mbsf.

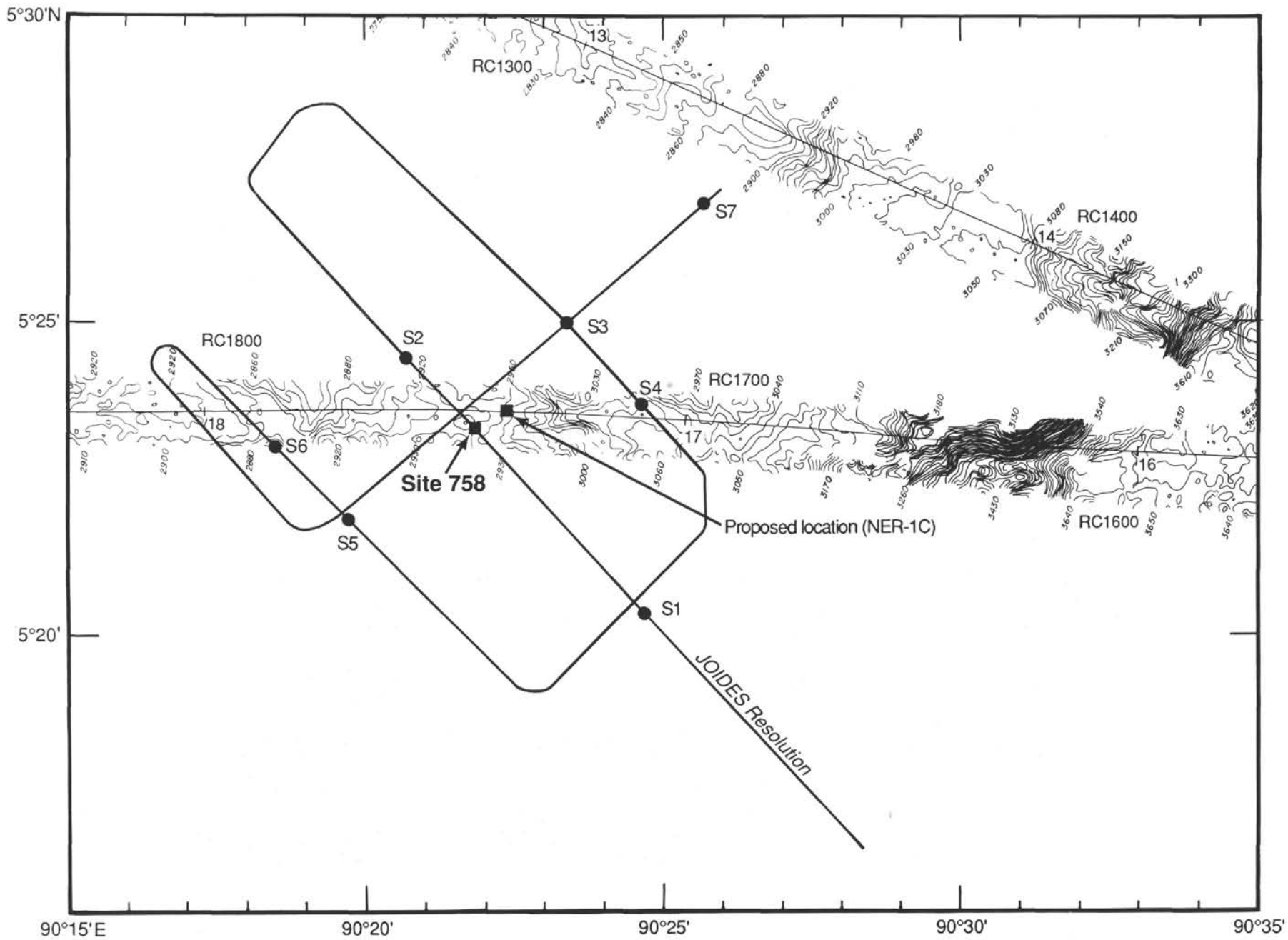


Figure 55. Northern Ninetyeast Ridge survey area. Tracks of the RC2705 survey and the *JOIDES Resolution* predrilling survey in the Site 758 area. Sea Beam bathymetry is shown along the RC2705 tracks. S1-S7 indicate locations of satellite fixes.

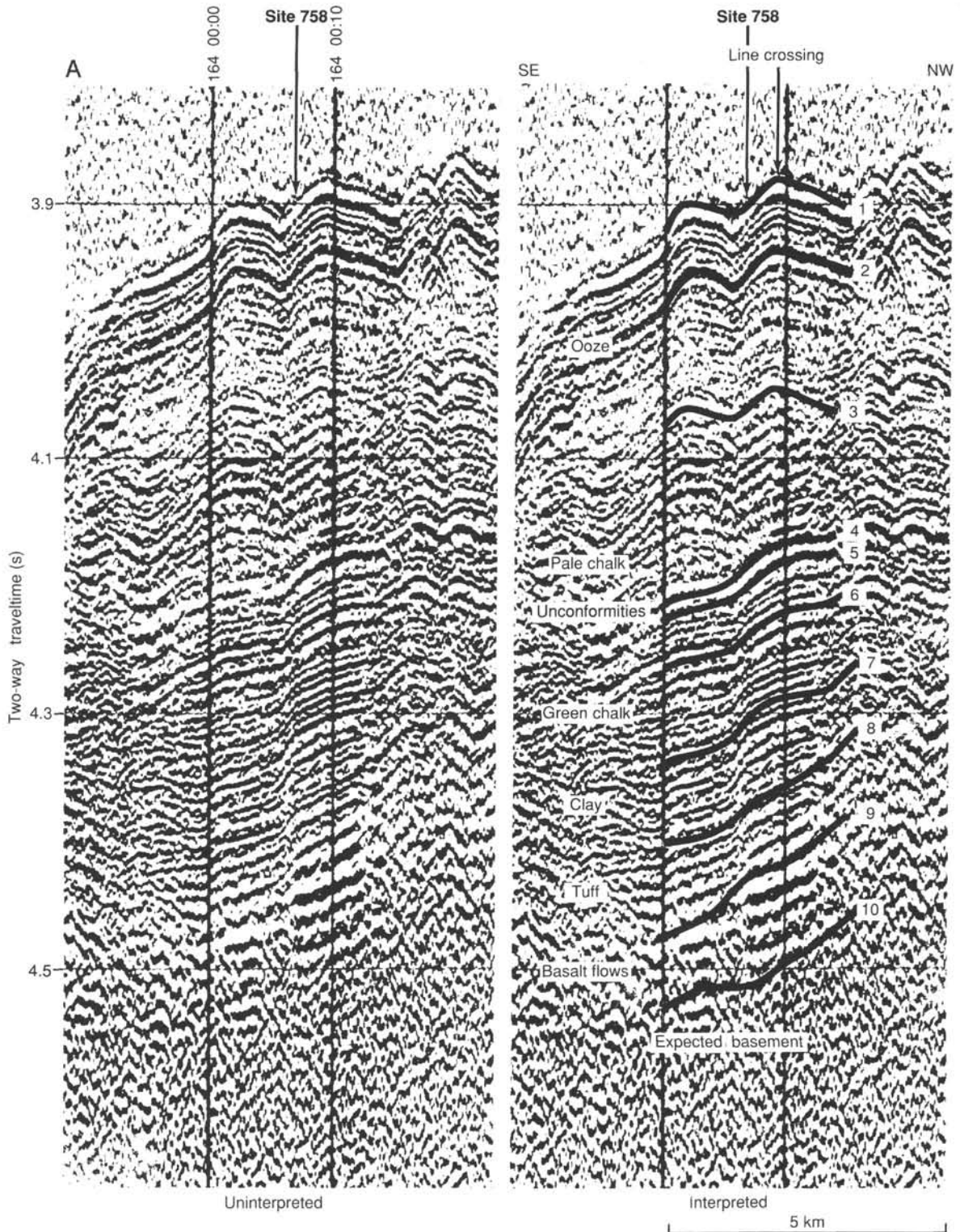


Figure 56. Seismic dip line across Site 758. **A.** Shipboard analog record, uninterpreted on the left and interpreted on the right. **B.** Same data reprocessed post-cruise with less vertical exaggeration. Figure 17 of the “Ninetyeast Ridge Underway Geophysics” chapter (this volume, back pocket) shows the reprocessed version of the entire survey.

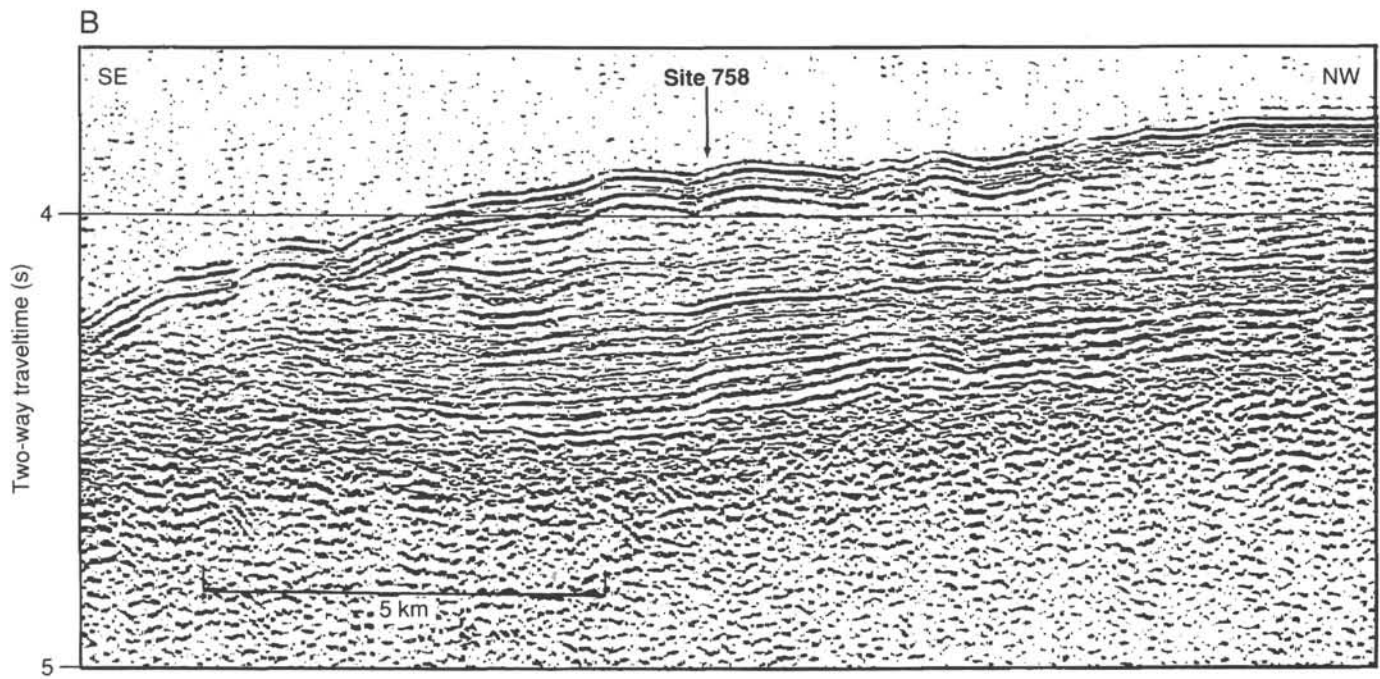


Figure 56 (continued).

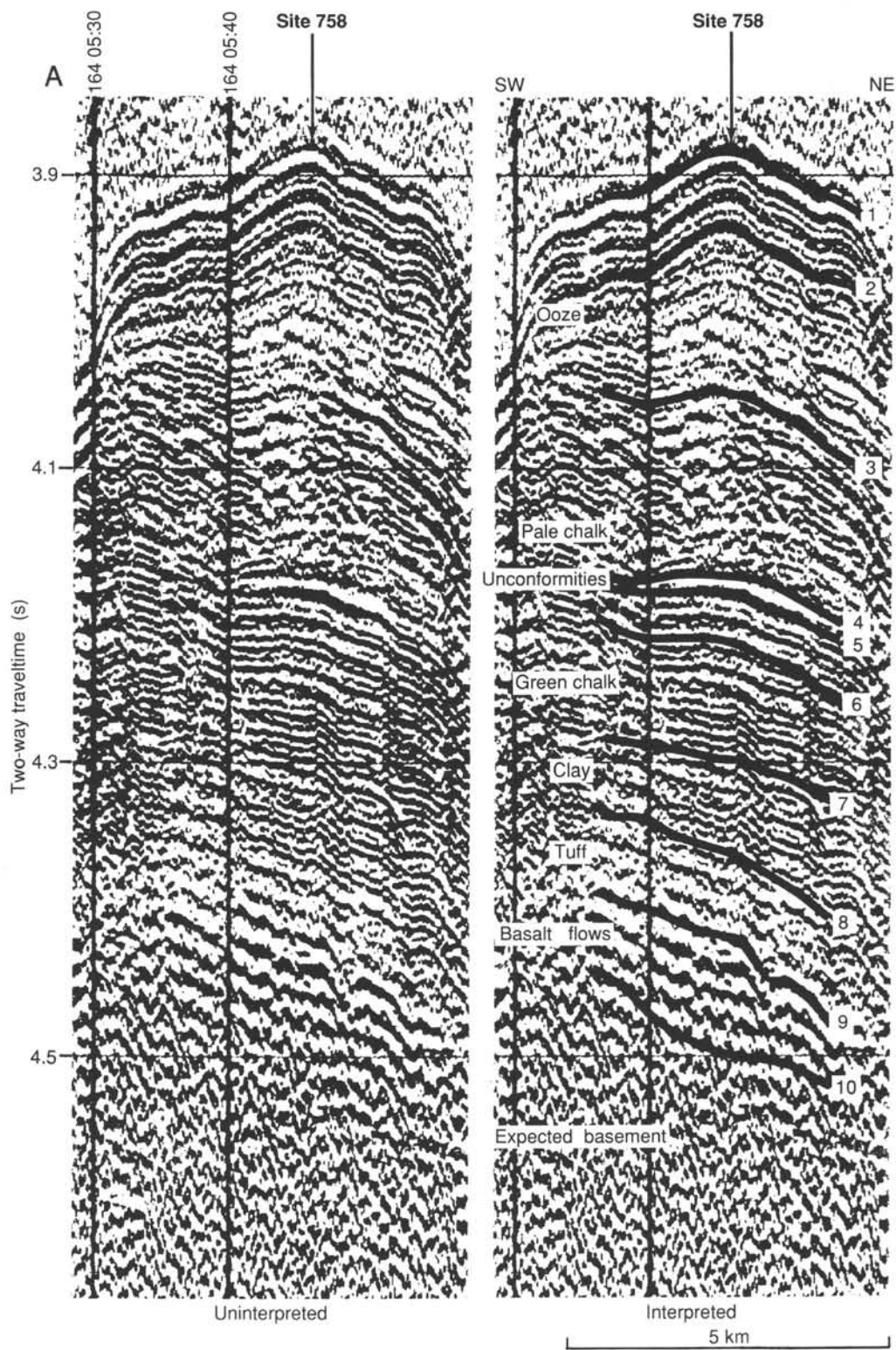


Figure 57. Seismic dip line across Site 758. A. Shipboard analog record, uninterpreted on the left and interpreted on the right. B. Same data reprocessed post-cruise with less vertical exaggeration.

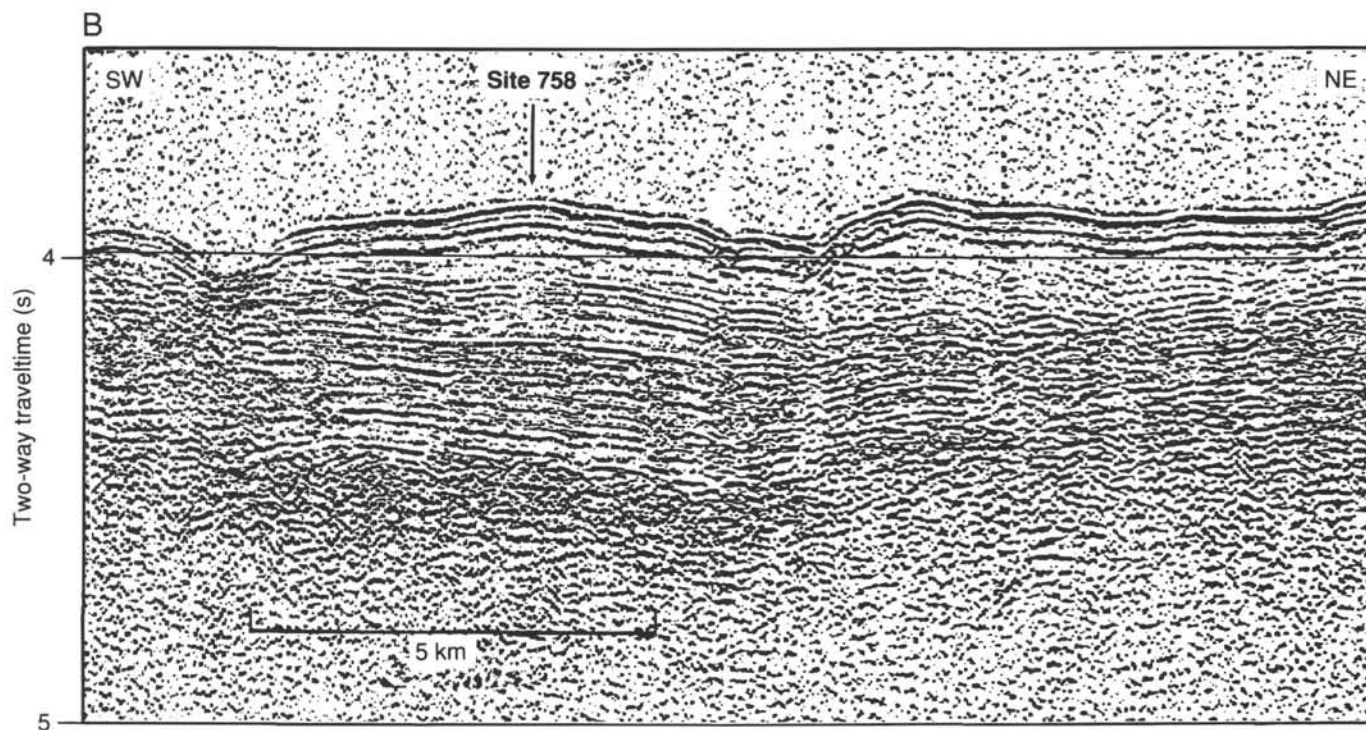


Figure 57 (continued).

Table 23. Reflector two-way traveltimes, Site 758.

Reflector	Two-way traveltime (s)	Remarks
1	3.900	Water bottom
2	3.952	
3	4.058	Ooze/pale chalk boundary
4	4.174	Probable unconformity at 232 mbsf
5	4.200	Large unconformity at 256 mbsf
6	4.242	Pale green and gray chalk and Cretaceous/Tertiary boundary
7	4.303	Green chalk/clay boundary
8	4.374	Clay/tuff boundary
9	4.432	Tuff/basalt flows boundary
10	4.514	Basalt flows/seismic basement boundary(?)

Table 24. Velocity model for calculating reflector depths, Site 758.

Reflector	Time (s TWT)	Depth (mbsf)	Model velocity (m/s)	Approximate velocity measured on physical-property samples (m/s)
1	3.900	0	1500	1500
2	3.952	40	1540	1500-1600
3	4.058	122	1540	1500-1600
4	4.174	232	1890	1500-1900
5	4.200	256	1890	1500-1900
6	4.242	296	1890	1500-1900
7	4.303	367	2330	1800-2100
8	4.374	431	1800	^a 1700-1800
9	4.432	493	2130	1600-2700
10	4.514	682	4600	3500-6000

^a Calculated without peaks.

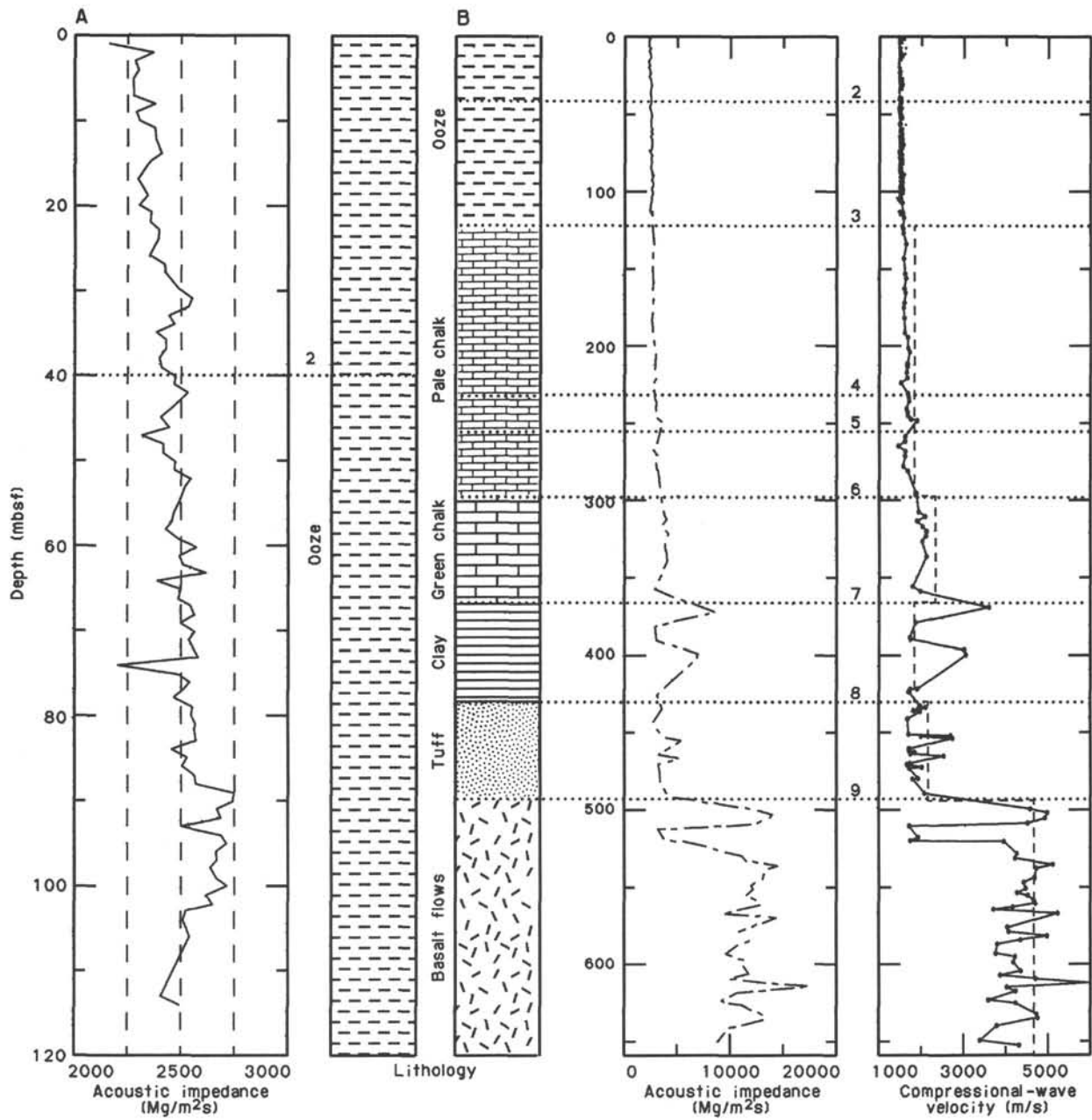


Figure 58. Correlation of seismic reflectors (numbered 2 to 10) to acoustic impedance and lithology at Site 758. **A.** Detailed impedance curve for 0–120 mbsf and lithology showing reflector 2. **B.** Acoustic impedance curve, measured velocities, seismic model velocities (dashed line), and seismic reflectors correlated with lithology.

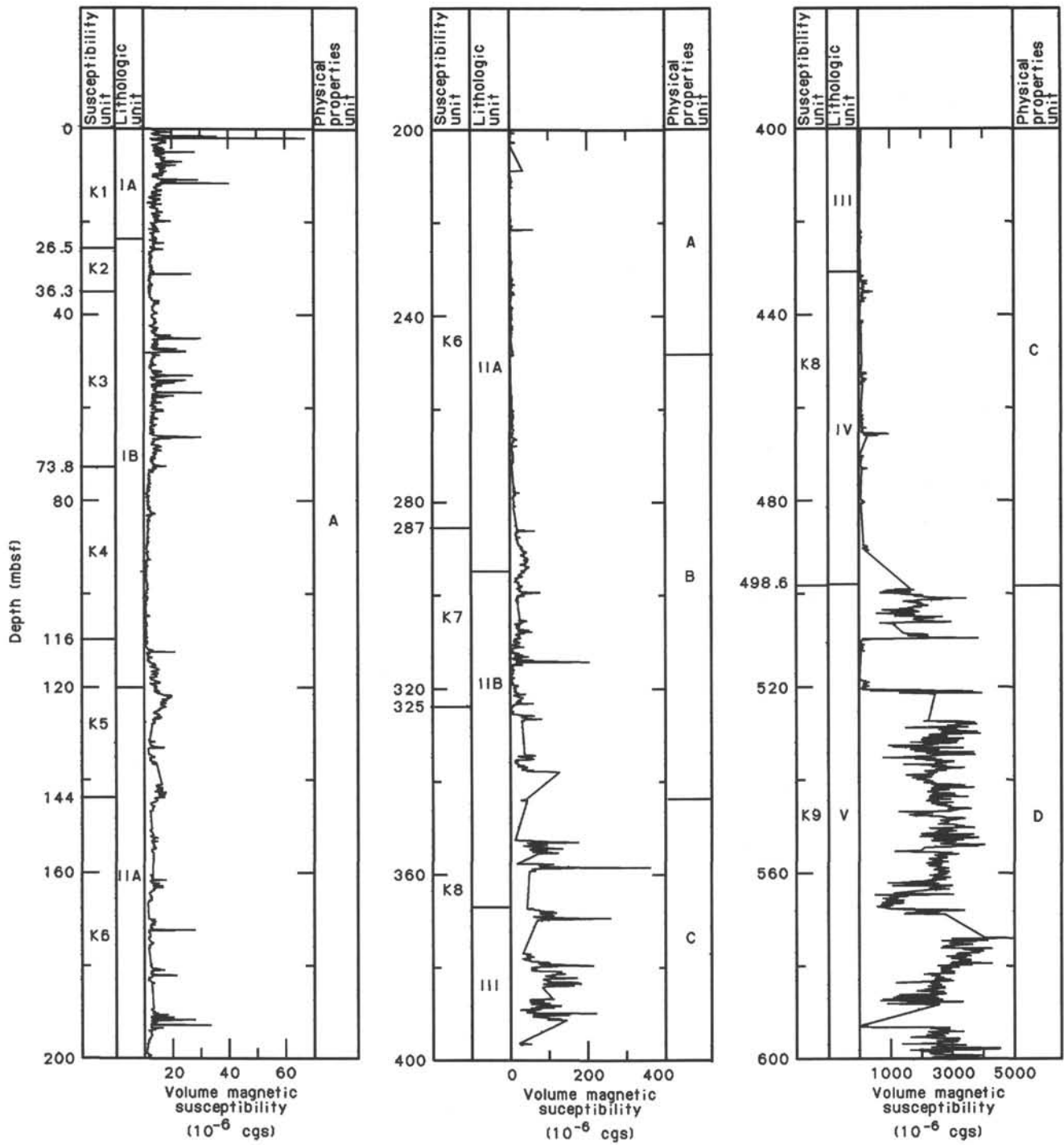


Figure 59. Susceptibility units defined in respect to depth for Hole 758A. The boundaries between lithologic Units I-V and physical-properties units A-D are shown for comparison.

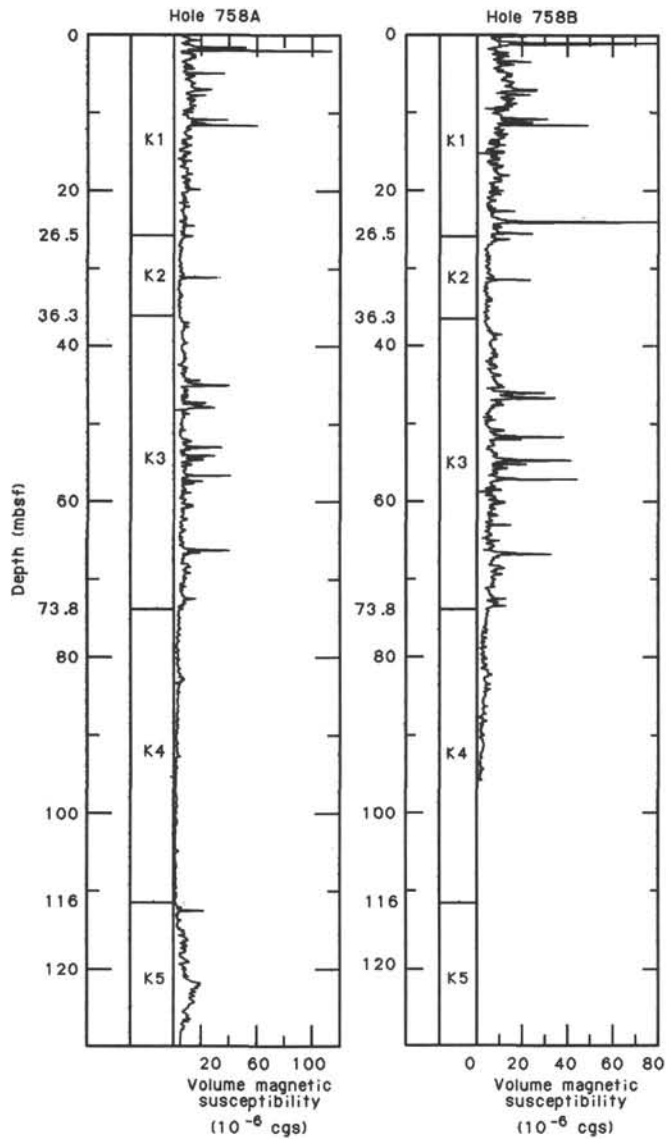


Figure 60. Correlation of susceptibility units K1 to K4 between Holes 758A and 758B.

Table 25. Susceptibility units and corresponding lithologic units in Hole 758A.

Susceptibility unit	Interval (mbsf)	Lithologic unit
K1	0.0-26.5	IA
K2	26.5-36.3	IB
K3	36.3-73.8	IB
K4	73.8-116	IB
K5	116-144 (151)	IB and IIA
K6	144 (151)-287	IIA
K7	287-325	IIA and IIB
K8	325-498.6	IIB, III, and IV
K9	498.6-	V

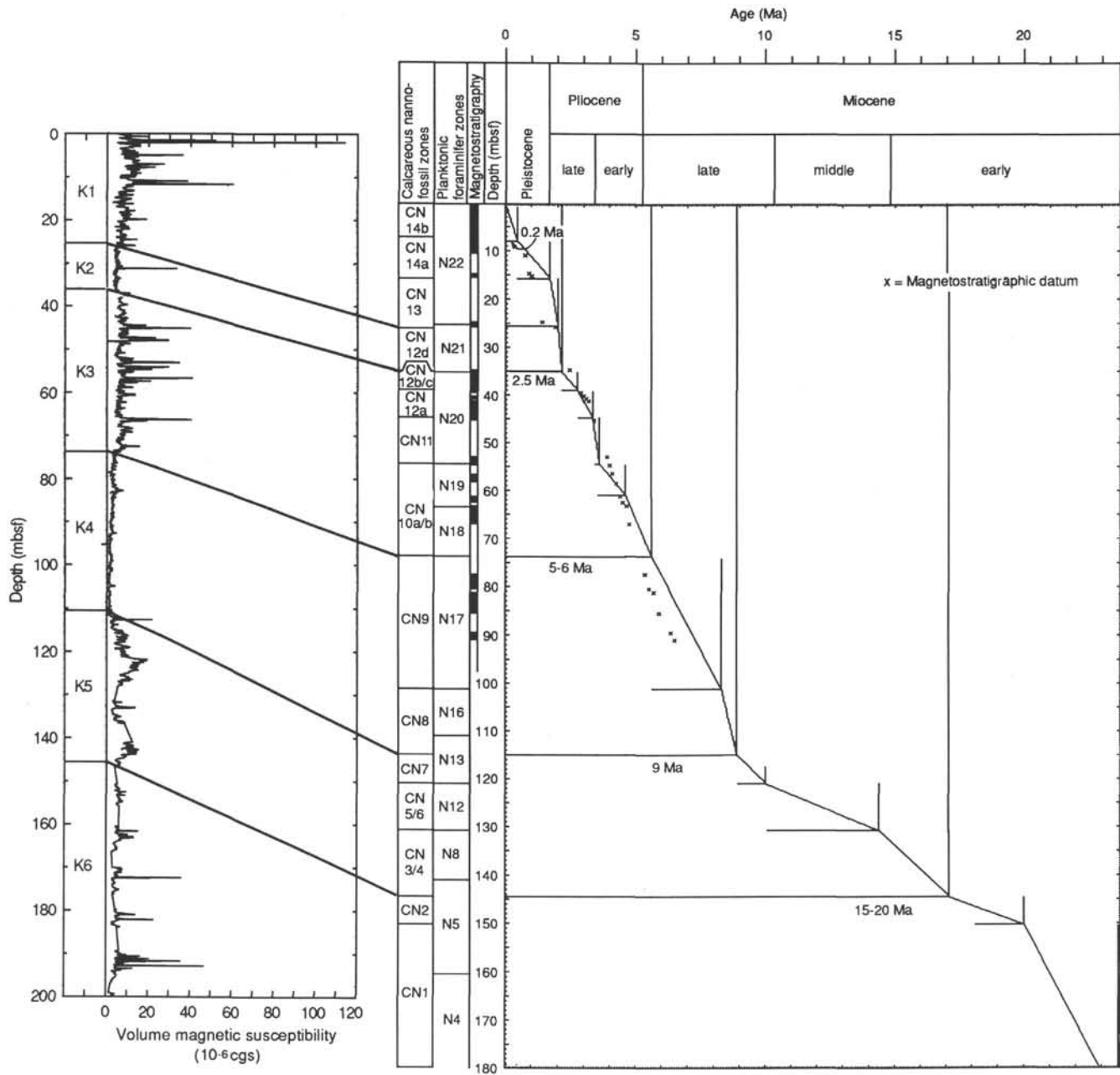


Figure 61. Dating of susceptibility unit boundaries through the Neogene age vs. depth record for Site 758.

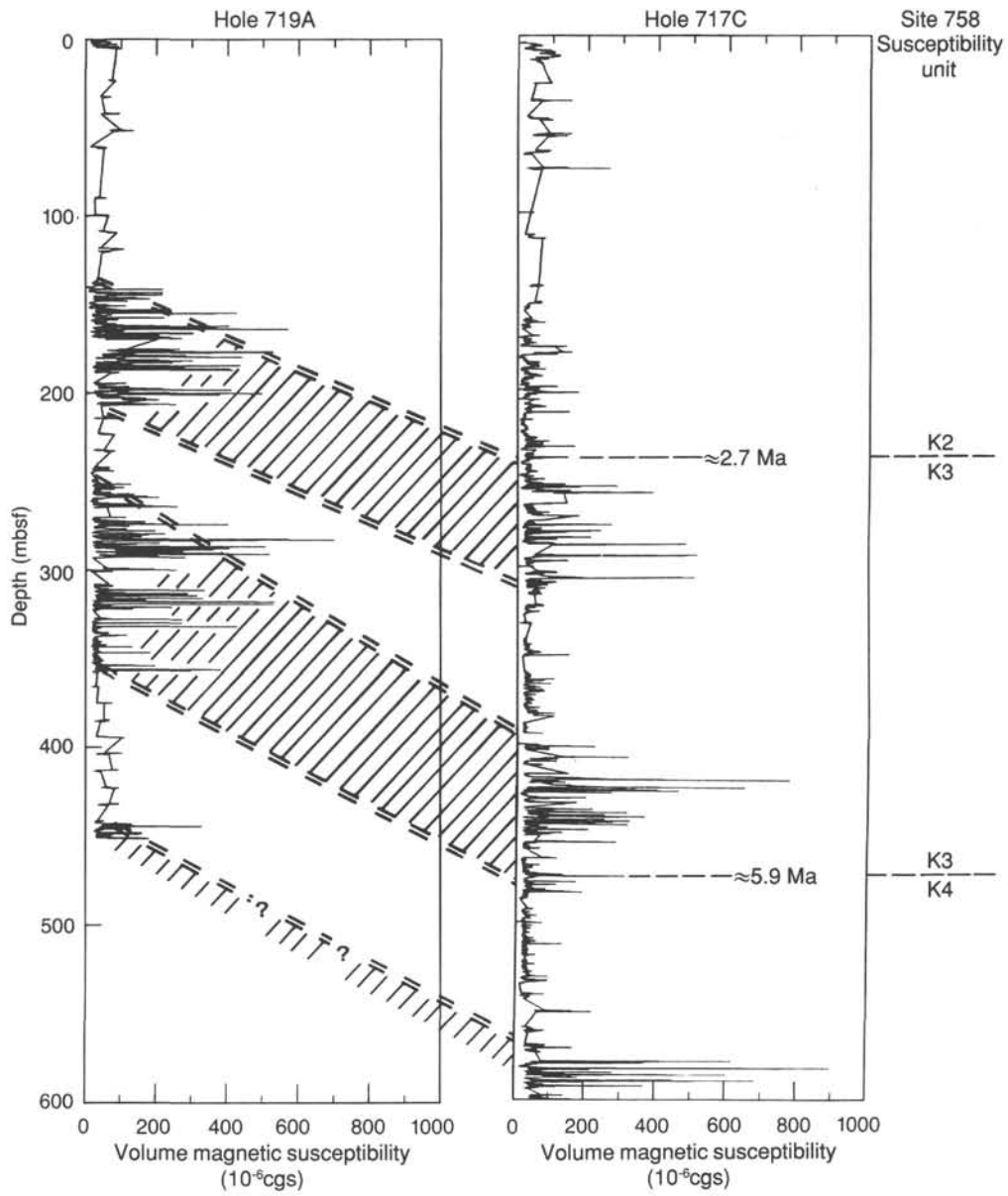


Figure 62. Comparison between susceptibility unit breaks identified at Site 758 and susceptibility unit boundaries identified in Holes 717C and 719A (Cochran, Stow, et al., 1989).

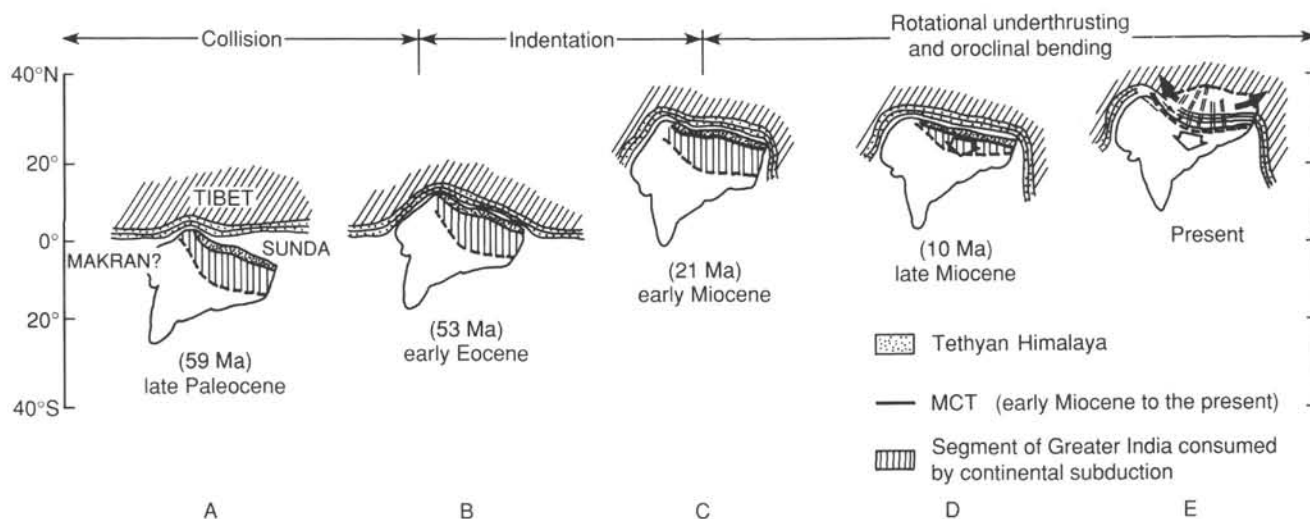


Figure 63. Schematic representation of the five (A-E) stages in the evolution of the India-Asia convergence (Klootwijk et al., 1985). Paleopositions of Greater India are derived from data in Morgan (1983) and Patriat and Achache (1984). At stage C, the Main Central Thrust (MCT) developed about 150 to 200 km south of the leading edge of Greater India (Tethyan Himalaya) and experienced clockwise progradation with respect to the Indian shield up to the present-day position of the Basement Thrust Front (Seeber et al., 1981). There is a causal relationship between rotational underthrusting, lithospheric downwarp, oroclinal bending, and extension in southern Tibet north of the MCT and (stage E) dextral displacement on the Pamir-Karakorum Fault. A = initial collision (late Paleocene); B = completion of suturing (early Eocene); C = onset of continental underthrusting (early Miocene); D = a late Miocene stage of large-scale rotational underthrusting; E = oroclinal bending during the Pliocene/Quaternary.